5-2009

Measurement and Modeling of Reduced-Gravity Fluid Distribution and Transport in Unsaturated Porous Plant-Growth Media

Robert Heinse
Utah State University

5-1-2009

Measurement and Modeling of Reduced-Gravity Fluid Distribution and Transport in Unsaturated Porous Plant-Growth Media

Robert Heinse

Recommended Citation

MEASUREMENT AND MODELING OF REDUCED-GRAVITY

FLUID DISTRIBUTION AND TRANSPORT IN UNSATURATED POROUS

PLANT-GROWTH MEDIA

by

Robert Heinse

A dissertation submitted in partial fulfillment
of the requirements for the degree

of

DOCTOR OF PHILOSOPHY

in

Soil Science

(Soil Physics)

Approved:

_____   _____
Dr. Scott B. Jones   Dr. Gail E. Bingham
Major Professor   Committee Member

_____   _____
Dr. Bruce Bugbee   Dr. Timothy E. Doyle
Committee Member   Committee Member

_____   _____
Dr. Ronald J. Ryel   Dr. Byron R. Burnham
Committee Member   Dean of Graduate Studies

UTAH STATE UNIVERSITY
Logan, Utah

2009

ABSTRACT

Measurement and Modeling of Reduced-Gravity Fluid Distribution and Transport in

Unsaturated Porous Plant-Growth Media

by

Robert Heinse, Doctor of Philosophy

Utah State University, 2009

Major Professor: Dr. Scott B. Jones
Department: Plants, Soils, and Climate

The effect of reduced gravity on the balanced management of liquid, gaseous and ionic fluxes in unsaturated porous media remains a central challenge for plant-based bio-regenerative life support systems needed for long-duration space missions. This research investigated how shifting capillary and gravitational forces alter the sample-scale transport and distribution of fluids in mm-sized porous ceramic aggregates. Measurements in variably saturated media conducted on the International Space Station in microgravity ($\sim 1 \cdot 10^{-3} g_{earth}$) and measurements during parabolic flight in variable gravity encompassing microgravity, terrestrial gravity and hypergravity ($\sim 1.8 g_{earth}$) were supported by numerical modeling based on fundamental, earth-derived soil-physical relationships. Measurements of water fluxes in rigid saturated media suggested Darcian flow unaffected by gravity. Observations of hydraulic potential and sample water content were used to estimate the primary draining and wetting water-retention characteristic (WRC). Terrestrial parameterizations of the WRC were largely unaffected by reduced gravity. However, because the WRC is hysteretic, heterogenous water-content distributions resulted within the confines of the primary draining and wetting characteristics. Ensuing distributions were fundamentally different from terrestrial observations and were stable in the absence of a significant gravity gradient. We showed that these distributions, though unexpected, could be predicted using the Richards equation. One consequence

of altered water distribution could be the reduction in, and increased tortuosity of, continuous gas-filled pathways for diffusive transport compared to terrestrial estimates. Measurements of oxygen diffusion in microgravity suggested reduced diffusivities during draining. These observations, particularly for the smaller particle-sized media, were suggestive of the delayed formation of critical air-filled pathways at lower water contents. This dissertation further uses a case history of a stratified root-zone developed based on water-retention characteristics of different particle-sized media. The root-zone design provided a more uniform water-content distribution at terrestrial gravity suggested to provide more optimal conditions for root growth. Additionally, the design and testing of a novel integrated sensor for measurements of water content based on the dissipation of heat and estimation of nutrient status based on electrical resistivity are discussed. These results should provide insights into microgravity fluid distribution and transport contributing to the design and implementation of controllable plant-growth systems for use in microgravity and future planetary habitats.

(240 pages)

Dedicated to my grandmother, Magda,
who once told me that what you have up there, nobody can take away

The one is the tale as it has come down to
us; of the other, there is more to say.

Günther Grass, *The Flounder*

ACKNOWLEDGMENTS

The help I have received in the writing of this dissertation is immeasurable and some of it has undoubtedly been forgotten or overlooked. I would like to acknowledge the patronage and assistance of all those that have accompanied me on this journey. Clearly, this endeavor has obvious links to the work of many scientists engaged in this research. I have gained much from their ideas, incredible support, inspiration and motivation. I recognize the important assistance and advice of many people in specific aspects of this dissertation in the acknowledgements at the end of individual chapters. For their contribution to this work as a whole, I express my gratitude as follows:

At the top of my list, I owe my academic advisor, Scott Jones, much gratitude for his continued teaching, trust and encouragement. I thank Scott for pioneering this project and for supporting me on this frontieresque journey towards plant growth in space (Who said the frontier closed in 1893?). Above all, I consider Scott my mentor and friend.

I am gratefull to my graduate committee, Gail Bingham, Bruce Bugbee, Tim Doyle and Ron Ryel for their support. I thank them for teaching, very inspiring discussions, and uncounted hints. I am much indebted to Gail for his sustained interest and drive of the science. I thank Bruce for sparking my interest in soil-plant-atmosphere interactions. His explanations, cooperation and guidance were important cornerstones for attaining the objectives of this dissertation.

I am deeply indebted to Dani Or, Markus Tuller and Susan Steinberg. I could not have wished for better collaborators and coaches. Your contributions, detailed comments and insight have been of immense value to me.

A warm, affectionate acknowledgment is due to colleagues, faculty and staff at the Department of Plants, Soils, and Climate. Colleagues at the Space Dynamics Laboratory are much appreciated for the friendly and very productive work atmosphere. I particularly appreciate the help and support of Shane Topham, Bill Mace, Seth Humphries, Kelly Lewis, Jimmy Suisse and Ricardo Estevez who for the many years provided the most congenial and supportive environment. I enjoyed discussing, solving problems and chatting over coffee with David Robinson, Inma Lebron-Robinson, Thijs Kelleners, Larry Hipps and Leanna Reynolds as well as many other friends. Those debts are not

easy to specify, so are others that I owe to all the other lovely people I have met during my time at USU—Vasile Turcu, Guy Serbin, Nil Banik, Tim Wright, Mark Blonquist, the late Robert Love and the π group—thanks for being around.

My parents, from an early age, instilled in me a sense of the possible and humility. Not just for their continued support during all the years of study they have my eternal respect and love.

No one deserves more thanks, however, than Jenn. A historian by trade, an artful writer by training and a passionate teacher by conviction, I give credit to any beauty in the writing to her. Jenn has taken me on a trail of difference and activism, a journey that deserves my deepest appreciation. This dissertation, then, is also for you.

Robert Hein

CONTENTS

LIST OF TABLES

LIST OF FIGURES

CHAPTER 1

INTRODUCTION

Plant growth in reduced gravity has been and continues to be an important part of space exploration research largely because of the need to incorporate plants in any long term, bio-regenerative life support system. While much research has been conducted on reduced gravity effects on plant development (for a review see for example: Monje et al., 2003; Musgrave et al., 2000; Stutte et al., 2006), the plant-rooting environment and physical processes that govern the flow and distribution of fluids in porous media has received far less attention. To date, uncertainties in water, nutrient, and air supply to plant roots have resulted in limited success in many plant-growth experiments in space (Porterfield et al., 2003) that are often attributed to limited understanding of fluid behavior and configuration in unsaturated particulate porous-media under reduced gravity (Ivanova et al., 2006; Steinberg et al., 2002). The current lack of control and quantification of the porous-media-plant-fluid relations hampers progress and development of resilient advanced life-support systems and necessitates the determination of porous-media physical characteristics in reduced gravity as a major soil physical subject.

Balanced fluxes of water and gases to the plant root via the porous plant-growth medium are antipodal and require the simultaneous and balanced existence of water-filled and gas-filled pathways for optimal root-zone fluxes. Water-filled pores provide a quasi barrier for the primarily diffusive gaseous fluxes required for root metabolism; providing for example exchange of Oxygen (sink) and CO_2 (source) with the atmosphere. Changes in the distribution of water-filled pores in porous plant-growth media consequently alter the existence and tortuosity of these crucial continuous gas-filled pathways. While a balance of water- and gas-filled pores can be established for terrestrial gravity conditions based on empirical estimates, the effects of reduced gravity on the distribution of water and ensuing transport parameters remains ambiguous. To achieve a favorable balance in reduced gravity, a combination of porous root-zone management and choice of porous media is sought. Both

rely on the detailed understanding of multiphase fluid distribution and transport characterized by the water-retention characteristic and hydraulic conductivity, and identified by the diffusive transport of Oxygen in unsaturated porous plant-growth media.

Plant growth experiments commonly utilize specialized root-zone systems promoting containment, hydration, nutrient supply and some degree of monitoring and controlling capabilities. The requirements for these root-zone hydration systems in microgravity (μg) have been outlined by Hoehn et al. (2000) to (a) supply appropriate nutrient concentration and composition, (b) maintain desired water content or water availability to plants over the entire growth cycle, (c) adjust water supply for each plant growth phase, and (d) allow adequate gas exchange for oxygenation, CO_2 and trace gas removal from the root zone. To date, these requirements have been fulfilled through the use of porous tube and membrane hydration systems (e.g., Bingham et al., 2002; Burtness et al., 2002; Dreschel et al., 1994; Hoehn et al., 2000; Morrow and Crabb, 2000; Morrow et al., 1993; Scovazzo et al., 2001).

The design and operation of these root-zone hydration systems implicitly assumed that water content and distribution in the porous medium could be uniformly maintained at a prescribed optimal level unaffected by μg conditions. The foundation for these predictions of water content and fluid transport is the water-retention characteristic. The water-retention characteristic links the water content to the matric potential (or suction) of water in porous media. Consequently, various systems have been designed to utilize suction in a porous membrane to indirectly manage the water content in the porous medium through matric potential control (Dreschel and Sager, 1989; Hoehn et al., 2003; Morrow et al., 1992). Some researchers have even controlled matric potentials in the media assuming that Earth-determined water retention characteristics are not altered in microgravity (Monje et al., 2005; Morrow et al., 1994; Steinberg and Henninger, 1997). In juxtaposition with these hydration systems, the control of liquid and gaseous fluxes in the root zone for optimal plant growth (Jones and Or, 1998) beg the question whether hydraulic properties of the porous plant-growth medium quantified under terrestrial gravity (Steinberg and Poritz, 2005) can be transferred to μg.

Presently favored growth media are mm-sized particles of stabilized baked clay (Steinberg and Poritz, 2005), with alternative soilless substrates like composted wheat straw (Gros et al., 2005) and

porous tube nutrient delivery systems (Dreschel and Sager, 1989) also being considered. The advantage of coarse-textured particulate porous media lies in the controllability of water contents where pores drain readily under slight suction, providing ample air-filled pore space for gas exchange with the root tissues. The particulate media systems further have the advantages of water storage and control via the matrix in the case of system malfunction. However, under reduced gravity conditions, capillary forces are dominant, potentially creating water distribution profiles and non-uniformities that are not observed on Earth (Jones and Or, 1999) and that could potentially reduce gas exchange rates (Chau et al., 2005).

Only a few space borne experiments have investigated water movement and control in μg (Bingham et al., 2000; Morrow and Crabb, 2000), but none have investigated the region where gas exchange becomes the limiting factor for plant growth. We hypothesize that under reduced gravity conditions, fluid flow and distribution in porous media are likely to be altered due to changes in buoyancy, dominance of capillary forces, particle rearrangement, enhanced fluid phase entrapment and vehicle vibration. Several studies have presented anecdotal evidence to support this hypothesis. For example, Podolsky and Mashinsky (1994) showed differences between water content distributions measured in μg aboard the MIR space station and measurements on Earth. The authors demonstrated reduced rates of capillary transport and enhanced preferential wetting in 1.5–2.5 mm baked clay aggregates (Perlite). These early observations pointed to enhanced capillary transport and promotion of phase entrapment in reduced gravity, the consequences for fluid behavior at the root module scale, however, remained unknown. Recently, Levine et al. (2003) reported that reduced gravity accentuated the role of pre-wetted surfaces for transport and the rearrangement of loosely packed particles. The authors partially confirmed the postulation of Jones and Or (1999) that microgravity enhances liquid- or gas-phase entrapment, affects macroscopic wetting and drainage processes, and sample scale hydraulic properties. Mohamed et al. (2002) further hypothesized that changes in the microstructure of porous media could significantly alter water retention and hydraulic conductivity.

Notwithstanding these recent advances, predictive capabilities for definitive design of plant growth modules remain ambiguous due to limited opportunities for reduced gravity experiments.

Short-term reduced gravity tests, for example during parabolic flight, offer a more accessible alternative to the more desirable long-duration experiments aboard orbiting spacecraft (Ivanova and Dandolov, 1992; Podolsky and Mashinsky, 1994). However, rare opportunities and high costs that limit the number of trials and repetitions required for obtaining reliable experimental data illustrate why results from past microgravity experiments have often been inconclusive and qualitative in nature. Additionally, the suitability and representativeness of short-term microgravity tests for long-term behavior under microgravity remains an open question. It is therefore not surprising that despite indications of altered liquid and gaseous behavior in reduced gravity, no official guidelines or selection criteria for plant-growth media in microgravity exist.

1.1 Research Objectives and Hypotheses

The primary objectives of this research were to study the effect of reduced gravity on the sample-scale behavior of fluids in partially saturated porous media with a special emphasis on physical root-zone conditions for reduced gravity. An integrative approach is proposed to address these topics, aiming at the following objectives:

i) To measure and model substrate-water retention and saturated hydraulic conductivity under reduced gravity conditions during microgravity (parabolic flight experiments) to elucidate potential differences in porous-media liquid behavior.

ii) To compare effective porous-media oxygen-diffusion coefficients and water retention characteristics measured in microgravity (orbiting spacecraft experiments) to terrestrial estimates to elucidate potential mechanisms contributing to gravity-dependent differences in porous-media fluid behavior.

iii) To examine and expand methods for optimizing physical root-zone conditions using an instrumented stratified porous-media column to provide testing capabilities for imitated microgravity liquid distributions. The optimization will link porous-media water-characteristics and gas diffusion into a general framework that describes the flow and distribution of fluids, and implements the gained knowledge to suggest design and development of engineered porous media that satisfy liquid, gaseous and solute flux requirements of plant roots in reduced gravity.

iv) To design, construct and test an integrative measurement approach to sense water-content and electrical conductivity amenable for use in space flight and planetary habitats.

The completion of the above objectives will contribute to the advancement of scientific knowledge by responding to the following hypotheses:

i) Reduced gravity alters the water retention characteristic thereby modifying the control of the liquid phase in particulate porous media used in microgravity root zones. The mechanism for altered water retention is believed to originate in modified pore size distributions as a result of the dominance of capillary forces, phase entrapment and particle separation.

ii) Reduced gravity (in particular microgravity) leads to a modified air-filled porosity configuration (i.e., based on the water content distribution) in porous media thereby modifying the bulk gas diffusion characteristic. The mechanism for altered gas phase transport in reduced gravity is believed to stem from a more disperse configuration of water-filled pores leading to more tortuous gas pathways compared to a higher gravity force environment.

iii) Engineering pore size distributions corresponding to the gravitational potential within a containerized porous-medium profile, approximates conditions expected in microgravity. Namely, a more uniform water content distribution is expected in microgravity while on earth a hydrostatic distribution is common to a free-draining homogeneous porous medium. Conditions leading to sub-optimal plant growth can be approximated and monitored using measurements and modeling of water content and water- and gaseous-fluxes.

iv) Integrating measurement and interpretation of water-content and electrical conductivity sensors at comparable sampling volumes advances present monitoring capabilities of microgravity root zones. Using dual-probe heat-pulse sensors over the current single-probe design will result in more accurate water content estimates and reduced dependence on empirical sensor calibration. The complex interpretation will allow the extraction of apparent solution electrical conductivities from measured bulk conductivities providing an indicator of nutrient status.

The remainder of this dissertation is organized as follows: Chapter 2 introduces water retention and saturated hydraulic conductivity measurements in variable gravity during parabolic flight. In

Chapter 3, the comparison of effective oxygen diffusion coefficients and implications of fluid configuration in porous media are evaluated in more detail, the statistical comparability of each parameter in this module are also surveyed in that chapter. Chapter 4 frames the design of porous-media root zones based on balanced fluxes of water and gases and proposes the use of a stratified porous media in an effort to optimize porous media for plant growth and provide a test bed for terrestrial microgravity plant research. Finally, Chapter 5 proposes means to evaluate the system performance using advanced water content/nutrient status sensor techniques. Repetition of some formulae and facts are thus inevitable in some parts of this dissertation. I wish the disposed reader will excuse this redundancy. In Appendix A, we describe some of the methodology and experimental setups used throughout this research and that in particular pioneers Chapter 2.

1.2 References

Bingham, G.E., I.G. Podolsky, T.S. Topham, and J.M. Mulholland. 2002. Lada: The ISS plant substrate microgravity testbed. SAE Technical Paper 2002-01-2388. SAE Int., Warrendale, PA.

Bingham, G.E., S.B. Jones, D. Or, I.G. Podolski, M.A. Levinskikh, V.N. Sytchov, T. Ivanova, P. Kostov, S. Sapunova, I. Dandolov, D.B. Bubenheim, and G. Jahns. 2000. Microgravity effects on water supply and substrate properties in porous matrix root support systems. Acta Astronautica 47:839-848.

Burtness, K., K. Norwood, T. Murdoch and H.G. Levine. 2002. Development of a porous tube based plant growth apparatus. SAE Technical Paper 2002-01-2389. SAE Int., Warrendale, PA.

Chau, J.F., D. Or, and M.C. Sukop. 2005. Simulation of gaseous diffusion in partially saturated porous media under variable gravity with lattice Boltzmann methods. Water Resour. Res. 41(8).

Dreschel, T.W., and J.C. Sager. 1989. Control of water and nutrients using a porous tube: a method for growing plants in space. HortScience 24:944-947.

Dreschel, T.W., C.S. Brown, W.C. Piastuch, C.R. Hinkle, and W.M. Knott. 1994. Porous Tube Plant Nutrient Delivery System development: A device for nutrient delivery in microgravity. Adv Space Res. 14:47-51.

Gros, J.B., C. Lasseur, A.A. Tikhomirov, N.S. Manukovsky, V.S. Kovalev, S.A. Ushakova, I.G. Zolotukhin, L.S. Tirranen, R.A. Karnachuk, and V.Y. Dorofeev. 2005. Testing soil-like substrate for growing plants in bioregenerative life support systems. Adv Space Res. 36:1312-1318.

Hoehn, A., P. Scovazzo, J. Clawson, T. Geissinger, W. Kalinowski, and J. Pineau. 2003. Design, Testing and Operation of Porous Media for Dehumidification and Nutrient Delivery in Microgravity Plant Growth Systems. SAE Technical Paper 2003-01-2614. SAE Int., Warrendale, PA.

Hoehn, A., P. Scovazzo, L. Stodieck, J. Clawson, W. Kalinowski, A. Rakow, D. Simmons, A.G. Heyenga, and M.H. Kliss. 2000. Microgravity root zone hydration systems. SAE Technical Paper 2000-01-2510:1-10. SAE Int., Warrendale, PA.

Ivanova, T.N., and I.W. Dandolov. 1992. Moistening of the substrate in microgravity. Microgravity sci. technol. 3:151-155.Jones, S.B., and D. Or. 1998. Design of porous media for optimal gas and liquid fluxes to plant roots. Soil Sci. Soc. Am. J. 62:563-573.

Ivanova, T., S. Doncheva, I. Ilieva, P. Kostov, S. Sapunova, and R. Dikova. 2006. Experiment investigating the influence of oxygen deficiency on plants grown in microgravity. SENS'2006 second scientific conference with international participation-Space, Ecology, Nanotechnology, Safety. Space Research Institute - Bulgarian Academy of Sciences, Creative House of the Bulgarian Academy of Sciences, Varna.

Jones, S.B., and D. Or. 1998. Design of porous media for optimal gas and liquid fluxes to plant roots. Soil Sci Soc Am J 62:563-573.

Jones, S.B., and D. Or. 1999. Microgravity effects on water flow and distribution in unsaturated porous media: Analysis of flight experiments. Water Resour. Res. 35:929-942.

Levine, H.G., G.K. Tynes, and J.H. Norikane. 2003. Fluid Behavior Under Microgravity Conditions Within Plant Nutrient Delivery Systems: Parabolic Flight Investigations. SAE Technical Paper 2003-01-2483. SAE Int., Warrendale, PA.

Mohamed, A.-M.O., H.E. Antia, and R.G. Gosine. 2002. Water flow in unsaturated soils in microgravity environment. J. Geotech. Geoenviron. Eng. 128:814-823.

Monje, O., G. Stutte, and D. Chapman. 2005. Microgravity does not alter plant stand gas exchange of wheat at moderate light levels and saturating CO_2 concentration. Planta 222:336-345.

Monje, O., G.W. Stutte, G.D. Goins, D.M. Porterfield, and G.E. Bingham. 2003. Farming in space: Environmental and biophysical concerns. Adv. Space Res. 31:151-167.

Morrow, R.C., and T.M. Crabb. 2000. Biomass Production System (BPS) plant growth unit. Adv. Space Res. 26:289-298.

Morrow, R.C., R.J. Bula, T.W. Tibbitts, and W.R. Dinauer. 1992. A matrix-based porous tube water and nutrient delivery system. SAE Technical Paper 921390. SAE Int., Warrendale, PA.

Morrow, R.C., W.R. Dinauer, R.J. Bula, and T.W. Tibbitts. 1993. The ASTROCULTURE-1 flight experiment: pressure control of the WCSAR porous tube nutrient delivery system. SAE Technical Paper 932282. SAE Int., Warrendale, PA.

Morrow, R.C., R.J. Bula, T.W. Tibbitts, and W.R. Dinauer. 1994. The ASTROCULTURE flight experiment series, validating technologies for growing plants in space. Adv. Space Res. 14:29-37.

Musgrave, M.E., A.X. Kuang, Y. Xiao, S.C. Stout, G.E. Bingham, L.G. Briarty, M.A. Levinskikh, V.N. Sychev, and I.G. Podolski. 2000. Gravity independence of seed-to-seed cycling in Brassica rapa. Planta 210:400-406.

Podolsky, I., and A. Mashinsky. 1994. Peculiarities of moisture transfer in capillary-porous soil substitutes during space flight. Adv. Space Res. 14:39-46.

Porterfield, D.M., G.S. Neichitailo, A.L. Mashinski, and M.E. Musgrave. 2003. Spaceflight hardware for conducting plant growth experiments in space: The early years 1960-2000. Adv. Space Res. 31:183-193.

Scovazzo, P., T.H. Illangasekare, A. Hoehn, and P. Todd. 2001. Modeling of two-phase flow in membranes and porous media in microgravity as applied to plant irrigation in space. Water Resour. Res. 37:1231-1243.

Steinberg, S.L., and D.L. Henninger. 1997. Response of the water status of soybean to changes in soil water potentials controlled by the water pressure in microporous tubes. Plant Cell Environ. 20:1506-1516.

Steinberg, S.L., and D. Poritz. 2005. Measurement of hydraulic characteristics of porous media used to grow plants in microgravity. Soil Sci. Soc. Am. J. 69:301-310.

Steinberg, S.L., D. Ming, and D. Henninger. 2002. Plant production systems for microgravity: Critical issues in water, air and solute transport through unsaturated porous media. NASA Tech. Mem. 2002-210774. Natl. Aeronautics and Space Admin., Houston, TX.

Stutte, G., O. Monje, R. Hatfield, A. Paul, R. Ferl, and C. Simone. 2006. Microgravity effects on leaf morphology, cell structure, carbon metabolism and mRNA expression of dwarf wheat. Planta 224:1038-1049.

CHAPTER 2

MEASUREMENTS AND MODELING OF VARIABLE GRAVITY EFFECTS ON WATER DISTRIBUTION AND FLOW IN UNSATURATED POROUS MEDIA[1]

2.1   Abstract

Liquid behavior in porous media under reduced gravity conditions is of considerable interest for various components of life support systems required for manned space missions. High costs and limited opportunities for spaceflight experiments hinder advances in reliable design and operation of elements involving fluids in unsaturated porous media such as plant growth facilities. We utilized parabolic flight experiments to characterize porous media hydraulic properties under variable gravity conditions deduced from variations in matric potential over a range of water contents. We designed and tested novel measurement cells that allowed dynamic control of water content (removal and addition) in particulate porous media during parabolic flight. Embedded time domain reflectometry (TDR) probes and fast responding tensiometers measured changes in water content and matric potential. For near-saturated conditions, we observed rapid establishment of equilibrium matric potentials during the recurring 20-s periods of induced microgravity. As media water content decreased, the concurrent decrease in hydraulic diffusivity resulted in limited attainment of equilibrium distributions of water content and matric potential in microgravity, and water content heterogeneity within the sample was strongly influenced by the preceding hypergravity phase. For steady fluxes through saturated columns, we observed rapid attainment of linear and constant hydraulic gradients during variable gravity, yielding saturated hydraulic conductivities similar to values measured under terrestrial gravity. Our results suggest that water distribution and retention

---

[1]The material for this chapter was previously published as: Heinse, R., S.B. Jones, S.L. Steinberg, M. Tuller and D. Or (2007). Measurements and Modeling of Variable Gravity Effects on Water Distribution and Flow in Unsaturated Porous Media. Vadose Zone J. 6:713-724.

behavior are sensitive to varied gravitational forces, whereas saturated hydraulic conductivity appears to be unaffected. Comparisons between measurements and simulations based on the Richards equation were in reasonable agreement, suggesting that fundamental laws of fluid flow and distribution for macroscopic transport derived on Earth are also applicable in microgravity.

2.2 Introduction

The National Aeronautics and Space Administrations's (NASA) and European Space Agency's (ESA) vision of life support for space missions considers growing plants as part of long-term, bioregenerative life support systems that would typically operate under microgravity (μg) conditions. Efficient and resilient growth systems require monitoring and accurate fluid management in the porous rooting environment to meet plant needs under the intense energy, mass, and volume constraints imposed during space flight (Steinberg et al., 2005). To date, water for plant growth systems was delivered through porous tubes and membranes (e.g., Bingham et al., 2002; Burtness et al., 2002; Dreschel et al., 1994; Hoehn et al., 2000; Morrow and Crabb, 2000; Morrow et al., 1993; Scovazzo et al., 2001). The design and operation of these root-zone hydration systems implicitly assumed that water content in the porous medium could be uniformly maintained at a prescribed optimal level unaffected by μg conditions. Various systems have been designed to utilize suction in the porous membrane to indirectly manage the water content in the porous medium through matric potential control (Dreschel and Sager, 1989; Hoehn et al., 2003; Morrow et al., 1992). Some researchers have even controlled matric potentials in the media assuming that Earth-determined water retention characteristics are not altered in microgravity (Monje et al., 2005; Morrow et al., 1994; Steinberg and Henninger, 1997). In juxtaposition with these hydration systems, the control of liquid and gaseous fluxes in the root zone for optimal plant growth (Jones and Or, 1998a) beg the question whether hydraulic properties of the porous plant-growth medium quantified under terrestrial gravity (Steinberg and Poritz, 2005) can be transferred to μg.

Under microgravity conditions, fluid flow and distribution in porous media could be altered due to changes in buoyancy, dominance of capillary forces, particle rearrangement, and vehicle vibration. Several studies have presented anecdotal evidence to support this hypothesis. For example,

Podolsky and Mashinsky (1994) showed differences between water content distributions measured in μg aboard the MIR space station and measurements on Earth. They demonstrated reduced rates of capillary transport and enhanced preferential wetting in 1.5–2.5 mm baked clay aggregates (Perlite). These early observations pointed to enhanced capillary transport and promotion of phase entrapment in reduced gravity, the consequences for liquid behavior at the root module scale, however, remained unknown.

Recently, Levine et al. (2003) reported that reduced gravity accentuates the role of pre-wetted surfaces for transport and the rearrangement of loosely packed particles. The authors partially confirmed the postulation of Jones and Or (1999) that microgravity enhances liquid- or gas-phase entrapment, affects macroscopic wetting and drainage processes, and sample scale hydraulic properties. The sample scale distribution of water was studied by Shah et al. (1993) who reported that during parabolic flight, fluid is pushed downward to the bottom of the substrate in hypergravity (1.8 times Earth's gravity) phases, and rises and distributes more uniformly under reduced gravity conditions. Mohamed et al. (2002) hypothesized that changes in the microstructure of porous media could significantly alter water retention and hydraulic conductivity. More recently, Reddi et al. (2005) studied the behavior of particles and pore fluid blobs at residual water contents in variable gravity. They concluded that microgravity had little effect on individual particles or the size of individual fluid blobs (i.e. blobs did not coalescence or break apart), but clusters of particles adhering to fluid blobs appeared to rearrange themselves. The preliminary observation of fluid flow and liquid configuration in porous micro-models during parabolic flight experiments by Or et al. (2004) suggested that the impact of reduced gravity is manifested at the meso-scale (cluster of pores) rather than at the single-pore level. Accordingly, sample-scale behavior of the spatial and temporal distribution of water in porous media depends on the physical behavior of water at the meso-scale.

Notwithstanding these recent advances, predictive capabilities for definitive design of plant growth modules remain ambiguous due to limited opportunities for reduced gravity experiments. Short-term reduced gravity tests during parabolic flights providing 20 seconds of reduced gravity per parabola offer a more accessible alternative to desirable long-duration space-flight experiments (Ivanova and Dandolov, 1992; Podolsky and Mashinsky, 1994). Rare opportunities and high costs

that limit the number of trials and repetitions required for obtaining reliable experimental data illustrate why results from past parabolic flight experiments are often inconclusive and qualitative in nature. Additionally, the suitability and representativeness of short-term microgravity tests for long-term behavior under microgravity remains an open question. Parabolic flight experiments are far from ideal for the task due to the short period of induced microgravity ($\sim$20 s) with limitations for hydraulic equilibration, the confounding background vibrations (g-jitter), and the ensuing hypergravity phase (1.8-g) required for proper flight trajectory.

Our study comprises results from more than 640 parabolas logged, with significant improvements in our understanding of the working environment and in measurement capabilities. In the following, we report results from water retention and saturated hydraulic conductivity experiments that were conducted during parabolic flight. We focus on spatial and temporal analyses of matric potentials under different water contents and variable gravitational acceleration, commenting on the applicability of hydraulic parameters obtained from short-term microgravity tests. We used estimated parameters and measured data for modeling transient matric potential distributions under microgravity with Hydrus-2D (Simunek et al., 1999). The specific objectives of this study were to (1) measure and analyze matric potentials as a function of water content in porous media during parabolic flight induced microgravity, (2) observe and quantify dynamic and non-equilibrium unsaturated flow in variable gravity, (3) assess the applicability of existing numerical models for unsaturated water flow and distribution in porous media to simulate hydraulic dynamics in reduced gravity, and (4) measure saturated hydraulic conductivity in earth-, hyper-, and microgravity

2.3 Theoretical Considerations

2.3.1 Governing Flow Equations

We briefly introduce here established models and parameterization schemes for describing water transport in unsaturated porous media. In this, we tacitly assume that basic laws of fluid flow for macroscopic transport derived on Earth are applicable to microgravity. The fundamental functional relationships include the volumetric water content q, matric potential h, pressure potential p, and the saturated hydraulic conductivity K_s. Recall that total hydraulic potential H is the sum

of the matric, pressure and gravitational potential z where matric (-) and pressure (+) potentials are mutually exclusive (i.e. $H = h + p + z$).

The Buckingham-Darcy law (Buckingham, 1907) relates the flux density with the hydraulic potential gradient dH/dx and the unsaturated hydraulic conductivity $K(h)$. The Richards (1931) equation, expressed in terms of water content, results from combining conservation of mass with the Buckingham-Darcy law:

$$\frac{\partial \theta}{\partial t} = \frac{\partial}{\partial x}\left[D(\theta)\frac{\partial \theta}{\partial x} - \rho_w g K(\theta)\right] \tag{2.1}$$

where ρ_w is the density of water, g is the acceleration due to gravity, and $D(\theta)$ is the soil-water diffusivity defined as $D(\theta) = K(\theta)dh/d\theta$ with $dh/d\theta$ the slope of the water retention function (i.e. reciprocal soil water capacity). To complete Eq. [2.1], the water retention and the unsaturated hydraulic conductivity functions describing porous media fluid behavior are cast in parameterized functional forms. The water retention may be parameterized with the van Genuchten (1980) model:

$$\Theta(h) = \frac{\theta - \theta_r}{\theta_s - \theta_r} = \begin{cases} [1 + (\alpha|h_m|)^n]^{-m} & \text{for} \quad h_m < 0 \\ 1 & \text{for} \quad h_m \geq 0 \end{cases} \tag{2.2}$$

α, n and m are empirical fitting parameters, where we use the simplification $m = 1 - 1/n$. The unsaturated hydraulic conductivity is then parameterized using the Mualem-van Genuchten expression in terms of these same parameters (Mualem, 1976; van Genuchten, 1980).

With numerical modeling, the challenge then is simulating the gravitational forces that induce the hydrodynamic conditions and adequately modeling the porous medium properties which describe the matric potential/water content relationship that drive transient and equilibrium conditions, especially when gravity forces approach zero. We selected Hydrus-2D (Simunek et al., 1999) because of the capability to simulate 1-g or 0-g conditions using the vertical or horizontal flow option (neglecting the gravity dependent term in Eq. [2.1]), respectively.

2.3.2 Equilibrium considerations

Characteristic Time and Length Scale

The extraction of static equilibrium matric potential values in microgravity under the dynamic conditions experienced in parabolic flight is constrained by the 20 s period of mg. Attainment of equilibrium following the transition from a fundamentally different distribution of matric potentials and water content in the preceding period of hypergravity may therefore be limited. For unsaturated conditions, some of these concerns can be addressed through the observation of matric potential measurements, which provide a rapid tensiometric response (i.e. <1 s) and indicate the level of equilibrium considering the temporal rate of change, where equilibrium conditions in 0-g are defined as:

$$\frac{dh}{dt} \to 0 \tag{2.3}$$

Because of minor gravitational accelerations during parabolic flight and due to the decreasing diffusivity with decreasing water content, we refer to quasi-steady state conditions indicating dh/dt approaches zero and becomes relatively small during each μg period.

Considering one-dimensional flow in 0-g and assuming that D is constant (i.e. uniform water content) and a unique function of water content (conveniently taken to be the drainage water retention function), Eq. [2.1] takes the form of the following differential equation (Childs and George, 1948):

$$\frac{d\theta}{dt} = D(\theta)\frac{\partial^2\theta}{\partial x^2} \tag{2.4}$$

Upon introduction of a dimensionless length $\hat{x} = x/L$ with the constant cell height L and dimensionless time $\hat{t} = t/t_0$ where t_0 is a characteristic time scale we can write:

$$\frac{d\theta}{d\hat{t}} = \frac{D(\theta)t_0}{L^2}\frac{\partial^2\theta}{\partial \hat{x}^2} \tag{2.5}$$

By inspection of Eq. [5] we may now define the characteristic time scale that un-dimensionalizes the differential equation:

$$t_0(\theta) = \frac{L^2}{D(\theta)} \tag{2.6}$$

The characteristic time scale can be thought of as a screening time. A perturbation at the boundary of an initially equilibrated hydrostatic system will decay with time with a characteristic time t_0. The question as to what the characteristic length of that process is may be deduced from the solution. A general solution to Eqs. [5] and [6] for D=const. and with a fixed boundary condition at $\hat{x} = 0$ has the form:

$$\theta(\hat{x}, \hat{t}) = \frac{1}{2} erf \left(\frac{\hat{x}}{2\sqrt{\hat{t}}} \right) \qquad (2.7)$$

From which we may infer that the characteristic diffusion length scale x_0 is proportional to the square root of diffusivity and time, and state:

$$x_0 \sim \sqrt{4D(\theta)t} \qquad (2.8)$$

The greater the lapse of time, the greater is the distance x_0 the perturbation has penetrated for a given diffusivity (i.e. at a given water content). Considering constant and uniformly distributed D implies $x/\sqrt{t}$ constant, hence a perturbation would progress as $1/\sqrt{t}$ along x.

Gravity and Capillarity Forces

In parabolic flight, the gravity-induced perturbation is not confined to a boundary, but is exerted on the sample as a whole where gravitational and capillary forces strive towards the establishment of a new equilibrium. The static bond number B_{os} describes this scaling of effects related to the gravity driven buoyancy force with respect to capillary force, given as (Auradou et al., 1999; Birovljev et al., 1991; Meheust et al., 2002):

$$B_{os} = \frac{\Delta\rho g \zeta}{\sigma/r} \qquad (2.9)$$

where $\Delta\rho$ describes the density difference between the liquid and gaseous phases, σ is the surface tension, r is the pore radius, and ζ the length scale. The characteristic capillary length for B_{os}=1 on Earth, is ζ_c=2.7 mm for the water/air interface, hence, at the pore scale ($\zeta = r$) for pores with radii larger than ζ_c gravity is expected to dominate (and conversely for $\zeta < \zeta_c$, capillary forces dominate). For Profile and Turface with typical pore sizes of 0.26 mm and 0.14 mm the role of reduced gravity on pore scale processes (e.g. liquid/gas interface configuration) is minor B_{os}= $9.1 \cdot 10^{-3}$ and $2.7 \cdot 10^{-3}$

at 1-g, respectively). However, at the sample scale and in the absence of viscous forces, we consider two length scales for the porous media samples, the typical pore size r and the system scale L (cell height or observation height). Substituting Eq. [2.9] into Eq. [2.1], and defining the characteristic length at the sample scale to be Lr (Nakajima and Stadler, 2006) yields:

$$\frac{\partial \theta}{\partial t} = \frac{\partial}{\partial x} \left[K(\theta) \left(\frac{\partial h}{\partial \theta} \frac{\partial h}{\partial x} - \frac{B_{os}\sigma}{Lr} \right) \right] \tag{2.10}$$

When the gravity force approaches zero (i.e. $B_{os} \to 0$) the right-hand term vanishes and Eq. [2.10] predicts a horizontal flow condition. In reality, the onset of instabilities in this regime (Auradou et al., 1999; Meheust et al., 2002) that are not predicted by Eq. [2.10] add complexity in the form of fingering. This additional complexity observed on Earth is likely to affect the flow and distribution of water in parabolic flight and space travel where the gravity force never equals zero, but reduces to values between 10^{-2} and 10^{-6}-g.

2.4 Materials and Methods

2.4.1 Parabolic Flight-Induced Variable Gravity

We conducted water retention and saturated hydraulic conductivity measurements during a 4-day flight campaign in February 2004 on board NASA's parabolic flight aircraft stationed at the Johnson Space Center in Houston, Texas. In May 2006, a second campaign provided additional water retention data, which were obtained with cells of smaller vertical extent (i.e. 1 cm tall). Each flight (1 per day) comprised four sets of 10 parabolas with intermittent 1-g turn-around periods. During each parabola, microgravity conditions existed for 20 to 25 s during free-fall in the apex of the parabolic aircraft trajectory (http://jsc-aircraft-ops.jsc.nasa.gov/Reduced_Gravity/index.html). An accelerometer onboard the aircraft measured gravitational accelerations in x (fore to aft), y (wing to wing), and z directions. The resulting normalized effective gravitational acceleration in z direction $g = g_{observed}/g_{Earth}$ had an oscillatory character, sequentially increasing to about 1.8-g (hypergravity) and then decreasing to near 0-g (microgravity). We also experienced small horizontal accelerations and variations in the vertical acceleration (g-jitter). Fig. 2.6a shows the change in gravitational

acceleration for two representative parabolas. In addition, Fig. 2.6a depicts changes in the aircraft cabin pressurization that compensate for variations in pressure with the parabolic flight trajectory. The pressure changes are in phase with the gravitational acceleration, decreasing nearly linearly in μg and increasing at a slightly accelerated rate in the beginning of 1.8-g traversing a pressure change of approximately 40 hPa.

2.4.2   Particulate Porous Media

The porous media used in this study were porous ceramic aggregates (Profile Products, Buffalo Grove, IL) sieved to particle size fractions of 0.25–1 mm (Profile), 0.25–2 mm (Mix) and 1–2 mm (Turface), and glass beads (MO-SCI, Rolla, MO) of 0.35–0.5 mm, 0.6–1 mm, 1–2 mm and 2.5–3.5 mm size fractions. The particle density of both the glass and porous ceramic aggregates is 2.5 g cm-3. Porous ceramic aggregates have been widely used in microgravity plant experiments (Levine et al., 2003; Norikane et al., 2004; Steinberg and Henninger, 1997; Stutte et al., 2005). The aggregates are stable and have moderate surface area for nutrient storage. Aggregated ceramics exhibit two distinct pore spaces: inter-aggregate and intra-aggregate pores. Only the inter-aggregate pore retention characteristics, particularly in the optimal range for liquid and gas supply of 0 to -25 cm H2O (1 cm H2O = 97.96 Pa) matric potential, are of interest for this study. Measured and fitted porous-media water retention characteristics for Turface, Mix and Profile are shown in Fig. 2.1 illustrating the hysteretic behavior of drainage and wetting processes. To obtain drainage and wetting data, we conducted repetitive measurements with shallow, 1 cm tall by 4 cm diameter cells. A syringe pump controlled water content, and tensiometers measured matric potentials. The van Genuchten (1980) model was fitted to measured data using the RETC software (van Genuchten et al., 1991). The fitted model parameters listed in Table 2.1 are in good agreement with those determined by Steinberg and Poritz (2005).

2.4.3   Experimental Design and Procedures

We designed four novel sample cells with differing vertical dimensions for measuring water retention during parabolic flight (Fig. 2.2). The first cell had a vertical dimension of 1 cm and was connected to a fast-responding transducer tensiometer (PX40-50BHG5V, Omega Engineering,

Stamford, CT). The second cell (Fig. 2.2b) had a vertical dimension of 2 cm and was equipped with a TDR probe (custom 10-cm 3-rod probe connected to a TDR100, Campbell Scientific, Logan, UT) in the center and three fast-responding transducer tensiometers. The third cell (Fig. 2.2c) had a height of 4 cm with TDR probes centered at elevations of 1 and 3 cm and four evenly distributed tensiometer ports. The fourth cell (Fig. 2.2d) was 7 cm high and equipped with three transducer-style tensiometers. To measure saturated hydraulic conductivity, cell inlets were connected to a syringe pump that provided alternating fluxes, and cell outlets were connected to collapsible reservoirs (Fig. 2.3).

The use of taller cells allowed monitoring of accentuated variable gravity effects due to increased hydrostatic forces in 1.8-g and more pronounced transition in matric potentials between 1.8-g and μg . The design of the shallower 1-cm and 2-cm, cells on the other hand, aimed at minimizing the time for steady state conditions by reducing hydrostatic induced water content differences within the cells. In the following, we briefly describe the various cell designs and experimental procedures. For detailed descriptions interested readers are referred to Heinse et al. (2005).

Retention Cell - 1 cm

The 1-cm cell consists of a 1 cm tall by 3.8 cm inner diameter cylindrical polyethylene container that was open to the atmosphere through a small hole ($\sim$1 mm in diameter) in the removable lid (Fig. 2.2a). A porous cup (5 mm pore size, Mott Metallurgical, Farmington, CT) connected to a hypodermic needle was centered in the cell and connected to a syringe. Water addition and removal was controlled and monitored by means of a high-resolution syringe pump (KDS 230, KD Scientific, Holliston, MA) connected to a datalogger (CR23x, Campbell Scientific, Logan, UT). During the experiment 0.67 ml of water was step-by-step withdrawn from the sample during 1.8-g periods. Upon desaturation of macropores the pumping direction was reversed to add water to the sample until satiation. Changes in matric potential as a function of water content and gravitational acceleration were monitored with a tensiometer positioned in the line connecting the porous cup with the syringe (i.e. measuring line pressure). Water content was inferred from pumped volumes of water with the porous media being completely saturated at the beginning of the experiment. Post-flight

analysis provided measures of bulk density for what were typically nine independent cells on each test day.

Retention Cell - 2 cm

The 2-cm cell consists of a 12 x 5 x 2 cm rigid wall container that is open to the atmosphere (Fig. 2.2a). The water addition and removal inlet that is connected to the syringe is in close hydraulic contact with the particulate medium through a sintered porous plate with 5 mm pore size (Mott Metallurgical, Farmington, CT) positioned at, and filling the entirety of, the bottom of the cell. Water addition and removal was controlled and monitored by means of a high-resolution syringe pump connected to a datalogger. During the experiment, a fixed volume of water (5 ml) was pumped stepwise into the sample during periods of 1.8-g. The changes in matric potential as a function of water content and gravitational acceleration were monitored with three tensiometers positioned at 0.5, 1 and 1.5 cm height and a TDR probe centered at z=1cm. The water content was inferred from TDR measurements using the following water content/dielectric relationship for 2–5 mm porous ceramic aggregates:

$$\theta_v = 0.0115\varepsilon^2 + 0.2456 \tag{2.11}$$

Retention Cell - 4 cm

The 4-cm cell (Fig. 2.2b) consists of a 12 x 5 x 4 cm rigid wall container. The changes in matric potential as a function of water content and gravitational acceleration were monitored by a set of four tensiometers located at 1, 1.5, 2.5 and 3 cm height, and two TDR probes centered at z=1 cm and 3 cm. Water addition and removal was achieved in the same fashion as outlined for the 2 cm cell above.

Retention Cell - 7 cm

The 7-cm cell (Fig. 2.2c) consists of a vertically oriented clear-polycarbonate cylinder with 2.5 cm inner diameter. Two stainless steel screens confine the particulate porous medium. The screen at the bottom of the cell is connected to a syringe, and the screen at the top of the cell is open to the atmosphere. Water removal was achieved by manually withdrawing water with a syringe in four

steps at volume increments of 5 ml to establish volumetric water contents ranging from 0.7 to 0.48. Matric potentials were measured with tensiometers positioned at 1, 3 and 5 cm heights.

Saturated Hydraulic Conductivity Cell

For the hydraulic conductivity experiments, the porous medium was packed into horizontal 48 cm long acrylic cylinders with 1.9 cm inner diameter (Fig. 2.3). Water was pumped from the syringe end into a flexible-wall bag at the distal end at alternating fixed fluxes. The flexible-wall bag was used to minimize the hydrostatic forces of water exerted by the reservoir, and allow the system to be in equilibrium with the cabin pressure. Five pressure transducers along the flow-domain (10 cm apart) measured the gradient in pressure potential. Experiments ran continuously to cover both μg and 1.8-g conditions.

2.5   Results and Discussion

We first discuss the hypothetical distribution of sample matric potential in hyper- and zero-gravity phases of a parabolic flight and illustrate redistribution after transition between the two stages. Next, we use a numerical model, Hydrus-2D, to evaluate the applicability of the Richards equation for modeling liquid behavior in microgravity. We compare model calculations with measured water content and matric potential data. We then focus on water retention characteristics measured in microgravity and compare results to measurements obtained in 1-g. In the final section, we discuss saturated hydraulic conductivity measured in microgravity.

2.5.1   Matric Potential Distribution in Variable Gravity

Vertical distributions of matric potentials under hydrostatic equilibrium for various gravitational conditions experienced during a parabolic flight are depicted in Fig. 2.4. In this hypothetical experiment, we consider a 4 cm tall cell packed with Turface, and assume an average matric potential of -4 cm maintained at the center of the sample. The system is then subjected to different gravitational accelerations ranging from 0 to 1.8-g to generate the static equilibrium distributions shown in Fig. 2.4.

In 1-g, we find a linear distribution of matric potentials ranging from -2 cm at the bottom of

the cell to -6 cm at the top. The sample water content distribution follows the primary drainage or wetting curves described by Eq. [2.2] and using parameters listed in Table 2.1.

For 1.8-g, the potential distribution changes and corresponds to the increase in the gravitational force. The potential at the bottom of the cell attains a value of -0.4 cm and at the top -7.6 cm. The corresponding water content distribution is obtained by scaling the matric potentials of the primary retention curves (i.e. $\theta(h_{1.8-g}) = 1.8 \cdot \theta(h_{1.8-g})$). Note that for the same average matric potential the water in the system is distributed differently. More water accumulates at the bottom of the cell, and less at the top.

If the cell were subjected to 0-g, the matric potential distribution would be constant and uniform throughout the porous medium. Consequently, the water content would have values that lie between the boundaries of the primary drainage and wetting curves. It would be possible to obtain secondary scanning curves between the water content values predicted by the primary curves. Hence, the spatial distribution of water content in the system may vary considerably as deviations between the top and bottom parts of the sample may follow different secondary retention curves. We therefore hypothesize that the water content in 0-g depends on the wetting/drainage history of individual pores and pore clusters prior to the 0-g phase.

For the experimental observations, the rapid transitions in gravitational acceleration between 1.8-g and μg may preclude attainment of equilibrium, and dynamic fluid behavior could dominate observations. In the following, the transition of matric potentials between 1.8-g and μg that drive the time-dependent redistribution of water and the consequences for measuring static-equilibrium water retention in variable gravity are discussed in more detail.

2.5.2 Transient and Equilibrium Analysis

In order to capture the effect of μg on hydraulic properties in unsaturated porous media, the transition following a perturbation caused by the ensuing hypergravity phase needs to decay reasonably fast, and a new equilibrium should be established. Clearly, the size of the sample and the hydraulic properties of the media determine this decay, but in addition, the establishment of this new μg equilibrium involves a shift in the relative influence of capillary- and gravitational-forces.

Recall Eq. [2.9] stating that at the pore scale under 1-g, capillarity dominates the shape of the interfacial configuration over gravity. Fig. 2.5a shows that this remains true even at 1.8-g. On the other hand, if one considers the effect of gravity at the sample scale ($\zeta \gg r$), one could argue that pores at different heights in the sample are interconnected and experience feedback suggesting the sample height or observation height determines the relative influence of gravitational to capillary force. Fig. 2.5a shows the Bond number using the pore scale and sample scale perspective. At the sample scale, for increasing cell heights the dominance of gravitational forces occurs in reduced gravitational fields compared to shallower cells. For the observation of equilibrium conditions in μg, it follows that the perturbation caused by the preceding hypergravity phase will be more pronounced as cell height increases. Keeping in mind that the time for the decay of this perturbation is limited to 20+ s, minimization of sample vertical extent for experiments in parabolic flight seems advantageous. This aspect is further illustrated in Fig. 2.5b depicting the characteristic time scale. Because the movement of water is controlled by the hydraulic diffusivity (Eq. [2.1]), the transition towards equilibrium is retarded at reduced water contents. The time required for reaching equilibrium conditions increases with cell height and pore size, where equilibrium conditions are reached relatively quickly (within seconds) at high water contents and shallow cell heights, while at low water content and for taller cells the transition to equilibrium can take considerably longer than 20 s.

2.5.3 Measurements in Parabolic Flight

Measured matric potentials obtained with the 7-cm cell during rapid transitions from 1.8-g to μg and vice versa (Fig. 2.6a) are shown for average water contents of 0.48, 0.56, 0.63 and 0.7 cm^3 cm^{-3} with potentials measured at 1, 3, and 5 cm heights (Figs. 6b-e). In the 1.8-g phase, the matric potentials diverged between the three monitoring elevations in accordance to the gravitational potential. In μg , the gradient rapidly decreased due to diminishing body forces and transitioned towards equilibrium. After the μg phase, the initial 1.8-g potential distribution was rapidly reestablished. Under near-saturated conditions (θ=0.7) all tensiometers measured a uniform matric potential indicating that equilibrium in μg was quickly attained, whereas the transition towards equilibrium at lower water contents (i.e. θ=0.63-0.48) became gradually slower. This progressive

delay in attaining equilibrium is attributable to the decrease in unsaturated hydraulic conductivity with decreasing water content scaled by the hydraulic capacity (Fig. 2.5). In this respect, it is noteworthy that subtle differences in the response rates at different elevations (e.g. compare 1 cm vs. 5 cm observation) indicate water content and unsaturated hydraulic conductivity heterogeneity at lower water contents within the sample (Fig. 2.6b-e). Temporal tensiometer responses at different sample elevations further indicate that different volume elements of the porous medium undergo different drainage or wetting processes simultaneously. At the lowest water content (Fig. 2.6b), the bottom tensiometer shows a reduction in matric potential (drainage) during μg, while the top tensiometer indicates an increase in matric potential (wetting). The middle tensiometer, on the other hand, at first shows an increase, followed by a decrease in potential. This apparent overcompensation likely arises from non-uniform water retention following different secondary curves within the profile coupled with the transition from drainage to wetting conditions.

Similar results as shown for the 7-cm retention cell were obtained for the 1-, 2- and 4-cm cells. The differences in observed matric potentials at different sample elevations and transitions to equilibrium, however, were more pronounced in the 7-cm cell.

2.5.4 Simulation of Fluid Behavior in Variable Gravity

In the following example, the Richards equation (Eq. [2.1]) and the van Genuchten/Mualem parametric models for water retention (Eq. [2.2]) and hydraulic conductivity are applied to calculate the transient matric potential distributions shown in Fig. 2.6g-j. In this simulation, we attempted to model the transition of matric potentials from an initially equilibrated matric potential distribution in 1.8-g to μg using Hydrus-2D concentrating on the first μg period shown in Fig. 2.6b-e. Hydrus-2D does not explicitly allow the simulation of 1.8-g conditions or variable gravity. However, the transition from 1.8-g to μg can be simulated using measured matric potentials in the sample at the end of the 1.8-g period as the initial condition, where the potentials at the upper and lower boundary of the domain were estimated based on a 1.8-g force (1.8 times distance) assuming static equilibrium. The initial process was specified to be drainage. For the van Genuchten parameterization, we used the Earth-based (1-g) parameters for Profile given in Table 2.1. For the saturated hydraulic conduc-

tivity, we used 0.2 cm s^{-1} to allow for a better fit. This conductivity is in the range of conductivities given in Table 2.2, which varied between 0.14 and 0.3 cm s^{-1} for packing densities between 0.62 and 0.67 g cm^{-3}.

A comparison of measured and modeled matric potentials showing the vertical distribution in μg as a function of time at three observation heights is shown in Fig. 2.6g-j. The results show good agreement between the measured and modeled matric potentials with respect to the transition following 1.8-g at the indicated water contents. Some of the perceptible discrepancies in Fig. 2.6g-i for the simulations at 1, 3 and 5 cm are partially attributed to the inability to specify simultaneous wetting and drainage as the initial conditions in Hydrus-2D. Notice in Fig. 2.6b that in 1.8-g most of the sample is following a drainage curve with exception of the lowest location (i.e. 1 cm). In the transition to μg, this scheme reverses and the bottommost location now appears to lose water, which results in drainage conditions at 1 cm and wetting conditions at 3 and 5 cm. Thus the modeled response at 1 cm more closely resembles the measurement because of a continuation of the initial drainage process (i.e. water moving upward). The modeled responses at 3 and 5 cm, however, transition to a wetting process immediately at the onset of μg, thus indicating that the simulation could improve if a variable gravity option were available.

While these limited simulations show reasonable agreement with the measurements, suggesting the applicability of Earth-based macroscopic transport models, they fail to describe a consistent bias toward a linear increase in measured matric potentials in μg. This bias appears to be a water content-dependent migration of the matric potential readings towards less negative potentials present in all three tensiometer readings, and is particularly perceptible at water contents of 0.63 and 0.56 (Fig. 2.6h-i). Changes in cabin pressure could contribute to this bias if some buffering of pressure changes were to occur within the porous medium. Discontinuous pockets of air could then absorb pressure changes, slowing the tensiometers response compared to the backside of the pressure transducer responding immediately to cabin pressure. Measurements in the 2 and 4-cm cells showed a similar bias, but at a much reduced amplitude ($<$2 mm), while this bias was not observed in measurements obtained with the 1-cm cell

2.5.5 Water Retention Characteristics in μg

Fig. 2.7 and 8 depict short-term (obtained at the end of the 20 s μg period) microgravity water retention characteristics for Profile, Mix and Turface obtained with the 1-, 2- and 4-cm retention cells. The 7-cm cell was not used because of difficulties in attaining equilibrium at lower water contents (Fig. 2.5) and the large differences in water content between top to bottom. Drainage and wetting data were obtained under quasi-steady state conditions at the end of the μg phase, where the distinction between drainage and wetting for μg conditions is solely based on the external addition or removal of water to the cell. As such, the classification does not consider the actual processes at the specific locations of potential measurement (i.e. drainage vs. wetting at the cell ends), and may be a poor image of the actual process.

In Fig. 2.7, we present water retention data obtained with the 1-cm cell. For the convenience of comparison, we also show the primary 1-g wetting and drainage retention curves (Fig.1). Parameterizations for Profile, Mix and Turface μg retention data of the van Genuchten (1980) model are given in Table 2.1. Wetting water retention data for Profile and Mix in Figs. 7a and b fell within the 95% confidence intervals of the primary wetting curves obtained at 1-g. For the drainage data, lower μg values were observed when compared with the 1-g primary drainage curve. For Turface wetting and drainage data in Fig. 2.7c, significantly reduced potentials were observed compared with the 1-g curves where all μg data fell below the 1-g primary wetting curve. This is contradictory to Turface wetting μg data measured in the 2-cm cell (Fig. 2.8a), which generally fell near the 1-g primary wetting curve. We partially attribute the observed decrease in μg potentials in the 1-cm cell to larger void spaces along the container wall, where the reduced response was likely enhanced by the larger particles sharing fewer contact points with the porous cup (i.e. Turface). For the measurements in the 2-cm cell, reduced μg drainage potentials compared with the 1-g curve were similar to the findings in Profile and Mix in Fig. 2.7. While μg wetting data found a lower bound near the 1-g primary wetting curve, the drainage data were not well described by, and fell below, the 1-g primary drainage curve. There are no drainage μg data that mimic the 1-g data, which suggests that either under these limited experimental conditions we cannot reproduce the 1-g curves, or the results are significantly different. While the dynamic and partially equilibrium limited measure-

ments contribute to the disparity, Steinberg and Poritz (2005) provide argument against the solitary contribution based on comparison of dynamic and static water retention in 1-g. They found more variation in dynamic measurements, especially in 1–2 mm Turface, but the measurements followed the static primary retention curves.

The observed disparities between the predicted 1-g curve and μg measurements are more likely to be attributed to the simultaneous wetting and drainage processes occurring spatially within different volume elements during microgravity (μg following 1.8-g). In a typical parabolic cycle, either we kept the cell water content constant or water was added or removed. Addition or removal of water occurred in the 1.8-g period and induced changes in water retention response as it transitioned between 1.8-g and μg . Water accumulated at the bottom of the cells during the 1.8-g phase would then move upward in response to the reduced gravitational force during μg . This would result in simultaneous drainage conditions in the lower part of the cell and wetting conditions in the upper part of the cell. For the addition of water in 1.8-g, wetting conditions dominate most volume elements in the cell. On the other hand, following the withdrawal of water in 1.8-g, most volume elements will be in a drainage mode at the end of the 1.8-g period, and potentially transition to a wetting mode in μg . Consequently, the measurements classified as drainage do not correspond well with the 1-g predicted primary drainage curve while the wetting data correspond much better in Fig. 2.7a,b and 8a. Measured temporal changes in the vertical distribution of matric potentials may indicate which process, (i.e. drainage or wetting) is occurring at a particular height in the cell. The measurements, however, do not uniquely indicate the water content or the movement of water, but rather track a response curve that may or may not involve water content changes.

Using localized rather than cell averaged water contents may then elucidate the water redistribution and water retention response. For this, TDR sensed water contents in Fig. 2.8b and c depict water retention curves for a 4 cm tall sample of Turface as a function of local water contents at elevations of z = 1 and 3 cm. Sensed water contents at these heights primarily reflected water content changes in response to the external addition and removal of water in the cell. The varying gravitational forces, however, did not appear to affect the water content readings. We observed a general lack of redistribution of water between the measurement heights, where the addition and removal of

water did not result in equal responses in the top and bottom location. The sensed water content at z=3 cm (top) varied significantly over the duration of the experiment, whereas the water content at z=1 cm (bottom) remained elevated. Minute changes in water content at the bottom location were sensed only at the lowest cell-average water content. We believe the reason for the apparent low sensitivity to gravity-induced redistribution of water is partially attributed to the averaging volume of the TDR probe, which is most heavily weighted around the rods (Robinson et al., 2003). More importantly, the TDR readings indicate an unanticipated lack of water redistribution between gravity force changes. The vertical heterogeneity in the water content distribution (Fig. 2.8b and c) is manifested in the measured water retention data for the bottom and top probe locations within the cell. These measurements show a wide distribution of water contents at comparable matric potentials in μg . This can be attributed to the energy state of water rapidly approaching a uniformly distributed quasi-static equilibrium with the dissipation of hydrostatic potentials, leaving no gradient to drive water movement (Fig. 2.4). The resulting water content distribution varies widely due to the narrow pore size distribution, hysteresis and to the hypergravity-induced distribution preceding μg . When transitioning to microgravity, the draining pores below and wetting pores above do not require significant changes in localized water content to reach sample-scale equilibrium potentials. In which case, upper and lower region water contents (i.e. referring to the vertical position in the cell) vary over the entire inter-aggregate water content range (compare Fig. 2.4) due to the relatively narrow pore-size distribution.

To further illustrate this argument, sensed water content and matric potential response data are shown in Fig. 2.9. The data represent matric potentials measured during two consecutive parabolas starting at 1.8-g, where consecutive readings of matric potential with time from two heights in the cell (z=1 and 3 cm) are plotted against TDR sensed water contents at these heights. For the two consecutive parabolas, it is evident that each data set (each at a different water content) experiences significant changes in matric potential that result in little movement of water based on TDR-determined water contents. The disparity in matric potentials between 1.8-g and μg is much greater at lower water contents and shows less disparity when water content is increased to near saturation. Note that water was pumped into the bottom of the cell during 1.8-g. Thus, the top and

bottom cell regions were not treated the same. Nevertheless, the measured response in the transition from 1.8-g to μg and back, traverses gravity induced alterations that are opposite in direction for the observations at the top and bottom locations. Notably, measured potentials in 1.8-g do not scale by a factor of 1.8 alone. For the bottom location, this can be explained by stating that the condition for scaling assumes a seepage face at the bottom boundary of the cell, yet in the experiment, water was not allowed to drain in 1.8-g. This resulted in more positive potentials than would be predicted under seepage conditions. For the top location, it is apparent that in 1.8-g more negative potentials are experienced than would be suggested by a 1.8-g force alone. We attribute this to local water content changes around the tensiometer cup that are not detected by the TDR sensors because of the disparity in their sampling volumes. The observed response in variable gravity indicates that matric potentials may fulfill quasi-steady state conditions involving minimal changes in water content that can be partially explained by hydrostatically scaling the measured response. Depending on the wetting and drainage history, sample volumes separated by only a few pore lengths can differ significantly in water content and direction of the wetting/drainage response that are more pronounced because of the repeated transition of 1.8-g to μg.

2.5.6   Saturated Hydraulic Conductivity

Hydraulic gradients were measured for prescribed fluxes through horizontally oriented saturated porous media columns. Several flux rates were used for each medium with measurements carried out continuously under the variable gravity conditions. Results are summarized in 2.10, where despite certain degree of measurement error, the experimental data plot within 1 standard deviation of the indicated lines of proportionality (i.e. indicating the mean saturated hydraulic conductivity). The results indicate that for the range of prescribed fluxes and porous media tested, the relationship between hydraulic gradient and flux can be described with a linear function (Buckingham-Darcy's law), corroborating the expected gravity-independence of saturated flow. In Heinse et al. (2005), we stressed that this independence was not observed when loose packing allowed changes in the arrangement of particles and pores during cycles of gravity. The coefficient of proportionality, the saturated hydraulic conductivity, for each medium is reported in Table 2.2, where the measured satu-

rated hydraulic conductivities for Profile and Turface were found to be comparable to measurements obtained by Steinberg and Poritz (2005).

2.6 Conclusions

In this study, we considered dynamic measurements of hydraulic properties in hysteretic porous media during parabolic-flight induced variable gravity, where the flight represents a challenging experimental environment in which acceleration frequently changes during the experiment. Consequently, the interpretation of parabolic flight data requires careful interpretation to account for the influence of dynamic accelerational forces, especially under unsaturated conditions. We developed a variety of cells to facilitate water retention and saturated hydraulic conductivity measurements, primarily for the microgravity portions of the flight. During dynamic measurements of water retention, we observed a transition of matric potentials during μg, where the non-linear response of the transition toward static equilibrium was a function of average water content with the transition slowing at decreased water contents. Transitioning from 1.8-g to μg and vice versa, matric potentials tracked secondary drainage or wetting curves simultaneously depending on the vertical position in the experimental cells. Minimal changes in water content fulfilled both the 1.8-g and the μg matric potential conditions, which resulted in significant spatial heterogeneity in the distribution of water contents maintained during variable gravity. The porous-media water retention characteristics were approximated for microgravity conditions from quasi-steady state conditions at the end of the μg phase. Despite the apparent influence of the hypergravity phase on dynamic water retention during μg, measurements suggested similar water retention characteristics in microgravity compared to 1-g for wetting conditions. Drainage water retention data generally fell below the 1-g measured data. This was attributed to the uncertain redistribution of water following the ensuing hypergravity phase. Long-term microgravity testing is recommended for more reliable and rigorous measurements of porous media water retention due to the prolonged steady state period and absence of dynamic constraints of the parabolic flight environment. The experiments and simulations described in this study present evidence of altered dynamics of liquid behavior in porous media, but seem to corroborate the applicability of the Buckingham-Darcy law and of the Richards

equation for describing macroscopic porous-medium fluid behavior under microgravity conditions with the gravity term approaching zero. Long-term microgravity questions remain, especially those regarding the fate of air-entrapment and its potential impact on fluid fluxes in porous media. Air entrapment alone could result in major differences in water retention, satiation and unsaturated hydraulic conductivity with enhancement of hysteretic behavior in sustained microgravity. Reduced gravity environments considering Lunar and Martian conditions add to the list of future research needs in anticipation of plant-growth facilities and porous media applications.

2.7 References

Auradou, H., K.J. Maloy, J. Schmittbuhl, A. Hansen, and D. Bideau. 1999. Competition between correlated buoyancy and uncorrelated capillary effects during drainage. Phys. Rev. E 60:7224-7234.

Bingham, G.E., I.G. Podolsky, T.S. Topham, and J.M. Mulholland. 2002. Lada: The ISS plant substrate microgravity testbed. SAE Technical Paper 2002-01-2388. SAE Int., Warrendale, PA.

Birovljev, A., L. Furuberg, J. Feder, T. Jssang, K.J. Mly, and A. Aharony. 1991. Gravity invasion percolation in two dimensions: Experiment and simulation. Physical Review Letters 67:584.

Blonquist, J.M., Jr., S.B. Jones, I. Lebron, and D.A. Robinson. 2006. Microstructural and phase configurational effects determining water content: Dielectric relationships of aggregated porous media. Water Resour. Res. 42. doi:10.1029/2005WR004418.

Buckingham, E. 1907. Studies on the movement of soil moisture Bull. 38. USDA, Bureau of Soils, Washington, DC.

Burtness, K., K. Norwood, T. Murdoch, and H.G. Levine. 2002. Development of a porous tube based plant growth apparatus. SAE Technical Paper 2002-01-2389. SAE Int., Warrendale, PA.

Childs, E.C., and N.C. George. 1948. Soil geometry and soil water equilibria. Discussions of the Faraday Society 3:78-85.

Dreschel, T.W., and J.C. Sager. 1989. Control of water and nutrients using a porous tube: A method for growing plants in space. HortScience 24:944-947.

Dreschel, T.W., C.S. Brown, W.C. Piastuch, C.R. Hinkle, and W.M. Knott. 1994. Porous Tube Plant Nutrient Delivery System development: a device for nutrient delivery in microgravity. Adv. Space Res. 14:47-51.

Heinse, R., S.B. Jones, S.D. Humphries, R.W. Mace, S.L. Steinberg, M. Tuller, R. Newman, and D. Or. 2005. Measurement of Porous Media Water Retention during Parabolic Flight Induced Microgravity. SAE Technical Paper 2005-01-2950. SAE Int., Warrendale, PA.

Hoehn, A., P. Scovazzo, J. Clawson, T. Geissinger, W. Kalinowski, and J. Pineau. 2003. Design, Testing and Operation of Porous Media for Dehumidification and Nutrient Delivery in Microgravity Plant Growth Systems. SAE Technical Paper 2003-01-2614. SAE Int., Warrendale, PA.

Hoehn, A., P. Scovazzo, L. Stodieck, J. Clawson, W. Kalinowski, A. Rakow, D. Simmons, A.G. Heyenga, and M.H. Kliss. 2000. Microgravity root zone hydration systems. SAE Technical Paper 2000-01-2510:1-10. SAE Int., Warrendale, PA.

Ivanova, T.N., and I.W. Dandolov. 1992. Moistening of the substrate in microgravity. Microgravity sci. technol. 3:151-155.Jones, S.B., and D. Or. 1998. Design of porous media for optimal gas and liquid fluxes to plant roots. Soil Sci. Soc. Am. J. 62:563-573.

Jones, S.B., and D. Or. 1999. Microgravity effects on water flow and distribution in unsaturated porous media: Analysis of flight experiments. Water Resour. Res. 35:929-942.

Levine, H.G., G.K. Tynes, and J.H. Norikane. 2003. Fluid Behavior Under Microgravity Conditions Within Plant Nutrient Delivery Systems: Parabolic Flight Investigations. SAE Technical Paper 2003-01-2483. SAE Int., Warrendale, PA.

Meheust, Y., G. Lovoll, K.J. Maloy, and J. Schmittbuhl. 2002. Interface scaling in a two-dimensional porous medium under combined viscous, gravity, and capillary effects. Phys. Rev. E 66:051603-1 - 051603-12.

Mohamed, A.-M.O., H.E. Antia, and R.G. Gosine. 2002. Water flow in unsaturated soils in microgravity environment. J. Geotech. Geoenviron. Eng. 128:814-823.

Monje, O., G. Stutte, and D. Chapman. 2005. Microgravity does not alter plant stand gas exchange of wheat at moderate light levels and saturating CO_2 concentration. Planta 222:336-345.

Morrow, R.C., and T.M. Crabb. 2000. Biomass production system (BPS) plant growth unit. Adv. Space Res. 26:289-298.

Morrow, R.C., R.J. Bula, T.W. Tibbitts, and W.R. Dinauer. 1992. A matrix-based porous tube water and nutrient delivery system. SAE Technical Paper 921390.

Morrow, R.C., W.R. Dinauer, R.J. Bula, and T.W. Tibbitts. 1993. The ASTROCULTURE-1 flight experiment: Pressure control of the WCSAR porous tube nutrient delivery system. SAE Technical Paper 932282. SAE Int., Warrendale, PA.

Morrow, R.C., R.J. Bula, T.W. Tibbitts, and W.R. Dinauer. 1994. The ASTROCULTURE flight experiment series, validating technologies for growing plants in space. Adv. Space Res. 14:29-37.

Mualem, Y. 1976. A new model for predicting the hydraulic conductivity of unsaturated porous media. Water Resour. Res. 12:513-522.

Nakajima, H., and A.T. Stadler. 2006. Centrifuge modeling of one-step outflow tests for unsaturated parameter estimations. Hydrology and Earth System Sciences Discussions 3:731-768.

Norikane, J.H., S.B. Jones, S.L. Steinberg, H.G. Levine, and D. Or. 2004. Porous media matric potential and water content measurements during parabolic flight. Habitation 10(2):117-26.

Or, D., S.B. Jones, M. Tuller, S. Steinberg, I. Alexander, N. Diadzic, L.N. Reddi, G. Kluitenberg, F.L. Ogden, and R. Heinse. 2004. Unsaturated flow in zero gravity—lessons and challenges. Agronomy Abstracts, ASA, Madison, WI.

Podolsky, I., and A. Mashinsky. 1994. Peculiarities of moisture transfer in capillary-porous soil substitutes during space flight. Adv. Space Res. 14:39-46.

Reddi, L.N., M. Xiao, and S.L. Steinberg. 2005. Discontinuous pore fluid distribution under microgravity—KC-135 flight investigations. Soil Sci. Soc. Am. J. 69:593-598.

Richards, L.A. 1931. Capillary conduction of liquids through porous mediums. Physics 1:318-333.

Scovazzo, P., T.H. Illangasekare, A. Hoehn, and P. Todd. 2001. Modeling of two-phase flow in membranes and porous media in microgravity as applied to plant irrigation in space. Water Resour. Res. 37:1231-1243.

Shah, S., W.E. Faller, A. Hoehn, M. Birdsong, and M.W. Luttges. 1993. Characterization of fluid distribution through a porous substrate under dynamic g conditions. Biomed. Sci. Instrum. 29:401-8.

Simunek, J., M. Sejna, and M.T.v. Genuchten. 1999. The HYDRUS-2D software package for simulating two-dimensional movement of water, heat, and multiple solutes in variably saturated media. Version 2.0, IGWMC - TPS - 53, International Ground Water Modeling Center, Colorado School of Mines, Golden.

Steinberg, S.L., and D.L. Henninger. 1997. Response of the water status of soybean to changes in soil water potentials controlled by the water pressure in microporous tubes. Plant Cell Environ. 20:1506-1516.

Steinberg, S.L., and D. Poritz. 2005. Measurement of Hydraulic Characteristics of Porous Media Used to Grow Plants in Microgravity. Soil Sci. Soc. Am. J. 69:301-310.

Steinberg, S.L., S.B. Jones, M. Xiao, L. Reddi, G. Kluitenberg, D. Or, J.I.D. Alexander, N. Daidzic, and M. Tuller. 2005. Challenges to understanding fluid behavior in plant growth media under microgravity. SAE Technical Paper 2005-01-2947. SAE Int., Warrendale, PA.

Stutte, G.W., O. Monje, G.D. Goins, and B.C. Tripathy. 2005. Microgravity effects on thylakoid, single leaf, and whole canopy photosynthesis of dwarf wheat. Planta 223:46-56.

van Genuchten, M.T. 1980. A closed-form equation for predicting the hydraulic conductivity of unsaturated soils. Soil Sci. Soc. Am. J. 44:892-898.

van Genuchten, M.T., F.J. Leij, and S.R. Yates. 1991. The RETC code for quantifying the hydraulic functions of unsaturated soils. U.S. Salinity Laboratory, USDA, ARS, Riverside, CA.

Table 2.1: Porous-medium hydraulic parameters for the van Genuchten (1980) water retention model. The prediction is based on measurements from the 1-cm cell.

Porous medium (size)		Drainage 1-g α cm^{-1}	n	$\theta_r^\dagger$ –cm^3 cm^{-3}–	θ_s –cm^3 cm^{-3}–	Microgravity α cm^{-1}	n	θ_r –cm^3 cm^{-3}–	θ_s –cm^3 cm^{-3}–
Turface (1–2 mm)		0.185	5.57	0.34	0.728	0.653	3.41	0.34	0.729
	lower*	0.181	5.08	0.34	0.717	0.608	2.98	0.34	0.719
	upper**	0.190	6.07	0.34	0.739	0.698	3.83	0.34	0.740
Mix (0.25–2 mm)		0.112	3.90	0.32	0.715	0.167	2.63	0.32	0.718
	lower	0.108	3.64	0.32	0.706	0.159	2.44	0.32	0.712
	upper	0.116	4.15	0.32	0.724	0.175	2.82	0.32	0.725
Profile (0.25–1 mm)		0.099	7.69	0.34	0.718	0.139	4.24	0.34	0.722
	lower	0.098	7.14	0.34	0.710	0.135	3.91	0.34	0.714
	upper	0.101	8.23	0.34	0.724	0.142	4.58	0.34	0.731

Porous medium (size)		Wetting 1-g α cm^{-1}	n	θ_r –cm^3 cm^{-3}–	θ_s –cm^3 cm^{-3}–	Microgravity α cm^{-1}	n	θ_r –cm^3 cm^{-3}–	θ_s –cm^3 cm^{-3}–
Turface (1–2 mm)		0.320	4.06	0.34	0.684	1.025	2.92	0.34	0.670
	lower	0.292	3.21	0.34	0.660	0.914	2.61	0.34	0.658
	upper	0.348	4.91	0.34	0.709	1.136	3.23	0.34	0.682
Mix (0.25–2 mm)		0.167	2.92	0.32	0.643	0.248	2.27	0.32	0.678
	lower	0.157	2.74	0.32	0.635	0.219	1.98	0.32	0.666
	upper	0.176	3.10	0.32	0.651	0.278	2.57	0.32	0.691
Profile (0.25–1 mm)		0.187	4.41	0.34	0.687	0.189	4.16	0.34	0.697
	lower	0.180	3.90	0.34	0.678	0.182	3.89	0.34	0.694
	upper	0.195	4.93	0.34	0.696	0.196	4.43	0.34	0.701

*, ** Lower and upper bounds of the 95% confidence interval, respectively.

† Residual water content (θ_r) was obtained from Blonquist et al. (2006) and kept invariable while fitting the saturated water content (θ_s) and the curve fitting parameters α and n in the van Genuchten model.

Table 2.2: Saturated hydraulic conductivity measured in variable gravity. In the case of multiple measurements at different bulk densities a range of conductivities is given.

Porous medium (size)	K_s cm s^{-1}
Turface (1–2 mm)	1.13
Profile (0.25–1 mm)	0.13–0.3
Glass beads (2.5–3.5 mm)	7.8
Glass beads (0.35–0.5 mm)	0.089
Glass beads (0.6–1 mm)	0.33
Glass beads (1–2 mm)	1.0–1.7
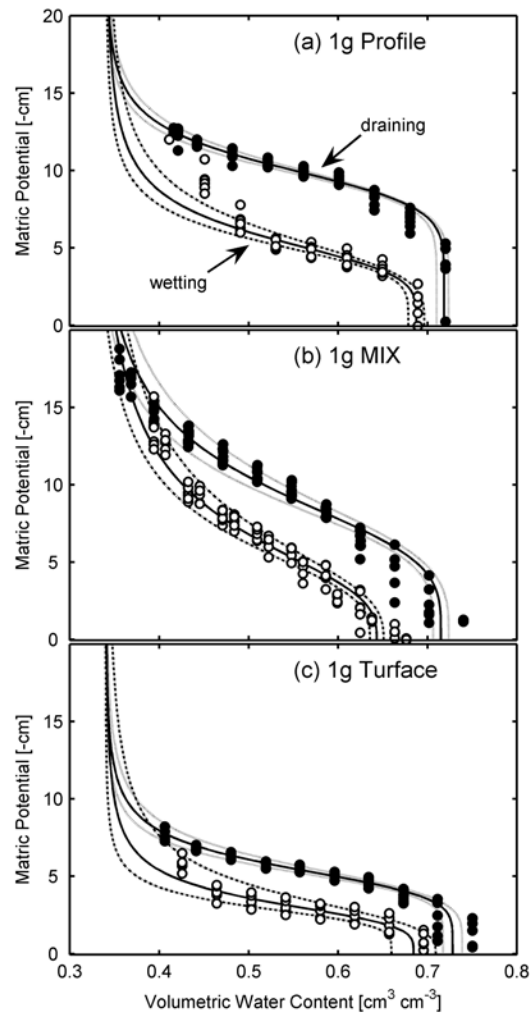
Fig. 2.1: Steady-state water retention curves measured in 1-g for (a) Profile (0.25–1 mm), (b) Mix (0.25–2 mm) and (c) Turface (1–2 mm). Solid lines represent the van Genuchten water retention model (Eq. [2.2]) fitted to six replicate measurements of drainage (●) and wetting (○) for processes within inter-aggregate pores. Dashed/dotted lines indicate the 95 percent confidence interval for the fitted retention curves.
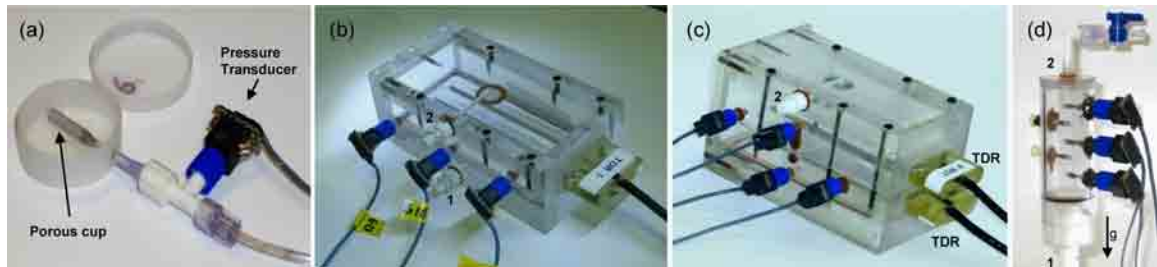
Fig. 2.2: (a) 1-cm water retention cell with pressure transducer connected to a porous cup embedded in and in hydraulic contact with the porous media. The porous cup was connected to a syringe pump that provided metered water addition and removal. (b) 2-cm water retention cell with (1) water inlet connected to sintered porous plate, (2) water outlet, pressure transducer ports, and centered time domain reflectometer (TDR) probe. (c) 4-cm water retention cell showing the vertical location of the two TDR probes. (d) 7-cm cell showing the pressure transducer positions and water inlet/outlet.
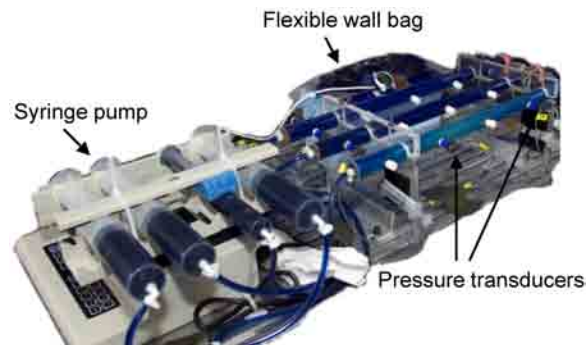
Fig. 2.3: Saturated hydraulic conductivity cells showing the pressure transducer locations. The water inlet was connected to a syringe pump for constant water fluxes using a bi-directional feed. The water outlet was connected to a collapsible reservoir.
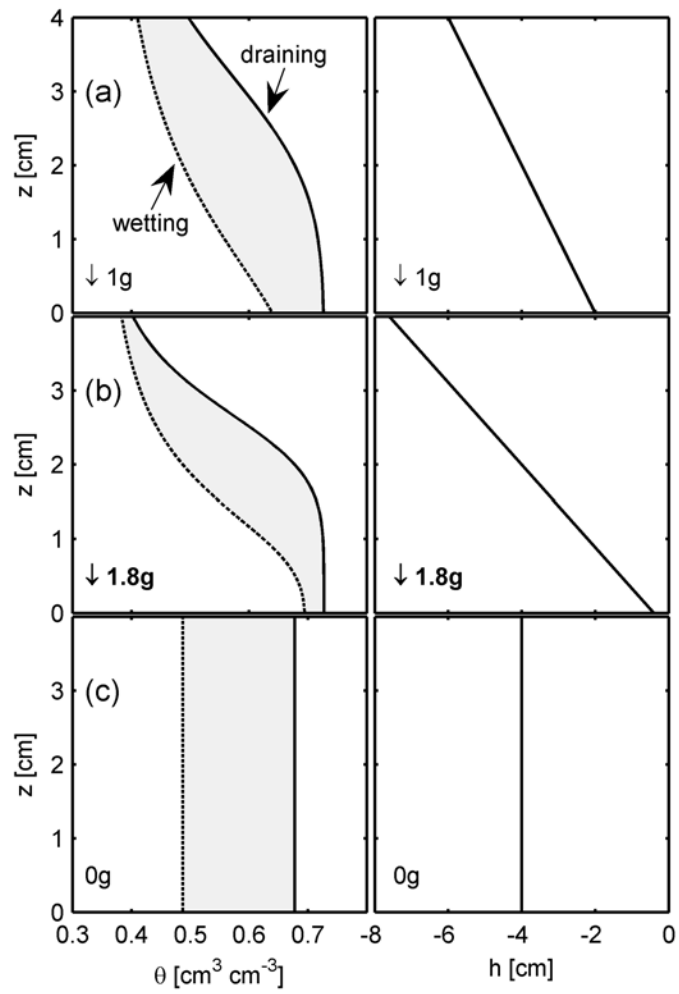
Fig. 2.4: Hypothetical diagram of the equilibrium distribution of water content and matric potentials in a 4 cm tall sample of Turface subjected to Earth's gravity (a), 1.8-g (b) and 0-g (c). The average matric potential (i.e. at the midpoint) is constant at -4 cm. The shaded area shows regions of validity for water content and potentials where the gravitational force scales the hydrostatic equilibrium distribution.
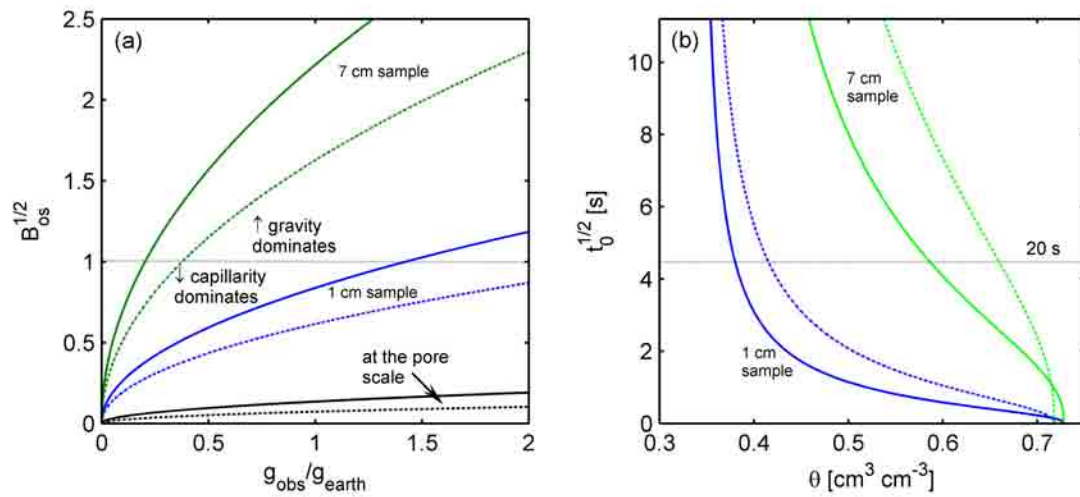
Fig. 2.5: (a) Dependence of static Bond numbers B_{os} on the normalized gravity force considering the pore scale and system/sample scale influence of gravity vs. capillarity. Solid lines are Turface and dashed lines are Profile. (b) Characteristic time scales for cell heights of 1 and 7 cm after Eq. [2.6], respectively.
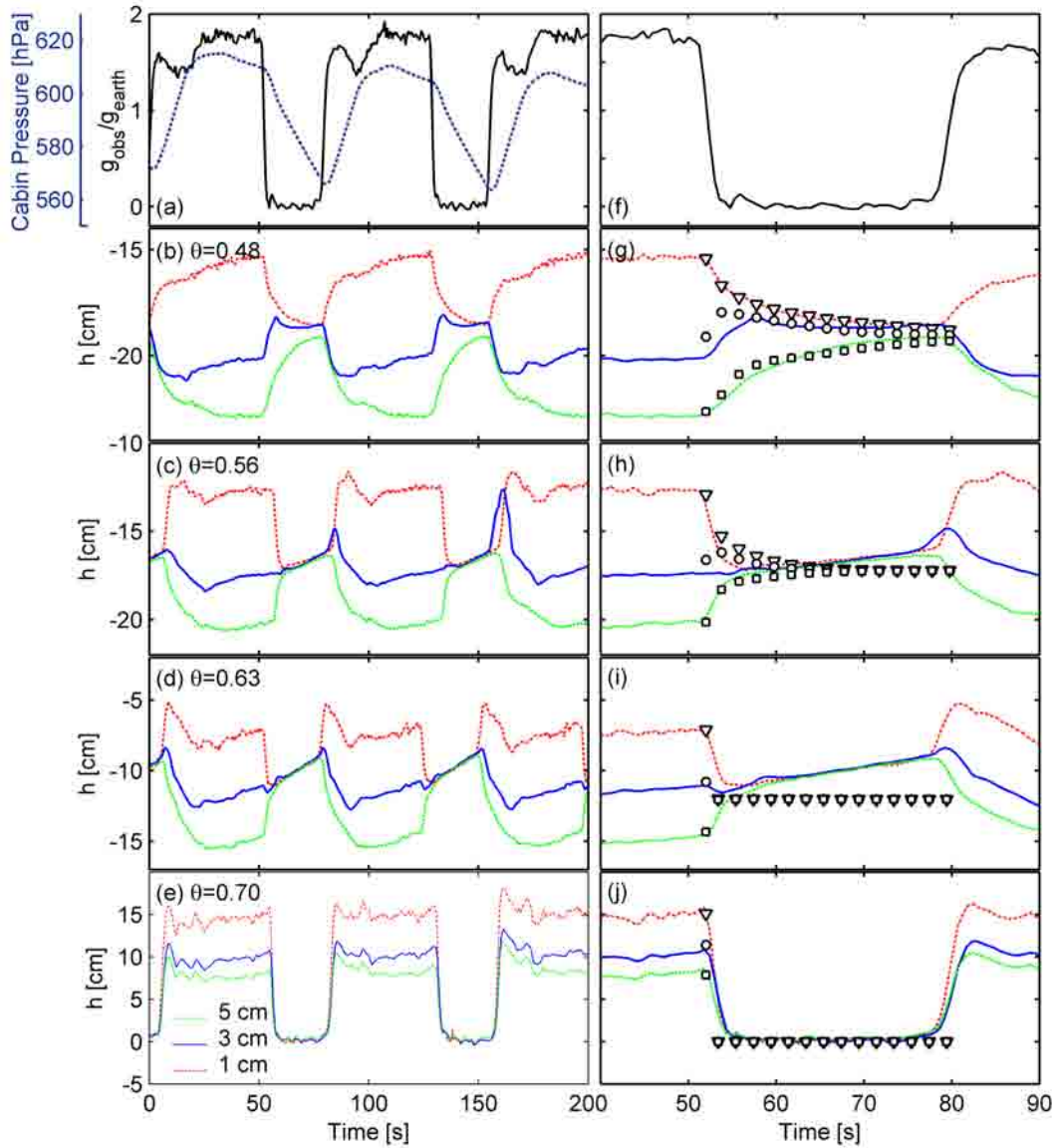
Fig. 2.6: Measured and modeled matric potentials as a response to variable gravity in the 7-cm cell for Profile. Figures on the left side (b—e) show measured matric potentials for three observation heights at z=1, 3 and 5 cm (Fig. 2.2) as a function of time for different water contents θ, where (a) depicts the gravitational acceleration and change in aircraft cabin pressure for plot (b). Figures on the right side compare measured (lines) and simulated (symbols) matric potentials in g following hypergravity (g-j). In (f), measured normalized gravitational accelerations are depicted for measurements shown in (g).
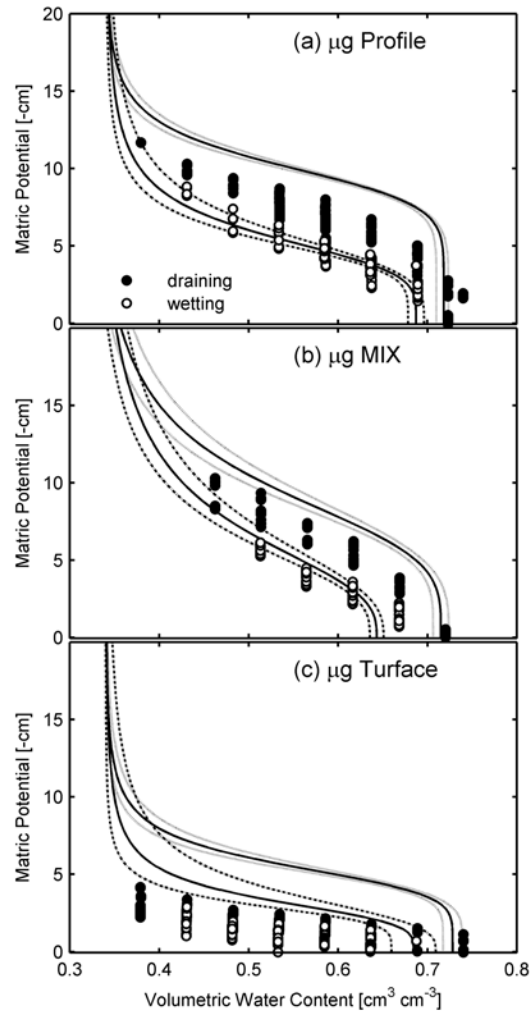
Fig. 2.7: Comparison of quasi-steady-state microgravity drainage and wetting water retention and steady-state 1-g porous-media water retention for Profile, Turface and a mixture of these obtained in the 1-cm cell. The solid lines are predicted 1-g retention curves (i.e. upper=drainage, lower=wetting). Dashed or dotted lines indicate the 95 percent confidence interval for the 1-g retention curves. Indicated water contents are shown as average sample values determined from pumping volumes. Matric potentials were measured at z=0.5 cm.
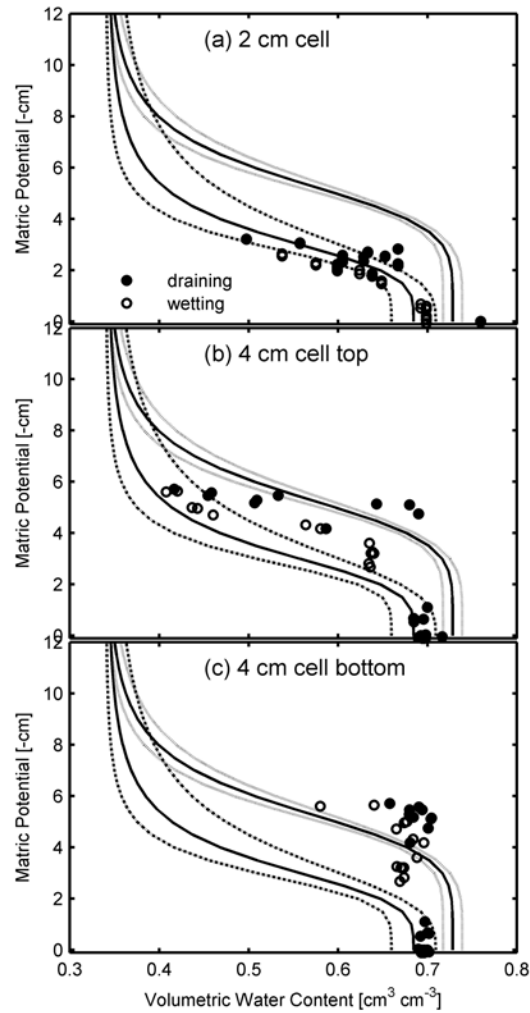
Fig. 2.8: Comparison of quasi-steady-state microgravity drainage and wetting water retention data with steady-state 1-g porous-media water retention curves for Turface. In (a) measurements in a 2 cm tall sample with water contents shown as average sample values determined from pumped volumes are shown. Matric potentials were measured at z=0.5 and 1 cm. Measurements utilizing a 4 cm tall sample with water contents shown as TDR measurements are depicted in (b) and (c), where water contents were measured at z=1 cm (bottom) and z=3 cm (top), respectively. The solid lines are predicted 1-g retention curves (i.e. upper=drainage, lower=wetting). Dashed or dotted lines indicate the 95 percent confidence interval for the 1-g retention curves.
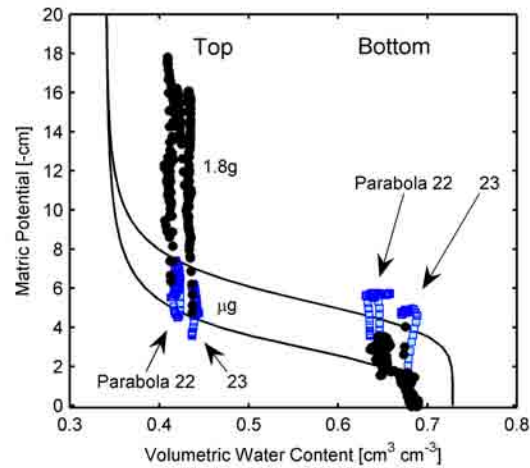
Fig. 2.9: Dynamic matric potential-water content response measured in Turface in the 4-cm cell during two consecutive parabolas at two vertical locations (z=1 and 3 cm, bottom and top, respectively). Five ml of water was added in the 1.8-g period in-between the parabolas with a syringe pump. Solid lines indicate the 1-g wetting and drainage water retention curves. Dotted lines indicate scaled water response curves for 1.8-g. Solid symbols (•) indicate 1.8-g, and open-faced symbols (○) indicate μg measured data.
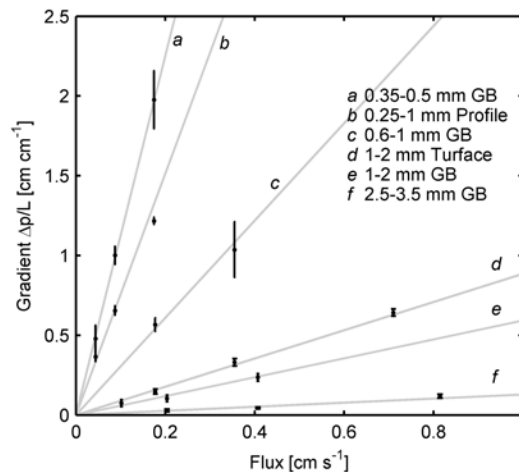
Fig. 2.10: Saturated-flow pressure gradients as a function of hydraulic flux for glass beads (GB), Profile and Turface measured in variable gravity. Error bars indicate the standard deviation, while solid lines denote the mean saturated hydraulic conductivity.

CHAPTER 3

MICROGRAVITY OXYGEN DIFFUSION AND WATER RETENTION MEASUREMENTS IN UNSATURATED POROUS MEDIA ABOARD THE ISS[1]

3.1 Abstract

The distribution of water controls directly or indirectly the management of water and air in particulate porous media. With the motivation to involve plants in future life-support systems in space, the question arises whether fluid behavior in porous media is altered when subjected to microgravitational accelerations ($\approx 10^{-6}$g$_{earth}$). While the consequences for fluid behavior at the sample scale have been observed in the form of hypoxia, the physical causes remain uncertain. The Optimization of Root Zone Substrates (ORZS) experiment was the first to directly measure porous-media water retention and oxygen diffusion parameters in prolonged microgravity. ORZS launched to the international space station on 12 May 2007, and the experiment was conducted from June to October 2007. Porous-ceramic aggregates tested included 1–2 mm Turface, 0.25–1 mm Profile and a 50:50 mixture of the two. Each medium had 3 replicates in a 9 cell array. The experiment used sealed dual-chamber diffusion cells controlled by an automated measurement system with water-content adjustment. Sensors measured matric potentials and water volumes in the media, along with oxygen concentrations in the two gas-filled chambers confining the medium. Effective oxygen-diffusion coefficients were determined from temporal oxygen-concentration measurements fitted to a Fickian-type relationship for the dual-chamber geometry. Ground-based determinations of matric potential and diffusion coefficients as a function of air-filled porosity were compared to microgravity data. Measured results pointed to enhanced hysteresis in oxygen-diffusion dependency on air-filled

---

porosity in microgravity. This indicated altered water-distribution patterns relative to earth-based measurements. Considering air invasion during drainage, we hypothesized that critical air-filled pathways form in microgravity at lower water contents due to the absence of hydrostatic force. The reason for the altered gas percolation threshold is not clear, but may have been affected by the diffusion-cell geometry boundary conditions, possibly leading to non-uniform water distributions not observed on earth. Water-retention parameters were not significantly different than Earth-based parameters, though gas diffusion parameters were significantly different for finer particle-sized media. The apparent reduction in the volume-averaged diffusive transport in microgravity will require adjustment in plant-growth system management protocols and model development for reliable response prediction of microgravity porous-medium systems.

3.2 Introduction

Predicting distribution and transport of fluids in porous media under microgravity (μg) conditions is vitally important for optimal design and management of plant-root-zone hydration systems for life support in space. Vigorous plant growth requires the favorable sustenance through fluxes of water, nutrients and gas exchanges by selection of an optimum (or least-restricting) root-zone substrate and maintenance of optimum water content. The challenge is to maximize the inversely related processes of gas and liquid transport (Jones and Or, 1998; Jones et al., 2005). If exposing root-zone substrates to reduced gravitational accelerations, the question arises if optimum conditions derived under terrestrial conditions are different. Indeed, plant research in microgravity has shown reduced biomass production compared to plants grown under terrestrial conditions using equal experimental systems and management protocols. There is consensus that plant physiological functions (cellular functions) are not primarily limiting (Ivanova et al., 2005; Monje et al., 2005; Musgrave et al., 2000), but that changes in the microgravity behavior of fluids impede that protocols established for successfully growing plants on Earth provide the same optimal physical environment for plants grown in reduced gravity. The discrepancy is mainly attributed to the significantly different distribution of water in microgravity (Ivanova et al., 2006; Steinberg et al., 2002). Difficulties in providing uniform substrate water contents in root modules and possibly resulting excessive irriga-

tion have consequently plagued many plant growth experiments in space. Low oxygen availability (hypoxia) in plants has been found to be symptomatic for these conditions as continuous gaseous pathways collapse (Bingham et al., 2000). For example, Porterfield et al. (2000) and Stout et al. (2001) have reported hypoxia in a variety of plants grown in different space greenhouses. Hypoxia is not the sole negative effect of reduced gas exchange rates, but plants rely on the removal of metabolic gases like carbon dioxide and ethylene (Veselova et al., 2003) through continuous air-filled pathways in unsaturated porous media, where gas diffusion is the primary transport process. The distribution and amount of water in porous media then impact the quantity and tortuosity of these continuous pathways, as gas diffusion in the water phase is roughly four to five orders of magnitude slower than in the gas phase; effectively providing a barrier for gaseous diffusion.

The problem is further complicated in the currently favored particulate plant-growth substrates with millimeter sized particles (Steinberg and Poritz, 2005) that show a rapid reduction in air-filled porosity (total porosity minus water content) within a narrow range of matric potentials; emphasizing the need to most accurately describe porous media fundamental processes like water retention and oxygen diffusion to manage the root-zone environment and avoid hypoxic conditions. Past studies have provided evidence of altered water behavior in porous media in microgravity, starting with the seminal work by Podolsky and Mashinsky (1994), who showed differences in water content distributions measured in μg aboard the MIR space station and measurements on Earth. Their observations pointed to enhanced capillary transport and the promotion of phase entrapment in reduced gravity. Jones and Or (1999) used a numerical model based on the Richards (1931) equation to simulate zero gravity conditions and concluded that narrower pore size distributions and reduced participation of larger pore sizes to water retention characteristics attributed to differences in experimental measurements from the space station MIR and the space shuttle to measurements conducted on Earth. Results in Chapter 2 suggested that the significant impact of reduced gravity is not on the water retention characteristic, but on the distribution of water in porous media. The authors used variable gravity testing during parabolic flight and concluded that the hysteretic nature of the soil water characteristic (SWC) determined the heterogeneous distribution of water based on the local history of wetting and draining processes. The impact of such possible alterations in water

distributions were studied by Chau et al. (2005). The authors predicted that relative diffusion coefficients may be reduced by up to 25 percent in zero gravity based on lattice Boltzmann simulations. However, no experiment has directly measured water retention or oxygen diffusion in long-term microgravity.

The only attempts to measure oxygen concentrations directly in space have been in-situ oxygen measurements conducted by Porterfield et al. (1997) that suggested sharp gradients in the root microenvironment. The authors observed signs of hypoxia in the plants grown while the bulk oxygen concentration in the agar growth medium was elevated, compared to 1g measurements. The difference was attributed to impaired oxygen resupply to the roots. In a follow-up experiment, Liao et al. (2004) measured oxygen uptake at the root scale in parabolic flight, where the oxygen bioavailability decreased in phase with the microgravity portion of the flight. However, the results were inconclusive. A large part of the problem stems from the fact that root-zone environment measurements that involve gas diffusion through partially wet substrates require longer periods of microgravity exposure than can be acquired by parabolic flights or drop towers.

The Optimization of Root Zone Substrates (ORZS) experiment was the first to measure gas diffusion and water retention in plant-growth substrates at varying water contents in sustained microgravity. ORZS is a successful continuation of space greenhouse experiments starting with the Bulgarian built SVET experiment that first flew on the space station MIR in 1990 (Ivanova et al., 1993). With the addition of the Gas Exchange Measurement System (GEMS) to the SVET greenhouse, measurement of physical plant growth parameters, including the root zone environment, were introduced (Ivanova et al., 1998). For example, GEMS measured soil water contents and air composition. With the advent of the International Space Station (ISS), the gained knowledge from the SVET and GEMS greenhouse perpetuated in a new space greenhouse called Lada (Bingham et al., 2002). Lada aims at advancing substrate management physics, plant production and cosmonaut-plant psychological benefits. Lada also provided the control module for the ORZS experiment. ORZS conducted side-by-side gas exchange and substrate water controllability measurements in μg, comparing triplicate samples of three aggregated porous media likely to be used in future NASA space greenhouses. The hardware was launched to the International Space Station (ISS) on May 12,

2007. The experiment began July 6 and ended October 9, 2007.

Our primary objectives were to investigate the effect of sustained reduced gravity on the diffusivity of oxygen in unsaturated porous plant-growth media and on the water retention and water configuration within the media. We (i) characterized oxygen diffusivity and water retention characteristics as a function of air-filled porosity under terrestrial- and microgravity conditions, (ii) provided predictive capabilities for diffusive transport in microgravity and (iii) described the impact of altered water distribution on oxygen diffusion pathways.

3.3   Theory

3.3.1   Gaseous Diffusion

The major mechanism for gas transport in porous media in the absence of convective forces is by diffusion in the gaseous and liquid phase, where the mean square displacement Δx of the diffusing gas molecules increases in proportion to the observation time t. The diffusivity D may then be introduced by the Einstein relation:

$$(\Delta x)^2 = 2Dt \tag{3.1}$$

In the case of normal diffusion in the bulk (sample) phase, the definition of D in Eq. [3.1] is equivalent to Fick's first law which correlates the diffusion flux-density $\vec{j}$ with the concentration gradient of the diffusant $\left(\dfrac{\partial c}{\partial x}\right)$, yielding the diffusivity D as the factor of proportionality:

$$\vec{j} = -D\frac{\partial c}{\partial x} \tag{3.2}$$

Because the diffusivity of oxygen in the water phase is roughly four orders of magnitude smaller then in free air, the transport in the liquid phase is often neglected, enabling simpler treatment of the theory. Using the equation of continuity, $\nabla \cdot \vec{j} = -\dfrac{\partial c}{\partial t}$, one arrives at the diffusion equation in one dimension (Fick's second law), assuming a constant D:

$$\frac{\partial c}{\partial t} = D\frac{\partial^2 c}{\partial x^2} \tag{3.3}$$

A solution to this partial differential equation for an initial concentration at the origin takes the form:

$$c(x,t) = const. \cdot \frac{1}{\sqrt{t}}e^{-\frac{x^2}{4Dt}} \tag{3.4}$$

The solution indicates that a perturbation will propagate as $\frac{1}{\sqrt{t}}$ with a decay proportional to the mean square displacement and inversely proportional to $4Dt$. The diffusivity may then be obtained from either measurements of $c(x,t)$ or measurements of the mean square displacement for long enough times using Eq.[3.4].

Estimation of Diffusivity Using a Dual-Chamber Device

Analytical solutions to Eq. [3.3] and [3.4] to determine the diffusivity using a dual chamber geometry monitoring the temporal change in diffusant concentrations in two cylindrical gas chambers sealed to the ends of a sample holder have been derived by Glauz and Rolston (1989) and are given in terms of the relative chamber dimensions by Rolston and Moldrup (2002). The temporal change in concentration $c(t)$ of a gas tracer is observed following the initializing establishment of a reduced concentration c_0 in the sink chamber, and can be described using:

$$c(t) = \left[\frac{1}{1 + \frac{1}{\gamma} + \frac{2}{\beta}} - \frac{A}{B}e^{-\alpha^2\tau}\right] - c_o + k \tag{3.5}$$

where $\tilde{t}$ describes the dimensionless characteristic time:

$$\tilde{t} = \frac{Dt}{L^2\varepsilon} \tag{3.6}$$

with the physical length of the substrate chamber L. γ and β define the dimensionless chamber geometries:

$$\gamma = \frac{H}{K}, \beta = \frac{H}{L\varepsilon} \tag{3.7}$$

where *H* and *K* describe the physical lengths of the source and sink chamber. The additional parameter *k* Eq. [3.5] not found in Glauz and Rolston (1989) was added to describe the effect of finite priming durations. The parameters *A*, *B* and α are given as:

$$\alpha = \sqrt{\frac{1}{2\beta}(1+\gamma) - \frac{1}{3\beta^2}(\gamma^2 - \gamma + 1) + \frac{2}{45\beta^3}(4\gamma^3 - 3\gamma^2 - 3\gamma + 4)} \tag{3.8}$$

$$A = \sqrt{\alpha^4 + \frac{\gamma^2}{\beta^4} + (1+\gamma^2)\left(\frac{\alpha}{\beta}\right)^2} \tag{3.9}$$

$$B = \alpha^4 \frac{\beta}{\gamma} + \alpha^2 \left(\frac{1}{\gamma\beta} + \frac{\gamma}{\beta} + \frac{1}{2\gamma} + \frac{1}{2}\right) + \frac{\gamma}{\beta^2} + \frac{\gamma}{2\beta^2} + \frac{1}{2\beta^2} \tag{3.10}$$

and for monitoring concentrations in the sink chamber, Eq. [3.9] is replaced by:

$$A = -\frac{\gamma}{\beta^2} - \frac{\alpha^2}{\gamma} \tag{3.11}$$

D may then be determined by fitting Eq. [3.5] to temporal observations of concentrations.

Effective Gaseous-Diffusion Coefficient in Variably-Saturated Porous Media

In porous media, the diffusivity introduced in Eq. [3.1] is understood as an effective diffusivity in the soil air phase in the presence of non-diffusive phases (i.e., solids and water). Commonly, a porous media factor ω (≤ 1) is introduced that relates the effective diffusivity D_s to the diffusivity in free air D_0 scaled by the availability and geometry of continuous air-filled pathways:

$$D_s = \omega D_0 \tag{3.12}$$

ω may be conceived as a separable contribution that includes the reduction in cross-sectional area given by the air-filled porosity ε (total porosity minus water content), the tortuosity of the pore space in the absence of water τ_p, and the increased tortuosity due to the partial saturation of the pore space τ_θ:

$$\omega = \varepsilon \tau_p \tau_\theta \tag{3.13}$$

The effective tortuosity τ_{eff} may then be estimated following Moldrup et al. (2001):

$$\tau_{eff} = \left(\frac{\varepsilon D_0}{D_s} \right)^{1/2} \tag{3.14}$$

and the effective pore connectivity may be estimated as:

$$\chi = \frac{D_s}{\varepsilon D_0} \tag{3.15}$$

Several empirical relationships utilizing parameterizations of the physical properties of the air-filled pore space have previously been applied successfully to predict D_s as a function of air-filled porosity. Because of the variability of pore structures, these are often soil-specific relationships, requiring an appropriate choice of model and fitting parameters. The majority of these relationships can be grouped under the following curvilinear format:

$$\frac{D_s}{D_0} = \omega = a\varepsilon\varepsilon^\delta \left(\frac{\varepsilon}{\phi} \right) \tag{3.16}$$

in which ϕ denotes the total, or macropore porosity. The factor a describes the diffusivity at the driest point, i.e., when $\varepsilon = \phi$. The exponent δ is a fitting parameter that describes the tortuosity of the pore space. The term $\frac{\varepsilon}{\phi}$ introduced by Moldrup et al. (2004), coined the water-induced linear reduction term, describes the additional tortuosity due to the presence of water in the pore space. A summary of relationships between D_s and ε is given in Table 3.1. Examples of these models are plotted in Fig. 3.1.

3.3.2   Gaseous Diffusion and Water Retention

Because the spatial distribution of water in the sample and the pore-size distribution affect the effective diffusivity of gases, a close relationship between $D_s(\varepsilon)$ and the water retention function is expected. For example, Moldrup et al. (2003) found similarity between the shape of the water retention and gas diffusivity curve when plotted against water content. The shape of the water retention function may be described in terms of the volumetric water content or water-filled porosity

$\theta = \phi - \varepsilon$ as a function of matric potential h (van Genuchten, 1980):

$$\Theta(h) = \frac{\theta - \theta_r}{\theta_s - \theta_r} = \begin{cases} [1 + (\alpha|h|)^n]^{-m} & \text{for} \quad h < 0 \\ 1 & \text{for} \quad h \geq 0 \end{cases} \tag{3.17}$$

where α, n and m are empirical fitting parameters, where we use the following simplification: $m = 1 - \frac{1}{n}$. Inclusion of water retention information, primarily at residual water contents, in estimating $D(\varepsilon)$ was found to provide more accurate estimates than models based on air-filled porosity alone (Moldrup et al., 2004). In a separate study, Caron and Nkongolo (2004) used water retention information in a simple scheme to estimate diffusivities in peat substrates. While no general transformation of water retention and gas diffusivity has been derived so far, these studies illustrate the considerable opportunities and benefits of measuring both in concert.

3.4 Materials and Methods

3.4.1 Porous Media

The porous media used in this study were porous ceramic aggregates (Profile Products, Buffalo Grove, IL) sieved to particle size fractions of 0.25–1 mm (Profile), 1–2 mm (Turface) and a mixture (50:50 by weight) of the two (Mix). The particle density of the aggregates is 2.5 g cm^{-3}. These porous ceramic aggregates have been widely used in microgravity plant experiments (Levine et al., 2003; Steinberg and Henninger, 1997; Stutte et al., 2005) and are expected to be used in future life support applications. The aggregates are stable, have moderate surface area for nutrient storage and exhibit two distinct pore spaces, inter-aggregate and intra-aggregate pores. Only the inter-aggregate pore retention characteristics, particularly in the optimal range for liquid and gas supply of 0 to -25 cm$_{H_2O}$ (1 cm$_{H_2O}$ = 97.96 Pa) matric potential, are of interest for this study. Terrestrial (1g) porous-media water retention characteristics for Profile, Turface and Mix have been parameterized in Chapter 2 and by Steinberg and Poritz (2005).

Packing and Prevention of Particle Rearrangement

Rearrangement of particles during launch to the International Space Station (i.e., vibration and increased g-force) and exposure to microgravity can result in changes in water retention (Xiao et al., 2008) and fluid pathways (Reddi et al., 2005) within the samples. These changes are difficult to predict and pose a separate effect to the targeted microgravity impacts on fluid distribution and transport not pursued in this paper. To prevent the rearrangement of particles and to ensure uniformity in the porous media samples, we used the following procedure: Oven-dry media was poured slowly (25 cm^3 min^{-1}) into the experimental cells, which were shaken on a vibration table. Packing under vibration was shown by Steinberg et al. (2005) to produce the highest packing density in Profile and Turface. The authors further showed that the presence of porous tubes and protruding sensors had only minor effects on the density. Vibration was stopped at the approximate fill level. The remaining porous media was then poured and compacted under tamping before pressing on porous screens that closed off the substrate chamber. The resulting packing densities are listed in Table 3.2.

3.4.2 Experimental Designs and Procedures

Gravity-Considerations on the Geometrical Cell Designs

Measurements were conducted with two separate experimental cell designs whose differences were in the container geometry and water supply strategy. The separation was necessary to minimize the vertical extent, and henceforth the hydrostatic vertical water-content distribution, of the sample in 1g for comparable test conditions to μg. In 1g, the horizontal (i.e., perpendicular to the gravity field) effective diffusion coefficient is an integral value resulting from stratified diffusion paths in parallel, where the gravity-induced water content distribution with the wettest stratum at the bottom and the driest stratum on top, control the diffusion coefficient (i.e., diffusion 'highway' in the driest stratum). Therefore, the Flat cells (Fig. 3.2a), used for experiments in 1g are rectangular in shape, exhibiting a vertical extent of 1.9 cm with water management and control through a sintered porous plate at the bottom of the cells. The Round cells (Fig. 3.2b) developed for the experiment in μg are cylindrical (5.08 cm i.d.), with a centered stainless-steel porous tube (0.4 cm o.d.) allowing axi-symmetrical management and control of water in μg. For both designs, nine cells were

combined into a unit capable of running independent diffusion and water retention experiments, allowing measurements in triplicate samples of Turface, Profile and Mix. The experiments were fully automated using the Lada control module on the ISS (Bingham et al., 2002), and required minimal cosmonaut intervention. For the detailed design and operation of the diffusion cells, we refer the reader to Jones et al. (2002; 2003a; 2003b); here we give a brief description of the measurement apparatus and conduction of the experiment.

Oxygen Diffusion and Water Retention Measurements

The experimental cells were sealed dual-chamber diffusion devices, designed following the theory of Glauz and Rolston (1989). Here we describe the Round cell illustrated in Fig. 3.2b; the general design and operation, however, applies to the Flat cell as well. The cell consists of three chambers separated at their interfaces with hydrophobic mesh screens. The center chamber was filled with the porous medium, while the two outer chambers were gas filled. Prior to the experiment, the substrate and gas chambers were purged with Nitrogen. The source chamber was then briefly (60 s at a flow rate of $3 \, \mathrm{l \, min^{-1}}$) flushed to reach atmospheric (cabin) conditions ($\approx 20 \, \%$ O_2). After hermetically sealing the cell, oxygen sensors in both gas chambers recorded the temporal changes in oxygen concentrations as gases diffused through the substrate in response to the O_2 concentration gradient. The closed system was then allowed to reach equilibrium. The effective diffusion coefficient D_s was determined using the observed temporal concentration by means of a non-linear least squares fit with the Levenberg-Marquardt optimization method to optimize Eq. [3.5], while adjusting c_0, D_s and k. Fitting was implemented with the "lsqcurvefit" function in the Matlab Optimization Toolbox version 3.0.2 (Mathworks Inc., Natick, MA).

Effective oxygen diffusivities were determined at eleven fixed sample pore-water volumes (i.e. water-content steps) in a multi-step in- and out-flow cycle. Bulk water content in the porous media was controlled and metered via a precision peristaltic pump capable of injecting and removing water through a stainless-steel porous membrane extending the entire length of the porous-media chamber. Fixed amounts of water were injected/removed, subject to pressure regulation to prevent bubbling of the membrane and avoid over-pressurization of the tensiometer. The water regulation was based

on measurements of a differential pressure-transducer tensiometer in line (i.e., measuring tube pressure) with the porous membrane using the membrane as the interface to the medium. Water contents were referenced to the residual water content at desaturation of the macropores (θ_r=0.37 cm^3 cm^{-3}) established prior to the experiment after initial cosmonaut priming (Fig. 3.3) of the air-dry porous media and computer-controlled wetting and draining cycle ending at approximately -30 cm of suction. The in-line tensiometers provided measurements of the bulk porous-media suction in-between pumping events. Another pressure-transducer tensiometer was located at the outside of the cell and connected to the substrate through a porous cup embedded in the outside wall. Water content in the porous media was further sensed with a single-probe heat-pulse sensor that was shown to be comparably accurate to dual-heat pulse-probe sensors, using a porous-media specific calibration (Heinse et al., 2006). However, the remainder of this paper uses metered water volumes as the measure of volumetric water content because of the higher measurement accuracy.

Control of Microbial Respiration

The use of oxygen as a tracer gas can be a disadvantage where microbial respiration can affect the estimation of diffusivity by reducing the concentration of oxygen in the porous-media sample, thus leading to over-prediction of the diffusivity. Jones et al. (2003b) established maximal respiration rates of up to 1 percent per day in Turface with the addition of a sucrose food source. Due to the short period required to estimate D_s (1 to 100 hours), and because respiration is limited at low diffusivities (i.e., at large characteristic time scales with low concentration gradients), the error is likely to be insignificant. Schjønning et al. (1999) estimated the potential error for agricultural soils to be less than 0.5 percent. Microbial respiration, if observable, is perceptible as a decrease in oxygen concentrations in both the source and sink chamber after an equilibrium concentration is reached. To limit microbial respiration, porous media samples were autoclaved at 121°C at 1.1 atm for 1 h before oven drying at 105°C. Experimental cells were wiped out with isopropyl alcohol (91 vol%). Tubing and porous membranes were flushed with a diluted (10 vol%) all-purpose cleaner solution (Mr. Clean, Procter & Gamble, Cincinnati, OH) and treated with a mix (17:3 by volume) of isopropyl alcohol (91 vol%) and a wetting agent (5 wt%, TWEEN 20). For the experiments, the introduction

and growth of microbes with the water was controlled using a 0.2 mg l^{-1} silver-nitrate biocide used in the Russian water system on the International Space Station (US National Research Council, 2000). Terrestrial measurements used de-ionized water processed with the silver-nitrate biocide.

3.4.3   Statistical Analysis

Model Fitting

Following Moldrup et al. (2000), three statistical measures were used to evaluate and compare the predictive gas diffusivity models. To evaluate prediction uncertainty, the root mean square error of the prediction was used:

$$RMSE = \left(\frac{1}{n} \sum_{i=1}^{n} e_i^2 \right)^{1/2} \tag{3.18}$$

where e_i is the residual between estimated and predicted values of D_s at a given air-filled porosity, and n is the number of observations in the data set. The bias was used to evaluate model over- (positive) or under-prediction (negative) of estimated $D_s(\varepsilon)$ values:

$$bias = \frac{1}{n} \sum_{i=1}^{n} e_i^2 \tag{3.19}$$

Analysis of Variance

Analysis of variance was used to comparatively evaluate the effect of gravity and cell design on oxygen diffusivities and water-retention characteristics using SAS statistical package software version 9.2 (SAS Inst. Inc., Gary, NC). For this, we singled out the SAPHIR model (Table 3.1) based on fitting results presented in Tables 3.3 and 3.4 discussed in section 3.6.1. Model fits to the oxygen diffusion/air-filled porosity observation were conducted using the MIXED Procedure. Prior to analysis of variance, data were transformed using a Box-Cox procedure (Box and Cox, 1964) to ensure homoscedasticity and normality of the log-normally distributed residuals e_{ijkm}, where the subscript m indexes the several observations in the wetting and draining sequences indexed by k within each combination of system (i.e., Flat, Round and ISS) indexed by i, and medium indexed by j. The linearized SAPHIR-like model in the analysis of variance followed as:

$$\log(D_{sdrv}) = \delta_{ijk} + \xi_{ijk} + e_{ijkm} \tag{3.20}$$

with an overall mean term μ and the following defined variables describing the observations and constants:

$$D_{sdrv} = \frac{\log D_s - \log D_0}{\log \varepsilon} - 1 \tag{3.21}$$

The mean effects regression coefficients δ_{ijk} and ξ_{ijk} are decomposed as:

$$\delta_{ijk} = \mu + \alpha_i + \beta_j + \gamma_k + (\alpha\beta)_{ij} + (\alpha\gamma)_{ik} + (\beta\gamma)_{jk} + (\alpha\beta\gamma)_{ijk} \tag{3.22}$$

and

$$\xi_{ijk} = \nu + \lambda_i + \rho_j + \tau_k + (\lambda\rho)_{ij} + (\lambda\tau)_{ik} + (\rho\tau)_{jk} + (\lambda\rho\tau)_{ijk} \tag{3.23}$$

Reverting the linear model back to the original response changes the relationship from additive in the exponent to multiplicative because of the log-normal distribution as follows:

$$D_s = D_0 \varepsilon^{e^{\delta_{ijk}\xi_{ijk}(\phi-\varepsilon)}} \tag{3.24}$$

To conduct the nonlinear regression for the analysis of the water retention observations, we used the NLMIXED Procedure. Procedure NLMIXED fits nonlinear mixed models by maximizing an approximation to the likelihood integrated over the random effects using the adaptive Gaussian quadrature for the integral approximations. We used the dual quasi-Newton algorithm to carry out the optimization.

3.5   Results

In the following, effective oxygen diffusivities as a function of air-filled porosities obtained in the three experimental systems (Flat 1g, Round 1g and ISS μg) for each of the three media (Turface, Profile and Mix) and opposing processes (wetting and draining) are compared. In the discussion, we detail on the performance of predictive models for the aggregated porous media and use them to statistically compare 1g to μg observations. In addition, we elaborate on the obtained water retention

characteristics at 1g and μg and discuss differences in the water distributions.

Average values for the porous-media packing densities and macropore porosities are given in Table 3.3. Reported porosities are reflections of an assumed microporosity of $0.37\ cm^3\ cm^{-3}$. While Round and ISS packing densities in the identical experimental cells agree well, packing densities in the Flat cells are slightly higher for Turface and lower for Profile and Mix, where packings of Turface in the Flat cell show the highest variability.

3.5.1 Terrestrial Estimates of $D_s(\varepsilon)$

Fig. 3.4(a–f) shows obtained effective oxygen diffusivities in the Flat and Round cells at 1g as a function of air-filled porosities. Diffusivities were estimated by fitting Eq. [3.5] with air-filled porosities obtained from bulk water volumes representing average air-filled porosities. Porosities of the media were estimated based on the mass of the packed media with the given particle density and cell volumes. The diffusivity in the air phase D_0 was taken as $11.4\ cm^2\ min^{-1}$. Input parameters for the cell geometries were taken from Jones et al. (2003b). Note that the two data sets (Flat and Round cell measurements) were obtained under different boundary conditions (i.e., cell geometry and water supply).

The diffusivity data in all media and systems suggest a near-linear increase in oxygen diffusivities with air-filled porosity. As expected, wetting diffusivities were higher at a given air-filled porosity compared to draining conditions. However, this hysteretic behavior was not very pronounced with exception of diffusivities in Profile obtained in the Flat cell. Here the draining diffusivities at intermediate air-filled porosities deviated visually from the wetting diffusivities. This behavior was not observed for the same medium in the Round cell. At a given air-filled porosity, the larger particle-sized Turface showed the highest diffusivity compared to Profile and Mix, which showed comparable diffusivities. While observations in Mix reached diffusivities close to zero at the lowest observed air-filled porosities ($\approx$0.08 $m^3\ cm^{-3}$), quasi-zero diffusivities were also attained for Profile in the Round cell, but not in the Flat cell. Observations in Turface for both the Flat and Round cells did not reach zero diffusivities at the lowest air-filled porosities, but retained a diffusivity of about 0.5 $cm^2\ min^{-1}$.

3.5.2 Microgravity Estimates of $D_s(\varepsilon)$

Fig. 3.4(g–i) shows obtained effective oxygen diffusivities on the ISS at μg as a function of air-filled porosities. For the measurements in microgravity, an incomplete data-set was collected due to premature termination of the experimen. This premature end of the experiment prevented us from collecting a complete data set where the missing measurements at steps 10 and 11 represent the dry end of the draining cycle. The complete experiment was also scheduled to repeat itself, but mechanical failure prevented this.

Wetting effective diffusivities at μg are visually in good agreement with data obtained at 1g. Draining data for Turface also appear to agree well with the 1g observations. The profound difference between the gravity regimes, however, is found for draining data in Profile, and to some extent in Mix, where a deviation is noted from the 1g observations in the draining cycle. With increasing air-filled porosities, diffusivities are increasing at a much slower rate than at 1g, suggesting that the air-filled connectivity in the draining process at equal air-filled porosities is reduced compared to 1g. This enhanced hysteresis in the diffusivity-air-filled porosity behavior is fundamentally different from the observations at 1g that exhibited less hysteretic behavior.

3.5.3 Model Comparison and Parameter Estimation for $D_s(\varepsilon)$

To aid in comparing the diffusivities in the different media, systems and processes, we evaluated the $D_s(\varepsilon)$ models listed in Table 3.1. For the model fitting, the diffusivities at the lowest air-filled porosity (i.e., at the turn-around in the draining wetting cycle) were classified as both draining and wetting. In fitting, we explicitly assumed that the macro-pore porosity ($\phi_m = \phi - 0.37$) equals the total porosity. This assumption reflects the hypothesis that the micropore region remains saturated under the exerted matric potentials, and that the diffusive transport of oxygen in the air-phase occurs exclusively in the macro-pore region. Table 3.3 and 3.4 list fitted model parameters and goodness-of-fit measures for the models given in Table 3.1 that were tested against the draining and wetting data. In Fig. 3.5 we show a scatter-plot comparison of estimated and predicted values for D_s.

3.5.4 Statistical Analysis of $D_s(\varepsilon)$

We used the log-transformed SAPHIR model (Eq. [3.24]) for the statistical analysis. Because this transformed model differs from the original SAPHIR model (Table 3.1), estimates of δ_s and ξ_s obtained using log transformation do not compare to direct fitting of models. However, the transformed model parameters quantify the differences between media, system and mode, albeit losing their physical meaning. Comparisons involving the parameter ξ_s were conducted under the assumption that $\delta_s = 0$ (i.e., when $\phi = \varepsilon$).

A selection of comparative statistics using the difference in estimated parameters for Flat (i.e., at 1g) and ISS (i.e., at μg) treatments, as well as draining and wetting, are given in Table 3.5. For the parameter δ_s, draining parameter estimates in the Flat cell were significantly different from draining parameter estimates in μg for all media. For wetting conditions, parameter estimates were not significantly different. For the parameter ξ_s, draining parameter estimates were different for Mix and Profile, but not for Turface. Wetting parameter estimates were significantly different between the Flat cell and μg for Mix, but not for Profile and Turface. Evaluating hysteresis in the draining and wetting modes for the media comparing parameter estimates from the Flat cell (i.e., at 1g), no significant difference was noted for parameters δ_s and ξ_s. At μg, parameter estimates for draining and wetting were significantly different for δ_s and ξ_s considering Mix and Profile, but were not significantly different for Turface.

3.5.5 Parameter Estimates of Porous-Media Water Retention

Water retention characteristic data obtained at 1g in the Flat and Round cells and at μg on the ISS are depicted in Fig. 3.6. Also shown are the fitted primary draining and wetting water retention curves to the observations using Eq. [3.17]. Fitting parameters α and n and goodness-of-fit measures are reported in Table 3.6. As with the diffusivity observations, the experimental malfunctions on the ISS prevented the collection of a complete data set, with two draining water content steps at the dry end missing.

Observations at 1g were self-consistent with some differences between the Flat and Round systems, likely due to the differing vertical extent of the experimental cells. At μg, we intermittently

experienced higher levels of noise in the potential readings compared to 1g, possibly due to a noisier power source. To retrieve consistent matric potential data, we filtered the individual matric-potential time series and averaged over reduced-noise time-windows at equilibrium conditions. Nevertheless, draining data in the individual cells (i.e., individual observations of potentials at a given water content) for Profile and Mix at μg were not self-consistent like they were at 1g, but appeared to deviate increasingly with decreasing water content.

To facilitate model fitting, the residual water content θ_r was kept invariant at 0.37 cm^3 cm^{-3}. Since experimental limitations forced the avoidance of saturated water contents, we further assumed a saturated water content θ_s of 0.7 cm^3 cm^{-3} for all systems, media and processes. In doing so, we effectively assumed some degree of air-entrapment, but ignored the process dependence of this entrapment (i.e., higher entrapment for wetting than draining) and further ignored the gravity dependence of entrapment. We did this because the measured data did not allow a substantiated analysis of air-entrapment because of the lack of data near saturation. In addition, owing to the malfunctions and the resulting lack of data at the dry end, we added the wetting data at θ=0.37 cm^3 cm^{-3} for $h < -25$ cm (i.e., at the asymptote) to help constrain the fit to the draining model.

3.5.6   Statistical Analysis of Porous-Media Water Retention

A selection of comparative statistics using the difference in estimated parameters for Flat cell and ISS, as well as draining and wetting, are given in Table 3.7. For the parameter α, estimates were significantly different for Mix under both wetting and draining conditions, but were not significantly different for Profile and Turface, with exception for Turface wetting conditions comparing Flat cell and μg estimates. For the parameter n, estimates for draining conditions were significantly different for Mix and Profile, but not for Turface. Under wetting conditions, no significant difference was noted for Mix and Profile. Turface estimates were significantly different for wetting conditions comparing Flat cell and μg. Evaluating hysteresis in the draining and wetting modes for the media comparing parameter estimates from the Flat cell, significant differences were noted for α parameters. For n parameters, no significant differences were noted for Mix and Profile. Parameter estimates of n for Turface were significantly different, comparing draining and wetting at 1g in the

Flat cell. At μg, no significant difference was noted for estimates of the parameter α for Mix and Profile, but not for Turface. For the parameter n, significant differences were noted for all media.

3.6   Discussion

3.6.1   Analysis of Predictive Models for $D_s(\varepsilon)$

In the following, models listed in Table 3.1 describing the effective oxygen diffusivities obtained in the Flat and Round cells at 1g as a function of air-filled porosities shown in Fig. 3.4 with fitting parameters listed in Table 3.3 are evaluated as to their ability to describe the observations. In Fig. 3.5 we show scatter plot comparisons of the predicted and observed data considering individual model parameter fits for the systems, media and processes in order to facilitate the statistical evaluation of reduced gravity effects based on predicted $D_s(\varepsilon)$.

Single Parameter Models

The Penman model, which was not fitted to the observations, was included for visual comparison purposes. The model was developed for dry media and assumes a linear variation of diffusivity with ε, as suggested by Buckingham (1904), using a constant tortuosity factor τ_{eff} of 0.66. It is not surprising then that the model greatly overestimated the observations for all treatments, and because of its linear nature, failed to capture the curvilinear shape of the observations. The Penman model did particularly poor for Mix and Profile, but did better in capturing the more linearly behaved Turface, especially for wetting conditions. Nevertheless, not needing a calibration (i.e., fitting), the Penman model did nevertheless well in predicting the diffusivities at the highest air-filled porosities, again capturing Turface well, but somewhat over-predicting Mix and Profile.

The PMQ model, extending the Penman model for partially saturated conditions and repacked soils, largely over-predicted diffusivities at $\varepsilon = \phi$, and tended to over-predict the observations at high air-filled porosities, while under-predicting the observations at low air-filled porosities. Nevertheless, the PMQ model provided reasonable estimates for Mix and Profile, but significantly under-predicted observations in Turface at low air-filled porosities.

The TPM did not provide a good fit to the data, generally under-predicting the observations at

high air-filled porosities and in part over-predicting the observations at low air-filled porosities. Part of the problem stems from the fact that we took the model literally; assuming that the ϕ^2 term does indeed describe $\dfrac{D_s}{D_0}$ at $\varepsilon = \phi$. We fully expect the TPM to perform better if ϕ^2 were treated as a fitting parameter or if measured observations were used for this condition as suggested by Moldrup et al. (2004). For the scope of our work, neither option was attractive, as each would have introduced additional variability.

The WLR model was the best fitting single parameter model. Turface under draining conditions was best described using a δ of 2.37, while under wetting conditions, $\delta=2.26$ and $\delta=2.33$ for the Flat and Round cells, respectively, were best. Profile and Mix were best described using an averaged exponent δ of 2.65 and 2.54 for wetting and draining, respectively. Due to its curvilinear format, the WLR model captured the observations of Mix and Profile very well with little bias, but generally underpredicted observations in Turface, particularly at low air-filled porosities, due to its non-linear shape.

Dual Parameter Models

With exception of the WLR model, the dual parameter models MQ, SAPHIR and Troeh generally described the observations better than the single parameter models, due to their greater flexibility in fitting the observations.

The Troeh model showed good agreement to the Turface observations, exhibiting little bias. Predictions in Mix and Profile, however, were slightly over-predicting the observations at low air-filled porosities, and under-predicting at high air-filled porosities. For the aggregated media, the second fitting parameter was found to be close to zero, suggesting that there was little impact of inactive air-filled pore space on the diffusion. With the second fitting parameter close to zero, the model may then be simplified to the form of $D_s = D_a\varepsilon^{\delta}$. This simplification effectively reduces the Troeh model to the models suggested by Marshall (1959) and Millington (1959) for completely dry soil, with the exception that the fitted exponent for the particulate porous media exceeded the suggested values of 4/3 and 3/2, with exception of Turface at draining, which seemed to be well described by a δ of 1.56. Surprisingly, the Troeh model implied little difference in the wetting ob-

servations among the media and systems. For the draining observations, the model further suggested that Turface may be described with an average δ of 1.56, while Profile and Mix may be described by an average δ=1.82, regardless of system highlighting the models relative insensitivity. For purposes of evaluating differences, the Troeh model seemed at a disadvantage, however, the good fit and stability (as the positive side of insensitivity) may lend the model suitability for conservative estimates in future modeling efforts.

The MQ model and the SAPHIR model provided the visually most appealing and almost identical fits to the observations. The SAPHIR model had slightly (statistically insignificant) lower RMS errors compared to the MQ model. Both models were able to capture the general shape of the observations in all media well, while showing little bias at low air-filled porosities, slightly under-predicting diffusivities.

The MQ model resolved differences in the observations related to media, system and process, with the values of the wetting parameter sets being lower compared to the draining parameters. For the observations under draining conditions, Mix parameter sets were in reasonable agreement with standard parameter sets suggested by Millington and Quirk (1961). The authors suggested the use of $\delta = \dfrac{10}{3}$ and ξ=2. In a later paper, Sallam et al. (1984) suggested a slightly reduced parameter δ of 3.1, placing values found in this study of δ=3.03 for the Flat cells and δ=3.85 for the Round cells close to the standard values. However, the Flat cell parameter ξ for Mix was found to be closer to the $\xi = \dfrac{2}{3}$ suggested by Millington and Quirk (1960). While Mix with the wider particle-size distribution compared to Profile and Turface compared well to the standard parameters in the above studies, Turface and Profile were not well described by these parameter sets at draining conditions with an even wider discrepancy at wetting conditions. Turface parameter sets suggested less curvature in the observations compared to Profile and Mix, with much smaller values for ξ ranging from 0 for wetting conditions to 0.15 and 0.3 for draining conditions. Similarly to the Troeh model, ξ values close to zero suggested that Turface may be well described by a simplified relationship according to $D_s = D_a \varepsilon^{\delta}$. In contrast to the Troeh model, however, Profile and Mix parameters for ξ showed divergent behavior between wetting and draining conditions, ranging from 0.85 to 2.4 for draining, and 0.31 to 0.86 for wetting conditions, with Mix showing the higher ξ

parameter values. Considering differences in Flat and Round cell model fits showed a general trend of lower parameters of and for the Flat cell. For example, Turface observations under draining conditions in the Flat cell were described with δ=1.63 and ξ=0.15, compared to δ=1.78 and ξ=0 in the Round cell. For wetting conditions, δ=1.41 and ξ=1.47 were found to describe the observations in the Flat and Round cell, respectively. Profile and Mix parameter sets showed similar behaviors.

The SAPHIR model appeared to best describe the observations in the Flat and Round cells. Turface parameter sets varied from the Profile and Mix parameter sets, with distinct differences in draining and wetting, as well as differences in the Flat and Round cell treatments. Mix observations in the Flat cell at draining conditions were well described using a parameter set of δ=0.62 and ξ=3.29 close to the one suggested by Thorbjørn et al. (2008). In their paper, the authors suggested that a δ=0.6 and ξ=3 comprised a good average parameter set to predict diffusivities in unstructured particulate porous media. For our observations at wetting conditions, however, a different parameter set of δ=0.61 and ξ=1 was found to describe the data. The reduction in the parameter ξ, also termed the water-blockage factor, to unity suggests that the reduction in diffusivities with air-filled porosity is primarily a function of the reduction in cross sectional area with increasing water content for wetting conditions, whereas, for draining conditions tortuosity increases non-linearly. For both wetting and draining conditions, the parameter δ, also termed the particle shape factor, is comparable. Because the particle shape factor describes the reduction in diffusivity due to the arrangement of the dry solids alone, there should not be a process-dependent change, giving us great confidence in the model's ability to separate effects in draining and wetting behavior under different gravity regimes. For the Turface observations in the Flat cell, δ varied between 0.49 and 0.41 for draining and wetting, respectively. The reduction in δ compared to Profile and Mix is consistent with Thorbjørn et al. (2008), where the authors suggested a lower δ for larger particle size media. For the water blockage factor ξ, we noted values of 0.24 and 0 for Turface under draining and wetting conditions, respectively, suggesting a lower water-induced disconnectivity in the larger particle sized media compared to the smaller particle sized Profile and Mix. This contradictory finding to Thorbjørn et al. (2008) implies reduced tortuosity when compared to Profile and Mix. The Round cell estimates showed similar behavior, but with increased ξ of 5.63 and 2.04 for wetting and drain-

ing respectively in Mix. Turface estimates were 0.61 and 0 for wetting and draining. The increased ξ for the Round cell estimates in Mix indicate that for any given air-filled porosity, diffusivities in the Round cell were lower compared to the Flat cell; perhaps caused by the different distribution of the water phase with an increased apparent water content ($\phi - \varepsilon$ in Table 3.1, SAPHIR) compared to the Flat cell. This apparent reduction in diffusivities may be partially attributed to the expected hydrostatic vertical distribution of water in the test cells, where the taller Round cell likely exhibits an increased gradient in water content with a region of below average water contents towards the top of the sample, and a region of above average water contents at the bottom that determine the lower apparent diffusivity.

3.6.2 Apparent Diffusivities under Hydrostatic Water Distributions at 1g

Because of the non-uniform distribution of water in a sample of height L at terrestrial gravity, the measured apparent (or mean) observations of diffusivity and air-filled porosity may not represent the true behavior of the diffusivity in a hydraulically homogenous sample. For horizontal diffusion (i.e., perpendicular to the gravity field), the expected apparent diffusivity of the 1g sample is the integral of the diffusivities determined by the equilibrium air-filled porosity distribution over the vertical extent of the sample divided by the height of the column:

$$\overline{D_s(\varepsilon)} = \frac{1}{L} \int_{h_{lb}}^{h_{ub}} D_s(\varepsilon) dh \tag{3.25}$$

where h_{lb} and h_{ub} indicate the lower and upper boundary hydraulic potentials. Fig. 3.7 compares observations of diffusivities considering horizontal diffusion at a point with modeled data in the Flat and Round cell samples with vertical extents of 2 and 5 cm, respectively. With increasing sample height, the error resulting from the mean observations $\overline{D_s(\varepsilon)}$ compared to the diffusivities at a given homogenous air-filled porosity $D_s(\overline{\varepsilon})$ increases, and is, as a fraction, most important at low air-filled porosities where the magnitude of the diffusivity is lowest.

3.6.3 Apparent Effects on Effective Diffusivities at μg

With 1g differences in the gravity induced water distribution in the Flat and Round cells being

perceptible in the model predictions, we opted to use the Flat cell estimates for means of comparison with μg results using the SAPHIR model (Table 3.1) fitted parameter estimates. Inferences about gravity-induced differences were made based on statistical conclusions using the SAPHIR-like model (Eq. [3.24]), herein indexed with *s*.

For wetting conditions, no significant differences were noted for all media comparing δ_s and ξ_s in the SAPHIR-like model, with the exception of Mix, where the parameter ξ_s differed significantly from the Flat cell estimate. The parameter ξ_s differed further comparing the Round cell estimate with μg (P < 0001). Comparing the model fitting estimates, Mix parameters for the particle shape factor δ in μg matched the Flat cell estimates at 1g, suggesting that minimum and maximum diffusivities at corresponding air-filled porosities were unaffected by μg. Estimates for ξ, however, were reduced to 0.25 compared to the terrestrial estimates of 1.01. This reduction is in concert with the reduction seen between the 5 and 2 cm tall samples at terrestrial gravity, making it likely that the vertical extent of the 2 cm tall Flat cell in 1g resulted in lower apparent diffusivities compared to the more homogenous distribution of water in the sample at μg.

The Turface estimate for δ at wetting was higher at 0.52 compared to the estimate of 0.41 at 1g, suggesting a slight, but insignificant reduction in maximum diffusivity at the highest air-filled porosity. As a note, the estimate for δ in the Round cell was 0.47. Because the particle shape factor ξ is less of a function of water distribution, but particle arrangement, the packing density affects the diffusivity in the dry media. Looking back to Table 3.2, packing densities for Turface were lowest for the ISS treatment with the highest density for the Flat and intermediate density for the Round treatment, respectively. With δ unchanged between the Flat, Round and ISS treatments, the change in ξ may then be partially attributed to the packing density differences and is likely not a manifestation of a gravity impact.

Comparing wetting and draining conditions, no significant differences in δ_s and ξ_s were noted for Mix and Profile comparing Flat cell wetting and draining estimates. In contrast, significant differences were noted comparing wetting and draining estimates in μg. This fundamentally different hysteresis behavior is attributed to a significantly different draining response in these media in μg. Comparing the model fitting estimates for the Flat cell, the particle shape factor δ remained largely

unchanged between the wetting and draining sequence, with a notable, but insignificant, increase in the water-blockage factor ξ under draining conditions. In μg, the particle shape factor δ differed significantly between the wetting and draining sequences, where for Mix and Profile δ more than doubled and ξ remained largely unchanged at values close to zero. No significant difference in the hysteretic behavior was noted for the larger particle-sized Turface.

For Turface under draining conditions, a significant difference was noted for δ_s, but not for ξ_s corresponding with the observed difference in the particle shape factor δ that showed an increase in μg compared to 1g estimates. Consideration of the shortened data set for draining conditions discussed above, one may be inclined to attribute the difference to the greater variability in the reduced data set with missing observations at high air-filled porosities. Considering the draining estimates for Mix and Profile, however, corroborated the divergent behavior in the draining process at μg compared to 1g where estimates of δ_s and ξ_s suggested a significant difference. Estimates of δ doubled for Mix and tripled for Profile, suggestive of the observed reduction in diffusivities with increased air-filled porosities that indicate a greater resistance to the diffusive transport. Because the water-blockage factor ξ is reduced to zero in μg, the increase in δ signifies an apparent change in the pore geometry, with a significant increase in apparent tortuosity. This increase in apparent tortuosity manifests itself as a perceived shift in the air-percolation threshold to higher air-filled porosities in μg. One may theorize that during wetting, small pores fill first and generate a more organized re-filling of pores compared to draining conditions. In the draining cycle, at a given water content, water will tend to be localized in larger pores with narrow necks. This will have less of an effect on air-filled pore connectivity than the more disperse distribution that will occur at the same water content during wetting. This dispersed distribution, however, is likely to occlude arterial pores important for maintaining high rates of gas diffusion, and is likely to explain reductions in diffusivity for the draining process at 1g. The enhanced reduction observed in μg, however, may be partially explained by an artifact of the experimental system (Fig. 3.8) that was not observed at 1g.

During draining, air percolates when the bubbling pressure threshold is surpassed. With the reduction of water-filled pore space indicated by the decreasing average water content in the draining sequence, air-filled porosity must increase. This increase, however, may not be uniform, but may

be concentrated in pores near the pervious sides of the experimental cells (i.e., the porous screens in Fig. 3.2b), leaving a cluster of water-filled pores in the center of the sample. Because of the speculated asymmetry of air-entry and water drainage, water filled pores which are not connected to air-filled clusters will remain water filled. As a consequence, no continuous air-filled pathway traversing the sample is established until a second threshold water content is reached when air-filled pore space has advanced to the center of the sample, allowing water in large pores to drain with incoming air. The existing air-filled porosity which previously did not contribute to the horizontal diffusion would then allow for rapid increases in diffusivity as the restriction subsides.

3.6.4   Apparent Effects on Water-Retention Characteristics at μg

The water-retention observations highlight some of the differences attributed to the hydrostatic water-content distributions. Using average water contents in the derivation of the water retention data, while using a quasi-point measurement for the matric potential, appears to distort parts of the retention behavior due to the neglect of changes in water content and hydraulic potential with elevation at terrestrial gravity. While matric potentials are expected to be more uniform throughout the sample with the lack of a gravitational potential, the water-content distribution may still be nonuniform.

Considering the wetting process, no significant differences were noted for the parameter n describing the pore-size distribution with exception of Turface. For Turface, n increased significantly. We attribute the difference to the averaging of water contents over the height of the sample in 1g that tends to smooth the apparent water-retention characteristic displaying a signature indicative of a wider pore-size distribution media (i.e., smaller n). Additionally, a shift in the air-entry value, related to the inverse of α, is attributable to the smoothing which is more perceptible for the larger particle-sized Turface. The smaller particle-sized media Profile and Mix have air-entry values comparable or greater than the vertical extents of the experimental cells in 1g, with a relatively smaller impact of the averaging on the water-retention characteristics. For Profile and Mix inconsistent conclusions have to be drawn as to the change in air-entry values at wetting comparing 1g and μg. The parameter α in Profile was shown to be significantly different in μg, but α for Mix was not

significantly different. Given that estimates for α varied significantly between the Flat and Round cell estimates, definitive conclusions cannot be drawn based on the available observations without further verification. For draining conditions, no significant differences were noted for estimates of α in the three media, with significant differences in the estimates for the parameter n for Mix and Profile. Turface estimates of n in μg were not significantly different from 1g.

Like for the diffusivity observations, water-retention observations under draining conditions were limited by an incomplete dataset. For the water-retention observations, particularly for the observations in Mix and Profile, inconsistent observations of matric potentials with increasing variation at decreasing water contents characterize the response. We speculate that the perceived inconsistency may be attributable to the discussed nonuniformity in the water-content distribution hypothesized for the draining process. This would result in spatially variable matric potentials necessarily bounded by the primary draining and wetting water-retention characteristic for pore-clusters showing water contents in contrast to neighboring clusters. With the given uncertainty in the water-retention response for draining conditions, no definitive conclusions on effects of microgravity can be drawn.

3.7 Conclusions

We presented oxygen diffusivity and matric potential measurements as a function of water content in variably-saturated aggregated porous media. Both wetting and draining processes were considered in both flattened rectangular and cylindrical experimental systems (diffusion cells) with differing vertical extents. We evaluated several fitted models describing the oxygen diffusivity/air-filled porosity characteristic and concluded that the SAPHIR model by Thorbjørn et al. (2008) best described our observations in the relatively coarse porous media compared to other models tested. Using the fitted SAPHIR model, we compared measurements conducted aboard the International Space Station in microgravity with earth-based measurements. For the oxygen diffusivity/air-filled porosity fitted parameters, no significant differences in the draining response were noted in μg. Observed significant differences in the draining response characterized by a higher air-percolation threshold and increased apparent tortuosity in Profile and Mix resulted in a significant difference

between the wetting and draining parameters not observed in 1g. While this reduction in diffusivity may explain signs of root-zone hypoxia from previous μg plant-growth experiments, the outcome is fundamentally different from measurements in 1g, and therefore, we offered a possible explanation based on the porous medium container geometry. This anomaly was not observed in 1g and is likely enhanced by microgravity, where in the draining sequence the air-entry takes place at the two gas chamber interfaces. We hypothesized this could create an asymmetrical distribution of water contents impeding diffusive transport between source and sink, where the effect was greater for smaller particle size. While results do not suggest a centrally different response in diffusivities at μg, they nevertheless highlight perceived changes in the configuration of water that affect the signature of observed volume-averaged effective diffusivities. With water-retention characteristics that, given the level of confidence, appear to be similar in μg, controlling water in porous substrates based on matric potentials (i.e., supply membrane suction) to ensure adequate aeration nevertheless suggests the need for adjustments in μg, because of the hydrostatic distribution of water in 1g that will generally allow for higher horizontal diffusivities compared to the more disperse distribution in μg. Our results further suggested that the distribution of water in μg may be nonuniform, with the possible creation of clusters of relatively more water-induced tortuous pathways, pointing to the need to more carefully study the impact of supply locations on resource fluxes in porous-media root zones. Because the signatures of measured oxygen diffusive transport and water retention characteristics do not allow for a unique reconstruction of the distribution of water in the sample, we suggest the need for further experimental study confirming key aspects of the speculated impacts of μg. Such studies might include approaches to measure spatial and temporal water content distribution, both with and without plants, in order to determine the extent of heterogeneity in microgravity porous media.

3.8   References

Bingham, G.E., I.G. Podolsky, T.S. Topham, and J.M. Mulholland. 2002. Lada: The ISS plant substrate microgravity testbed. SAE Technical Paper 2002-01-2388. SAE Int., Warrendale, PA.

Bingham, G.E., S.B. Jones, D. Or, I.G. Podolski, M.A. Levinskikh, V.N. Sytchov, T. Ivanova, P. Kostov, S. Sapunova, I. Dandolov, D.B. Bubenheim, and G. Jahns. 2000. Microgravity effects on water supply and substrate properties in porous matrix root support systems. Acta Astronautica 47:839-848.

Box, G.E.P., and D.R. Cox. 1964. An analysis of transformations. J. Royal Statistical Soc. Series B 26:1-78.

Buckingham, E. 1904. Contributions to our knowledge of the aeration of soils. Bull. 25. USDA, Bureau of Soils, Washington, DC.

Caron, J., and N.V. Nkongolo. 2004. Assessing gas diffusion coefficients in growing media from in situ water flow and storage measurements. Vadose Zone J. 3:300-311.

Chau, J.F., D. Or, and M.C. Sukop. 2005. Simulation of gaseous diffusion in partially saturated porous media under variable gravity with lattice Boltzmann methods. Water Resour. Res. 41(8).

Glauz, R.D., and D.E. Rolston. 1989. Optimal design of two-chamber, gas diffusion cells. Soil Sci. Soc. Am. J. 53:1619-1624.

Heinse, R., G. Kluitenberg, K.S. Lewis, R.S. Austin, P.J. Shouse, G.B. Bingham, and S.B. Jones. 2006. Integration of Heat Capacity and Electrical Conductivity Sensors for Root Module Water and Nutrient Assessment. SAE Technical Paper 2005-01-2950. SAE Int., Warrendale, PA.

Ivanova, T., S. Doncheva, I. Ilieva, P. Kostov, S. Sapunova, and R. Dikova. 2006. Experiment investigating the influence of oxygen deficiency on plants grown in microgravity. SENS'2006 second scientific conference with international participation-Space, Ecology, Nanotechnology, Safety. Space Research Institute - Bulgarian Academy of Sciences, Creative House of the Bulgarian Academy of Sciences, Varna.

Ivanova, T.N., Yu.A. Bercovich, A.L. Mashinskiy, and G.I. Meleshko. 1993. The first "space" vegetables have been grown in the "SVET" greenhouse using controlled environmental conditions. Acta Astronautica 29:639-44.

Ivanova, T.N., S.M. Sapunova, P.T. Kostov, and I.I. Ilieva. 2005. Recent advances in the development of the SVET space greenhouse equipment, pp. 722-727. IEEE.

Ivanova, T.N., P.T. Kostov, S.M. Sapunova, I.W. Dandolov, F.B. Salisbury, G.E. Bingham, V.N. Sytchov, M.A. Levinskikh, I.G. Podolski, D.B. Bubenheim, and G. Jahns. 1998. Six-month space greenhouse experiments - a step to creation of future biological life support systems. Acta Astronautica 42:11-23.

Jones, S.B., and D. Or. 1998. Design of porous media for optimal gas and liquid fluxes to plant roots. Soil Sci. Soc. Am. J. 62:563-573.

Jones, S.B., and D. Or. 1999. Microgravity effects on water flow and distribution in unsaturated porous media: Analysis of flight experiments. Water Resour. Res. 35:929-942.

Jones, S.B., D. Or, and G.E. Bingham. 2003a. Gas diffusion measurement and modeling in coarse-textured porous media. Vadose Zone J 2:602-610.

Jones, S.B., D. Or, G.E. Bingham, and R.C. Morrow. 2002. ORZS: Optimization of root zone substrates for microgravity. SAE Technical Paper 2002-01-2380. SAE Int., Warrendale, PA.

Jones, S.B., R. Heinse, G.E. Bingham, and D. Or. 2005. Modeling and design of optimal growth media from plant-based gas and liquid fluxes. SAE Technical Paper 2005-01-2949. SAE Int., Warrendale, PA.

Jones, S.B., G.E. Bingham, T.S. Topham, D. Or, I.G. Podolsky, and O. Strugov. 2003b. An automated oxygen diffusion measurement system for porous media in microgravity. SAE Technical Paper 2002-01-2380. SAE Int., Warrendale, PA.

Laing, C. 2004. A mechanical design to support the research of optimum root zone substrates. Utah State University, Logan, UT.

Levine, H.G., G.K. Tynes, and J.H. Norikane. 2003. Fluid behavior under microgravity conditions within plant nutrient delivery systems: Parabolic flight investigations. SAE Technical Paper 2003-01-2483. SAE Int., Warrendale, PA.

Liao, J., G. Liu, O. Monje, G.W. Stutte, and D.M. Porterfield. 2004. Induction of hypoxic root metabolism results from physical limitations in O2 bioavailability in microgravity. Adv. Space Res. 34:1579-1584.

Marshall, T.J. 1959. The diffusion of gases through porous media. J. Soil Sci. 10:79-82.

Millington, R.J. 1959. Gas diffusion in porous media. Science (Washington, DC) 130:1200-1207.

Millington, R.J., and J.M. Quirk. 1960. Transport in porous media. 7th International Congress of Soil Science. SSSA, Madison, WI.

Millington, R.J., and J.M. Quirk. 1961. Permeability of porous solids. Trans. Faraday Soc. 57:1200-1207.

Moldrup, P., T. Olesen, D.E. Rolston, and T. Yamaguchi. 1997. Modeling diffusion and reaction in soil: VII. Predicting gas and ion diffusivity in undisturbed and sieved soil. Soil Sci. 162:632-640.

Moldrup, P., T. Olesen, P. Schjonning, T. Yamaguchi, and D.E. Rolston. 2000. Predicting the gas diffusion coefficient in undisturbed soil from soil water characteristics. Soil Sci. Soc. Am. J. 64:94-100.

Moldrup, P., T. Olesen, T. Komatsu, P. Schjonning, and D.E. Rolston. 2001. Tortuosity, diffusivity, and permeability in the soil liquid and gaseous phases. Soil Sci. Soc. Am. J. 65:613-623.

Moldrup, P., S. Yoshikawa, T. Olesen, T. Komatsu, and D.E. Rolston. 2003. Gas diffusivity in undisturbed volcanic ash soils: Test of soil-water-characteristic-based prediction models. Soil Sci. Soc. Am. J. 67:41-51.

Moldrup, P., T. Olesen, S. Yoshikawa, T. Komatsu, and D.E. Rolston. 2004. Three-porosity model for predicting the gas diffusion coefficient in undisturbed soil. Soil Sci. Soc. Am. J. 68:750-759.

Monje, O., G. Stutte, and D. Chapman. 2005. Microgravity does not alter plant stand gas exchange of wheat at moderate light levels and saturating CO2 concentration. Planta 222:336-345.

Musgrave, M.E., A.X. Kuang, Y. Xiao, S.C. Stout, G.E. Bingham, L.G. Briarty, M.A. Levinskikh, V.N. Sychev, and I.G. Podolski. 2000. Gravity independence of seed-to-seed cycling in Brassica rapa. Planta 210:400-406.

Penman, H.L. 1940. Gas and vapor movement in soil: The diffusion of vapors through porous solids. J. Agric. Sci. 30:437-462.

Podolsky, I., and A. Mashinsky. 1994. Peculiarities of moisture transfer in capillary-porous soil substitutes during space flight. Adv. Space Res. 14:39-46.

Porterfield, D.M., S.W. Matthews, C.J. Daugherty, and M.E. Musgrave. 1997. Spaceflight exposure effects on transcription, activity, and localization of alcohol dehydrogenase in the roots of *Arabidopsis thaliana*. Plant Physiol. 113:685-693.

Porterfield, D.M., D.J. Barta, D.W. Ming, R.C. Morrow, and M.E. Musgrave. 2000. ASTROCULTURE (TM) root metabolism and cytochemical analysis. Adv. Space Res. 26:315-8.

Reddi, L.N., M. Xiao, and S.L. Steinberg. 2005. Discontinuous pore fluid distribution under microgravity–KC-135 flight investigations. Soil Sci. Soc. Am. J. 69:593-598.

Richards, L.A. 1931. Capillary conduction of liquids through porous mediums. Physics 1:318-333.

Rolston, D.E., and P. Moldrup. 2002. Gas diffusivity, p. 1113-1139. In J. H. Dane and G. C. Topp, eds. Methods of soils analysis. Part 4. SSSA, Madison, WI.

Sallam, A., W.A. Jury, and J. Letey. 1984. Measurement of gas diffusion coefficient under relatively low air-filled porosity. Soil Sci. Soc. Am. J. 48:3-6.

Schjønning, P., I.K. Thomsen, J.P. Mberg, H. de Jonge, K. Kristensen, and B.T. Christensen. 1999. Turnover of organic matter in differently textured soils: I. Physical characteristics of structurally disturbed and intact soils. Geoderma 89:177-198.

Steinberg, S., G. Kluitenberg, S.B. Jones, N. Diadzic, L. Reddi, M. Xiao, M. Tuller, R. Newman, D. Or, and I.D. Alexander. 2005. Physical and hydraulic properties of baked ceramic aggregates used for plant growth medium. J. Amer. Soc. Hort. Sci. 130:767-774.

Steinberg, S.L., and D.L. Henninger. 1997. Response of the water status of soybean to changes in soil water potentials controlled by the water pressure in microporous tubes. Plant Cell Environ. 20:1506-1516.

Steinberg, S.L., and D. Poritz. 2005. Measurement of hydraulic characteristics of porous media used to grow plants in microgravity. Soil Sci. Soc. Am. J. 69:301-310.

Steinberg, S.L., D. Ming, and D. Henninger. 2002. Plant production systems for microgravity: Critical issues in water, air and solute transport through unsaturated porous media. NASA Tech. Mem. 2002-210774. Natl. Aeronautics and Space Admin., Houston, TX.

Stout, S.C., D.M. Porterfield, L.G. Briarty, A. Kuang, and M.E. Musgrave. 2001. Evidence of root zone hypoxia in *Brassica rapa L.* grown in microgravity. Intl. J. Plant Scie. 162:249-255.

Stutte, G.W., O. Monje, G.D. Goins, and B.C. Tripathy. 2005. Microgravity effects on thylakoid, single leaf, and whole canopy photosynthesis of dwarf wheat. Planta 223:46-56.

Thorbjørn, A., P. Moldrup, H. Blendstrup, T. Komatsu and D.E. Rolston. 2008. A gas diffusivity model based on air-, solid-, and water-phase resistance in variably saturated soil. Vadose Zone J. 7(4):1276-1286.

Troeh, F.R., J.D. Jabro, and D. Kirkham. 1982. Gaseous diffusion equations for porous materials. Geoderma 27:239-253.

US National Research Council. 2000. Methods for developing spacecraft water exposure guidelines: Report of the Subcommittee on Spacecraft Water Exposure Guidelines, Committee on Toxicology, Board on Environmental Studies and Toxicology, Washington, DC.

van Genuchten, M.T. 1980. A closed-form equation for predicting the hydraulic conductivity of unsaturated soils. Soil Sci. Soc. Am. J. 44:892-898.

Veselova, T.D., G.M. Il'ina, M.A. Levinskikh, and V.N. Sychev. 2003. Ethylene is responsible for a disturbed development of plant reproductive system under conditions of space flight. Russian J. Plant Phys. 50:339-354.

Xiao, M., L.N. Reddi, and S. Steinberg. 2008. Variation of soil water characteristics due to particle rearrangement. Submitted to ASCE Int. J. Geomechanics.

Table 3.1: Summary of commonly used relationships between relative effective diffusivity D_s/D_0 and air-filled porosity ε for partially saturated porous media. For the ease of notation, δ and ξ are being used to describe the first and, if applicable, second fitting parameter. ϕ denotes the total or macropore porosity.

Source	$\dfrac{D_s}{D_0} =$	Notation
Penman (1940)	0.66ε	Penman
Moldrup et al. (1997)	$0.66\varepsilon\left(\dfrac{\varepsilon}{\phi}\right)^{\frac{12-\delta}{3}}$	PMQ
Moldrup et al. (2004)	$\phi^2\left(\dfrac{\varepsilon}{\phi}\right)^{\delta}$	TPM
Moldrup et al. (2004)	$\varepsilon^{\delta}\left(\dfrac{\varepsilon}{\phi}\right)$	WLR
Millington and Quirk (1960, 1961)	$\dfrac{\varepsilon^{\delta}}{\phi^{\xi}}$	MQ
Thorbjørn et al. (2008)	$\varepsilon^{1+\delta+\xi(\phi-\varepsilon)}$	SAPHIR
Troeh et al. (1982)	$\left(\dfrac{\varepsilon-\xi}{1-\xi}\right)^{\delta}$	Troeh

Table 3.2: Average packing densities $\overline{\rho_b}$ and macropore porosities $\overline{\phi_{macro}}$ (assuming a micropore porosity of 0.37 cm^3 cm^{-3}) for triplicate measurements in the Flat, Round and ISS treatments. The standard deviations (SD) for these properties are also given.

System	Media	$\bar{\rho_b}$	SD_{ρ_b}	ϕ_{macro}	$SD_{\phi_{macro}}$
		–g cm^3–		–cm^3 cm^{-3}–	
	Turface	0.682	0.029	0.357	0.011
Flat	Profile	0.683	0.012	0.357	0.005
	Mix	0.699	0.006	0.351	0.003
	Turface	0.665	0.003	0.364	0.001
Round	Profile	0.704	0.001	0.348	0.001
	Mix	0.716	0.013	0.343	0.005
	Turface	0.652	0.005	0.369	0.002
ISS	Profile	0.705	0.002	0.348	0.001
	Mix	0.713	0.008	0.345	0.003

Table 3.3: Fitted gas diffusivity model parameters for the Flat and Round cell observations at 1g. For the model descriptions compare Table 3.3.1. The lower and upper bounds (*lb* and *ub*, respectively) of the 95 percent confidence interval for the estimated parameters are given in addition to the models *RMSE* and *bias*.

System	Media	Model	Draining δ	δ 95% CI lb	ub	ξ	ξ 95% CI lb	ub	RMSE	bias	Wetting δ	δ 95% CI lb	ub	ξ	ξ 95% CI lb	ub	RMSE	bias
Flat cell	Turface	Penman	2.00						0.466	0.394	2.00						0.255	0.220
		PMQ	1.45	-1.28	4.19				0.717	0.100	4.63	3.05	6.20				0.658	0.153
		TMP	0.67	0.32	1.02				0.543	-0.266	0.43	0.14	0.73				0.557	-0.289
		WLR	2.37	2.32	2.43				0.272	-0.129	2.26	2.20	2.33				0.367	-0.168
		MQ	1.63	1.43	1.82	0.15	-0.08	0.37	0.190	-0.031	1.41	1.30	1.52	0.00	-0.14	0.14	0.128	-0.025
		SAPHIR	0.49	0.44	0.54	0.24	-0.27	0.75	0.192	-0.027	0.41	0.38	0.45	0.00	-0.30	0.30	0.128	-0.025
		Troeh	1.59	1.40	1.78	0.03	-0.03	0.09	0.191	-0.006	1.62	1.50	1.73	0.07	0.03	0.11	0.099	-0.001
	Mix	Penman	2.00						0.932	0.884	2.00						0.741	0.707
		PMQ	0.00	-3.83	3.83				0.814	0.462	0.00	-3.80	3.80				0.806	0.295
		TMP	1.86	1.29	2.42				0.322	-0.108	1.25	0.83	1.68				0.379	-0.143
		WLR	2.67	2.62	2.72				0.180	0.001	2.55	2.49	2.60				0.215	-0.040
		MQ	3.03	2.56	3.51	1.41	0.88	1.93	0.174	-0.020	2.05	1.74	2.36	0.44	0.08	0.79	0.190	0.004
		SAPHIR	0.63	0.56	0.71	3.29	2.02	4.55	0.176	-0.022	0.61	0.55	0.68	1.01	0.20	1.82	0.189	0.003
		Troeh	1.82	1.42	2.22	0.00	-0.10	0.10	0.256	0.042	1.68	1.43	1.93	0.00	-0.07	0.07	0.210	0.031
	Profile	Penman	2.00						0.822	0.779	2.00						0.512	0.502
		PMQ	0.00	-3.33	3.33				0.747	0.313	1.53	-1.47	4.52				0.789	0.171
		TMP	1.43	1.07	1.79				0.297	-0.114	0.80	0.52	1.09				0.391	-0.188
		WLR	2.61	2.57	2.65				0.145	-0.055	2.44	2.38	2.50				0.271	-0.118
		MQ	2.41	2.13	2.70	0.77	0.45	1.10	0.142	-0.039	1.57	1.47	1.66	0.00	-0.12	0.12	0.088	-0.007
		SAPHIR	0.65	0.59	0.71	1.69	0.92	2.45	0.147	-0.040	0.57	0.54	0.59	0.00	-0.26	0.26	0.088	-0.007
		Troeh	1.76	1.51	2.00	0.00	-0.07	0.07	0.183	0.007	1.63	1.54	1.72	0.02	-0.01	0.05	0.085	0.001
Round cell	Turface	Penman	2.00						0.537	0.470	2.00						0.382	0.335
		PMQ	0.39	-1.85	2.63				0.558	-0.037	3.48	1.39	5.58				0.743	0.164
		TMP	0.79	0.44	1.13				0.499	-0.208	0.59	0.28	0.89				0.524	-0.259
		WLR	2.37	2.32	2.42				0.254	-0.087	2.33	2.26	2.40				0.369	-0.146
		MQ	1.78	1.52	2.03	0.30	-0.01	0.61	0.211	-0.021	1.47	1.30	1.64	0.00	-0.21	0.21	0.186	-0.016
		SAPHIR	0.49	0.42	0.55	0.61	-0.07	1.28	0.213	-0.020	0.47	0.42	0.52	0.00	-0.46	0.46	0.186	-0.016
		Troeh	1.54	1.33	1.74	0.00	-0.06	0.06	0.222	0.002	1.61	1.42	1.80	0.04	-0.02	0.10	0.179	0.001
	Mix	Penman	2.00						0.943	0.897	2.00						0.756	0.732
		PMQ	0.00	-2.56	2.56				0.571	0.377	0.00	-3.16	3.16				0.705	0.364
		TMP	1.97	1.35	2.58				0.329	-0.075	1.35	0.85	1.85				0.380	-0.145
		WLR	2.64	2.59	2.70				0.181	0.047	2.55	2.52	2.58				0.127	0.007
		MQ	3.85	3.36	4.34	2.39	1.84	2.94	0.126	0.000	2.42	2.16	2.69	0.86	0.56	1.16	0.125	0.014
		SAPHIR	0.48	0.41	0.55	5.63	4.32	6.94	0.125	-0.003	0.57	0.52	0.61	2.04	1.35	2.73	0.122	0.012
		Troeh	1.83	1.37	2.28	0.00	-0.11	0.11	0.279	0.070	1.69	1.46	1.92	0.00	-0.06	0.06	0.194	0.053
	Profile	Penman	2.00						0.902	0.882	2.00						0.697	0.681
		PMQ	0.00	-1.76	1.76				0.439	0.229	0.00	-2.87	2.87				0.652	0.178
		TMP	1.61	1.37	1.86				0.176	-0.025	1.14	0.81	1.48				0.324	-0.112
		WLR	2.64	2.61	2.67				0.096	-0.005	2.51	2.47	2.56				0.176	-0.042
		MQ	2.52	2.21	2.83	0.85	0.48	1.23	0.096	0.000	1.92	1.71	2.14	0.31	0.06	0.57	0.133	0.008
		SAPHIR	0.69	0.62	0.76	1.87	1.04	2.70	0.095	-0.001	0.62	0.56	0.67	0.70	0.12	1.28	0.133	0.008
		Troeh	1.84	1.61	2.07	0.00	-0.06	0.06	0.128	0.028	1.67	1.50	1.84	0.00	-0.05	0.05	0.146	0.027

Table 3.4: Fitted gas diffusivity model parameters for the ISS observations at μg. For the models descriptions compare Table 3.3.1. The lower and upper bounds of the 95 percent confidence interval for the estimated parameters are given in addition to the models *RMSE* and *bias*.

| | | | Draining | | | | | | | | Wetting | | | | | | | |
| | | | | δ 95 % CI | | | ξ 95 % CI | | Statistics | | | δ 95 % CI | | | ξ 95 % CI | | Statistics | |
System	Media	Model	δ	lb	ub	ξ	lb	ub	RMSE	bias	δ	lb	ub	ξ	lb	ub	RMSE	bias
ISS	**Turface**	Penman	2.00						0.604	0.571	2.00						0.416	0.394
		PMQ	3.25	1.74	4.76				0.289	-0.101	3.34	-0.27	6.94				0.854	0.214
		TMP	0.97	0.80	1.13				0.130	-0.011	0.65	0.30	1.00				0.415	-0.208
		WLR	2.30	2.19	2.42				0.218	-0.090	2.40	2.29	2.52				0.382	-0.182
		MQ	1.62	1.08	2.15	0.00	-0.80	0.80	0.141	-0.030	1.52	1.30	1.74	0.00	-0.27	0.27	0.158	-0.037
		SAPHIR	0.62	0.37	0.87	0.00	-1.56	1.56	0.141	-0.030	0.52	0.46	0.59	0.00	-0.58	0.58	0.158	-0.037
		Troeh	2.17	1.39	2.94	0.15	-0.06	0.36	0.110	-0.001	1.88	1.62	2.13	0.11	0.03	0.20	0.112	0.001
	Mix	Penman	2.00						0.998	0.929	2.00						0.594	0.581
		PMQ	0.00	-2.62	2.62				0.258	0.073	0.36	-4.95	5.68				0.776	0.182
		TMP	2.71	2.07	3.34				0.125	-0.033	1.04	0.59	1.49				0.346	-0.149
		WLR	2.95	2.73	3.16				0.128	-0.048	2.50	2.43	2.56				0.192	-0.087
		MQ	2.23	0.47	3.99	0.00	-2.55	2.55	0.117	-0.029	1.72	1.56	1.87	0.12	-0.06	0.30	0.083	0.000
		SAPHIR	1.23	0.51	1.96	0.00	-5.22	5.22	0.117	-0.029	0.60	0.56	0.64	0.25	-0.16	0.66	0.083	0.000
		Troeh	3.77	-0.69	8.23	0.31	-0.61	1.22	0.105	-0.002	1.62	1.50	1.74	0.00	-0.03	0.03	0.087	0.009
	Profile	Penman	2.00						1.166	1.086	2.00						0.720	0.709
		PMQ	0.00	-5.18	5.18				0.388	0.216	0.00	-7.63	7.63				0.879	0.236
		TMP	5.00	3.41	6.59				0.080	-0.044	1.19	0.76	1.63				0.241	-0.086
		WLR	3.57	3.19	3.96				0.070	-0.039	2.59	2.48	2.70				0.226	-0.087
		MQ	2.83	-1.16	6.82	0.00	-5.66	5.66	0.063	-0.030	1.71	1.45	1.97	0.00	-0.31	0.31	0.104	0.007
		SAPHIR	1.83	0.33	3.34	0.00	-11.6	11.58	0.063	-0.030	0.71	0.64	0.78	0.00	-0.71	0.71	0.104	0.007
		Troeh	2119	$-2 \cdot 10^7$	$2 \cdot 10^7$	382	$-4 \cdot 10^5$	$4 \cdot 10^5$	0.037	-0.001	1.71	1.48	1.94	0.00	-0.06	0.06	0.104	0.007

Table 3.5: Evaluation of differences in parameter estimates for δ and ξ in Eq. [3.24] using Student's t-test under the null hypothesis. The estimate gives the difference in parameters for the listed cases given as combinations of system, medium and mode with the corresponding standard error. The sign of the estimate corresponds with the direction of change for the compared cases. Probabilities subscripted with b indicate statistical significance.

Parameter	System	Medium	Mode	System	Medium	Mode	Estimate $\pm$ SD	DF	t Value	Pr > $|$t$|$†
δ‡	Flat	Mix	Draining	Flat	Mix	Wetting	0.29 ± 0.24	454	1.2	0.219
δ‡	Flat	Profile	Draining	Flat	Profile	Wetting	0.41 ± 0.23	454	1.8	0.078
δ‡	Flat	Turface	Draining	Flat	Turface	Wetting	0.12 ± 0.24	454	0.5	0.628
δ‡	Flat	Mix	Draining	ISS	Mix	Draining	-3.11 ± 0.50	454	-6.2	<.0001^b
δ‡	Flat	Mix	Wetting	ISS	Mix	Wetting	-0.57 ± 0.29	454	-2.0	0.050
δ‡	Flat	Profile	Draining	ISS	Profile	Draining	-2.64 ± 0.60	454	-4.4	<.0001^b
δ‡	Flat	Profile	Wetting	ISS	Profile	Wetting	0.36 ± 0.33	454	1.1	0.282
δ‡	Flat	Turface	Draining	ISS	Mix	Draining	-2.12 ± 0.50	454	-4.2	<.0001^b
δ‡	Flat	Turface	Wetting	ISS	Turface	Wetting	-0.15 ± 0.29	454	-0.5	0.601
δ‡	ISS	Mix	Draining	ISS	Mix	Wetting	2.84 ± 0.52	454	5.5	<.0001^b
δ‡	ISS	Profile	Draining	ISS	Profile	Wetting	3.41 ± 0.63	454	5.4	<.0001^b
δ‡	ISS	Turface	Draining	ISS	Turface	Wetting	0.93 ± 0.52	454	1.8	0.071
ξ	Flat	Mix	Draining	Flat	Mix	Wetting	-0.20 ± 0.47	454	-0.4	0.677
ξ	Flat	Profile	Draining	Flat	Profile	Wetting	-0.23 ± 0.45	454	-0.5	0.616
ξ	Flat	Turface	Draining	Flat	Turface	Wetting	0.17 ± 0.47	454	0.4	0.720
ξ	Flat	Mix	Draining	ISS	Mix	Draining	5.54 ± 0.90	454	6.2	<.0001^b
ξ	Flat	Mix	Wetting	ISS	Mix	Wetting	1.52 ± 0.53	454	2.9	0.005^b
ξ	Flat	Profile	Draining	ISS	Profile	Draining	3.45 ± 1.07	454	3.2	0.001^b
ξ	Flat	Profile	Wetting	ISS	Profile	Wetting	-1.28 ± 0.62	454	-2.1	0.038
ξ	Flat	Turface	Draining	ISS	Turface	Draining	1.23 ± 0.89	454	1.4	0.169
ξ	Flat	Turface	Wetting	ISS	Turface	Wetting	-0.17 ± 0.54	454	-0.3	0.752
ξ	ISS	Mix	Draining	ISS	Mix	Wetting	-4.22 ± 0.93	454	-4.5	<.0001^b
ξ	ISS	Profile	Draining	ISS	Profile	Wetting	-4.96 ± 1.15	454	-4.3	<.0001^b
ξ	ISS	Turface	Draining	ISS	Turface	Wetting	-1.23 ± 0.93	454	-1.3	0.187

SD: standard deviation; DF: degrees of freedom; t: Student's t-test applied to difference between two parameter estimates
† considering $\alpha = 0.05$
‡ for $\xi = 0$

Table 3.6: Parameters of the fitted van Genuchten model (Eq. [3.17]). The residual and saturated water contents θ_r and θ_s were kept invariant at 0.37 cm³ cm⁻³ and 0.7 cm³ cm⁻³, respectively.

System	Media	Wetting								Draining							
		α	α 95 % CI		n	n 95 % CI		Statistics		α	α 95 % CI		n	n 95 % CI		Statistics	
		–g cm³–	lb	ub		lb	ub	RMSE	bias	–g cm³–	lb	ub		lb	ub	RMSE	bias
Flat	Turface	0.490	0.447	0.532	2.713	2.414	3.013	0.020	0.002	0.294	0.251	0.338	3.091	2.431	3.750	0.030	0.007
	Mix	0.146	0.140	0.153	4.072	3.560	4.584	0.020	0.000	0.103	0.098	0.108	4.435	3.818	5.052	0.020	0.003
	Profile	0.126	0.121	0.131	4.633	3.911	5.356	0.024	0.001	0.085	0.083	0.087	5.357	4.758	5.956	0.016	0.003
Round	Turface	0.256	0.235	0.276	3.796	3.164	4.427	0.032	0.007	0.169	0.162	0.177	4.708	4.003	5.413	0.020	0.001
	Mix	0.179	0.152	0.206	3.113	2.344	3.881	0.037	0.009	0.130	0.116	0.144	3.036	2.610	3.461	0.024	0.003
	Profile	0.146	0.137	0.155	3.824	3.117	4.531	0.025	0.002	0.089	0.086	0.092	4.341	3.949	4.733	0.014	0.001
ISS	Turface	0.282	0.270	0.294	5.273	4.055	6.490	0.026	-0.001	0.222	0.195	0.250	3.918	2.271	5.566	0.020	0.000
	Mix	0.286	0.272	0.299	3.480	3.101	3.858	0.012	0.001	0.197	0.152	0.241	2.758	2.009	3.508	0.031	0.006
	Profile	0.133	0.124	0.142	4.641	3.333	5.948	0.028	0.001	0.100	0.086	0.114	3.513	2.503	4.523	0.028	0.006

Table 3.7: Evaluation of differences in parameter estimates for α and *n* in Eq. [3.17] using Student's *t*-test under the null hypothesis. The estimate gives the mean difference in parameters for the listed cases given as combinations of system, medium and mode with the corresponding standard error. The sign of the estimate corresponds with the direction of change for the compared cases. Probabilities subscripted with ♭ indicate statistical significance.

Parameter	System	Medium	Mode	System	Medium	Mode	Estimate ± SD	DF	t Value	Pr > |t|†
α	Flat	Mix	Wetting	Flat	Mix	Draining	0.04 ± 0.00	7	12.6	<.0001♭
α	Flat	Profile	Wetting	Flat	Profile	Draining	0.04 ± 0.00	7	18.3	<.0001♭
α	Flat	Turface	Wetting	Flat	Turface	Draining	0.23 ± 0.02	7	9.9	<.0001♭
α	Flat	Mix	Draining	ISS	Mix	Draining	-0.19 ± 0.06	7	-3.1	0.017♭
α	Flat	Mix	Wetting	ISS	Mix	Wetting	-0.15 ± 0.01	7	-13.0	<.0001♭
α	Flat	Profile	Draining	ISS	Profile	Draining	-0.03 ± 0.01	7	-2.8	0.028
α	Flat	Profile	Wetting	ISS	Profile	Wetting	-0.01 ± 0.00	7	-2.7	0.030
α	Flat	Turface	Draining	ISS	Turface	Draining	0.04 ± 0.01	7	2.7	0.029
α	Flat	Turface	Wetting	ISS	Turface	Wetting	0.21 ± 0.02	7	8.7	<.0001♭
α	ISS	Mix	Wetting	ISS	Mix	Draining	0.01 ± 0.06	7	0.2	0.881
α	ISS	Profile	Wetting	ISS	Profile	Draining	0.02 ± 0.01	7	1.9	0.106
α	ISS	Turface	Wetting	ISS	Turface	Draining	0.06 ± 0.01	7	5.4	<.0001♭
n	Flat	Mix	Wetting	Flat	Mix	Draining	-0.29 ± 0.30	7	-1.0	0.365
n	Flat	Profile	Wetting	Flat	Profile	Draining	-0.75 ± 0.35	7	-2.1	0.073
n	Flat	Turface	Wetting	Flat	Turface	Draining	-0.83 ± 0.22	7	-3.7	0.007♭
n	Flat	Mix	Draining	ISS	Mix	Draining	2.36 ± 0.32	7	7.4	<.0001♭
n	Flat	Mix	Wetting	ISS	Mix	Wetting	0.76 ± 0.33	7	2.3	0.052
n	Flat	Profile	Draining	ISS	Profile	Draining	2.57 ± 0.42	7	6.1	<.0001♭
n	Flat	Profile	Wetting	ISS	Profile	Wetting	-0.04 ± 0.48	7	-0.1	0.941
n	Flat	Turface	Draining	ISS	Turface	Draining	-0.52 ± 0.56	7	-0.9	0.382
n	Flat	Turface	Wetting	ISS	Turface	Wetting	-2.50 ± 0.39	7	-6.4	<.0001♭
n	ISS	Mix	Wetting	ISS	Mix	Draining	1.31 ± 0.31	7	4.2	0.004♭
n	ISS	Profile	Wetting	ISS	Profile	Draining	1.86 ± 0.49	7	3.8	0.006♭
n	ISS	Turface	Wetting	ISS	Turface	Draining	1.15 ± 0.64	7	1.8	0.116

SD: standard deviation; DF: degrees of freedom; t: Student's t-test applied to difference between two parameter estimates
† considering α=0.05
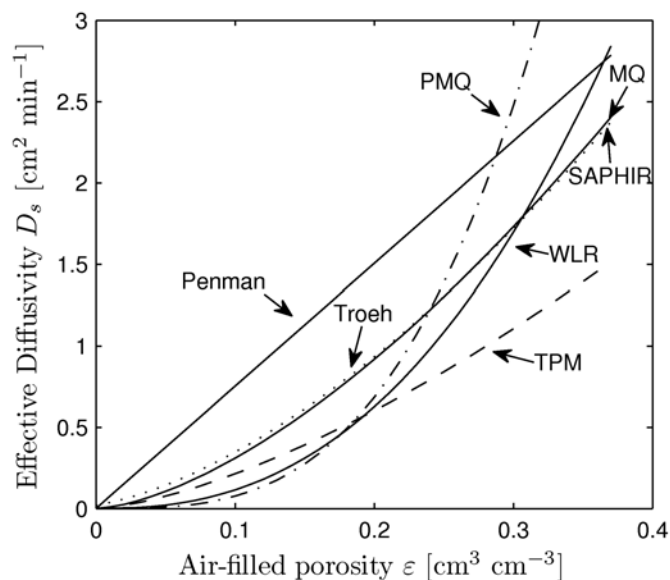
Fig. 3.1: Illustration of shape differences in the models describing effective diffusivity as a function of air-filled porosity given in Table 3.1. Depicted functions are examples of fitted models (i.e., not using standard parameter sets) to the aggregated porous media used in this study with a diffusivity in air D_0 of 11.4 cm^2 min^{-1}. Note that subtle differences in the Troeh- (dotted line), and MQ- and SAPHIR-model (solid line) plots are obscured through the line thickness.
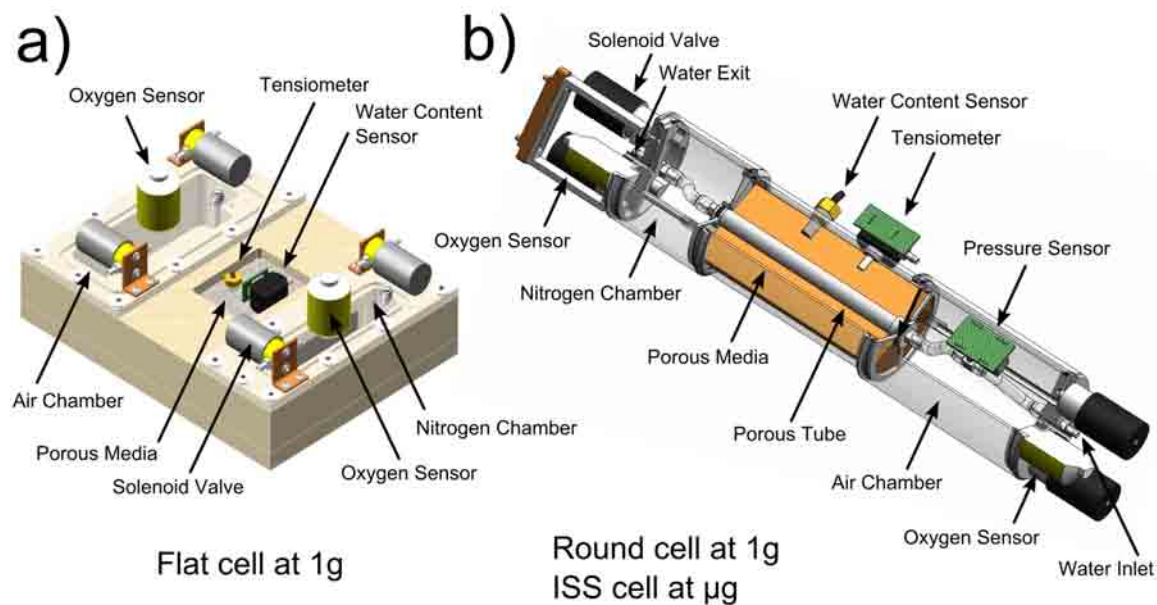
Fig. 3.2: Schematic drawings of the Flat (a) and Round/ISS (b) cells depicting the porous media and gas chambers as well as sensor locations. Part (b) was drawn after Laing (2004).

Fig. 3.3: Cosmonaut Oleg Kotov priming the experiment with water on the International Space Station in July 2007. The porous media were launched oven dry. Air in the tubes and porous membranes was replaced with water through manual Cosmonaut intervention facilitating the first wet-up of the porous media in the process. An automated procedure then continued to wet up the media to a matric potential of -2 cm_{H_2O} and subsequently drained the media to a potential of -30 cm_{H_2O}, at which point the automated experiments began. The cut-out shows heterogeneous wetting patterns observed in Turface, Mix and Profile during priming, leaving behind dry clusters of media.
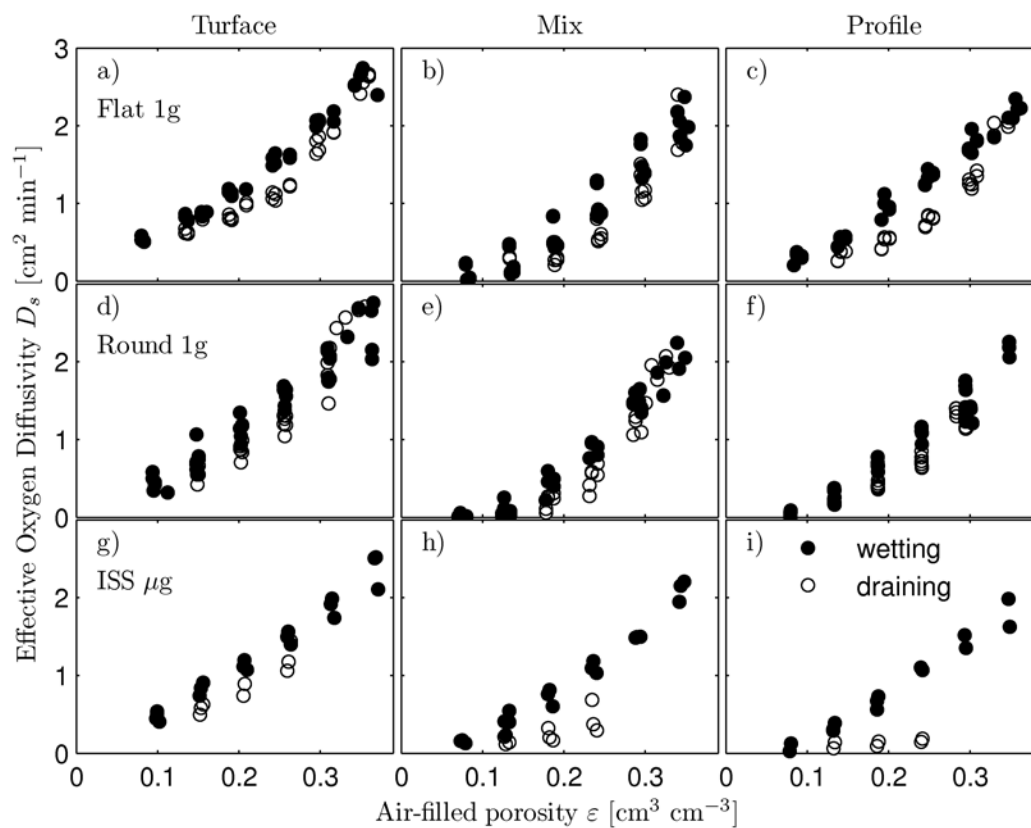
Fig. 3.4: Oxygen diffusion observations in three different particle-sized aggregate media: Turface, Profile and Mix. Top and center rows compare measurements at 1g collected in apparatuses with vertical extents of 1.9 cm (Flat) and 5 cm (Round), respectively, illustrating the influence of the vertical distribution of water in 1g with gravity. Bottom row shows measurements at μg on the ISS. Note the departure in Profile and Mix draining data.
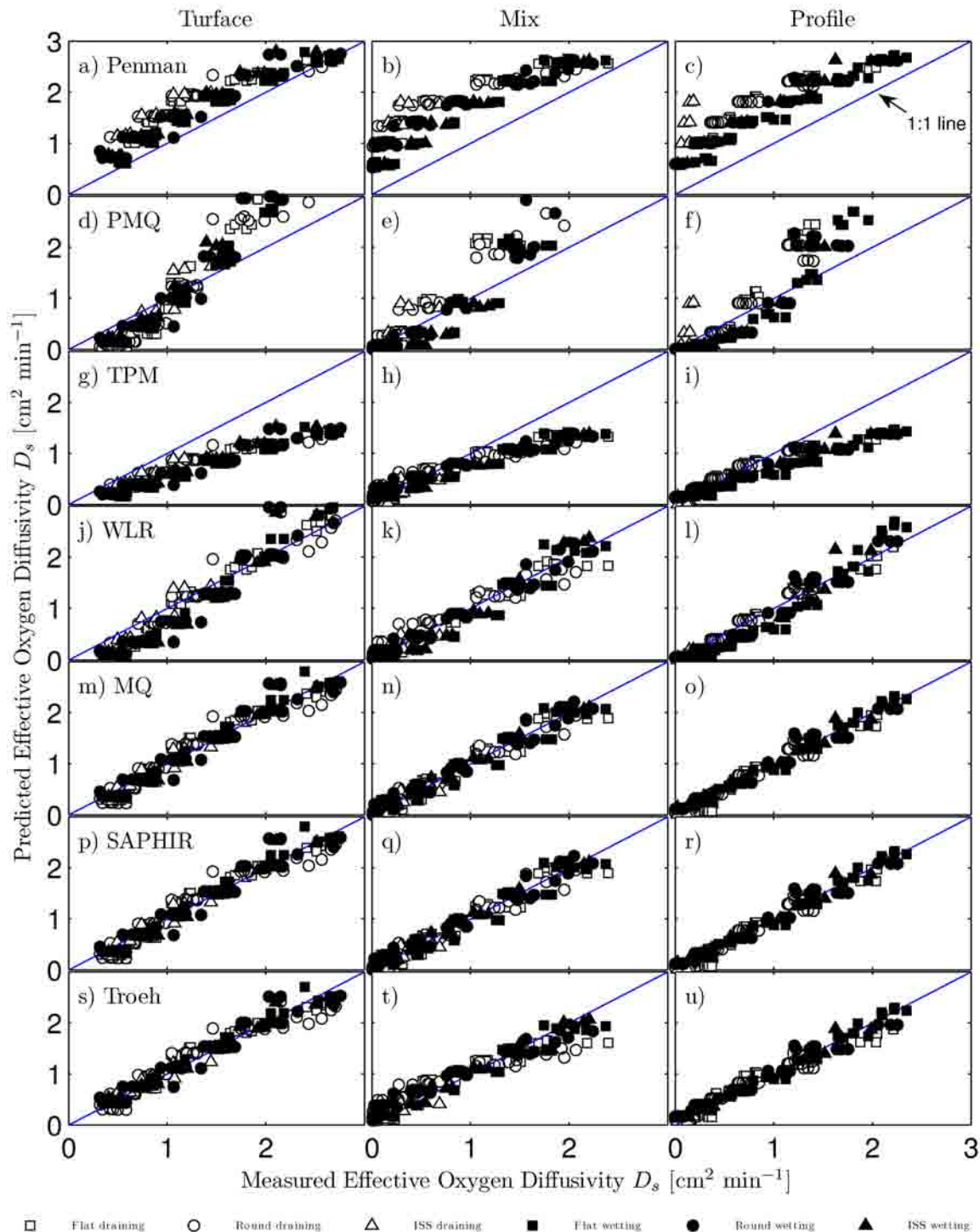
Fig. 3.5: Scatter-plot comparison of predicted and measured effective oxygen diffusivities in the Flat, Round and ISS treatments for draining and wetting conditions in the Turface, Mix and Profile media. Model predictions are: (a–c) Penman, (d–f) Penman-Millington and Quirk, (g–i) Three-Porosity Model, (m–o) Millington and Quirk, (p–r) SAPHIR and (s–u) Troeh gas diffusivity model (compare Table 3.1). Predicted diffusivities are given based on individually fitted parameterizations for the media, system and process (Table 3.3 and 3.4).
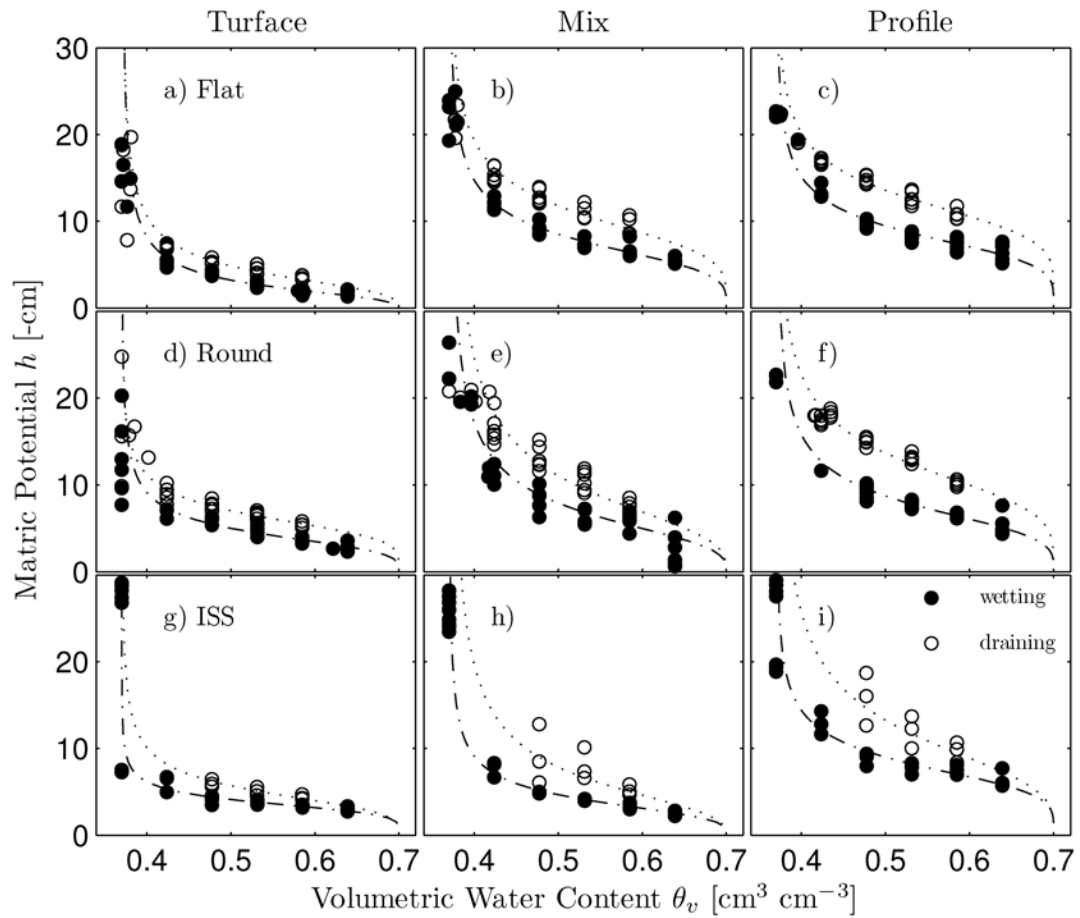
Fig. 3.6: Water retention observations in the Flat, Round and ISS measurements. Dotted and dash-dotted lines indicate the fitted van Genuchten model (Eq. [3.17]) to the draining and wetting observations, respectively.
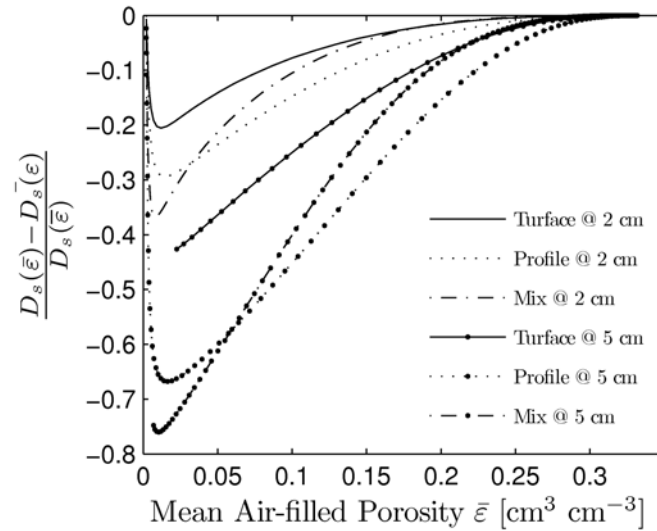
Fig. 3.7: Illustration of the relative error in modeled mean diffusivities $\overline{D_s(\varepsilon)}$ relative to the local diffusivity $D_s(\bar{\varepsilon})$ for samples of two vertical heights (2 cm and 5 cm), representing the Flat and Round cells, respectively. Estimates of the error were derived using Eq. [3.25] with terrestrial estimates of the van Genuchten water retention function for draining conditions and utilizing the SAPHIR diffusivity model with Flat cell derived parameter sets relative to the diffusivity at a constant air-filled porosity representing the mean.
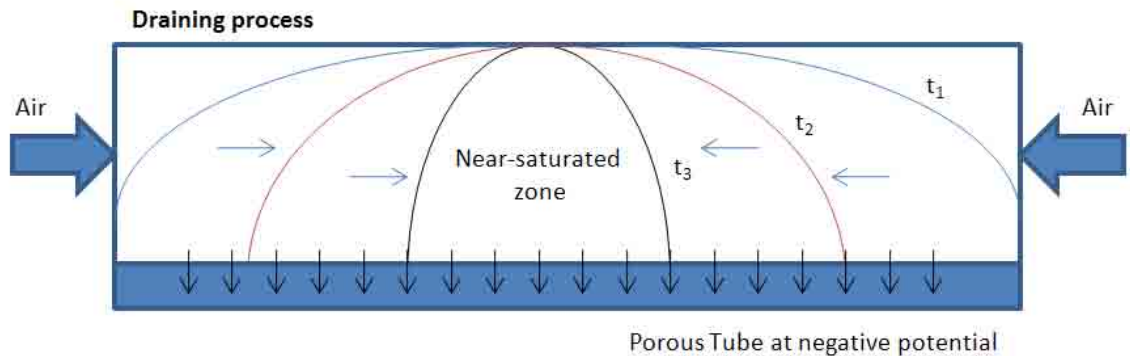
Fig. 3.8: Schematic showing the hypothesized explanation of reduced gas diffusivities measured in microgravity on the ISS. The water-content distribution suggests the draining process begins from the air-supply boundaries at each end. As the stepwise draining process continues, the progressively diminishing center region remains water filled, limiting the diffusive flux of oxygen from one side to the other. Note that only one half of the axisymmetric diffusion cell is shown.

CHAPTER 4

ON GRAVITY CONSIDERATIONS FOR OPTIMAL ROOT-ZONE FLUXES IN UNSATURATED POROUS MEDIA: FRAMEWORK AND CASE STUDIES [1]

4.1 Abstract

The modeling, designing and testing of root zones providing optimal supplies of plant needs is essential for reliable and resilient research-based bioregenerative life support systems that operate in partial- or microgravity. High root densities, limited volumes and gravity-induced changes in water content distributions remain central challenges for maintaining a favorable water/air-exchange balance. In this chapter, we i) discuss root-zone design considerations from a soil-physical standpoint, ii) suggest a stratified root-zone design amenable for imitating the more disperse microgravity liquid distribution in a gravitational environment, and iii) evaluate the effect of high root densities on the physical root-zone environment. In a first case study, we developed a unique root-zone system using stratified Ottawa sands where capillary driven saturation was maintained between 50 and 80 percent. The benefits of the root-zone design include maintaining more uniform water content and on-demand supply of resources within the porous-media profile compared with the dynamic range of water contents in conventional homogenous particle-sized medium designs in earth's gravity. In a second case study, we measured water-retention characteristics in Turface and Profile aggregates comparing bulk media and macroscopic rhizosphere properties. The macroscopic water-retention characteristics were unaffected at root-densities of up to 0.03 cm^3_{root} cm^{-3}_{soil}. However, we suggest an increasing underestimation of plant-available water is possible with increasing root densities. This will likely prove to be an important consideration for operation and management of restricted root zones where temporal changes of root-zone hydraulic properties should be included.

---

[1] The material for this chapter is part of a collaborative work with contributions by Scott B. Jones and Bruce Bugbee.

4.2 Introduction

Plant growth continues to be a key part of space exploration research motivated by the need to incorporate plants in any long term, bioregenerative life support system. While much research has been conducted in the areas of microgravity (μg) plant growth (Monje et al., 2003; Porterfield et al., 2003), the important issue of the plant-rooting environment and associated physical processes that govern the flow and distribution of fluids in porous media lacks a general framework that addresses different gravity environments for future space missions. With the current focus of the National Aeronautics and Space Administration (NASA) to look at Lunar and Martian outposts, there is a need to consider root systems that operate in partial gravity.

One of the major problems in previous microgravity plant research has been the lack of control and quantification of the growth-media-plant-fluid relations (Steinberg et al., 2002). Despite indications of altered liquid and gaseous fluxes in reduced gravity, there are currently no official guidelines or selection criteria for selecting plant growth media for microgravity. The presently favored growth media are mm-sized particles of baked clay (Steinberg and Poritz, 2005). Alternative soilless substrates like composted wheat straw (Gros et al., 2005) and porous tube nutrient delivery systems (Dreschel and Sager, 1989) are also being considered. The advantage of coarse-textured particulate porous media lies in the controllability of water content where pores drain readily after watering, providing ample air-filled pore space for gas exchange with the root tissues. The particulate media systems have the further advantages of water storage and control via the matrix in the case of system malfunction. However, under reduced gravity conditions, capillary forces are dominant, creating water distribution profiles and non-uniformities that are not observed on Earth (see Chapter 2; Jones and Or, 1999) and that could reduce gas exchange rates (Chau et al., 2005). Few space borne experiments have investigated water movement and control in μg, but none have investigated the region where gas exchange becomes the limiting factor for plant growth. The gas exchange in the root zone provides both oxygen supply and the removal of metabolic gases. Consequently, the importance of air-filled pores for vigorous plant growth has been emphasized by many researchers (for a review see: Gliński and Sępniewski, 1985). For example, Bunt (1988) suggested that while there is no optimal value of air-filled porosity, there is agreement that 10–25 percent is desirable. Some of

the uncertainty in quantifying optimal air-filled porosity is attributed to the variability in tolerance of different plant species to poor aeration, the effects of different environmental and management factors, and to the use of different methods of determining air-filled porosity. More importantly, while the air-filed porosity is a good descriptor of the storage of gases, it is primarily the diffusive gas-exchange rate along with the rate of respiration that determines the composition of the soil air. The rate of gas exchange, and in that capacity the gas diffusion coefficient, is therefore a more appropriate descriptor of soil aeration (Caron and Nkongolo, 1999), where Cook and Knight (2003) pointed out that it is highly unlikely that there is a single critical value to describe soil aeration.

The controllability of optimal root-zone conditions is further intricate for restricted root zones because of root densities that are typically 10 times higher than in containers in greenhouse grown plants, and 100 times greater than field grown plants. The successive demand for aeration and water per unit volume is therefore much larger than in conventional crop production. While terrestrial plant-growth media have been researched considerably in the past four decades (Rivire and Caron, 2001), the emphasis has been on characterizing the physical properties of different growth substrates (Milks et al., 1989), optimizing the proportions of these materials (Bunt, 1984) and managing irrigation (Rivire et al., 1990). Building on this research, the least limiting water range was proposed as a structural quality index that defines a range of soil water content within which plant growth is least limited by water potential, aeration, and mechanical resistance (da Silva and Kay, 1997; da Silva et al., 1994). However, much of this research has considered optimizing homogenous and isotropic media ignoring or explicitly accepting hydrostatic water content differences in the soil profile.

In reduced gravity, hydrostatic water content differences are reduced and hysteretic water content differences become more dominant (see Chapter 2). In this context, the question arises if homogenous porous media are the ideal root-zone design for reduced gravity and how root-zone performance in homogenous porous media can be evaluated in terrestrial gravity with respect to microgravity. Recent research by Henry et al. (2006) has considered non-uniform root zones that provide vertically more homogeneous conditions for root growth. The authors successfully used strata of increasingly finer particle sizes to homogenize the water content distribution in a soil column where the free-draining column was drip irrigated at the upper surface. Inherent in the de-

signs by Henry et al. (2006) as well as previous efforts at designing and managing optimized root zones was the assumption that hydraulic properties of the porous-media root zone are unaffected by roots. The question arises whether initial conditions used in the designs are altered with progressing root development. In particular, the questions stands if hydraulic properties of the root-zone media, largely determined through the pore-size distribution, undergo temporal changes as roots selectively occupy pores, reducing the overall porosity and altering the pore size distribution of the media. Through the physical elongation, radial expansion and exchanges with their immediate environment (i.e. water and mineral absorption, exudation of chemical compounds), roots are known to modify the soil physico-chemical conditions. Considerable research in root-adherent soil has shown increased bulk density in the immediate root vicinity (e.g. Whalley et al., 2004; Young, 1998), aggregation of soil particles due to biological exudates of roots and microbial colonies (Traore 2000) and changes in the hydrophilic and hydrophobic properties of the media (Hallett et al., 2003; Read et al., 2003). Most of the physical changes are concentrated around the root with for example bulk density changes decreasing exponentially with distance from the root (Dexter, 1987). Considering water retention characteristics, Whalley et al. (2005) studied differences between porous media adjacent to roots and bulk media. The authors concluded that rhizosphere media contained larger pores and tended to be drier at a given matric potential than bulk media. In contrast, research on the effects of increased bulk density due to compaction by Bruand and Cousin (1995) has shown that changes in the pore size distribution are primarily due to a decrease in the number of larger pores with resulting reductions in water retention primarily near saturation. Richard et al. (2001) and Assouline (2006) suggested further that compaction increases the amount of smaller pores with an related increase in water retention at low matric potentials. Because the pore size distribution and the resulting distribution of water so crucially determine fluxes of water, gases and nutrients to the roots, the water retention characteristic need to be quantified in light of increasing root densities to predict the long term viability of engineered root zones. Modifications of the porous-media rhizosphere by root penetration particularly need to be considered when multiple successive croppings could potentially compound the effects on porous-media hydraulic properties.

There is a lack of research combining flux-based root-zone characterization framing water-

content distributions in different gravity regimes and related hydraulic properties. Our aim was to analyze how terrestrial root zones can be developed to simulate the more homogenous water-content distribution in microgravity based on matric-potential driven water contents. For that purpose we designed a stratified root zone and studied (i) the water-retention properties of Ottawa sands, (ii) the hydrostatically driven water-content distribution in the stratified design and (iii) evaluated the improved root-zone performance on theoretic ground compared to a conventional homogenous porous-media root zone through liquid and gaseous flux potentials. We further aimed to analyze potential temporal changes to rhizosphere porous-media hydraulic properties. For that purpose we selected a course aggregated porous medium in two different particle sizes and studied (i) the bulk and rhizosphere water-retention characteristics using pea roots in partially restricted root zones and (ii) hypothesized on the effects of root-growth on the plant-available water and monitored water contents using electric, dielectric and heat-flux-based sensors.

4.3   Porous-Media Root-Zone Design Considerations

For plant hydration and nutrient delivery systems in micro- and partial- gravity, it is desirable to minimize the root volume, water use and nutrient application while retaining plant vigor and yield. The aim is to maintain adequate air-filled pore connectivity and water transfer rates to maximize the advantageous (usable) plant-rooting volume through optimization of the porous-media physical characteristics. The design optimization must balance the water transfer performance with the gas exchange penalty where the presence of plant roots and microbes and their requirements for liquid and gaseous content and fluxes pose an important dynamic component for media selection and characterization. The intensive growth conditions associated with the use of small containers and desirable high efficiency of growth which relies on gas exchange, further add to the complexity of the problem.

The water content θ_v and the gas content θ_a in porous media are intricately linked and may be described in terms of their volumes in porous media:

$$\theta_v = \frac{V_w}{V_t} = \frac{V_w + V_a - V_a}{V_t} = n - \theta_a \tag{4.1}$$

where V_w is the volume of water, V_a the gas-filled volume and V_t the total porous media volume. n is the porous-media porosity $\left(n = \dfrac{V_w + V_a}{V_t} \right)$. Looking ahead to Fig. 4.2, in gravity dominated environments, the gravity-driven distribution of water in homogenous porous media is non-uniform and non-linear, providing only a partially-optimized root zone profile. In capillarity dominated environments, the distribution of water is expected to be more disperse, providing, at least in terms of water content, the potential of choice of one optimally engineered porous media. However, along with the more uniform water content distribution comes the cost of having a root zone that is less forgiving. Because of the hydrostatic water content at Earth's gravity, a homogenous porous media is likely to be more forgiving (albeit less optimal) than in reduced gravity, providing a wider range of water contents in the root zone that roots may choose to occupy. This range is likely to be narrower at reduced gravity. Considering partial gravity, one may approach the optimization problem through vertical stratification using a combination of porous media sizes, thus simulating in part the more homogeneous distribution of water in the root zone. Of course, optimizing for an optimal water content distribution can only be part of the effort as water and gas fluxes as well as nutrient supplies to the roots are the primary resource determinants for the plant. It can be shown however that these fluxes are intricately linked to the water content distribution.

Because the water and gas fluxes depend on their respective contents, determining an optimal porous media to satisfy the root requirements, one may approach the problem by establishing a representative water content profile. The focus can then turn towards evaluating the gas and water movement through the profile. The efficiency of the system in maximizing water and gaseous fluxes is related to the restriction in water movement through the least saturated volume element and for the gas movement in the most saturated volume element. A further restriction to the fluxes may be in the water and gas consumption/production. One may use a modified Fick's law to describe the water and oxygen transport mechanisms in unsaturated porous media. Analytical solutions are presented to estimate both the fluxes that reach volume elements in the root zone and the fluxes entering the roots. For this, one may separate macro-fluxes, occurring between the supply source and distal media locations, and micro-fluxes, which occur in the nearby vicinity of plant roots similar to work of many researchers (e.g., Cook and Knight, 2003; De Willigen and van Noordwijk, 1984;

Gliński and Sępniewski, 1985).

Under the intensive growth conditions in constrained volumes, the assumption of steady-state fluxes is used to simplify the system under consideration. Where water contents near roots are maintained at a level such that hydraulic conductivity is not limiting water uptake by roots, virtual steady-state conditions exist. Lang and Gardner (1970) demonstrated this upper limit at which plant roots can maintain a given rate of water uptake: it occurs when the unsaturated hydraulic conductivity of the media in the vicinity of roots decreases more rapidly than the increase in the water potential gradient between the root surface and the bulk media. Gardner (1960) theorized that these gradients are small if the soil is not drier than -10 m$_{H2O}$. Experimental observations by Schmidhalter (1997) corroborated that significant gradients between the root and soil do not occur when pre-dawn soil matric potentials were lower than -2.6 m$_{H2O}$ in a silt-loam soil. The author measured gradients in maize and sunflower plants in the order of -20 to -70 m$_{H_2O}$ cm^{-1} under dry and water-stressed conditions. However, the study also suggested that plant species behave differently showing that gradients in wheat and barley were generally insignificant. This may partially be determined by the root/soil contact as illustrated in Fig. 4.1. For unsaturated soils, water films and menisci near the root provide supply of water to the root at low resistivities, while non-contact areas which are air-filled can provide gas exchange. With increasing root diameters this contact resistance increases faster compared to smaller diameter roots as water content decreases.

In this context, aggregated porous media, like Turface which are used in space greenhouses (Steinberg and Poritz, 2005), will tend to develop larger potential gradients between the soil and root. Because of larger particle sizes than most field soils, these media will have a faster increase in contact resistance with fewer contact points with the root and a more marked decrease in unsaturated hydraulic conductivity than typical field soils (Hsieh et al., 1972). Further, if roots are confined to a small volume, gradients are more likely to develop. Under the plant water potentials that result from a root-media gradient of up to -70 m$_{H2O}$, plant stomata close—reducing CO$_2$ uptake, and limiting cell expansion. On Earth, night periods allow the equilibration of water near the root surfaces with the bulk media, allowing cell expansion to recover. However, many microgravity experiments use longer light periods or constant illumination to correct for lower light levels (Bugbee and Salis-

bury, 1989), which with gradients of this size may significantly stunt plant growth.

The development of roots is further affected by environmental factors such as mechanical impedance, aeration, temperature, and availability of water and nutrients. While the mechanical impedance, water retention and aeration are functions of the texture and structure of the porous medium, the root distribution and architecture are partially determined by genetic factors and environmental stimuli and constraints. With the limited volumes of containers used in commercial plant production and space-greenhouse experiments, atypically-high root densities are induced that may result in temporal and spatial modifications of the physical root environment. Such modifications may counter the design of porous-media root zones under static conditions and would require the inclusion of predictive capabilities describing the temporal alterations in hydraulic behavior with the design considerations or the adjustment in the operation of such root zones.

4.3.1   Macroscopic Porous-Media Characterization

Fluxes in Porous-Media Root Zones

The transport of plant resources in porous medium including water and nutrients as well as gases can be cast in general terms using transport theory. Considering a one-dimensional root zone, one may supplement the differential form of the mass balance equation with a sink/source term describing uptake and release of resources by plant roots:

$$\frac{\partial \mu}{\partial t} = \frac{\partial v_z}{\partial z} - S_z(z,t) \tag{4.2}$$

where μ is the content (or energy potential) of the resource, z is the physical separation, v_z is the flux density and S_z is a distributed sink/source rate. The planar flux density can be defined using Fick's first law:

$$v_z = -D\frac{\partial \mu}{\partial t} \tag{4.3}$$

where D is the diffusivity (in the case of radial geometries describing fluxes to a cylindrical root, a

factor of $2\pi r$ is added). Combining [4.2] and [4.3] results in:

$$\frac{\partial \mu}{\partial t} = \frac{\partial}{\partial z}\left[-D\frac{\partial \mu}{\partial z} = \right] - S_z(z,t) \tag{4.4}$$

Eq. [4.4] can be used to predict the performance of the root zone. While notoriously hard to solve, solutions exist for specific conditions and parameterizations discussed below.

For steady-state diffusion $\left(\dfrac{\partial \mu}{\partial t} = 0\right)$ and assuming a constant diffusivity, Eq. [4.4] can be written as:

$$\frac{\partial^2 \mu}{\partial x^2} + \frac{S(z,t)}{D} = 0 \tag{4.5}$$

van Bavel (1951) presented a solution for Eq. [4.5] considering a constant and uniform source/sink in a porous media underlain by an impervious boundary at depth L (e.g., a water table for gaseous fluxes or an air-interface for liquid fluxes) and an ambient content (μ_0) at the surface. The boundary conditions are:

$$S = \text{const.} \quad \text{at} \quad 0 \leq x \leq L$$

$$\mu = \mu_0 \quad \text{at} \quad x = 0 \tag{4.6}$$

$$\frac{\partial \mu}{\partial x} = 0 \quad \text{at} \quad x = L$$

We may then integrate Eq. [4.5] twice and apply the boundary conditions. The solution for the content distribution in the porous-media profile is:

$$\mu(x) = \mu_0 + \frac{S}{D}\left(Lx - \frac{x^2}{2}\right) \tag{4.7}$$

The prediction of content distributions as a function of path length for steady-state conditions using Eq. [4.7] provides a framework for estimating macro and subsequent micro fluxes from the source boundary to the plant root. However, the assumed constant diffusivity in Eq. [4.7] is not an accurate description of diffusivity profiles that are determined by content profiles as well as source and sink rates and distributions. One may then revert to using an effective diffusivity integrating over the domain between source and point-of-interest dividing the domain into infinitesimal small layers with

constant diffusivity. The effective diffusivity for such a layered non-uniform porous-media profile with liquid and gaseous fluxes perpendicular to the layering can be estimated based on harmonic averaging of individual diffusivities of each layer:

$$D_{\text{eff}} = \frac{\displaystyle\sum_{i=1}^{I} \Delta z_i}{\displaystyle\sum_{i=1}^{I} \frac{\Delta z_i}{D_i^s(\mu_i)}} \tag{4.8}$$

where D_{eff} is the effective diffusivity for the entire domain. $D_i(\mu_i)$ represents the diffusivity of discrete layers i of thickness Δz_i and content μ, and I is the total number of layers within the domain.

Analytical Descriptions and Parameterizations of Diffusivities and Root Fluxes

For liquid fluxes in porous media, Eq. [4.3] is identified as the Buckingham-Darcy law in the absence of gravity and Eq. [4.4] is identified as the Richards (1931) equation where the (always positive) porous-media liquid diffusivity for unsaturated conditions is given as:

$$D_s^l = K \frac{\partial h}{\partial \theta} \tag{4.9}$$

K denotes the hydraulic conductivity, h the matric potential describing the surface interactions between water and porous-media solids, and θ is the volumetric water content. $\frac{\partial h}{\partial \theta}$ is the inverse of the slope of the soil water characteristic curve ($\theta(h)$) describing the physical environment consisting of volumes of air, liquid and solids in terms of the energy status of water in the media as a functional relationship between water content and matric potential. Several parameterizations of the soil water characteristic and the unsaturated hydraulic conductivity are known. In order to enable a compact formulation we introduce the normalized water content (i.e. saturation index):

$$\Theta = \frac{\theta - \theta_r}{\theta_s - \theta_r} \tag{4.10}$$

where θ_s is the saturated volumetric water content and θ_r is the residual volumetric water content, respectively. The soil water characteristic curve may then be parameterized using the van Genuchten

(1980) relationship:

$$\Theta(h) = \left[\frac{1}{1 + (\alpha |\psi|)^n} \right]^m \tag{4.11}$$

where α, m and n are empirical parameters. For well-sorted sand filters, Hazen (1911) developed the following empirical model to predict the saturated hydraulic conductivity in cm s^{-1}:

$$K_s = 100 \cdot d_{10}^2 \tag{4.12}$$

where d_{10} is the particle size in cm for which ten percent of the soil is finer. The unsaturated hydraulic conductivity as a function of water content in connection with the statistical pore-size distribution model of Mualem (1976) may then be expressed in terms of matric potential using parameters of the van Genuchten (1980) model (Eq. [4.11]):

$$K(h) = K_s \frac{\left[\left(1 - (\alpha |h|)^{n-1}\right) \left[1 + (\alpha |h|)^n \right]^m \right]^2}{\left[1 + (\alpha |h|)^n \right]^{\frac{m}{2}}} \tag{4.13}$$

Frequently the simplification $m = 1 - \frac{1}{n}$ is used. Both the water retention characteristic and the unsaturated hydraulic conductivity function are hysteretic, meaning that a set of parameters describing the primary, process dependent (i.e. draining and wetting) functions are needed for the closure of the model.

Several forms of the water uptake function $S(z,t)$ exist. Here we give a conceptually simple form. The uptake integrated over the root zone equals the potential transpiration rate governed by atmospheric conditions under optimal water conditions (i.e. not limited). Feddes et al. (1978) described S as a function of matric potential assuming a homogenous root distribution according to:

$$S(h) = \beta(h) S_p \tag{4.14}$$

where $\beta(h)$ is a dimensionless function of matric potential and S_p is the potential water uptake by roots. Under non-optimal conditions (i.e. water or solute stress), S_p is reduced by means of $\beta(h)$. A simple shape of $\beta(h)$ as a trapezoid was given by Feddes et al. (1978). The values of the input variables for $\beta(h)$ are crop specific and can be found in the literature (e.g. Wesseling et al., 1991).

Diffusion is the dominant component for gaseous fluxes within a porous media having negligible air pressure gradients (Collin and Rasmuson, 1988). The driving force for diffusion is a gas concentration or partial pressure gradient. Such gradients develop around plant roots as O_2 is being consumed for respiration and CO_2 and other metabolic gases are released. The effective gas diffusion flux density (v_z) in air may be written according to Eq. [4.3] as:

$$v_z = -D^a \frac{dc_g}{dx}$$

(4.15)

where D_a is the diffusion coefficient in free air, and c_g is the gas concentration. The apparent diffusion coefficient D_s^g in a porous medium is lower than in air due to limited and tortuous pathways in the presence of water filled pores and solid particles. Moldrup et al. (2000) derived an expression for the apparent gas diffusion coefficient D_s^g as a function of air-filled pore space in sieved and repacked porous media given as:

$$D_s^g = D^a \theta_a \frac{\theta_a^\delta}{n}$$

(4.16)

where n is the porosity and θ_a is the gas-filled porosity of the medium. A fitting exponent $\delta = 1.5$ was found to be a good approximation for most unstructured media (Moldrup et al., 2000).

4.3.2 Water-Content Distributions in Planetary- and Zero-Gravity

The previous relationships relating fluxes of water and gases to plant roots as a function of media parameters (porosity, hydraulic conductivity, water retention characteristic) can be used to design a porous medium. The intricate dependency on the liquid distribution requires different solutions for varying gravity regimes, where gravity and hysteresis determine the spatial and temporal distribution of water. Additional considerations concern the water supply strategies including the location and operation of sources and sinks as well as the balancing of opposing processes (e.g. while lunar gravity may call for gravel-sized media for an optimal liquid distribution, root establishment and cation exchange capacity likely would make particles of this size prohibitive). The capillary rise equation can be used to predict the liquid distribution based on the height of rise h as

a function of the radius of a capillary tube *r* which can be related to the porous-media pore size:

$$h = \frac{2\sigma\cos(\gamma)}{\rho_w g r} \qquad (4.17)$$

where σ is the surface tension of liquid, γ is the contact angle of the solid-liquid interface, ρ_w is the density of liquid and *g* is the gravitational acceleration. When exposing porous media to Earth (1g), Martian (0.38g), Lunar (0.165g) or zero-gravity (0g), the capillary rise scales with the reciprocal gravitational force according to Eq. [4.17]. One can then use the parameterized soil water characteristic to predict the steady-state distribution of water for given boundary conditions. Figure 4.2 shows the distribution of water at four gravity regimes illustrating the very different distributions of water in a 10 cm tall root zone at identical management (i.e. average hydraulic potential). Note that the average water content is not identical for the distributions despite equal average hydraulic potentials.

Case Studies

4.4 Terrestrial Simulation of More Uniform Water-Content Distributions Using a Stratified Root Zone

4.4.1 Motivation

Testing designed root zones intended for plant growth in microgravity under terrestrial condition as well as providing guidelines for media selection at planetary gravities would greatly benefit from an experimental test bed that could simulate reduced-gravity water content distributions. For this, we propose to combine the method of Jones and Or (1998) with a novel terrestrial approach for maintaining vertically more uniform water contents in porous-media root zones using stratified media to offset the effects of gravity similar to Henry et al. (2006). In Jones and Or (1998), the authors formulated an optimization problem leading to media selection based on design fluxes. The authors combined media properties in terms of hydraulic and structural parameters with physiological information (e.g., optimal oxygen concentration and water content) to express gas and liquid fluxes to

plant roots for a homogeneous root-zone. To provide a test bed, we therefore propose to abandon the textural homogeneity of the porous media in order to create a more homogenous water content distribution following Henry et al. (2006). In the authors approach, differing grades of Ottawa sands provided variations in particle and pore sizes related to the capillary rise or energy of water held in the porous media Eq. [4.17]. The authors used strata of increasingly finer particle sizes create a more uniform water-content distribution in a sand column where the free-draining column was drip irrigated at the upper surface and drained with a hanging 7 cm fiberglass wick at the bottom outlet. Problems arose when water build up in the strata (i.e., above the soil water content discontinuities) because of disparities in the matric potentials, requiring more positive pressure potentials before water moved into the next underlying stratum. This problem can be diverted by reversing the direction of irrigation where water is drawn upward against gravity by capillary forces. Looking ahead to Fig. 4.5, a porous media design based on the wetting water retention curves (water is drawn upward by capillary action from a free water surface) of sands can be designed. Each curve associated with a different particle size distribution provides a guide for stratifying depths based on hydrostatic conditions.

4.4.2 Materials and Methods

Porous Media

We used Ottawa sands ($\rho_s = 2.64$ g cm^{-3}, 1:1 aspect ratio) with varying particle sizes obtained from the following sources: 20–30 grit (Coarse), 20117-088 (VWR, West Chester, PA); 30-40 grit (Medium), EM-SX0075-3 (VWR, West Chester, PA); 40-50 grit (Fine), 50 grit Wedron sand (Cinder Co., Lindon, UT). To estimate the water retention characteristics of the sands, paired measurements of matric potential and water content were carried out in 1 cm tall, 2.5 cm i.d. cylindrical cells described in Chapter 2.

Experimental Setup and Hydration

We designed a column (25 cm tall, 10 cm inner diameter) that allowed the establishment and maintenance of a shallow saturated zone at the bottom of the root zone through a small (>0.4 mm i.d.)

port using a Mariotte device. The Mariotte device provided on demand replenishment of water while maintaining a constant hydraulic potential distribution in the column under steady-state conditions. Fig. 4.3 shows an open-faced (for illustrative purposes only) root-zone column with possible sensor placements for monitoring water content and electrical conductivity (not used in this study).

Experiments were conducted under monitored environmental conditions in a greenhouse at the Crop Physiology Laboratory at Utah State University, Logan, UT. Six instrumented root-zone columns were prepared with uniformly packed strata. To assure uniformity, mixing and packing of media for each stratum was conducted slightly wet to prevent particle size segregation (Lebron and Robinson, 2003).

Hydration of the media was maintained on-demand using individual Mariotte devices for each column. Water use was monitored hourly by suction (negative pressure) measurements in the airspace of the Mariotte devices, corresponding to the height of water in each device.Pressures were monitored using differential pressure transducers (PX40-15G5V, Omega Engineering, Stamford, CT). Water lost from each Mariotte device provided an indirect measure of water use. Evapotranspiration was determined by taking the difference in the suction between two consecutive hours and converting the value to mm h^{-1}. Pan evaporation was estimated in a similar fashion using an additional column with an open water surface.

4.4.3 Stratified Root-Zone Results and Discussion

In this subsection, we present measurements and design parameters leading to the assembly of the stratified root zone. We argue for the design effectiveness based on predicted distributions of water- and air-filled pores with subsequent diffusivities and propose a design-effectiveness descriptor in the ratio of effective gaseous and liquid diffusivities.

Water-Retention-Based Media Stratification

Water retention characteristics for the Ottawa-sand particle-size classes are depicted in Fig. 4.4 with parameterizations of the van Genuchten (1980) model (Eq. [4.11]) given in Table 4.1. Fitted saturated water contents θ_s and the parameters α, describing the air-entry value, compared well to estimates by Schroth et al. (1996) which were used in the root-zone design by Henry et al. (2006).

The fitting parameter *n* for the primary draining water-retention curves, however, differed from the estimates reported in Schroth et al. (1996). This may partially be attributable to the different source for the sands, where the lower *n* values indicate a wider pore-size distribution for the sands used in this and the Henry et al. (2006) study compared to sands tested by Schroth et al. (1996) at identical upper and lower sieve boundaries (i.e. mesh sizes). Using the assumption of a 25 cm tall column at hydrostatic equilibrium under wetting conditions, layers of Coarse and Medium sands and mixtures thereof were found appropriate for maintaining the desired water content range. To obtain media with suitable retention characteristics, mixtures of the media were prepared for the use in two strata (2 and 4). Indicated mixtures are given as a mass fraction of the constituents. In stratifying the Ottawa sand classes, the water content distribution was optimized based on the wetting water retention curves. Strata boundaries were chosen to retain saturation between 50 and 85 percent (shaded area in Fig. 4.5). In Fig. 4.5, from stratum 1 (Coarse) at the bottom between 0 and 6.75 cm a water content between 0.34 and 0.17 cm^3 cm^{-3} is predicted. The next stratum up (2:1 mix of Coarse and Medium) shows increased water content back up to 0.26 cm^3 cm^{-3} at the interface with stratum 1 and decreasing again to 0.17 cm^3 cm^{-3} at its top interface where it again transitions in stratum 3 (Medium) back up to 0.26 cm^3 cm^{-3} and so on. A similar approach could be applied to a different gravity environment using the capillary rise principle (Eq. [4.17]) to make inferences about the effect of Lunar or Martian gravity on the water distribution in a given porous medium.

Predicted Root-Zone Performance and Advantages over Conventional Designs

Fig. 4.6 shows predicted water-content distributions and related liquid and gaseous transport properties comparing the stratified with a homogenous porous-media root-zone design. For purposes of comparison, Medium Ottawa sand was chosen as a representative conventional design. Based on the water content distributions estimated using Eq. [4.16] with parameters listed in Table 4.1 shown in Fig. 4.6a, the unsaturated hydraulic conductivities (Fig. 4.6b) and liquid diffusivities (Fig. 4.6c) were predicted using Eq. [4.13] and [4.9], respectively. For the estimation of the unsaturated hydraulic conductivities, we estimated the saturated hydraulic conductivities using Eq. [4.12]

with effective particle size diameters d_{10}= (0.707, 0.56, 0.42 and 0.285) mm, for strata 1 through 4, respectively. In Fig. 4.6d we depict gaseous diffusivities estimated using Eq. [4.16].

Compared to the homogenous medium design, unsaturated hydraulic conductivities in the stratified media are equal or higher with exception of stratum 2. Notably, the unsaturated hydraulic conductivity in the topmost stratum (4) is significantly higher than in the homogenous medium. The benefits of that are evidenced in the liquid diffusivities where the achieved higher diffusivities in the topmost layer functionally outweighs the reduction in diffusivities in the lower strata compared to the homogenous medium. Concerning the gaseous diffusivity, the stratified media realizes higher diffusivities in the lower strata at the expense of lower diffusivities in the topmost stratum. More importantly, the balance of antipodal liquid and gaseous diffusivities providing optimal fluxes of root resources determines root health and plant vigor. For that it is further imperative to include information on pervious and impervious boundaries to the root zone allowing exchange of gases with the atmosphere and supply of liquids. For the root zone under consideration, the topmost boundary is pervious to gases while the bottommost boundary is pervious to liquids. As a result, the direction of liquid fluxes in the media is upward while the direction of gaseous fluxes are downward given a consumptive use that establishes a gradient with respect to concentrations at the pervious supply boundaries.

Because these fluxes to a given volume element in the root zone are an integral process limited by the lowest diffusivity along the pathway, comparing diffusivities for a volume element as descriptors of design effectiveness alone would be inappropriate. As a better descriptor we suggest the ratio of effective diffusivities of the gaseous and liquid phase. Using Eq. [4.16] we may estimate the vertical distribution of effective (or apparent) diffusivities for the gaseous and liquid phases where the ratio attempts to describe the balance between the two. The ratio descriptor is similar to the gas diffusion fingerprint (GDF) plot suggested by Moldrup et al. (2003). The authors used the incremental relative change (IRC) in gaseous diffusivity with respect to a change in air-filled porosity (i.e. change in water content) as a descriptor, where high IRC values at a given matric potential indicate an optimal aeration potential (i.e. suggesting a high connectivity of the air-filled pore space). We feel that the change in liquid diffusivities is more descriptive than the

change in water content in relation to the IRC in gaseous diffusivities; including information on connected water-filled pathways along with gas-filled pathways. In addition, the use of effective diffusivities allows for root-zone design effectiveness evaluations with respect to path lengths to supply locations not feasible when using diffusivities alone. In the case of multiple supply location and multi-domain geometries, the ratio of effective diffusivities may easily be generalized as the superposition of effective diffusivities for each volume element with respect to each supply source:

$$S_k = \frac{\sum_{i=1}^{I} D^s_{g\,\mathrm{eff}\,k,i}}{\sum_{j=1}^{J} D^w_{g\,\mathrm{eff}\,k,j}} \tag{4.18}$$

where S_k is the ratio descriptor for the kth volume element with the subscripts i and j referencing the gaseous and liquid supply sources, respectively. Care needs to be taken however in providing an optimal range of values for the ratio because root demands likely vary among species and microbial communities likely pose dynamic demands with complex feedbacks that may be spatially distributed and are difficult to predict in the scope of this chapter. It is further important to remember that plants are quite adaptable to root-zone conditions making a single optimal value for the ratio unlikely.

The ratio of effective diffusivities for the root-zone in Fig. 4.5 is shown in Fig. 4.6e comparing the stratified root-zone with the homogenous medium design. In both cases, low values characterize the bottommost and topmost volume elements of the root zone. For the bottommost volume elements, the ratio is close to zero because of low effective gaseous diffusivities with respect to high effective liquid diffusivities indicating that gas exchange may be limiting in this region. In contrast, for the topmost volume elements, the ratio is close to zero because of high effective gaseous diffusivities with respect to low effective liquid diffusivities indicating that hydration may be limiting in this region. High values of the ratio descriptor are attained in the center of the root zone suggesting that balanced effective gaseous and liquid diffusivities characterize this region. Comparing the stratified root zone with the homogenous root zone, it is notable that the region of high ratio descriptor is extended for the stratified design suggestive of a more optimal distribution of usable porous media for root exploration compared to a conventional homogenous-medium design.

Verification of the Water Content Distribution

Fig. 4.7 depicts gravimetrically-determined water contents sampled at the end of the experiment in three columns. water contents shown are integrative values over given depth intervals and were determined using sampled gravimetric water contents. Gravimetric water contents were used to estimate the volumetric water contents using pre-determined average bulk densities ρ_b=(1.75, 1.72, 1.46, 1.55) g cm^{-3} for strata 1-4, respectively. In cases where samples spanned a strata interface, a weighted bulk density was used. In Fig. 4.7, water contents were over-predicted for stratum 1 with the exception of the bottommost samples which exhibited water contents exceeding the saturated water content of the Coarse sand. For these samples, water contents were likely higher due to sampling in the saturated layer with collection of excess water. In contrast, reduced water contents compared to predicted values in the Coarse sand above the water table may in part be attributable to a loss of water during sampling caused by the dispersion of particles and accompanied loss of water holding capacity which is more perceptible in the Coarse sand than in the finer and wider pore-size distribution sands used in strata 2–4. Sampled water contents in strata 2 and 3 generally agreed well with predicted water contents. Water contents in Stratum 4 showed inconsistent results, but remained within the desired water content range (shaded area in Fig. 4.7) for the height interval corresponding to the predicted water content.

The measured water-content distribution in Fig. 4.7 reflects the assumed hydrostatic distribution. With increasing evapotranspiration, however, the assumed water content profile may only be maintained up to some threshold. This threshold is reached when the water extraction rate exceeds the resupply rate at any given time and vertical position along the transport pathway. In that case, water contents, primarily at the upper strata interface, may be reduced resulting in a local reduction in unsaturated hydraulic conductivity further reducing the rate of water resupply. If the water demand is reduced, and ample time is given for recovery (e.g. during dark periods), the system can recover and re-establish equilibrium conditions. If however, the demand continuously outstrips the supply, a condition can be created where the system cannot stabilize itself, and can result in a hydraulic disconnect. This disconnect would likely first affect the interface between strata 3 and 4, resulting in the draining of strata four. The plant may then continue to extract water from the

underlying strata if an existing root system allows. If the demand continues to grow, the establishment of disconnects may progress downward, but at increasingly higher thresholds. The advantage of the stratified root zone compared to a homogenous medium design is found in the reduction in thresholds for the failure in steady-state conditions because of the hypothetically more uniform distribution of roots in such a system with the accompanied distribution of uptake, reducing the probability of failure by reducing the demand per volume element in the root zone.

4.5 Bulk and Rhizosphere Water-Retention Properties

4.5.1 Motivation

Root proliferation may modify porous-media properties by altering the quantity and size distribution of pores controlling the water-retention characteristic and hydraulic conductivity. Therefore it seems likely that increasing root density should decrease the total porosity (or saturated water content) and may alter the slope and shape of the water-retention characteristic curve. As a consequence, water management based on macroscopic criteria (i.e. management set points using the water-retention characteristic) may require temporal adjustments. While field-grown plants result in root densities in the order of 1–2 percent of the porous media volume (e.g. Fageria et al., 2006), containerized plant growth in coarse aggregate media may result in significantly higher root volumes. For example, Steinberg et al. (2005) suggested a 10 percent change in available macroporosity for plants grown in Turface. At such high root volumes, water held in the roots may further contribute to an overestimation of water contents with current sensing techniques providing an integral signal.

4.5.2 Materials and Methods

Porous Media

We used coarse aggregate media (Profile Products, Buffalo Grove, IL) sieved to particle size fractions of 0.25–1 mm (Profile) and 1–2 mm (Turface). The particle density of the aggregates is 2.5 g cm^{-3}. These media have been widely used in microgravity plant experiments (Levine et al., 2003; Steinberg and Henninger, 1997; Stutte et al., 2005) and are expected to be used in future

life support applications. The aggregates are stable, have moderate surface area for nutrient storage and exhibit two distinct pore spaces, inter-aggregate and intra-aggregate pores. Only the inter-aggregate pore retention characteristics, particularly in the optimal range for liquid and gas supply of 0 to -25 cm_{H_2O} matric potential, are of interest for this study. The porous-media water retention characteristics for Profile and Turface have been parameterized in Chapter 2 and by Steinberg and Poritz (2005).

Plant Materials

EarliGreen pea plants (*Pisum sativum*), a dwarf variety, (obtained from the USU Crop Physiology Laboratory, Logan, UT) were used in this work. The plants exhibit a fast life cycle (24 days to first flower), short height, and excellent growth in low light (Crop Physiology Laboratory at Utah State University). Seed germination was initiated by hydrating the refrigerated seeds in water for 12 hours and then planting the seeds in a 4-noded quad plus center node directly into the media at 1 cm depth (i.e. having a 1-2 mm overburden). Germination rates were 100 percent after 5-6 days.

Water Retention and Root Measurements

Experiments were conducted in a temperature-controlled room with temperatures ranging from 26-28°C with a relative humidity ranging from 21-28 percent. Fig. 4.8 shows the setup with three of six samples using Buchner funnels (Pyrex 36060, Corning Life Sciences, Lowell, MA; 350 ml capacity, 8.0 cm disc diameter) for the root chamber. Porous-media samples were packed under tamping to a height of ≈ 3 cm at a mean bulk density of 0.68 g cm^{-3} on top of the fritted porous plates (pore size 4-5.5 μm). Hydration was achieved on-demand using a single Mariotte bottle connected to the porous plates which formed the interface to the porous medium. Hydraulic potentials were set to 0 cm_{H_2O} at the porous plate with capillary action drawing water into the media. Lighting was achieved with four cool-white fluorescent lights with a light intensity of 105 μmol$_{photons}$ m^{-2} s^{-1} at ≈ 15 cm below the light source. The light period was 16 hours. Plants were grown for two trials (i.e., in Turface and Profile) for 28 days past planting. The rooting volume was not restrained vertically (i.e. allowed to expand with root proliferation). The Buchner funnels were initially covered with Parafilm to minimize evaporative water losses during the germination state

with a small hole (> 0.5 mm) allowing for pressure equilibrium with the atmosphere. Nutrients (at a low concentration to avoid osmotic potentials) were applied in liquid form on days 7 and 18 using 2 ml of premixed plant-food (0.02% N, 0.02% P, 0.02% K; Pour and Feed, Scotts Miracle Grow, Marysville, OH) directly to the porous media.

Water retention characteristics in the six samples were determined with an automated method using the fritted porous plates connected to a precision peristaltic pump (KDS 230, KD Scientific, Holliston, MA). Fast responding pressure transducers (PX40-15G5V, Omega Engineering, Stamford, CT) installed horizontally in line between the funnels and the pump measured the hydraulic potential, where the height of the fritted porous plate corresponded to the midpoint of the transducer membranes (i.e., measuring hydraulic potentials as the negative "tube pressure" with reference to the porous plate). Water-retention measurements were conducted immediately before seed planting and repeated every seven days thereafter. To minimize water uptake by the plant and evaporation during measurements, shoots were shielded from light and covered with a plastic bag. Measurements started at a matric potential of -30 cm_{H_2O} (i.e. referencing water content to the macropore residual water content θ_r=0.37 cm^3 cm^{-3}) with the pump adding fixed volumes (5 ml) in multiple steps (wetting). Upon reaching approximate satiation, the direction of pumping was reversed until a matric potential of -30 cm_{H_2O} (draining) was attained. Static equilibrium conditions were attained after each pumping step before proceeding. Water contents at each step were determined from the induced changes in water volumes with the known porosity.

Plants were harvested after 29 days to determine the mass of roots and shoots. The root fresh mass was measured after careful removal of adhering particles through washing and rinsing and separation of roots and shoots. Dry mass of roots and shoots was determined after oven drying at 65°C for 48 hours. Root distributions were visually evaluated.

4.5.3   Water-Retention Results and Discussion

Table 4.2 lists root and shoot properties at 29 days after planting. The mean root-volume fractions relative to the total volume were 0.016 and 0.03 cm$^3_{root}$ cm$^{-3}_{soil}$ for the Profile and Turface treatments, respectively. Considering only the macro-pore volume, mean root fractions were 0.041

and 0.076 $\mathrm{cm}^3_{root}\ \mathrm{cm}^{-3}_{macropore}$ for Profile and Turface treatments, respectively.

Measured hydraulic potentials in the root chambers were corrected for hydrostatic differences in the media by shifting the readings to represent the matric potential in the center of the sample. Fig. 4.9 compares obtained water-retention observations for the bulk media collected before seed planting and rhizosphere media collected at day 28 for Profile (a) and Turface (b), respectively. Also shown are the predicted water-retention characteristics using the van Genuchten model (Eq. [4.11]) with parameters from Chapter 2. Fitted parameters α, n and θ_s were determined using a non-linear least squares approach with the Levenberg-Marquardt optimization method for Eq. [4.11] to the observations of water content and matric potential while keeping θ_r fixed at 0.37 $\mathrm{cm}^3\ \mathrm{cm}^{-3}$. Fitting was implemented with the "lsqcurvefit" function in the Matlab Optimization Toolbox version 3.0.2 (Mathworks Inc., Natick, MA). Table 4.3 lists the fitted parameters.

Water retention characteristics for the bulk and rhizosphere media were similar for both the Profile and Turface media. Parameters α, inversely related to the air-entry potential, were almost identical between bulk and rhizosphere estimates with exception of Profile at wetting conditions where α is larger suggesting a decrease in air-entry pressure. Parameters n, describing the slope of the retention curve, were generally larger for the rhizosphere estimates with exception of Turface at draining conditions where n was lower. However, differences in n were not significant, indicated by the overlapping 95 percent confidence intervals for the estimates. Similarly, the difference in α was not significant considering the 95 percent confidence interval for the estimate in Chapter 2. Further, estimates for the saturated water content θ_s were not significantly different between bulk and rhizosphere treatments.

Root volumes increased vertically with a mean height in the root chamber of 3.2 cm for Profile and 3.3 cm for Turface at day 29. The increase in height corresponds approximately to the developed root volume suggesting that root development resulted in an equivalent decrease in bulk density with an overall increase in pore sizes now occupied by roots. However, visual observation of the rooting system revealed that a large quantity of roots developed at the porous plate interface with a higher root density in the medium immediately above the porous plate. For plant development this suggests that water was limiting in the media. For the water retention characterization it suggests that a

significant part of the root proliferation did not take place in the mediums pore space and therefore a measurable signature suggestive of a change in rhizosphere water-retention characteristics was not observed at this rooting density.

Hypothesized Root-Induced Pore Volume Changes

The physical characteristics of the porous media are crucial design parameters because they determine the physical aspects of root functions and resource supplies. If used as a design characterization for matric-suction based root-zone hydration systems, the modifications of the porous-media rhizosphere need to be considered, particularly, when multiple successive plantings compound the effects on porous-media hydraulic properties. In addition to changes in pore-size distributions primarily affecting the function of optimally designed root zones, changes in overall pore volume affecting the monitoring of root zones need to be considered. Of these, water content measurements are critical for the accurate determination of plant-available water and the estimation of freely available ions. Indirect volume-based water content determinations fail to separate between water held in the porous media and water held in the roots. For example, Gerke and Kuchenbuch (2007) measured water held inside the roots and found that up to 20 percent of the total soil water content can be in the roots for field grown maize at high root densities. Estimates based on the dielectric properties (e.g. time domain reflectometry) will fail to make that distinction and prove problematic because of their integrative signal (Mojid and Cho, 2004). Estimates based on electrical properties (e.g. electrical resistivity imaging), suffering from the equivalency problem, will also fail to make that distinction for fresh roots, but recent research has shown that older roots may be distinguishable from fresh roots by their much higher electrical resistivity (Hagrey, 2007). Estimates based on the measurement of heat capacity (e.g., heat-pulse sensors) may also be unable to distinguish water held in roots from water held in pores. In most cases then, plant available water will likely be overestimated if root water is not considered.

For the change in porosity with root proliferation we consider two scenarios:

i) Restricted Root Zone

If the root-zone volume is restricted, the total volume with roots V_2 equals the total volume of the bulk media V_1:

$$V_2 = V_1 \tag{4.19}$$

$$V_{\phi2} = V_{\phi1} - V_r \tag{4.20}$$

where V_r is the root volume and V_ϕ is the pore volume with the indices 1 and 2 describing the case without roots and with roots, respectively. It may be speculated that the reduction in pore volume would likely shift the pore size distribution to smaller pore sizes as roots preferentially occupy larger pores.

ii) Unrestricted Root Zone

If the root-zone volume is allowed to expand, the total volume with roots will increase compared to the total volume of the bulk media V_1 according to:

$$V_2 = V_1 + \kappa V_r \tag{4.21}$$

$$V_{\phi2} = V_{\phi1} - (1-\kappa)V_r \tag{4.22}$$

Part of the roots will occupy existing pore space while part of the root expansion will lead to an increase in total volume. The factor κ $(0 \leq \kappa \leq 1)$, defined as:

$$\kappa = \frac{V_2 - V_1}{V_r} \tag{4.23}$$

scales the proportional occupation of existing pore space $V_{\phi1}$ to newly created pore space by expansion. Again, the reduction in pore space will likely shift the pore size distribution to smaller pore sizes, but may be less pronounced than in the restricted root-zone case.

It can easily be shown that case 1 is a special condition of case 2 with $\kappa = 0$. For a given media with an initial bulk density ρ_{b1}, the introduction of roots would decrease the bulk density to a value

ρ_{b2} because of the change in total Volume. The saturated water content of the rhizosphere media is then directly related to the saturated water content of the bulk media and the bulk densities:

$$\theta_{s2} = \theta_{s1} \frac{(V_{\phi1} - (1-\kappa)V_r)\,V_1}{(V_1 + \kappa V_r)V_{\phi1}} = \theta_{s1} \left(\frac{\rho_s - \rho_{b2}}{\rho_s - \rho_{b1}} \right) \tag{4.24}$$

where ρ_s is the solids particle density. The residual water content θ_r can be considered unaffected by a change in pore size distribution and bulk density on a mass basis ($\theta_{rm} = \dfrac{m_w}{m_s}$), where m_w and m_s denote the mass of water and dry media solids, respectively Consequently, the volumetric residual water content of the rhizosphere soil θ_{r2} is given by:

$$\theta_{r2} = \theta_{r1} \left(\frac{V_1}{V_1 + \kappa V_r} \right) = \theta_{r1} \left(\frac{\rho_{b2}}{\rho_{b1}} \right) \tag{4.25}$$

Fig. 4.10(inset) shows the change in residual and saturated water contents using the example of the Turface media considering only the primary draining water-retention characteristic. For a restricted root zone (i.e. $\kappa = 0$), the residual water content remains unchanged compared to the bulk media with a marked decrease in saturated water content corresponding to the occupation of pores by roots (in this case 10 percent). For the unrestricted root-zones (i.e. $\kappa > 0$), both the residual and saturated water content decrease, where higher κ values characterize a larger decrease. The resulting predictions of readily plant-available water defined as $\theta - \theta_r$ in Fig. 4.10 show a reduction compared to the bulk media. Notably, the highest reduction is predicted for the restricted root-zone. Unrestricted root zones are characterized by a reduction in plant-available water that scales with $1 - \kappa$, meaning that root zones where root proliferation results in the 1:1 creation of additional root-zone volume are predicted to experience the lowest decrease in plant-available water.

For water-content measurements, water held in roots occupying some of the pore space integrated over by the volume-averaging sensors, sense a water content closer to the bulk mediums water content at a given matric potential. The overestimation (i.e. some part of $\theta_{s1} - \theta_{s1}$) depends on κ, where a value of zero, corresponding to the restricted root zone, exhibits the highest overestimation with the maximal pore fraction occupied by roots. The overestimation depends further on the root water content, where Gerke and Kuchenbuch (2007) estimated the water content of well

watered maize to be ≈ 0.8 cm^3 cm^{-3}. However, because the water status of the roots (i.e. the root water content) varies with the porous-media hydraulic potential, root age and species, the water-content overestimations may be difficult to predict accurately. Nevertheless, the fraction of water held in roots relative to the bulk volumes water content is significant at high root densities and particularly in restricted root zones and should be considered when estimating water contents based on volume-averaging sensors.

4.6   Summary and Conclusions

The physical characteristics of the porous media are crucial design characteristics because they determine the physical aspects of root function such as water, nutrient and gas exchange that are most relevant to root growth and plant vigor. Of these, water retention characteristics provide critical information on the distribution of water and air in root zones and are critical for the optimization of water and gaseous fluxes to plant roots in different gravity environments.

In a first case study we designed a root-zone system based on wetting water-retention characteristics of vertically-increasing finer particle-sized media providing a more homogenous water-content distribution under terrestrial gravity compared to conventional homogenous-medium results. The design offers a more uniform water content profile leading to a potentially more homogenous root distribution. This is achieved by extending the region where antipodal fluxes of water and gases are balanced and provides a terrestrial test bed for microgravity root-zone performance. The design framework may further be easily adapted for planetary gravity, like Lunar or Martian gravity, and provides the basis for media selection including planetary regolith.

In a second case study, we considered how roots change the physical root-zone environment and in particular the water-retention characteristic, which underlies the root-zone optimization problem. The limited results from this study do not support the suggestion that macroscopic water-retention characteristics are significantly altered by root proliferation. We attributed part of this conclusion to experimental challenges that should be addressed in future experiments. The main challenge is establishing a uniform root distribution in the sample and prevention of the development of a root mat on the porous membrane. We advocate that root effects on the porous-media

root zone should be more intensely studied before media optimizations can be applied. We further suggest that more research should be conducted on the inclusion of water held in roots for volume-averaging water-content monitoring sensors crucial to managing a root environment to sustain plant growth.

Current soil-water flow models based on the Richards equation describe water movement only in the capillary pores. Plant effects on soil water are considered only as a sink term accounting for root-water uptake. While root distribution, soil hydraulic properties and water content data are used for the closure of the models, complex feedback reactions and impacts of root systems both spatially and temporally on the state variables (i.e. water content and matric potential) and hydraulic properties (i.e. changes in density, pore size distribution, hydraulic conductivity) are mostly neglected. We suggest further study aiming at the inclusion of temporal root modifications of the porous-media hydraulic properties which affect the transport and retention of water. We further suggest the need to study more closely the transport of water from the bulk media to the immediate root vicinity and finally into the root to explain differences in plant vigor seen in restricted root zones in microgravity.

4.7 References

Assouline, S. 2006. Modeling the relationship between soil bulk density and the water retention curve. Vadose Zone J. 5:554-563.

Blonquist, J.M., Jr., S.B. Jones, I. Lebron, and D.A. Robinson. 2006. Microstructural and phase configurational effects determining water content: Dielectric relationships of aggregated porous media. Water Resour. Res. 42.

Bruand, A., and I. Cousin. 1995. Variation of textural porosity of a clay-loam soil during compaction. European J. Soil Sci. 46:377-385.

Bugbee, B., and F.B. Salisbury. 1989. Current and potential productivity of wheat for a controlled environment life support system. Adv. Space Res. 9:5-15.

Bunt, A.C. 1984. Physical properties on mixtures of peats and minerals of different particle size and bulk density for potting substrates. Acta Hort. (ISHS) 150:143-154.

Bunt, A.C. 1988. Media and mixes for container-grown plants: A manual on the preparation and use of growing media for pot plants. Unwin Hyman, London.

Caron, J., and V.K.N. Nkongolo. 1999. Aeration in growing media: recent developments. Acta Hortic. 481:545-551.

Collin, M., and A. Rasmuson. 1988. A comparison of gas diffusivity models for unsaturated porous media. Soil Sci. Soc. Am. J. 52:1559-1565.

Cook, F.J., and J.H. Knight. 2003. Oxygen transport to plant roots: Modeling for physical understanding of soil aeration. Soil Sci. Soc. Am. J. 67:20-31.

da Silva, A.P., and B.D. Kay. 1997. Estimating the least limiting water range of soils from properties and management. Soil Sci. Soc. Am. J. 61:877-883.

da Silva, A.P., B.D. Kay, and E. Perfect. 1994. Characterization of the least limiting water range of soils. Soil Sci. Soc. Am. J. 58:1775-1781.

De Willigen, P., and M. van Noordwijk. 1984. Mathematical models on diffusion of oxygen to and within plant roots, with special emphasis on effects of soil-root contact: I Derivation of the Model. Plant and Soil 77:215-231.

Dreschel, T.W., and J.C. Sager. 1989. Control of water and nutrients using a porous tube: a method for growing plants in space. HortScience 24:944-947.

Fageria, N.K., V.C. Baligar, and R.B. Clark. 2006. Physiology of Crop Production. Food Products Press, An Imprint of the Haworth Press, New York.

Feddes, R.A., P.J. Kowalik, and H. Zaradny. 1978. Simulation of field water use and crop yield. In: Feddes et al., ed. Water Uptake by Plant Roots. John Wiley & Sons, New York.

Gardner, W.R. 1960. Dynamic aspects of water availability to plants. Soil Sci. 89:63-73.

Gerke, H.H., and R.O. Kuchenbuch. 2007. Root effects on soil water and hydraulic properties. Biologia 62:557-561.

Gliński, J., and W. Sępniewski. 1985. Soil Aeration and Its Role for Plants. CRC Press, Inc., Boca Raton, USA.

Gros, J.B., C. Lasseur, A.A. Tikhomirov, N.S. Manukovsky, V.S. Kovalev, S.A. Ushakova, I.G. Zolotukhin, L.S. Tirranen, R.A. Karnachuk, and V.Y. Dorofeev. 2005. Testing soil-like substrate for growing plants in bioregenerative life support systems. Adv. in Space Res. 36:1312-1318.

Hagrey, S.A.A. 2007. Geophysical imaging of root-zone, trunk, and moisture heterogeneity. J. Exp. Bot. doi:10.1093/jxb/erl237

Hallett, P.D., D.C. Gordon, and A.G. Bengough. 2003. Plant influence on rhizosphere hydraulic properties: direct measurements using a miniaturized infiltrometer. New Phytologist 157:597-603.

Henry, A., W. Doucette, J. Norton, S. Jones, J. Chard, and B. Bugbee. 2006. An axenic plant culture system for optimal growth in long-term studies. J. Env. Quality 35:590-598.

Hsieh, J.J.C., W.H. Gardner, and G.S. Campbell. 1972. Experimental control of soil water content in the vicinity of root hairs. Soil Sci. Soc. Am. J. 36:418-421.

Jones, S.B., and D. Or. 1998. Design of porous media for optimal gas and liquid fluxes to plant roots. Soil Sci. Soc. Am. J. 62:563-573.

Jones, S.B., and D. Or. 1999. Microgravity effects on water flow and distribution in unsaturated porous media: Analysis of flight experiments. Water Resour. Res. 35:929-942.

Lang, A.R.G., and W.R. Gardner. 1970. Limitation to Water Flux from Soils to Plants. Agron J 62:693-695.

Lebron, I., and D.A. Robinson. 2003. Particle size segregation during hand packing of coarse granular materials and impacts on local pore-scale structure. Vadose Zone J. 2:330-337.

Levine, H.G., G.K. Tynes, and J.H. Norikane. 2003. Fluid behavior under microgravity conditions within plant nutrient delivery systems: Parabolic flight investigations. SAE Technical Paper 2003-01-2483. SAE Int., Warrendale, PA.

Milks, R.R., W.C. Fonteno, and R.A. Larson. 1989. Hydrology of horticultural substrates: II. Predicting physical properties of media in containers. J. Amer. Soc. Horta. Sci. 114:53-56.

Mojid, M.A., and H. Cho. 2004. Evaluation of the time-domain reflectometry (TDR)-measured composite dielectric constant of root-mixed soils for estimating soil-water content and root density. J. Hydrology 295:263-275.

Moldrup, P., S. Yoshikawa, T. Olesen, T. Komatsu, and D.E. Rolston. 2003. Gas diffusivity in undisturbed volcanic ash soils: Test of soil-water-characteristic-based prediction models. Soil Sci. Soc. Am. J. 67:41-51.

Moldrup, P., T. Olesen, J. Gamst, P. Schjonning, T. Yamaguchi, and D.E. Rolston. 2000. Predicting the gas diffusion coefficient in repacked soil: Water-induced linear reduction model. Soil Sci. Soc. Am. J. 64:1588-1594.

Monje, O., G.W. Stutte, G.D. Goins, D.M. Porterfield, and G.E. Bingham. 2003. Farming in space: Environmental and biophysical concerns. Adv. Space Res. 31:151-167.

Mualem, Y. 1976. A new model for predicting the hydraulic conductivity of unsaturated porous media. Water Resour. Res. 12:513-522.

Porterfield, D.M., G.S. Neichitailo, A.L. Mashinski, and M.E. Musgrave. 2003. Spaceflight hardware for conducting plant growth experiments in space: The early years 1960-2000. Adv. Space Res. 31:183-193.

Read, D.B., A.G. Bengough, P.J. Gregory, J.W. Crawford, D. Robinson, C.M. Scrimgeour, I.M. Young, K. Zhang, and X. Zhang. 2003. Plant roots release phospholipid surfactants that modify the physical and chemical properties of soil. New Phytologist 157:315-326.

Richard, G., I. Cousin, J.F. Sillon, A. Bruand, and J. Gurif. 2001. Effect of compaction on the porosity of a silty soil: Influence on unsaturated hydraulic properties. European J. Soil Sci. 52:49-58.

Richards, L.A. 1931. Capillary conduction of liquids through porous mediums. Physics 1:318-333.

Rivire, L.M., and J. Caron. 2001. Research on substrates: State of the art and need for the coming 10 years. Acta Hort. (ISHS) 548:29-42.

Rivire , L.M., J.C. Foucard, and F. Lemaire. 1990. Irrigation of container crops according to the substrate. Scientia Horticulturae 43:339-349.

Schmidhalter, U. 1997. The gradient between pre-dawn rhizoplane and bulk soil matric potentials, and its relation to the pre-dawn root and leaf water potentials of four species. Plant, Cell and Environ. 20:953-960.

Schroth, M.H., J.D. Istok, S.J. Ahearn, and J.S. Selker. 1996. Characterization of miller-similar silica sands for laboratory hydrologic studies. Soil Sci. Soc. Am. J. 60:1331-1339.

Steinberg, S.L., and D.L. Henninger. 1997. Response of the Water Status of Soybean to Changes in Soil Water Potentials Controlled by the Water Pressure in Microporous Tubes. Plant Cell Environm. 20:1506-1516.

Steinberg, S.L., and D. Poritz. 2005. Measurement of hydraulic characteristics of porous media used to grow plants in microgravity. Soil Sci. Soc. Am. J. 69:301-310.

Steinberg, S.L., D. Ming, and D. Henninger. 2002. Plant production systems for microgravity: Critical issues in water, air and solute transport through unsaturated porous media. NASA Tech. Mem. 2002-210774. Natl. Aeronautics and Space Admin., Houston, TX.

Steinberg, S.L., S.B. Jones, M. Xiao, L. Reddi, G. Kluitenberg, D. Or, J.I.D. Alexander, N. Daidzic, and M. Tuller. 2005. Challenges to understanding fluid behavior in plant growth media under microgravity. SAE Technical Paper 2005-01-2947. SAE Int., Warrendale, PA.

Stutte, G.W., O. Monje, G.D. Goins, and B.C. Tripathy. 2005. Microgravity effects on thylakoid, single leaf, and whole canopy photosynthesis of dwarf wheat. Planta 223:46-56.

van Bavel, C.H.M. 1951. A soil aeration theory based on diffusion. Soil Sci. 72:33-46.

van Genuchten, M.T. 1980. A closed-form equation for predicting the hydraulic conductivity of unsaturated soils. Soil Sci. Soc. Am. J. 44:892-898.

Wesseling, J.G., J.A. Elbers, P. Kabat, and B.J.v.d. Broek. 1991. SWATRE, instructions manual for input. p. 55. In Wesseling et al., ed. Internal report. DLO-The Winand Staring Centre, Wageningen, The Netherlands.

Whalley, W.R., P.B. Leeds-Harrison, P.K. Leech, B. Riseley, and N.R.A. Bird. 2004. The hydraulic properties of soil at root-soil interface. Soil Sci. 169:90-99.

Whalley, W.R., B. Riseley, P.B. Leeds-Harrison, N.R.A. Bird, P.K. Leech, and W.P. Adderley. 2005. Structural differences between bulk and rhizosphere soil. European J. Soil Sci. 56:353-360.

Young, I.M. 1998. Biophysical interactions at the root-soil interface: A review. J. Agricultural Sci. 130:1-7.

Table 4.1: van Genuchten (1980) parameterizations of the primary draining and wetting water retention characteristics for the Ottawa sands and the respective mixtures used in the stratified sand column. The parameters for Fine are also given though it was used only as a mixture in the column experiment. Mixtures indicate parts by weight. α, n and θ_s were determined using a nonlinear least squares fit with the Levenberg-Marquardt optimization method to optimize Eq. [4.11] to measured water contents and matric potentials while keeping θ_r fixed. Fitting was implemented with the "lsqcurvefit" function in the Matlab Optimization Toolbox version 3.0.2 (Mathworks Inc., Natick, MA).

Porous medium [stratum]	Draining				Wetting			
	α	n	$\theta_r^\dagger$	θ_s	α	n	$\theta_r^\dagger$	θ_s
	cm^{-1}		–cm^3 cm^{-3}–		cm^{-1}		–cm^3 cm^{-3}–	
Coarse [1]	0.086	6.23	0.01	0.36	0.166	4.28	0.01	0.35
lower‡	0.080	5.26		0.32	0.151	3.45		0.34
upper‡	0.093	7.20		0.40	0.181	5.11		0.35
Coarse-Medium (2:1) [2]	0.063	4.67	0.01	0.37	0.113	3.23	0.01	0.33
lower	0.060	4.00		0.34	0.101	2.82		0.31
upper	0.067	5.33		0.39	0.124	3.63		0.35
Medium [3]	0.042	6.78	0.01	0.35	0.074	4.78	0.01	0.31
lower	0.041	5.89		0.33	0.068	4.04		0.29
upper	0.043	7.67		0.37	0.080	5.52		0.34
Medium-Fine (1:1) [4]	0.031	6.17	0.01	0.35	0.051	3.94	0.01	0.31
lower	0.030	5.30		0.35	0.045	3.24		0.29
upper	0.031	7.04		0.36	0.057	4.63		0.33
Fine	0.074	3.25	0.01	0.38	0.034	4.37	0.01	0.40
lower	0.062	2.40		0.35	0.033	3.91		0.40
upper	0.087	4.09		0.42	0.035	4.83		0.41

† Residual water content θ_r was kept invariant while fitting the saturated water content θ_s and the curve-fitting parameters α and n in the van Genuchten model.

‡ Lower and upper bounds of the 95 % confidence interval, respectively.

Table 4.2: Fresh and dry mass of pea roots and shoots expressed in grams per plant after 28 day treatments.

	Profile			Turface		
	Root	Root	Shoot	Root	Root	Shoot
V_t	m_{fresh}	m_{dry}	m_{dry}	m_{fresh}	m_{dry}	m_{dry}
cm^3	g	g	g	g	g	g
161	2.12	0.34	0.62	3.82	0.36	0.95
161	3.06	0.43	0.8	5.14	0.62	0.93
161	2.68	0.37	0.66	6.13	0.73	1.07
161				4.33	0.41	0.76

Table 4.3: Porous media parameters of the van Genuchten (1980) water retention model comparing bulk and rhizosphere estimates.

	Profile							
	Bulk Media				Bulk Rhizosphere			
Process	α	n	$\theta_r^{\dagger}$	θ_s	α	n	$\theta_r^{\dagger}$	θ_s
	cm^{-1}		–cm^3 cm^{-3}–		cm^{-1}		–cm^3 cm^{-3}–	
Wetting	0.172	4.85	0.37	0.66	0.223	3.41	0.37	0.66
lower‡	0.163	4.00	0.37	0.64	0.201	2.92	0.37	0.65
upper‡	0.181	5.71	0.37	0.67	0.244	3.91	0.37	0.68
Draining	0.108	6.74	0.37	0.66	0.109	5.81	0.37	0.68
lower	0.105	5.86	0.37	0.65	0.106	5.31	0.37	0.67
upper	0.112	7.62	0.37	0.68	0.111	6.31	0.37	0.69
	Turface							
Wetting	0.350	4.16	0.37	0.66	0.398	3.83	0.37	0.67
lower	0.332	3.75	0.37	0.65	0.366	3.19	0.37	0.65
upper	0.368	4.56	0.37	0.68	0.430	4.47	0.37	0.68
Draining	0.202	5.52	0.37	0.67	0.201	6.64	0.37	0.67
lower	0.192	4.55	0.37	0.65	0.192	5.42	0.37	0.65
upper	0.212	6.50	0.37	0.69	0.210	7.86	0.37	0.69

† Residual water content θ_r was taken from Blonquist et al. (2006) and kept invariant while fitting the saturated water content θ_s and the curve-fitting parameters α and n in the van Genuchten model.

‡ Lower and upper bounds of the 95 % confidence interval, respectively.
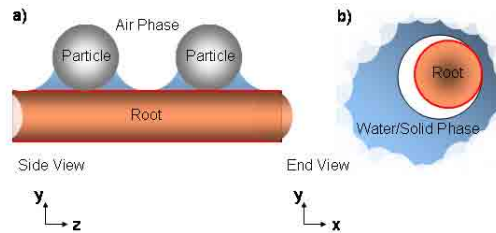
Fig. 4.1: Illustration of partial root-soil and root-air contact providing simultaneous transport of water and gasses at the pore-scale.
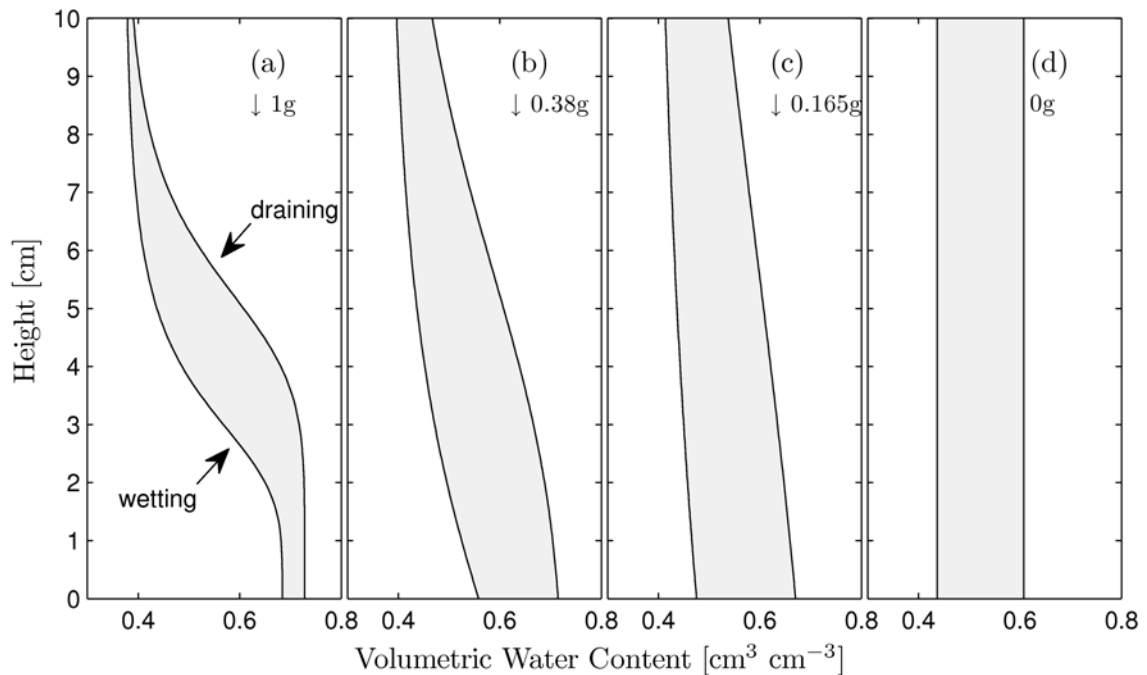
Fig. 4.2: Hypothetical steady-state equilibrium distribution of water contents in a 10 cm tall sample of porous ceramic-aggregate Turface subjected to (a) Earth's, (b) Martian, (c) Lunar and (d) zero-gravity. The average hydraulic potential (i.e. at the midpoint) is constant at -5 cm. The shaded area shows the regions of validity for water contents bounded by the primary draining and wetting water retention curves where the hydrostatic distribution of hydraulic potentials scales with the gravitational force.

Fig. 4.3: Plant-growth column used in the stratified porous-media root zone experiments. The 25 cm tall column allows hydration via the establishment of a shallow saturated zone at the bottom of the root zone using a small port at the base. The inside look shows the possible placement of integrated dual-probe heat-pulse sensors amenable for the estimation of water content and electrical conductivity.
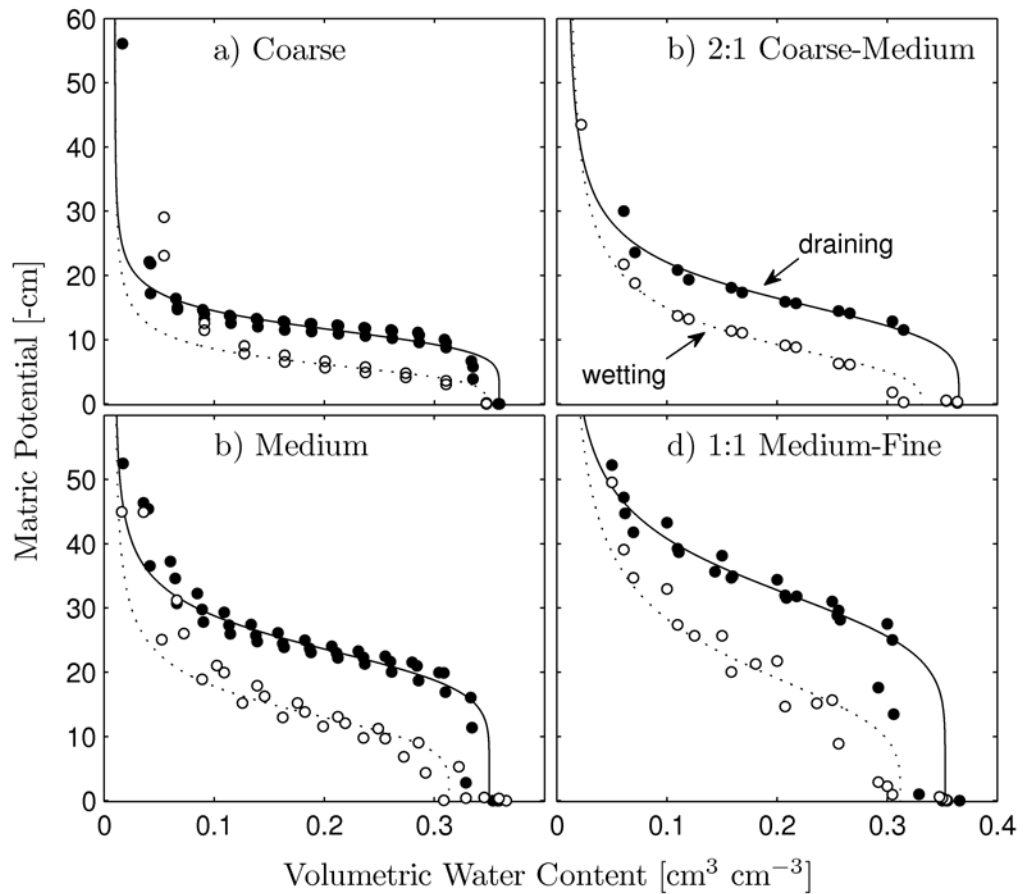
Fig. 4.4: Water retention characteristics of four particle-size classes of Ottawa sands. Solid and dotted lines represent fitted van Genuchten models to the replicate wetting (closed symbols) and draining (open symbols) data with parameterizations given in Table 4.1.
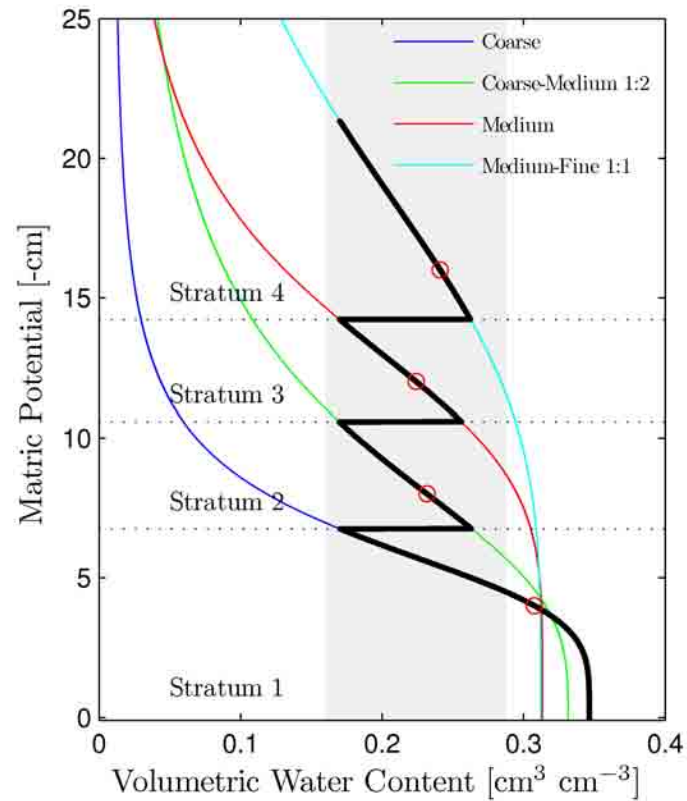
Fig. 4.5: Depiction of the stratified porous-media root zone providing more uniform water contents than a conventional homogenous medium design. The wetting water-retention curves shown illustrate the vertical change in water content (i.e. with the gravitational field) where the predicted water content (bold line) increases in the next higher stratum at the interface based on smaller pore-sized media holding more water at that hydraulic potential (vertical position in the profile).
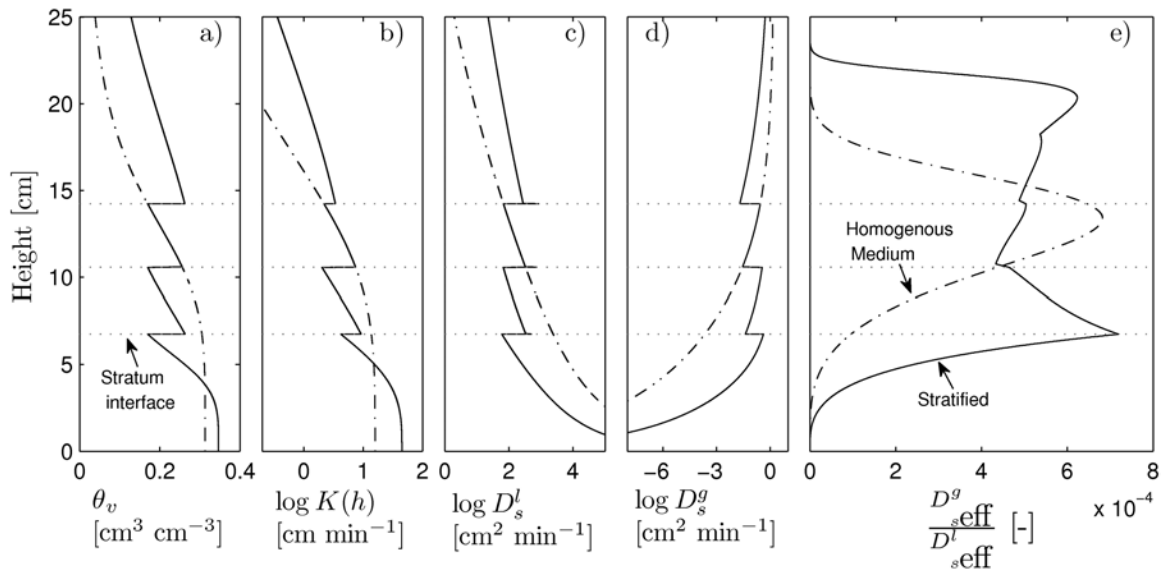
Fig. 4.6: Predicted root zone performance comparing a homogenous porous medium design with the proposed stratified design. For the estimation of unsaturated hydraulic conductivities $K(h)$, liquid diffusivities D_g^w and gaseous diffusivities D_g^a see the text. The ratio of effective diffusivities shown in (e) is proposed as a design-effectiveness descriptor suggesting a wider range in optimal root zone (i.e. where liquid and gaseous fluxes are balanced) for the stratified design compared to the homogenous medium-sand design.
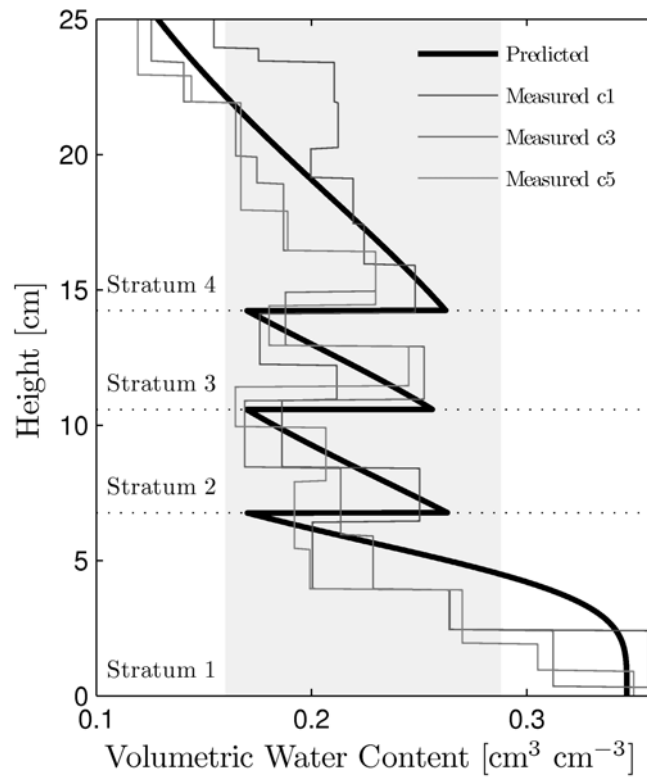
Fig. 4.7: Comparison of predicted and gravimetrically determined volumetric water-content distributions in three columns with stratified root zones. Gravimetric water contents were sampled over depth intervals indicated in the plot and thus represent vertically averaged values. Column identifiers c1, c3 and c5 point to columns 1, 3 and 5 out of a total of 6 tested, respectively.
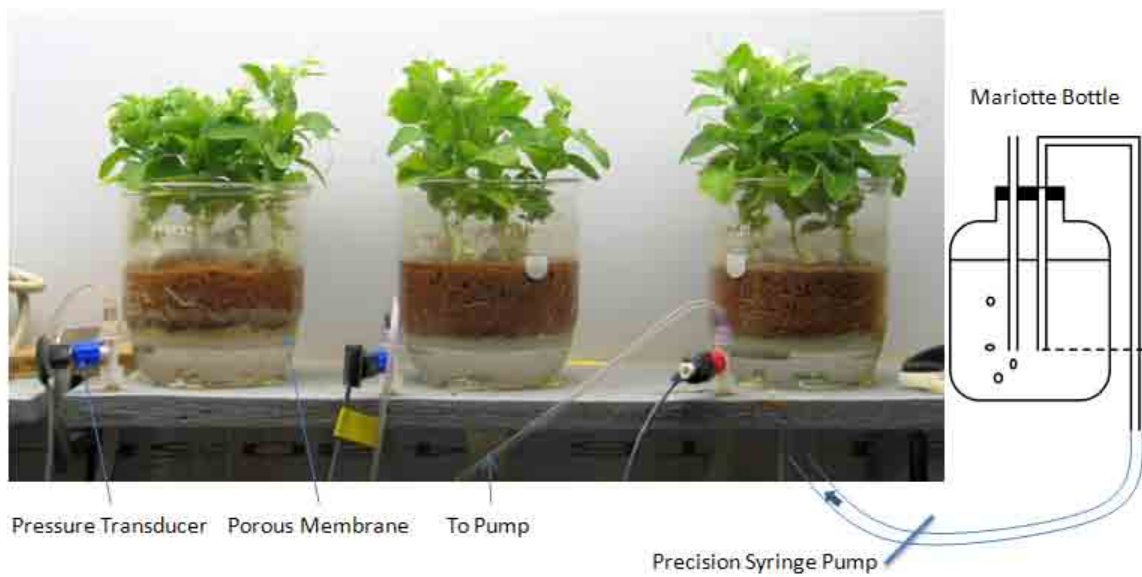
Fig. 4.8: Buchner-funnel root chambers for water retention measurements. The Mariotte-Bottle provided on demand water supply maintaining a hydraulic potential of 0 cm$_{H_2O}$ at the porous membrane. For water retention measurements, the water supply was interrupted and a computer-controlled precision syringe pump provided changes in water volume in the bulk root zone while the plants were covered and darkened to minimize evapotranspiratory losses.
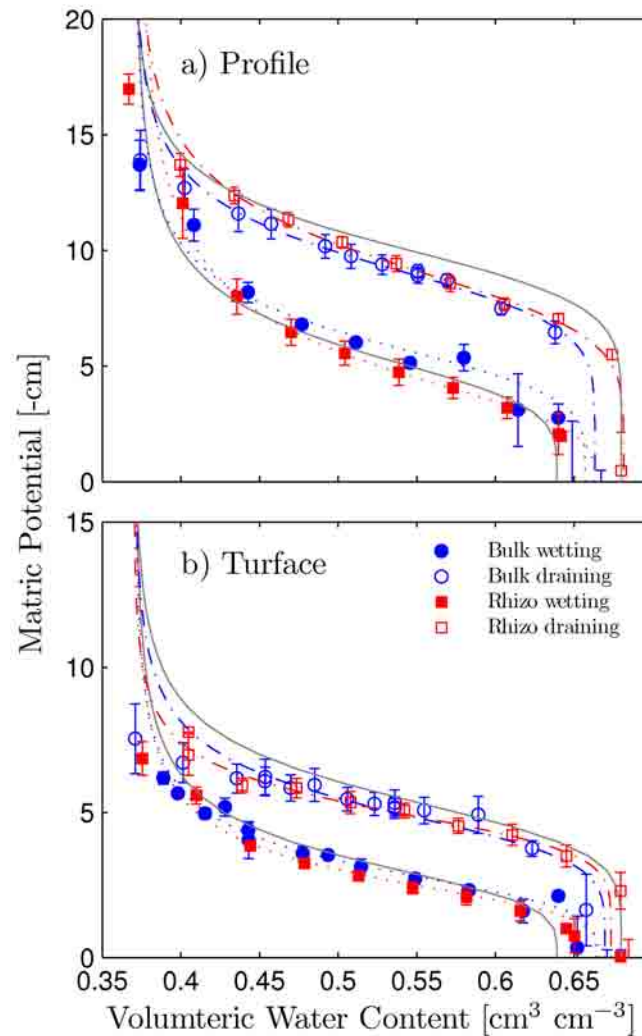
Fig. 4.9: Water retention characteristics measured in Profile (a) and Turface (b) comparing bulk media with bulk rhizosphere properties. For comparison, solid lines represent predicted characteristics using parameters given in Heinse et al. (2007). Dotted and dash-dotted lines represent fitted van Genuchten models to the replicate wetting (closed symbols) and drying (open symbols) data. Errorbars indicate the standard error in the replicate measurements at given water contents.
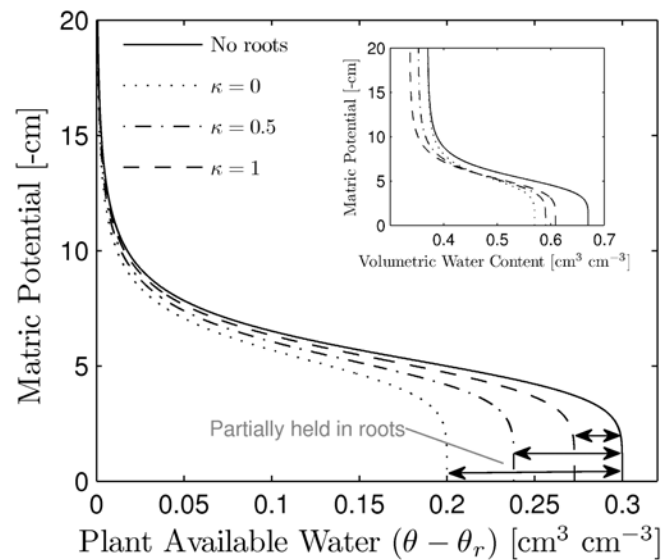
Fig. 4.10: Plant available water in restricted and unrestricted root zones comparing the bulk media with no roots and cases with 10 percent roots per volume in Turface for the primary draining process. The parameter κ indicates the fractional root expansion with root development. $\kappa = 0$ indicates the case when the root-zone volume is restricted, $\kappa = 1$ indicates a case where the root-zone volume is allowed to expand and root development results in the total expansion. The insert shows the corresponding water-retention characteristics considering only the changes in residual and saturated water contents. Also indicated is the range of apparent water-content overestimation (water that is held in the roots occupying pore space within the media) using volume-averaging indirect water-content sensors.

CHAPTER 5

INTEGRATION OF HEAT CAPACITY AND ELECTRICAL CONDUCTIVITY SENSORS FOR ROOT MODULE WATER AND NUTRIENT ASSESSMENT[1]

5.1 Abstract

Management of water content and nutrient status during space flight is a critical element for successful plant production systems. Our objectives were to determine if dual-probe heat-pulse (DPHP) sensors could improve water content determination accuracy over single-probe heat-pulse (SPHP) sensors, and to test a design using coupled heat-pulse and direct-current electrical conductivity sensors, paired as a 4-electrode array. The DPHP predicted water content correlated well with independently measured water contents based on a physically-derived one-point calibration model. SPHP water content prediction was comparable to the dual-probe sensors when using an empirical relationship. Pooled regression analysis showed that water content for both sensors was accurate with a root-mean square error of 0.02 cm^3 cm^{-3}. Electrical conductivity was measured in both saturated flow-through and static unsaturated measurements. Model predictions of solution electrical conductivity as a function of water contents were well correlated for water contents above 0.2 cm^3 cm^{-3}. Combining the dual-needle heat-pulse probe water content determination with electrical conductivity measurements provides improved root-zone environment assessment and management capabilities.

5.2 Introduction

Water content and nutrient status is a critical need for plant production systems that utilize restricted root zones. The heat-pulse method has been a common method for estimating volumetric water content where mass, volume, power and safety constraints associated with payloads destined for space necessitated the development of small-scale low-power sensors. While the soil physics community began revisiting dual-probe heat-pulse (DPHP) methods with improvements in electronics technology in the 1980s, spaceflight applications called for the retrofitting of existing hardware using nail-like and miniaturized single-probe heat-pulse (SPHP) sensors for measuring water content (Bingham et al., 2002; Hoehn et al., 2000; Levine et al., 2003; Morrow et al., 2001). Recently, Newman et al. (2005) successfully applied the DPHP method in coarse-textured porous media considered for plant growth in space. The major advantages of the DPHP over the SPHP method is the greater consistency with theory and the availability of analytical solutions, allowing an estimation of the soil water content using a physically-based approach. Sensing water content with SPHP sensors is commonly based on empirical, calibrated relationships (Morrow et al., 2001). One additional advantage of the DPHP method is the versatility of the setup. Recently scientists have proposed multi-functional sensors combining heat-pulse measurements with electrical conductivity measurements (Bristow et al., 2001; Mori et al., 2003), dielectric measurements (Ren et al., 2005), and water flux determinations (Mori et al., 2005; Ochsner et al., 2005). The benefit of the multi-functional probe is the possibility of measuring independent physical properties at a comparable scale. This is particularly important considering the spatial and temporal heterogeneity in the root zone. The addition of two needles to the DPHP sensor, to facilitate electrical conductivity measurements, which can be related to solution nutrient status, has shown promise using equidistant parallel needles in a Wenner array (Bristow et al., 2001; Mori et al., 2003). In this paper, we test whether difficulties in using the Wenner array at low conductivities can be partially improved by increasing the spacing between the potential electrodes. The electrode spacing determines the sensitivity and the signal to noise ratio of the array. We expect that the benefit of the increased spacing will be most significant at low water contents and electrical conductivities. We further investigated the problem of water content determination with SPHP and DPHP methods and the integrated use of DPHP sen-

sors to measure electrical conductivity in a 4-electrode array. Our objectives were to: (1) evaluate if dual-probe heat-pulse sensors can improve water content determination accuracy compared to single-probe heat-pulse sensors, and (2) construct and test a novel sensor providing nutrient status from electrical conductivity measurements at a scale (i.e., sensor or root zone) appropriate for space applications. Combining the DPHP sensor with the capability for electrical conductivity measurements potentially provides improved water-content-determination accuracy and nutrient assessment. Emphasis on integrating porous-media root module and sensor components with porous-media design will create novel management capabilities unavailable in present microgravity plant-growth systems.

5.3   Theoretical Considerations

5.3.1   Heat-Capacity-Based Water Content Sensing

The specific heat capacity c of a porous medium has been shown to be linearly related to the volumetric water content of porous media (Campbell et al., 1991):

$$\theta_v = \frac{\rho c - \rho_b c_s}{\rho_w c_w} \tag{5.1}$$

ρ_b denotes the bulk density, c the specific heat-capacity, and θ_v the volumetric water content. The subscripts s and w refer to the solid and liquid phase, respectively. The contribution of the air phase is neglected because of the relatively low density and heat capacity compared to the solid and liquid phase. Generally, the experimental methodology for measuring the specific heat capacity is based on the application of a heat pulse to a source, and analysis of the temperature response at the source (SPHP) or at some distance from the source (DPHP). Commonly, SPHP data are analyzed empirically by a linear fitting of the measured maximum temperature change to water contents. For the DPHP method, Campbell et al. (1991) developed an analytical inverse relationship between the maximum temperature rise at the temperature probe and the volumetric heat capacity of the medium following an instantaneous heat pulse:

$$\rho c = \frac{q}{e \pi r^2 T_m} \tag{5.2}$$

T_m denotes the maximum temperature increase at a distance r following the application of a heat pulse taken as the applied power per length of probe q, and e is the Euler's number. Campbell et al. (1991) found that calibrating for apparent probe spacing r_{app} rather than the physical spacing between the needles improved the water content prediction accuracy. Knight and Kluitenberg (2004) proposed a computationally simplified version of a physically based equation derived by Kluitenberg et al. (1993) that accounts for the finite heat application as opposed to an instantaneous heat pulse:

$$\rho c = \frac{q}{e \pi r_{app}^2 T_m} \left(1 - \frac{\varepsilon^2}{8} \left\{ \frac{1}{3} + \varepsilon \left[\frac{1}{3} + \frac{\varepsilon}{8} \left(\frac{5}{2} + \frac{7\varepsilon}{3} \right) \right] \right\} \right) \tag{5.3}$$

where $\varepsilon = t_o/t_m$, t_o is the duration of the heat-pulse, and t_m is the time from the initiation of the pulse to the occurrence of the temperature maximum.

5.3.2 Electrical Conductivity

The bulk electrical conductivity represents the integrative conductivity of all contributing conductors (pore fluid, matrix), and is dependent on the water content of the media. Archie (1942) formulated an expression that relates the bulk electrical conductivity σ_b to the porosity Φ, the relative saturation S, the electrical conductivity of the pore fluid σ_w, and the conductivity of the matrix σ_g:

$$\sigma_b = \frac{1}{a} \Phi^m S_w^n \sigma_w + \sigma_g \tag{5.4}$$

with a, m and n being fitting parameters. After calibration, Eq. (5.4) provides a means to estimate the solution electrical conductivity from measurements of the bulk conductivity and volumetric water content. The calibration consists of fitting Eq. (5.4) to measured bulk conductivities at known solution conductivities and water contents. Measuring the electrical conductivity may be achieved with direct current resistivity methods that refer to stationary fields and currents, but also include

slowly alternating fields and currents.

Given two electrodes A and B, and two electrodes M and N at spacings r (Fig. (5.1)), the difference in potential between M and N equals:

$$V = \frac{I}{2\pi\sigma}\left[\left(\frac{1}{r_{AM}} - \frac{1}{r_{AN}}\right) - \left(\frac{1}{r_{BM}} - \frac{1}{r_{BN}}\right)\right]^{-1} \tag{5.5}$$

The 2π term indicates measurements at the surface of a half sphere. A multitude of electrode arrays exist. Measuring the potential difference and the induced current, multiplied by a geometry factor, results in the apparent conductivity:

$$\sigma_a = \frac{I}{2\pi U}f(r) \tag{5.6}$$

where

$$G = \frac{f(r)}{2\pi} \tag{5.7}$$

is called the geometry or configuration factor.

The geometry factor can be determined experimentally in a medium with known conductivity. Because the medium is generally not homogenous and isotropic, the determined conductivity is referred to as the apparent conductivity. If the medium is homogeneous and isotropic, the apparent conductivity equals the specific conductivity of the medium.

5.4   Materials and Methods

5.4.1   Porous Media

The porous media used in this study were porous ceramic aggregates (Aimcor, Deerfield, IL) sieved to size fractions of 0.25–1 mm (Profile), and 1–2 mm (Turface). Porous ceramic aggregates have been widely used in microgravity plant experiments (Levine et al., 2003; Norikane et al., 2004; Steinberg and Henninger, 1997; Stutte et al., 2005). The aggregates are stable, have moderate surface area for nutrient storage, are easily separated from roots, and are re-useable. The aggregates

exhibit a dual-pore character made up of inter-aggregate and intra-aggregate pores. Only the intra-aggregate pore retention characteristics are of interest for these studies, particularly in the range of 0 to -25 cm H_2O matric potential used for plant growth.

5.4.2 Shallow-Sample Cell Setup

Heat-pulse sensors were installed in an experimental setup for microgravity water-retention experiments used by Heinse et al. (2005). The experimental system consists of clear-Lexan rectangular containers (internal dimensions: 12 cm long, 5 cm wide and 2 cm high). The average water content of the media was controlled using a water addition/removal system which consisted of water inlet, water outlet and porous plate. The inlet, connected to the porous plate, fills the entirety of the bottom of the cell, allowing control of water in the media at suction (negative pressure) without air passing through the plate. The gravitational effect on the water content distribution is minimized because of the small vertical extent. The heat-pulse sensors were installed horizontally at a height of 1 cm. Sensors were held in place using silicone sealant to allow for non-destructive removal while ensuring air- and water-sealed conditions. Figure 5.2 shows the sensors installed in the cell. The horizontal spacing between the probes is approximately 3 cm.

5.4.3 Pseudo Root Module Setup

Testing the ability of the multi-needle electrical conductivity sensors to monitor changes in electrical conductivity at the root module scale used a container shown in Fig. 5.3. Three DPHP sensors were installed vertically from the bottom of the container (30 cm by 15 cm, 15 cm tall). The container was packed with porous media to a height of 12 cm. The sensors were placed in a line, and were spaced 7.5 cm apart. On one side, the container was packed with 0.25-1 mm ceramic aggregates vacuum-saturated with tap water (σ_w=0.042 S m^{-1}), and on the other side, with 0.25–1 mm ceramic aggregates saturated and vacuumed in tap water mixed with slow release fertilizer (Osmocote 19-6-12, Scotts-Sierra Horticultural Products, Marysville, OH). The concentration of the fertilizer was 0.0185 cm^3 cm^{-3}.

5.4.4 Heat-Pulse Sensors

The single-probe heat-pulse (SPHP) sensors tested were developed at Space Dynamics Laboratory (SDL), Logan, Utah, and are being used in the Optimization of Root Zone Substrates (ORSZ) flight experiment (Jones et al., 2002) and as a modified version in the LADA plant growth chamber (Bingham et al., 2002). The sensors contain a single heating and temperature-sensing element (model LM50BIM3, National Semiconductor, Santa Clara, CA), and have a stainless-steel tip.

The dual-probe heat-pulse sensors (DPHP) were developed and constructed following the procedure of Ham and Benson (2004). The DPHP sensors consist of two parallel stainless steel needles spaced 6 mm apart. One needle contains a line heat source while the other contains a thermistor.

5.4.5 Heat-Pulse Measurements

The shallow-sample cell was packed with porous media saturated under vacuum to minimize air-entrapment. Following the incremental addition of the media (about 2 cm^3), the cell was tapped to ascertain uniform bulk density. The specific heats (Turface: 832 J kg^{-1} K^{-1}, Profile: 848 J kg^{-1} K^{-1} at 30°C) of the saturated ceramic aggregates as a function of temperature were measured by Thermophysical Properties Research Laboratories, West Lafayette, IN. The initial temperature (room temperature, about 24°C) of the individual sensors was measured prior to applying a heat-pulse. The SPHP sensors were heated for a period of 20 s by applying a constant potential of 12 V ($q \cong 1677$ J m^{-1}). Fifteen-minute intervals were given to allow temperatures to return to the initial temperature before the next heating event. The temperature was monitored after heating was terminated, and the maximum temperature difference, T_m, was recorded. The DPHP sensors were heated for a period of 8 s ($q \cong 744$ J m^{-1}). Temperature was then monitored after heating was terminated, and the maximum temperature difference, time to maximum tm, and applied heat were recorded. The apparent probe spacing *rapp* for the DPHP sensors was then calculated using saturated measurements of q, T_m and t_m (Eq. (5.3)). Water was then manually withdrawn from the bottom of the cell with a syringe in 7 ml increments until the approximate desaturation of macropores, where the water withdrawal was reversed up to satiation. Volumetric water contents of the medium were calculated at the end of the experiment using destructive measurements of the

bulk density with known cell volume following the experiments. SPHP and DPHP measurements were conducted sequentially in 15 min intervals after a 15 min wait to static equilibrium after each water content change.

5.4.6   Electrical Conductivity Sensor

A common electrical conductivity measurement configuration consists of four electrodes. For this study, the configuration consisted of two DPHP sensors. The physical arrangement of electrodes has infinite possibilities; all involve a current induction with two electrodes and a measurement of potential with two separate electrodes. To avoid polarization effects, an alternating current (e.g., 400 Hz) was used. The measured apparent electrical conductance (g=V/I) was used to calculate the bulk electrical conductivity σ_b using a calibrated configuration factor G that depends on the electrode array, electrode spacing and boundary conditions.

The two main considerations in determining the most suitable electrode configuration are the sensitivity distribution and the signal to noise ratio. The sensitivity describes a change in the measured apparent conductivity with respect to a conductivity change in a small volume element in the porous medium (Spitzer, 1998). A positive sensitivity indicates an increase in the apparent conductivity from an increase in the intrinsic conductivity in the cell. A negative sensitivity suggests inverse behavior where an increase in the intrinsic conductivity leads to a decrease in apparent conductivity. The sensitivity data can be used to analyze the resolving power of electrode configurations in both horizontal and vertical directions (Furche and Weller, 2002). In this study, we used SensInv2D (Geotomographie, Neuwied, Germany) to calculate the sensitivity distributions. As for the signal to noise ratio (S/N ratio), the larger spacing between M and N (the potential drop measurement) compared to the commonly used Wenner array, results in a larger potential difference at a small geometry factor. The larger potential drop can be read with greater accuracy by a data-logger, while the small geometry factor ensures that errors in the potential drop measurements are not multiplied by a large geometry factor.

5.4.7   Electrical Conductivity Measurements

Two DPHP sensors, spaced 3 cm apart (center to center), were used to construct the 4-electrode

array. First, the cell was filled with four liquids of known electrical conductivity in the range of 0.4–5.4 S m^{-1}. The increase in electrical conductivity of the liquids was achieved by adding Potassium Bromide to tap water. The electrical conductivity of the fluids was measured by an electrical conductivity meter (Accumet 20, Fisher Scientific, Hampton, NH). Using Eq. (5.6), the geometry factor was determined experimentally from measurements of the electrical conductance. The average geometry factor was 0.068 cm^{-1} with a standard deviation of 0.002 cm^{-1}.

Second, we packed the cell with 1–2 mm porous media in analogy to the heat pulse measurements. The initial packing used porous media saturated with tap water (0.042 S m^{-1}). The cell was then connected to a pumping mechanism (Masterflex, Cole Parmer, Vernon Hills, IL), and potassium bromide infused water at a conductivity of 0.68 S m^{-1} was pumped through the cell at a flow rate of 4 cm^3 min^{-1}. We then switched back to pumping tap water through the cell. Reference σ_w measurements were conducted at the cell's outlet. The apparent electrical conductivity was calculated using Eq. (5.6) with the previously determined geometry factor. We used a least-squares algorithm to optimize for the parameters a and m in Archie's equation (Eq. (5.4)) by comparison with the reference σ_w measurements.

Third, we disconnected the pump and connected a syringe to the bottom of the cell. Water was manually withdrawn from the bottom of the cell with the syringe in 5 ml increments until the approximate desaturation of macropores, where the water withdrawal was reversed up to satiation. Volumetric water contents of the medium were calculated using destructive measurements of the bulk density with known cell volume following the experiments. We used a least squares algorithm to optimize for the parameter n in Archie's equation (Eq. (5.4)) using previously determined parameters a and m by comparison with the reference sw measurements.

5.4.8 Data Acquisition and Control System

The data acquisition and control system (DACS) included several data-loggers, multiplexers and custom circuits. Control of the heat pulse (HP) measurements and electrical conductivity measurements were separated and electrically isolated for initial testing and development, and have subsequently been incorporated into a single DACS (Fig. 5.4).

The heat pulse DACS consisted of a CR10X data-logger with two AM416 multiplexers (Campbell Scientific, Logan, UT), a 1 Ω current-sensing shunt resistor (Model VPR5, 0.1% tolerance, Vishay Resistors, Malvern, PA), a 5 $k\Omega$ resistor (Model S102K, 0.1% tolerance, Vishay Resistors, Malvern, PA), and a 12 V battery. One multiplexer was used for the heater probe selection and the other multiplexer was used for all temperature probes. The data-logger was used for the timing and recording of the heat pulse and temperature measurements. The switched 12 V terminal of the data-logger was used to apply power to each heater for 8 s. Heat transmitted was measured by placing the 1 Ω shunt in series with the heater probe. Ohm's law was used to determine the current in the heater by measuring the voltage drop across the shunt. The thermistors were measured using a four-wire half-bridge circuit that utilized the 5 $k\Omega$ resistor as a reference.

The electrical conductivity DACS consisted of a data-logger (Model CR21X, Campbell Scientific, Logan, UT), one multiplexer (Model AM416, Campbell Scientific, Logan, UT), one 12 V battery, an isolated current supply circuit (four optical isolators with transistor output) shown in Fig. (5.4), and two D-size 1.5 V batteries. The data-loggers' excitation port acted as a 400 Hz alternating current switch that controlled the output and polarity of the current driver circuit. The constant current driver was composed of a PS-2501-4 optical isolator, a 100 Ω resistor, a 22 $k\Omega$ resistor, and a 1 $k\Omega$ current-sensing resistor.

5.5 Results and Discussion

5.5.1 Heat-Pulse Probe Comparison

Estimates of volumetric water content in 0.25–1 mm and 1–2 mm ceramic aggregates obtained using the SPHP (θ_{SPHP}) and DPHP (θ_{DPHP}) method are shown in Fig. 5.7. The symbols represent water content values from individual sensors paired with average cell water contents (θ_{cell}). The data shows good agreement between θ_{DPHP} and θ_{cell}. The maximum residual between θ_{DPHP} and θ_{cell} in Profile (Fig. 5.7a) is 0.11 cm^3 cm^{-3} at $\theta_{cell} = 0.68$ cm^3 cm^{-3}. It is at this water content that we find the most pronounced spread between the water content estimates. Further, notice that one of the sensors (Sensor 3: circles) overestimates water contents down to θ_{cell}=0.49 cm^3 cm^{-3}. At the lowest water content, all Sensors estimate the water content in agreement. Apparently, water in the cell does

not distribute horizontally in a uniform manner following water content changes. We speculate that water was preferentially withdrawn from the part of the cell sensitive to measurements of Sensor 3. Notice that Sensors 1 and 2 do not register a change in water content at the first water withdrawal step (0.75 to 0.68 cm^3 cm^{-3}). One explanation for the water content heterogeneity is that while packing the media saturated, segregation in particle size took place at each packing increment, resulting in horizontal layering (the cell was packed vertically). The slight DPHP underestimation noticeable for Sensors 1 and 2 throughout the whole water content range has previously been reported (Basinger et al., 2003; Bristow et al., 2001).

In the case of 1–2 mm ceramic aggregates (Fig. 5.7b) the sensor under-predicts water contents in the range of 0.4–0.6 cm^3 cm^{-3}. We attribute this in part to the vertical gradient in water content. The volume sensitive to the heat-pulse measurement likely has a lower water content compared to the average water content. Steinberg and Poritz (2005) demonstrated that 1–2 mm ceramic aggregates drain over a relatively small range of suction comparable to the 2 cm vertical extent of the cell. Further, contact problems between the probe and the particles may have affected the predictions. The diameter of the probe is similar to the particle size resulting in fewer contact points between the probe and the media.

When comparing DPHP and SPHP performance based on the analytical approach that does not require calibration other than fitting probe spacing to measure-ments made in saturated media, it is apparent that the DPHP method shows good accuracy for the entire water content range. The SPHP performance based on media specific calibrations shown in Fig. 5.7 (c and d) shows the water content estimates based on a best-fit linear calibration. The effects of the heterogeneous water content distribution in 0.25–1 mm aggregates are more pronounced when compared to the DPHP estimates. The reason for this difference could be the result of the smaller sampling volume of the SPHP sensor.

Statistical results for the pooled measurements of the three SPHP and DPHP in each of the two porous media are given in Fig. 5.7. The average apparent probe spacing (r_{app}) and standard deviation for each probe are listed showing less variation in r_{app} for 0.25–1 mm ceramic aggregates. At least five water content determinations were made for each probe at saturation to obtain the

fitted *rapp*-values. The root mean squared error was also computed for the difference in DPHP and SPHP determinations compared to the independently measured values over the entire range of water contents. These values indicate that the SPHP sensor errors are comparable to the DPHP errors.

5.5.2 Electrical Conductivity

Determining nutrient status from bulk electrical conductivity measurements necessitates estimating the solution electrical conductivity from the bulk measurement. Below we present estimates of solution electrical conductivity in saturated and unsaturated media followed by information on sensitivity and robustness of the electrical conductivity measurements. We demonstrate the need for caution interpreting bulk electrical conductivity measurements because the integration takes place over a complex volume, which in turn is dependent on constituent physical properties. This is illustrated by time-dependent measurements that track diffusion of solutes in a porous medium.

Saturated Measurements with a Solute Pulse

A solute pulse was passed through the shallow-sample cell filled with 1–2 mm ceramic aggregates, and the bulk electrical conductivity was measured. The bulk electrical conductivity values were determined from the electrode configuration calibration in Eq. (5.6). Solution electrical conductivities were estimated solving Eq. (5.4) and optimizing parameters *a* and *m* (*a*=0.64, *m*=1.7). The estimated solution electrical conductivity was compared in Fig. 5.6 with the measured effluent electrical conductivity measured at the cell outlet using an EC meter. The over-prediction in the salinizing and the under-prediction in the desalinizing period are attributed to the temporal and spatial separation between the 4-electrode probe and the EC meter in addition to diffusion into the aggregates and adsorption of the salt on the solid. Because the EC meter is located at the outlet of the cell, changes in σ_w in the cell are first sensed by the 4-electrode array, with the EC meter lagging behind. Further, the EC meter measures the effluent exiting the cell after a complicated mixing process between tap and saline water in the cell (convective) and inside the aggregates (diffusive). The data in Fig. 5.8 indicates the difference in ion dispersion of the pulse front moving through the cell.

Unsaturated Static Measurements

To evaluate the 4-electrode array response under unsaturated static-equilibrium conditions, the volumetric water content was adjusted using a syringe. For purposes of evaluating the σ_w prediction methodology, we used the syringe-controlled (bulk) water content instead of the heat-pulse sensed water content. The results in Fig. 5.7 show measured data for glass beads and macropore data in ceramic aggregates (i.e., micropores were not drained).

Modeled results were obtained by fitting parameters *a*, *m*, and *n* to the experimental data. Fitted values for 1–2 mm glass beads were 0.33, 1.5, 1 and for 1–2 mm ceramic aggregates were 0.64, 1.7, 1.0 for *a*, *m*, and *n*, respectively. Notice that coincidentally the total porosity of the glass beads is equivalent to the microporosity of the 1–2 mm ceramic aggregates (i.e. the macropores of the ceramic aggregate finish draining near the saturation of the glass beads). Both data sets exhibit a linear relationship between bulk conductivity and water content (for glass bead θ greater than 0.2) indicated by a saturation exponent *n*=1 for both materials. We attribute the linear relationship to the contribution of the solid phase conductivity in the case of 1–2 mm ceramic aggregates, and more importantly, to the presence of water films prohibiting the electrical isolation of water absorbed in the particles or held in pore crevices (Suman and Knight, 1997). Bulk conductivities measured below 0.2 water content are reduced compared to the model. We attribute this to measurement deficiencies at such low conductivities (see subsection Measurement Sensitivity).

Using the fitted model, i.e., Eq. (5.4), it is possible to predict the solution electrical conductivity from the bulk conductivity measurements.

Figure 5.9 illustrates the capability of the 4-electrode array to provide solution electrical conductivity estimates from bulk water content determinations. It is evident, that the accuracy of the σ_w prediction is limited by the accuracy of sensing water content.

Measurement Sensitivity

The conductivity measurement is not equally sensitive to all volume elements because the apparent conductivity is an integral measurement lumping a complicated three-dimensional conductivity distribution into a single value. Electrodes may be configured in several ways were each exhibits

a characteristic distribution of sensitivity. Some volume elements will be more influential in the bulk measurement than others. Figure 5.8 illustrates the two-dimensional sensitivity distributions for the Focused and Wenner electrode configurations. The Focused array refers to the configuration used in this study (AB=3.6 cm, MN=2.4 cm). The equidistant Wenner array uses AB=3.6 cm and MN=1.8 cm. Features common to these distributions are that the greatest sensitivities are observed around the electrodes and at the container surface between the electrodes, and that the sensitivity decreases moving away from the electrodes. Distinctions can be made between the configurations considered. For example, the Wenner configuration has relatively constant sensitivities laterally and resolves the half-space uniformly. This is why the Wenner configuration is preferred for mapping. The focused array shows slightly higher sensitivities at larger radial distances at the expense of increased sensitivities in the immediate surroundings of the electrodes. The major difference, however, is the slightly reduced lateral homogeneity of the sensitivity distribution for the focused compared to the Wenner configuration.

While the sensitivity is a quantity aiding in data interpretation and optimization of a configuration for a given target, the robustness of the conductivity measurement is determined by the range, accuracy and precision of the voltage and current measurement and the geometry factor calibration (Eq. (5.5)). Conductivities of unsaturated porous media can vary over several orders of magnitude with the degree of saturation and the solution electrical conductivity. It is therefore the conductivity that primarily determines the voltage and current measurement. Provided a constant current driver operates in its optimal range, the voltage measurements determine the measurement precision. It is hence desirable to measure large voltages at small geometry factors. Figure 5.9 demonstrates voltage drop and geometry factor, as a function of the spacing between AM (compare Fig. 5.1) for a symmetrical configuration were the outer electrodes (AB) are the current electrodes.

Notice that at high conductivities (for example saline, saturated conditions) and large spacings between AM (i.e. MN very small), the maximum resolution of the data-logger (in the 2.5 mV range: 0.33 mV) limits the precision of the measurement. More importantly, small perturbations in the configuration of the electrodes at large AB will result in increased error propagation for the conductivity estimation (multiplication of a small erroneous conductance with large geometry

factor). Compared to the Wenner configuration, the focused configuration uses an increased spacing between the potential electrodes which results in larger measured voltages at smaller geometry factors.

For low conductivities (e.g., unsaturated conditions), it is the ability to induce a current across electrodes AB that becomes the limiting factor for measurements. It is likely that the constant current driver will not operate optimally under these conditions, i.e. higher voltage generation across AB, suggesting larger gradients are needed to drive a current under low conductive conditions. This may result in significantly reduced current induction, which in turn results in a reduced potential drop across electrodes MN. It is under these conditions that the S/N ratio decreases. If the spacing between the current electrodes is fixed, it is beneficial to sense a larger potential drop at reduced currents.

Saturated Measurements of Solute Diffusion

We chose five configurations for the electrical conductivity measurements. The configurations and the measured configuration factors are given in Table 5.2. Solution electrical conductivity was predicted using Eq. (5.4). The parameters a=0.64, and m=1.7 were taken from parameter optimizations described in subsection Saturated Measurements with a Solute Pulse.

Solution electrical conductivities as a function of time are shown in Fig. 5.10. Measurements were initiated immediately after packing. The predicted initial solution electrical conductivity (0.045 S m^{-1}) corresponds well with the measured σ_w of the tap water used for saturating and packing the porous media. As the fertilizer started to release ions, the sensed sw increased in both sides of the container. In the part of the pseudo root module packed with fertilizer, σ_w increased by a factor of five in a period of 24 hours. In the part with no fertilizer the sensed solution electrical conductivity also increased, but to only about half the magnitude. This increase is indicative of a diffusive transport of ions from the higher concentration in the fertilized part towards the low concentration. Note that for the measurements in the fertilized part of the module, the rate of increase in electrical conductivity changed from an initial rapid increase to a much slower rate. We speculate that ions entering solution out of the fertilizer pellets contributed to the initial rapid increase.

As these ions were taken out of solution by sorption onto/into the aggregates, the rate of increase decreased because of the reduced contribution of free ions in solution.

5.6 Conclusions

Long-term plant growth in containerized media can suffer from salt buildup due to slow release fertilizers or nutrient solution additions. This occurs due to excess plant nutrient additions and a lack of free drainage that would remove excess salts. The ability to monitor nutrient status of plant growth media could minimize or eliminate this problem and provide researchers with valuable spatial and temporal information on water potential and content within the root zone. The integrated measurement method presented here provides a relatively accurate and robust approach for estimating volumetric water content and nutrient status via solution electrical conductivity in unsaturated porous media.

We considered single-probe and dual-probe heat-pulse sensors to estimate water contents in a multi-step outflow experiment. We conclude that the accuracy of the dual-probe sensors is comparable to the single-probe sensors. The dual-probe sensor, which comprises two needle-sized probes, has the advantage of a single point calibration (i.e., under saturated conditions). In cases where the particle size was on the order of the dual-probe sensor's needle diameter, we attributed water content estimate variations to contact resistance as fewer particles were in contact with the probe. In the current mode of operation, the dual-probe sensors consume less than half the power compared to the single-probe sensors.

We showed results of two dual-probe heat-pulse sensors combined to form a 4-electrode configuration for measuring electrical conductivity. It was shown that variations in the bulk electrical conductivity due to water content changes were well described using Archie's Law for water contents above 0.2 cm^3 cm^{-3}. The numerical estimates indicate that the saturation was linearly related to bulk electrical conductivity in the range of water contents tested. These results demonstrate the ability of the integrated electrical conductivity sensors to accurately predict the solution electrical conductivity under unsaturated conditions. We pointed to the advantages of using a larger spread between the potential electrodes over the equidistant Wenner configuration. In this case, signal

to noise ratios can be improved with small sacrifices to lateral uniformity in the sensitivity distribution of those configurations. The benefit of such configurations will be most noticeable at low conductivities where current induction limits measurement sensitivity.

The integrated heat-pulse and electrical conductivity measurement method for water content and bulk electrical conductivity determination provides valuable management and assessment tools for containerized plant growth media. The tool gives researchers a means to study the effect of water content, and nutrient release and uptake in the root zone at a scale suitable for current plant production units used in spaceflight applications.

5.7   References

Archie, G.E. 1942. The electrical resistivity log as an aid in determining some reservoirs characteristics. J. Petroleum Technology 5:1-8.

Basinger, J.M., G.J. Kluitenberg, J.M. Ham, J.M. Frank, P.L. Barnes, and M.B. Kirkham. 2003. Laboratory evaluation of the dual-probe heat-pulse method for measuring soil water content. Vadose Zone J. 2:389-399.

Bingham, G.E., I.G. Podolsky, T.S. Topham, and J.M. Mulholland. 2002. Lada: The ISS plant substrate microgravity testbed. SAE Technical Paper 2002-01-2388. SAE Int., Warrendale, PA.

Bristow, K.L., G.J. Kluitenberg, C.J. Goding, and T.S. Fitzgerald. 2001. A small multi-needle probe for measuring soil thermal properties, water content and electrical conductivity Comput. Electron. Agric. 31:265-280.

Campbell, G.S., C. Calissendorff, and J.H. Williams. 1991. Probe for measuring soil specific heat using a heat-pulse method. Soil Sci. Soc. Am. J. 55:291-293.

Furche, M., and A. Weller. 2002. Sensitivity distributions of different borehole electrode configurations considering a model with a cylindrical coaxial boundary. Geophysical J. International 149:338-348.

Ham, J.M., and E.J. Benson. 2004. On the construction and calibration of dual-probe heat capacity sensors. Soil Sci. Soc. Am. J. 68:1185-1190.

Heinse, R., S.B. Jones, S.D. Humphries, R.W. Mace, S.L. Steinberg, M. Tuller, R. Newman, and D. Or. 2005. Measurement of porous media water retention during parabolic flight induced microgravity. SAE Technical Paper 2005-01-2950. SAE Int., Warrendale, PA.

Hoehn, A., P. Scovazzo, L. Stodieck, J. Clawson, W. Kalinowski, A. Rakow, D. Simmons, A.G. Heyenga, and M.H. Kliss. 2000. Microgravity root zone hydration systems. SAE Technical Paper 2000-01-2510:1-10. SAE Int., Warrendale, PA.

Jones, S.B., D. Or, G.E. Bingham, and R.C. Morrow. 2002. ORZS: Optimization of root zone substrates for microgravity. SAE Technical Paper 2002-01-2380. SAE Int., Warrendale, PA.

Kluitenberg, G.J., J.M. Ham, and K.L. Bristow. 1993. Error analysis of the heat pulse method for measuring soil volumetric heat-capacity. Soil Sci. Soc. Am. J. 57:1444-1451.

Knight, J.H., and G.J. Kluitenberg. 2004. Simplified computational approach for dual-probe heat-pulse method. Soil Sci. Soc. Am. J. 68:447-449.

Levine, H.G., G.K. Tynes, and J.H. Norikane. 2003. Fluid behavior under microgravity conditions within plant nutrient delivery systems: Parabolic flight investigations. SAE Technical Paper 2003-01-2483. SAE Int., Warrendale, PA.

Mori, Y., J.W. Hopmans, A.P. Mortensen, and G.J. Kluitenberg. 2003. Multi-functional heat pulse probe for the simultaneous measurement of soil water content, solute concentration, and heat transport parameters. Vadose Zone J. 2:561-571.

Mori, Y., J.W. Hopmans, A.P. Mortensen, and G.J. Kluitenberg. 2005. Estimation of vadose zone water flux from multi-functional heat pulse probe measurements. Soil Sci. Soc. Am. J. 69:599-606.

Morrow, R.C., T.M. Crabb, R.J. Anderson, and D.J. Smith. 2001. A microprocessor based soil moisture sensor system for space based plant growth units. SAE Technical Paper 2001-01-2178. SAE Int., Warrendale, PA.

Newman, R.M., G.J. Kluitenberg, and S.L. Steinberg. 2005. Evaluation of the Dual-Probe Heat-Pulse Method for Measuring Water Content in Spaceflight Plant Growth Systems. SAE Technical Paper 2005-01-2951. SAE Int., Warrendale, PA.

Norikane, J.H., S.B. Jones, S.L. Steinberg, H.G. Levine, and D. Or. 2004. Porous media matric potential and water content measurements during parabolic flight. Habitation 10(2):117-26.

Ochsner, T.E., R. Horton, G.J. Kluitenberg, and Q. Wang. 2005. Evaluation of the heat pulse ratio method for measuring soil water flux. Soil Sci. Soc. Am. J. 69:757-765.

Ren, T., Z. Ju, Y. Gong, and R. Horton. 2005. Comparing heat-pulse and time domain reflectometry soil water contents from thermo-time domain reflectometry probes. Vadose Zone J. 4:1080-1086.

Spitzer, K. 1998. The three-dimensional DC sensitivity for surface and subsurface sources. Geophysical J. International 134:736-746.

Steinberg, S.L., and D.L. Henninger. 1997. Response of the water status of soybean to changes in soil water potentials controlled by the water pressure in microporous tubes. Plant Cell Environ. 20:1506-1516.

Steinberg, S.L., and D. Poritz. 2005. Measurement of hydraulic characteristics of porous media used to grow plants in microgravity. Soil Sci. Soc. Am. J. 69:301-310.

Stutte, G.W., O. Monje, G.D. Goins, and B.C. Tripathy. 2005. Microgravity effects on thylakoid, single leaf, and whole canopy photosynthesis of dwarf wheat. Planta 223:46 - 56.

Suman, R.J., and R.J. Knight. 1997. Effects of pore structure and wettability on the electrical resistivity of partially saturated rocks—A network study. Geophysics 62:1151-1162.

Table 5.1: Pooled apparent probe spacing (r_{app}), and standard deviation (STDEV) for the DPHP sensors used in the DPHP water content prediction, and linear least squares model for predicting the SPHP water content prediction based on maximum temperature rise T_m.

Porous Media	Sensor	Prediction	r_{app} mm	STDEV mm
1–2 mm	DPHP	Eq. 1–3	5.54	0.17
aggregate	SPHP	$\theta_{SPHP}=2.27T_m$-0.30		
0.25–1 mm	DPHP	Eq. 1–3	5.53	0.14
aggregate	SPHP	$\theta_{SPHP}=2.22T_m$-0.27		

Table 5.2: Electrode configurations, geometry factors (G) and standard deviation of geometry factors (STDEVG). V and I indicate voltage measurement across M-N and current induction across A-B, respectively (compare Fig. 5.7). Lower case roman numerals indicate probe configurations.

Configuration	M-N (V)	A-B (I)	G m	STDEVG m
i	2-3	1-4	0.0521	0.0004
ii	4-5	3-6	0.0516	0.0007
iii	1-6	2-3	0.0849	0.0008
iv	1-6	4-5	0.0865	0.0007
v	1-6	2-5	0.0422	0.0005
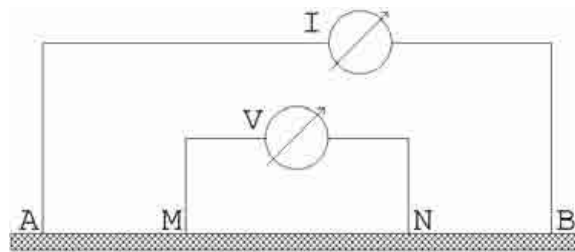
Fig. 5.1: Four-electrode configuration for apparent electrical conductivity measurements showing current induction (I) and potential difference (V) measurements.
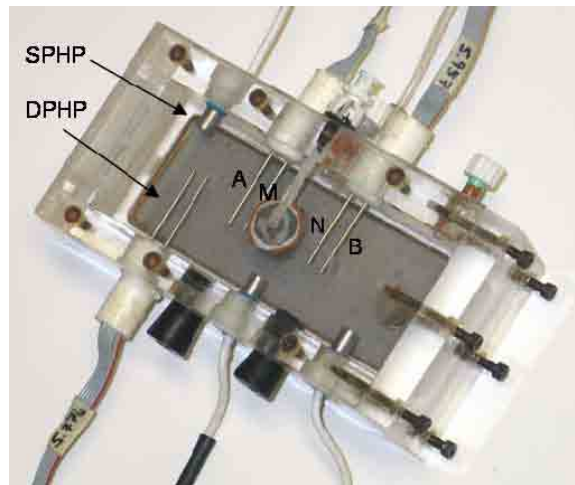
Fig. 5.2: Shallow sample cell (12x5x2 cm) showing the installment of the single-probe heat-pulse (SPHP) and dual-probe heat-pulse (DPHP) sensors. Letters AMNB indicate the DPHP sensors used for the electrical conductivity measurements.
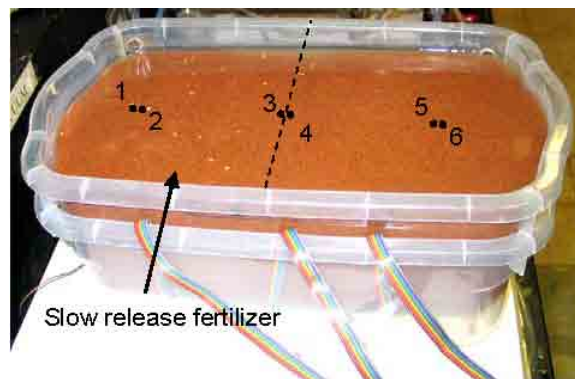
Fig. 5.3: Photograph of the pseudo root module experimental setup showing the porous media filled container. The three DPHP sensors are indicated (dots), and their probes numbered. Sensors were installed vertically from the bottom of the container spaced 7.5 cm apart. The cell was packed with 0.25–1 mm ceramic aggregate, were the left half of the container was mixed with slow release fertilizer.
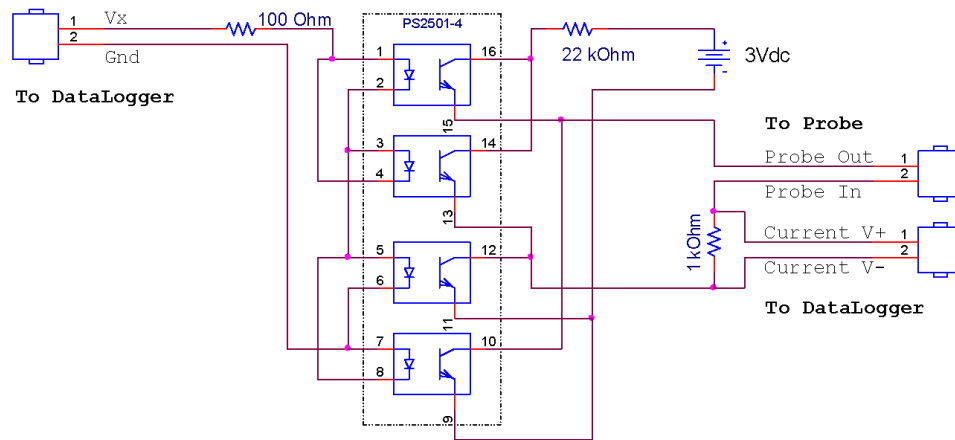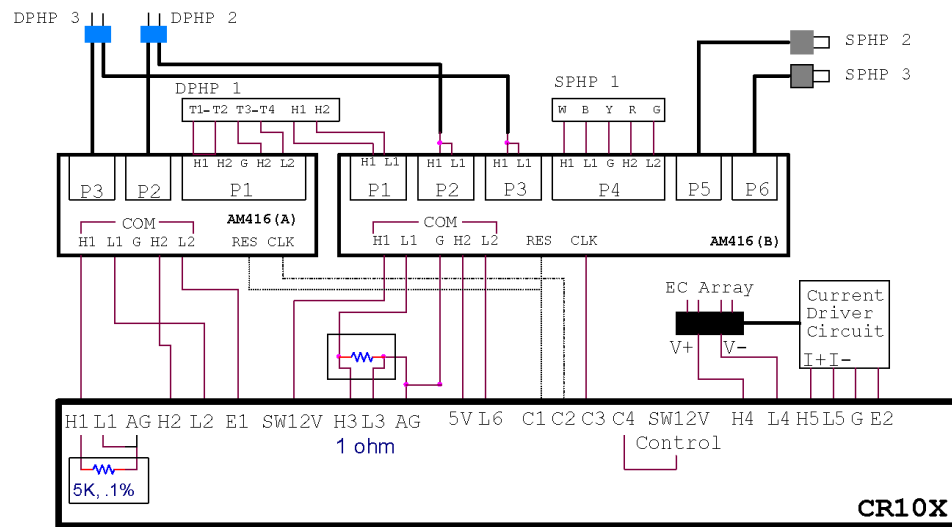
Fig. 5.4: Data acquisition and control system circuit diagram showing the single- and dual-probe heat-pulse sensor and electrical conductivity measurement wiring (top), and constant current driver (bottom).
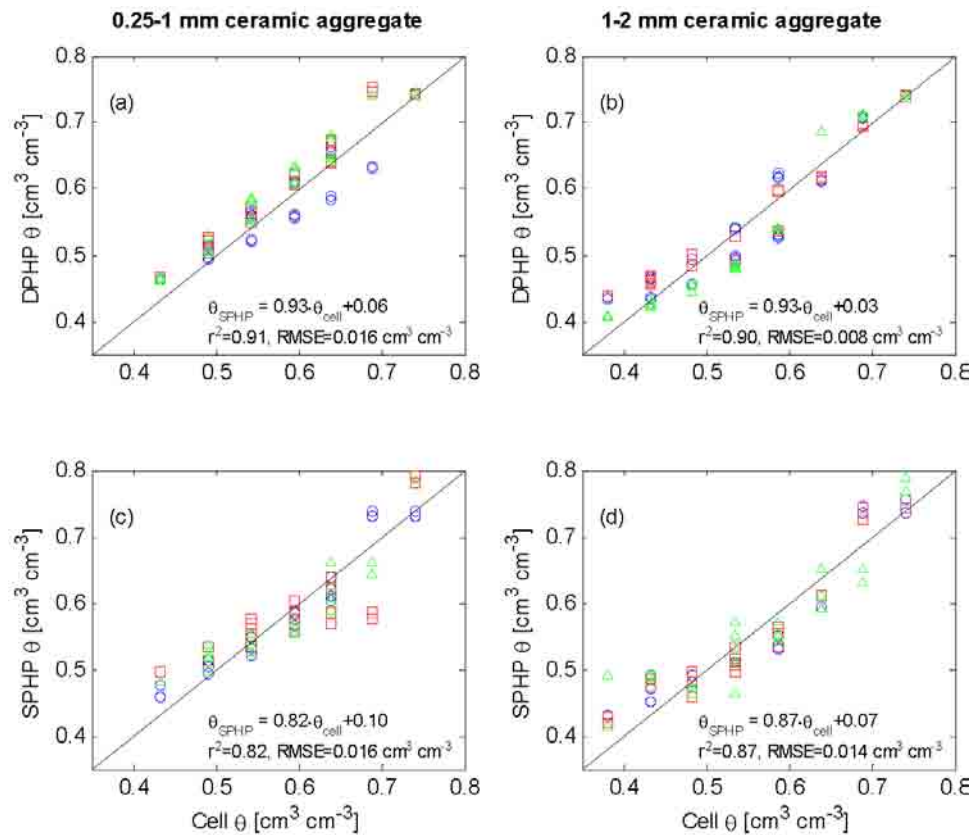
Fig. 5.5: Comparison of predicted with independently measured volumetric water contents for two ceramic aggregates. (a+b) DPHP predictions using the analytical approach. (c+d) SPHP estimates based on empirical linear best fit. The solid line indicates the 1:1 line. Slope and intercept (line not shown) of the statistical analysis of the water content relationship between DPHP, SPHP and cell water content are given in the inset. The square of the correlation coefficient (r^2) and the root mean square error (RMSE) for the water content prediction in 1–2 mm (ρ_b=0.65 g cm^{-3}) and 0.25–1mm (ρ_b=0.647 g cm^{-3}) ceramic aggregates are also given.
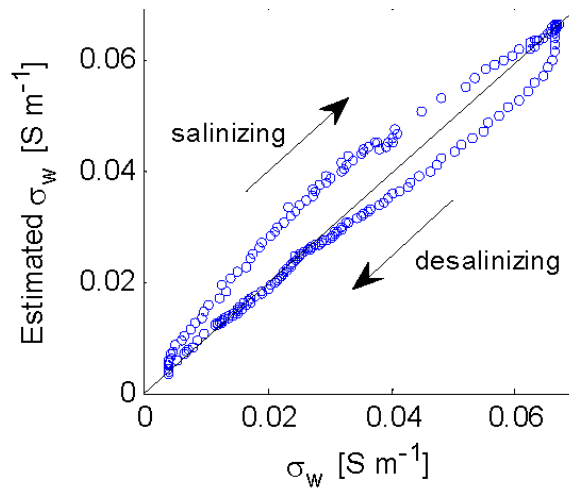
Fig. 5.6: Measured and estimated solution electrical conductivity obtained at steady state saturated flow (q=4 ml min^{-1}). A saline pulse (σ_w=0.68 S m^{-1}) was passed through tap-water saturated 1–2 mm ceramic aggregate (salinizing) until steady state conductivities were reached; at which point tap water was re-introduced to the cell (desalinizing). Estimated σ_w determined from σ_b measured inside the cell, while σ_w was measured at the outlet of the cell.
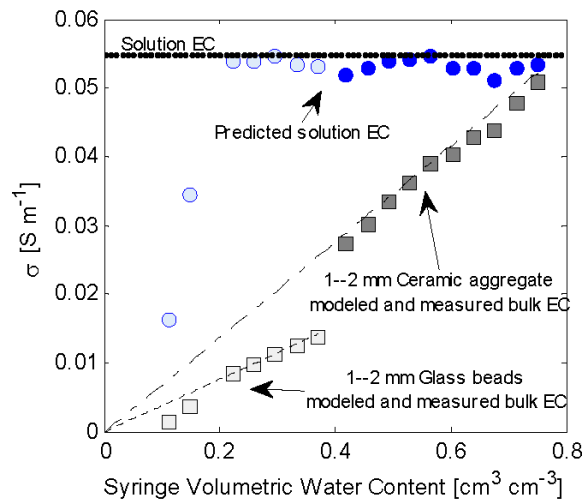
Fig. 5.7: Predicted solution electrical conductivity (circles) as a function of average (syringe) water content for 1–2 mm glass beads and 1–2 mm ceramic aggregates. Dashed lines indicate fitted models to the bulk electrical conductivity measurements (Eq. (5.4)). Convergence of bulk EC and solution EC near saturation in ceramic aggregates is coincidental and partially attributed to surface conductance of aggregates.
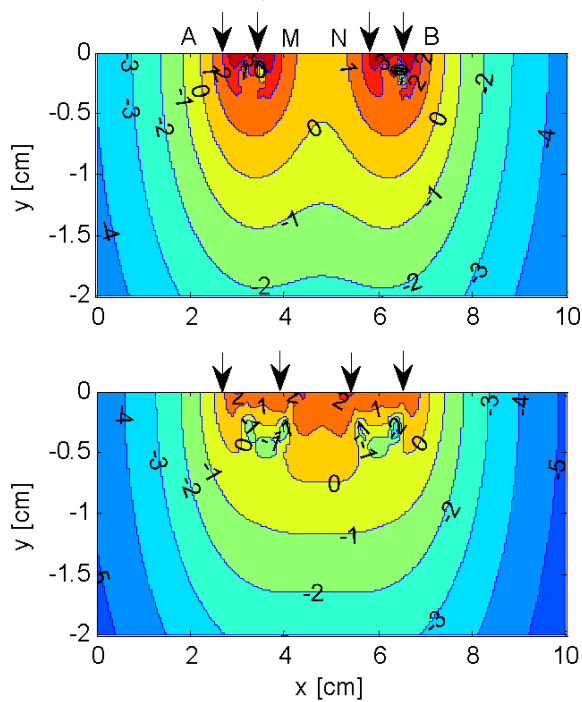
Fig. 5.8: Absolute sensitivity distribution on a log-scale for the Focused (used in the shallow sample cell) (top) and Wenner (bottom) electrode configuration assuming a homogeneous half space.
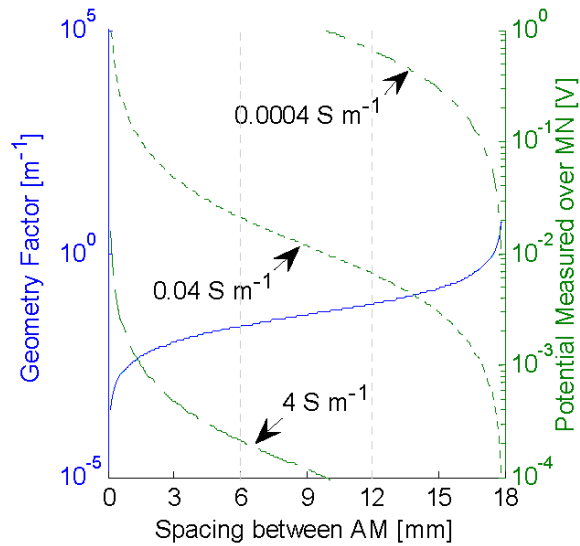
Fig. 5.9: Geometry factor and potential drop over the potential electrodes (MN) as a function of the spacing between AM for a symmetrical electrode configuration. The calculations using Eq. (5.5) assume a homogeneous half space with conductivities indicated in the figure. The total spread between the current electrodes AB (constant current 0.048 A) is held constant at 36 mm. The spacing between AM for the focused configuration is 6 mm (indicated by the gray dashed line), and the spacing for the equidistant Wenner configuration is 12 mm (see Fig. (5.4)).
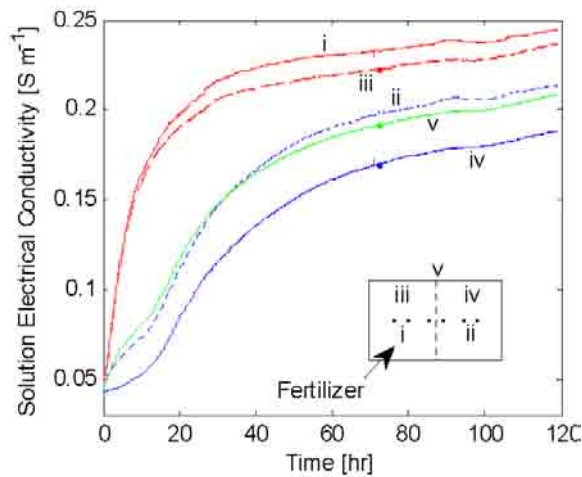
Fig. 5.10: Change in solution electrical conductivity as a function of time for five electrode configurations during a slow release fertilizer experiment. Electrical conductivity measurements were made using 4-electrode configurations employing DPHP sensors. The approximate volume sensitive to the measurements is indicated in the inclusion. Detailed information on the configurations can be found in Table 2.

CHAPTER 6

SUMMARY AND CONCLUSIONS

At the core of this research stood the question whether and how the hydraulic performance of porous plant-growth media changes in the absence, or partial presence, of gravity. Past plant growth experiments in microgravity had indicated the former, but have improved in the past 35 years to produce vigorous plants, with multiple examples of successful seed to seed experiments (albeit under low light conditions, reducing the demand on the root-zone resource supply). Has the notion of gravity effects passed? Certainly not, but space greenhouses have adapted using trial and error and empirical adjustment to control set points and choice of mm-sized media. Little of this advance was based on improved deterministic understanding of the complex interactions of fluids and matrix in reduced gravity. Perspectively, this comes as no surprise as these interactions are still the subject of intense research for soils under terrestrial gravity conditions where we have much higher accessibility to experimentation and execution of multiphase models. Studying multiphase flow in reduced gravity on the other hand is very much opportunity limited. The list of long duration space experiments targeting multiphase flow in coarse-textured porous media is stunningly short. Whilst pore scale effects (foremost contact angle issues) in reduced gravity have been studied more intensely, upscaling these singular effects to predict performance at the root-module scale has not produced the needed answers. A few researchers have studied sample-scale multiphase flow in short-duration reduced gravity using drop towers or parabolic flight. However, these environments bring their own challenges, foremost the short duration, that limit the power of the conclusions gained from these experiments. A convenient diversion from the experimental limitations is the attempt to predict root-zone performance using numerical modeling of multiphase flow. There are no indications that fundamental relationships derived on Earth are not applicable in reduced gravity. However, accentuated hysteretic-bound heterogeneities, enhanced phase entrapment, preferential wetting and particle rearrangement are likely to produce phase distributions not observed on earth. Quantifying these

distributions will consequently facilitate advanced modeling of reduced-gravity root-zone performance and enable the development of improved, resourceful root-zones for microgravity in space travel and partial gravity on planetary habitats.

6.1   Summary of Findings

The results presented in the body of this dissertation included the improved characterization of the spatio-temporal behavior of porous-media-water and -gases in variable and reduced gravity by studying the water retention, saturated flow and gaseous diffusion in unsaturated particulate porous media. Furthermore, an integrated method for sensing soil water and nutrient concentration, specifically for restricted root-zones, was developed, improving the accuracy and capability of root-zone monitoring systems.

In Chapter 2, measurements during parabolic-flight induced variable gravity showed the dynamic behavior of matric potentials during transitions from 1.8g to μg. We found that the non-linear migration toward static equilibrium was a function of hydraulic diffusivity with the transition slowing at decreased water contents. While transitioning from 1.8g to μg and vice versa, matric potentials tracked secondary drainage or wetting water-retention curves simultaneously depending on the vertical position in the experimental cells, illustrating that minimal changes in water content fulfilled both the 1.8g and the μg matric potential conditions. The resultant spatial heterogeneity in the distribution of water contents, maintained during variable gravity, pointed toward history-dependent heterogeneous water contents in μg amid uniform hydraulic potentials. This finding falsified one of the implicit assumptions of root-zone water contents in microgravity. While reduced gravity forces result in reduced water content gradients with diminished gravity potentials, the hysteretic nature of the water-content/matric potential relationship could maintain water content differences within the root zone. In the case of Turface (1–2 mm particle size), this could result in significant water content gradients. For example, at a matric potential of -4 cm, water contents could traverse a range of 0.5–0.67 cm^3 cm^{-3}. Measurements in parabolic flight approximated microgravity water-retention characteristics from quasi-steady state conditions at the end of the μg phase. Despite the apparent influence of the hypergravity phase on dynamic water retention, measurements suggested

similar water-retention characteristics compared to 1g for wetting conditions. Drainage water retention data generally fell below the 1g measured data, with the disparity being attributed to the uncertain redistribution of water following the ensuing hypergravity phase. Water retention results highlighted open questions about the long-term applicability of parabolic flight experiments raised by the timescale of some processes in excess of the 20 s of μg and the dynamic constraints with the ensuing hypergravity phase required for proper flight trajectory. Saturated hydraulic conductivities measured during parabolic flight were found to be in close agreement with measurements conducted on the ground. Results indicated that the relationship between hydraulic gradient and flux could be described with a linear function (Buckingham-Darcy's law), corroborating the expected gravity-independence of saturated flow when rigid pore structures were maintained (i.e. no particle rearrangement). Simulations of experimental data presented evidence of altered dynamics of liquid behavior in porous media, but corroborated the applicability of the Richards equation for describing macroscopic porous-medium fluid behavior under microgravity conditions with the gravity term approaching zero.

Chapter 3 detailed measurements aboard the international space station (ISS) investigating the effect of reduced gravity on porous-media diffusive oxygen-transport and water-retention considering wetting and draining processes not limited by dynamic constraints. Results suggested that accounts of fluid transport were part of a larger story of fluid distribution when gravitational and capillary forces are shifting. Considerations on the terrestrial hydrostatic distribution of water contents in samples of vertical extents exceeding the air-entry value suggested higher horizontal effective-diffusion rates compared to a sample with uniformly-distributed water contents. For the oxygen diffusion observations in microgravity, no significant differences from terrestrial observations for the draining characteristic were noted. For the wetting characteristics, however, significant deviations from terrestrial observations displaying enhanced hysteretic behavior, with increased air-percolation thresholds and increased apparent tortuosity not observed on earth, were noted. This reduction in oxygen diffusion rates was most notable for the smaller particle-sized Profile (0.25–1 mm) while also being perceived in Mix (0.25–1 mm), but not in the larger particle-sized Turface (1–2 mm). We attributed the difference to a significantly different distribution of water in the sample in micro-

gravity not experienced on earth where the lack of a hydrostatic distribution lead to a speculated asymmetrical draining pattern with isolated water-filled pores retarding rapid diffusive transport. While partially speculative, the results suggest no significant impact of microgravity on the diffusive transport per se, but suggest a significant impact on the fluid distribution affecting the sample scale (i.e. effective) diffusive transport. With sample-scale water-retention characteristics largely unaffected by microgravity, the observed differences demonstrated the unanticipated behavior in fluid distributions with fluid transport in pursuit of a capillary equilibrium within the hysteretic, contingent energy potential of water. Altered water distribution patterns, relative to earth-based measurements, leading to the formation of a critical air-filled pathway at higher saturation in microgravity (i.e., due to the absence of hydrostatic water distribution) would require adjustment in plant-growth system management protocols and possible model development for reliable response prediction of microgravity systems.

Chapter 4 described balanced root-zone fluxes based on the distribution of water in plant-growth media. We addressed the lack of a terrestrial testbed capable of simulating the more disperse matric-potential driven water-content distribution. We designed a stratified root-zone based on wetting water-retention characteristics and theorized on the targeted design fluxes of water and gases that could provide a more optimal root zone. The benefits of the optimized system design included maintaining a more uniform water content and on-demand supply of water compared with the dynamic range of water content in conventional designs with uniform media. While the optimized design describes a possible root-zone scheme for terrestrial gravity, we demonstrated the adaptability for the use of similar systems under planetary gravity conditions. We further tested the ramifications of roots altering their physical and hydraulic environment theorizing that high root densities and restricted root zones increase the resource-supply demand per root-volume element and could alter the pore-size distribution and saturated water content. While our limited results did not suggest a significant change in measured water-retention characteristics in rhizosphere media compared to bulk porous media, we advocated for the inclusion of corrective models describing the reduction in plant-available water. We further pointed out that an overprediction of plant-available water is likely at high root densities using state-of-the-art volume-averaging water-content sensors

that fail to distinguish between water held in pores and water held in roots. When controlling hydration based on water-retention characteristics or water content sensing, the development of predictive capabilities describing the temporal changes in root-zone hydraulics with root proliferation were suggested.

In Chapter 5, we presented an integrated measurement method providing a relatively accurate and robust approach for estimating volumetric water content and nutrient status via solution electrical conductivity in unsaturated porous media. We found the water-content sensing accuracy of the dual-probe sensor to be comparable to the currently used single-probe sensor. The dual-probe sensor, which consisted of two needle-sized probes, has the advantage of a physical, single-point calibration over an empirical calibration required for the single-probe sensor. In the current mode of operation, the dual-probe sensors consumed less than half the power compared to the single-probe sensors. We showed results of two dual-probe heat-pulse sensors combined to form a 4-electrode configuration for measuring electrical conductivity. Variations in the bulk electrical conductivity due to water-content changes were well described using a modified Archie's Law for water contents in the macropore region. The numerical estimates indicated that the saturation was linearly related to bulk electrical conductivity in the range of water contents tested. These results demonstrated the ability of the integrated electrical conductivity sensors to accurately predict the solution electrical conductivity under unsaturated conditions. We pointed to the advantages of using a larger spread between the potential electrodes over the equidistant Wenner configuration, where signal-to-noise ratios could be improved with small sacrifices to lateral uniformity in the sensitivity distribution. The benefit of this configuration would be most noticeable at low conductivities where current induction limits measurement sensitivity. The integrated heat-pulse and electrical conductivity measurement method for water content and bulk electrical conductivity determination provides a valuable management and assessment tool for containerized plant-growth media. The tool gives researchers a means to study the effect of water content, and nutrient release and uptake in the root zone at a scale suitable for current plant production units used in spaceflight applications.

6.2   Confounding Issues that Might Impact μg Root-Zone Performance

Because space is our Manifest Destiny, it is important to move beyond confounding micro-gravity effects and develop research-based bioregenerative life support systems. While the results and conceptual understandings shown in this research show great promise for future development, management and optimization of root zones in micro- and planetary- gravity, a number of factors could serve to confound these objectives if not properly studied. These include variations in the distribution of fluids in microgravity, variations in the sample-scale physical properties of porous media with root growth, microscale fluxes of water and gases, and the distribution and release of slow release fertilizer.

Distribution of Fluid in Microgravity

Indications of altered distributions of fluid within the physical framework, but not observed on earth, appear to contribute to stunted, often unexplained plant vigor in mirogravity. Effects of reduced gravity may manifest themselves in altered fluid distribution and transport, especially when considering a shift from silt-sized to sand-sized particles. This has implications on water film thickness, unsaturated hydraulic conductivity and diffusion path lengths at pore-scales that we have little experience with. Soil physical principles can be applied to unlock these challenges of controlling fluids in porous rooting environments and should be coupled with tomographic reconstructions of fluid distributions.

Hydraulic Properties of Rooted Media

In designing root zones with physical conditions that allow for more optimal plant growth, the question stands, at what root density will initial conditions be altered with progressing root development. In particular, the questions stands if hydraulic properties of the root-zone media, largely determined through the pore size distribution, undergo a temporal change as roots selectively occupy pores and alter the bulk density of the media. Because the distribution of water so crucially determines fluxes of water, gases and nutrients to the roots, the water retention characteristic needs to be quantified as a function of increasing root densities to predict the long term applicability of root zones designs.

Microscale Fluxes of Water and Gases

Along with the hydraulic properties of rooted media come ramifications of roots altering their microenvironment rarely addressed on earth much less in microgravity. With the current direction of using coarse particulate porous media there is a need to study the contact resistance for water and gaseous fluxes from the bulk media to the roots. With indications of root hypoxia the impact of microgravity on the development and thickness of water films around plant roots further gains in significance.

Supply, Distribution and Monitoring of Fertilizer

While hydrostatic water distributions on earth and free draining root zones provide predictable fertilizer distributions and removal of excess nutrients, microgravity root zones, particularly considering finite and restricted volumes, could suffer from the accumulation of excess salts. With the lack of drainage comes the need to dose nutrients according to plant needs. Because electrical conductivity sensors fail to distinguish between ions, the accumulation of undesirable ions could be misinterpreted as a balanced nutrient concentration. Further, with hysteretic water-content differences mapped on a constant water supply-source the redistribution of nutrients from a slow-release fertilizer may be limited to diffusive transfer, where water fluxes through the root zone may bypass a significant portion of nutrient pellets.

6.3   Future Directions

The results of the current research show that while water-retention characteristics and diffusivity responses are not fundamentally different, a number of issues exist which warrant further investigation and extent beyond the currently considered scope. Future research should focus on a number of areas, namely:

1. Use of engineered plant-growth media with manufactured pore-size distributions and possible use of hydrophobic and hydrophillic pathways.

2. Optimization of supply source distributions for water flux, nutrient release and gas exchange.

3. Temporal changes in root-zone and rhizosphere properties including the impact of microgravity on the microscale transport from the bulk media to the plant root.

4. Development of root-zones for planetary habitats with the use of processed local regolith based on gravity force and capillarity.

5. Upscaling and development of plant-production systems for bioregenerative life support for long-term missions and habitat establishment less restricted by limited volumes and energy (i.e. farming in space).

6.4 Conclusions

The distribution of water directly or indirectly controls the management of water, air and nutrients in coarse-textured porous plant-growth substrates. With the motivation to involve plants in future life support systems in space, we posed the question whether fluid behavior in porous substrates is altered when subjected to microgravitational accelerations. Central to unraveling this question was the water retention characteristic; an often used control parameter for managing water supply to plants in space. In order to differentiate between changes in water content, water configuration, and pore-scale restrictions, we developed experiments which allowed for distinctions in retention characteristics to be made based on measurements in parabolic flight and on the ISS. These measurements highlighted an important feature of capillary dominated water configuration: The enhanced heterogeneity of water content under reduced gravity gradients. We found this heterogeneity to be dependent on whether a pore was draining or imbibing prior to the induced change. This dependence resulted in significant water content gradients maintained at separations of only a few pore lengths in variable gravity. One consequence of this altered distribution at the root-module scale is the abridged existence and increased tortuosity of continuous gas-filled pathways for diffusive transport. These pathways represent, in part, the hypothesized limitation for the exchange of respiratory gases, and therefore distinguish the changes in reduced-gravity capillary dominated processes that affect the configuration and transport of fluids in porous media.

APPENDICES

APPENDIX A

MEASUREMENT OF POROUS MEDIA WATER RETENTION DURING PARABOLIC FLIGHT INDUCED MICROGRAVITY[1]

A.1 Abstract

Bioregenerative life-support systems proposed for long-duration space missions require an understanding of the physical processes that govern distribution and transport of fluids in particulate porous plant-growth media. Our objectives were to develop hardware and instrumentation to measure porous-medium water retention and hydraulic transport properties during parabolic-flight induced microgravity. Automated measurements complimented periodic manual operations in three separate experiments using porous ceramic aggregates and glass beads. The water content was adjusted in multiple steps in periods of 1.8g. Continuous hydraulic potential measurements provided information on water retention. The short duration of microgravity limited the occurrence of equilibrium potentials under partially saturated conditions. Measured pressure gradients under fixed flow rates were largely unaffected by gravity force in saturated cylindrical porous-medium-filled flow cells. High resolution video imagery provided details on water imbibition rates into dry and previously wetted porous media. Additional analysis of these data will provide insight into the effects of reduced gravity on porous medium hydraulic properties.

A.2 Introduction

Motivated by the need to involve plants in any long-term, bio-regenerative, life-support system, plant growth in microgravity (μg) has been and continues to be an important part of space-

---

[1]The material for this appendix was previously published as: R. Heinse, S.D. Humphries, R.W. Mace, S.B. Jones, S.L. Steinberg, M. Tuller, R. Newman and D. Or.: "Measurement of Porous Media Water Retention during Parabolic Flight Induced Microgravity." SAE Technical Paper 2005-01-2950. The 35th International Conference on Environmental Systems (ICES) and the 8th European Symposium on Space Environmental Control Systems (ESSECS), Rome, Italy, July 11–14, 2005. Reprinted with permission from SAE Paper # 2005-01-2950* ©2005** SAE International.

exploration research. For optimal and scientifically-quantifiable plant-growth experiments the rooting environment needs to be well controlled and monitored to maintain desirable high efficiency growth conditions under intense energy, mass, and volume constraints. Most plant growth studies in particulate porous media have suffered from inadequate control regarding the root-zone environment, where much of this difficulty is attributed to the limited understanding of the fundamental physical principles of water and air distribution and transport under microgravity conditions (Steinberg et al., 2002). The narrow band of optimal liquid and gaseous fluxes for plant growth (Jones and Or, 1998) make it necessary to quantify hydraulic characteristics of the porous media to allow predictability and transferability of results for future design and management that have the potential to improve efficiency and reliability of plant-growth support systems.

Under microgravity conditions, water is assumed to distribute uniformly within homogeneous porous media. In reality air entrapment and altered hydrodynamics may significantly change flow and distribution of fluids. Recent work focused on porous-media fluid physics in microgravity has led to a number of hypotheses and observations. For example, preliminary observations from parabolic flight experiments (Or et al., 2004) suggest that, when observing flow and liquid configuration in porous micro-models, the impact of reduced gravity is manifested at the meso-scale (cluster of pores) rather than at the single-pore level. Levine et al. (2003) reported that reduced gravity accentuates the role of pre-wetted surfaces for transport and the rearrangement of loosely packed particles. Jones and Or (1999) postulated that microgravity enhances liquid- or gas-phase entrapment, affects macroscopic imbibition and drainage processes, and sample scale hydraulic properties.

Predicting and testing water and air transport in porous media in microgravity is limited by the lack of frequent long-duration experiments in orbit. Therefore, systems are often designed and tested under terrestrial gravity conditions where actual fluid distribution and potential microgravity effects cannot be easily studied. Alternatively, short periods of reduced gravity testing using parabolic flights (~ 20 s of reduced gravity) are possible.

The objectives of this study were to develop and test hardware and instrumentation amenable to quantify porous-medium water retention, saturated hydraulic conductivity and imbibition during

parabolic-flight induced microgravity using porous media samples of calcined clays and glass beads.

While the proposed measurements of water retention and saturated hydraulic conductivity are common place in agricultural soils on earth, collecting reproducible data in coarse textured porous media under varying water contents in the strenuous environment of an aircraft is more challenging. Body parts weighing 1.8 times their normal weight coupled with the challenge of stabilizing ones own body during periods of weightlessness, cause difficulty in carrying out simple tasks such as writing and navigating one's own hand in a controlled fashion. The automation of some experimental functions was therefore central. Norikane et al. (2004) attempted to measure matric potentials in calcined clays during parabolic flight. The measurements suffered from the vertical orientation of the partially sealed porous-medium container and unreferenced pressure measurement that were affected by changes in cabin pressure.

Learning from past experience, the measurement system required complete automation with periodic manual adjustments to comply with the physically strenuous measurement conditions on the aircraft.

A.3   Theoretical Considerations

In porous media, flow and distribution of fluid phases is controlled by the geometry of the pores, the aspect ratio, and the degree of interconnectivity of the pore system. The intricate geometry of the substrate and the large surface area induce matric forces between the water and the solid matrix. The sum of matric, gravitational and pressure potentials may be called the hydraulic potential. Conveniently, the hydraulic potential is expressed in terms of the height of a water column (1 cm = 98 Pa).

The gradient in hydraulic potential drives the transport of water in porous media. Darcy (1856) specified the relationship between the gradient in potential ∇h and the fluid flux $\vec{q}$:

$$\vec{q} = -K\nabla h \qquad\qquad (A.1)$$

where the hydraulic conductivity K is a constant for saturated flow under steady-state conditions (Ks). In unsaturated media, however, the hydraulic conductivity decreases as the hydraulic

potential h decreases. This is due to the decreasing number of saturated pores as the water content decreases:

The porous-medium water characteristic relates volumetric water content (θ_v) and hydraulic potential (h). A widely used parametric model for predicting water content as a function of hydraulic potential was proposed by van Genuchten (1980), given as:

$$\Theta(h) = \frac{(\theta_v - \theta_r)}{(\theta_s - \theta_r)} = \left[\frac{1}{1 + (\alpha |h|)^n} \right]^m \tag{A.2}$$

where Θ is the saturation. The subscripts s and r refer to saturated and residual water content, and α, n and m are empirical (fitting) parameters. Commonly, m is estimated to be: $m = 1 - n^{-1}$. The unsaturated hydraulic conductivity may be estimated as a function of porous-media water characteristics, using the van Genuchten (1980) parameters:

$$K(h) = K_s \left[\Theta(h)\right]^{\frac{1}{2}} \left[1 - \left(1 - \{\Theta(h)\}^{\frac{n}{n-1}} \right)^{\frac{n-1}{n}} \right]^2 \tag{A.3}$$

Equations (25) and (26) can be used to predict liquid content and fluxes within porous media.

A.4   Materials and Methods

A.4.1   Parabolic Flight

The flight campaign on board NASA's KC-135 aircraft was flown over the course of 4 days in February 2004. Microgravity conditions existed for about 20 s during free-fall in the cyclic-parabolic trajectory flown by the aircraft. The flight comprised of 4 sets of 10 parabolas, each with a $1g$ recovery period in between the parabola sets. A three component accelerometer on board the aircraft measured the gravitational acceleration. The resulting normalized effective gravitational acceleration $g = g_{observed}/g_{earth}$ had an oscillatory character and included small negative values. The effective gravitational acceleration values present during the parabolic flight increased to about $1.8g$, then decreased to about $0g$, and repeated. Because of the nature of the parabolic flight, small horizontal accelerations were also experienced.

A.4.2 Porous Media

Water retention, hydraulic conductivity, and imbibition cells were packed with different porous media. The porous media studied were porous ceramic aggregates and glass beads. Porous ceramic aggregates have frequently been used in microgravity plant experiments (Levine, 2002, Steinberg and Henninger, 1997, Norikane et al., 2004). The porous ceramic aggregates (Aimcor, Deerfield, Ill.) were sieved to size fractions of 0.25–1 mm (Profile) and 1–2 mm (Turface). Turface and Profile were rinsed to remove fines that could potentially clog the porous plate. Glass beads (MO-SCI, Rolla, Mo.) of 0.35–0.5 mm, 0.6–1 mm, 1–2 mm and 2.5–3.5 mm size fractions were also tested.

The mean particle density of all media was 2.5 g cm^{-3}. Porous media cells were packed saturated with water. Bulk density uniformity was ensured by tapping. Resulting packing densities are quantified in Tables (A.1) and (A.2).

A.4.3 Water Retention Experiment Description

Experimental Overview

Experiments were launched with saturated porous media. Signals from all sensors were recorded by a data-logger (CR23x, Campbell Scientific, Logan, Utah). The data-logger actuated a microprocessor-controlled precision syringe pump (KDS 200, KD Scientific, Holliston, Mass.). Water was withdrawn or pumped into the porous-media samples in multiple steps at a constant flow-rate, in order to record several cycles of drainage and wetting. The pumping time and flow rate were used to reference the volumetric water content θ_v.

Two water retention cells were tested simultaneously on each flight day. The cells were kept open to cabin air through the outlet tube and were maintained at cabin temperature. Each cell was connected to a water filled syringe (60 ml syringe) via a 3.175 mm inner-diameter tube. All syringes were mounted on a single pump. Water was delivered from the water source, via the pump, to the cells at a rate of 15 ml min^{-1} during periods of 1.8g. A fixed volume (5 ml) was pumped per step up to a maximum predefined total volume (40 ml). When the pump was on, one line pressure sensor measured the dynamic pressure of the water being pumped. That sensor was used to cease the pump if either the pressure got too high during pumping in or too low during pumping out. This prevented

the pressure from decreasing to the point where air bubbles were drawn through the porous plate (bubbling pressure) during pumping out (drainage). The pump would reverse direction after each set of 10 parabolas.

Additional tubes attached to the water outlet of the cells were connected to a storage reservoir (container filled with sponges) that readily absorbed any water leaving the cell. This prevented water from being drawn back into the cell during pumping out (drainage) while ensuring that no water left the storage reservoir in periods of $0g$ to imperil hardware or personnel. Custom-made optical bubble detectors, which were attached to the outlet tubes, were calibrated to control pumping by initiation of flow in $1.8g$ and cessation of flow when water exited the cell. When all cells were satiated (i.e. water exited out of all cells) the pump would cease and resume in the reverse direction in the next set of parabolas.

Final water contents and bulk densities were determined by destructive sampling following the flight. Water contents during the experiment were referenced to the porosity of the media—assuming the media was saturated at the beginning of the experiment—using the known changes in volume of water pumped in or out of the cells.

Water Retention Cell

The water retention cell shown in Figure (A.1) consists of a clear acrylic rectangular container of constant volume (internal dimensions: 12 cm long, 5 cm wide and 2 cm high). The cell contained tensiometers to measure matric potential in the porous media. To control medium water content, a syringe pump provides water addition/removal. The inlet at the bottom was used to supply water. The open outlet at the top facilitated pressure equilibrium with the cabin. The water inlet was connected to a sintered porous plate at the bottom of the cell that allowed control of water in the media without air passing the plate. Two different porous plates were tested: (1) a 3.175 mm thick porous plastic plate with 10 μm pore size (Porex Porous Products Group, model X-9948 T3 sheet, Fairburn, Ga.), and (2) a porous stainless steel plate with 5 μm pore size (Mott Metallurgical, Farmington, Conn.). In order to make the porous plates hydrophilic, they were soaked with a surfactant (20% Tween 20, Sigma-Aldrich Co., St. Louis, Mo. and 80% isopropyl alcohol), allowed to dry for

approximately 30 minutes and rinsed with de-ionized water.

Water Content Control

Five methods were used to control or monitor water content in the cell:

1. Tensiometers measured the hydraulic potential of water in the media. The tensiometer measurements were not used as a control mechanism.

2. A line pressure sensor monitored the pressure between the porous plate and pump. If the absolute pressure passed a threshold of 20 cm, the pump stopped, and resumed during the next $1.8g$ phase if the cutoff-threshold was met. The line pressure sensor used a 15 psi range differential-pressure transducer (OMEGA Engineering Inc. model PX40-15GV5, Stanford, Conn.).

3. Time Domain Reflectometry (TDR) measured the water content in the media on the basis of a change in dielectric properties. The TDR was used to monitor changes in water content only, and was not used as a control mechanism.

4. A syringe pump controlled water addition or removal from the media via a pre-set flow rate and data-logger control.

5. A calibrated bubble sensor detected excess water leaving the cell at the outlet. The bubble sensors controlled the direction of pumping when satiation (natural saturation) was reached.

Tensiometers

Each retention cell had a set of three tensiometers to measure the hydraulic potential of the media inside the cell. Two different designs were tested: i) all three tensiometers at the same elevation ($z=1$ cm), and ii) the tensiometers at different heights ($z_1=0.5$ cm, $z_2=1$ cm, and $z_3=1.5$ cm).

The tensiometers were open to the cabin air, and used differential pressure transducers (OMEGA Engineering Inc. model PX40-50BHG5V, Stanford, Conn.) connected to the medium with hypodermic needles, attached to a 2 mm diameter by 2 mm length porous stainless-steal cup ($10\,\mu$m pore

size, Mott Metallurgical, Farmington, Conn.). The goal was for the fluid within the tensiometer to reach equilibrium with the pore fluids controlled by the semi-porous membrane that prevented air from entering the probe. The tensiometers were calibrated with a hanging water column over the range of potential anticipated in the tests. The tensiometers were accurate to ± 0.5 cm.

Time Domain Reflectometer

The volumetric water content was measured by Time Domain Reflectometry (TDR). The TDR instrument (TDR100, Campbell Scientific Inc., Logan, Utah) was connected to a custom 3-rod sensor (100 mm long, 3.20 mm diameter rods and 12.0 mm rod spacing) that was aligned horizontally in the cell. A calibration function was established in $1g$, measuring the water content and permittivity in the cell. The fitted 3rd order polynomial is given as:

$$\theta_v = p_0 + p_1\sqrt{\varepsilon} + p_2\sqrt{\varepsilon}^2 + p_3\sqrt{\varepsilon}^3 \tag{A.4}$$

with p_3=0.007648, p_2=-0.1387, p_1=0.9236, and p_0=-1.556.

Bubble Sensor

Custom built bubble detectors were calibrated to sense the presence of water or air in a clear tube. An 890 nm wavelength phototransistor (Fairchild Semiconductor, model L14N1, South Portland, Maine) sensed changes in the intensity of transmitted infrared radiation from a matching wavelength infrared LED source (Fairchild Semiconductor, model QEE122, South Portland, Maine) across the tube.

A.4.4 Saturated Hydraulic Conductivity

The experimental system shown in Figure (A.2) consisted of 48 cm long cylindrical cells with a cross sectional area of 2.83 cm^2. They were horizontally aligned with the wings of the aircraft to avoid secondary accelerations. Saturated hydraulic conductivity (K_s) was determined for the porous media described in Table (A.2). Variable packing densities were established to test the influence of density on *Ks* during microgravity (Table A.2). Screens at each end contained the porous media while dyed water was pumped through the cells at variable fixed fluxes. During parabolas 1–20 a flow rate of 30 ml min^{-1} was used. This flow rate was set to 15 ml min^{-1}

during parabolas 21–30, and 7.5 ml min^{-1} during parabolas 31–40. Pressure differences along the flow cell were measured to determine saturated hydraulic conductivity using Equation (24). To measure the pressure differences, we installed five ports along the cell, located 10 cm apart, for pressure transducer readings (see Figure A.8). Each transducer (OMEGA Engineering Inc. model PX40, Stanford, Conn.) measured the difference between media hydraulic potential and cabin pressure. Experiments were run continuously to span both 0g and 1.8g conditions with pump reversal occurring periodically. A collapsible reservoir at the distal end opposite the pump provided pressure stabilization with cabin pressure.

A.4.5   Imbibition Cells

Water imbibition into different porous media was observed using video imagery and a porous medium container/water reservoir pictured in Figure (A.3). The porous medium was separated from the water reservoir by a 0.25 mm stainless steel screen. The water reservoir consisted of a thin-walled latex membrane, which allowed water to move into and out of the substrate under 0g without imposing any pressure or resistance to flow. Video imagery of water imbibition into different porous media was recorded at the rate of 15 frames per second and a resolution of 600 x 800 pixels per square inch. The video camera was a Micropix M-1024 (CCD Direct, Ann Arbor, Mich.), controlled by manufacturer supplied software (Fire-i). A clock mounted at the side of the substrate provided both a time record and an indicator of gravity level. Prior to the initial parabola, the water level was raised to lie just under the separation screen. This ensured that once microgravity was achieved, a slight advance would bring water in contact with the porous medium and the water would flow freely under capillary force and near zero potential at the boundary.

A.5   Results

A.5.1   Water Retention

Water Content

Water content of the media was calculated from the pump flow rate and pumping time, and

modified based on bubble detector sensor readings. The calculated water content in the cell was unchanged irrespective of pumping when the bubble sensor detected water in the outlet tube, suggesting additional water was flowing through the cell to the overflow reservoir.

Known water contents at the set points (i.e., initial water content at saturation and final water content from oven drying) helped to confirm the strategy. The reported volumetric water content represents a bulk volumetric water content in the cell.

The TDR water content sensor was beneficial for verification of relative changes in water content, though the pump provided more accurate measurements after corrections. Figure (A.4) shows the mismatch between TDR-and pump-determined volumetric water content in the cell. Discrepancies between pump and TDR are partially attributed to the disparity between the TDR-probe sampling volume (centered in the cell and concentrated around the probe) and the cell volume, which was roughly double in size.

Hydraulic potential

The hydraulic potential, measured by the tensiometers using pre-flight calibration, was adjusted for offset to read zero potential in the initial parabola at saturation in $0g$ periods. Based on ground testing, the tensiometers are assumed to have been in equilibrium with the media.

Figure (A.5) and (A.6) depict typical time series of tensiometer responses to varying effective gravitational acceleration and volumetric water content for 1–2 mm porous ceramic aggregates. Several interesting observations include hydrostatic forces, originating from water in the overflow line, secondary accelerations, and water content-dependent transitions toward equilibrium conditions. Excess water standing in the overflow tube manifests itself as positive pressure–up to 30 cm of head–which recedes under unsaturated conditions, and recurs after water content is increased to a satiated state.

Figure (A.5a) shows the response of tensiometers at different heights in the cell for 3 consecutive parabolas at constant water content near saturation. The response is indicative of the redistribution of water in the cell as the gravitational acceleration cycles between $1.8g$ and $0g$. The potential at the lower tensiometer decreases during periods of $0g$ as water rises from the satiated layer at the

bottom of the cell. The potential at the upper and centered tensiometers increases due to the upward movement of water. At the end of the 20 s $0g$ period, water is distributed uniformly in the cell at this water content, indicated by the convergence of hydraulic potential readings at different heights.

At lower water contents the transition in potentials between $1.8g$ and $0g$ becomes more accentuated. The increase in hydraulic potential difference between $1.8g$ and $0g$ with decreasing water content is depicted in Figure (A.5b). Also notably, the slope of the transition in $0g$ increases with decreasing water content, suggesting that unsaturated hydraulic conductivity becomes the limiting factor in reaching steady state in the 20 s of $0g$ allotted for equilibration. Further, the upper tensiometer appears to become hydraulically disconnected at lower water content. As a technical note, the use of a wick attached to the porous cup and distributed within the porous medium could help maintain hydraulic continuity.

Equilibrium Condition Estimation

Time series analysis of tensiometer readings exhibited hydraulic potential transitions toward steady state, which represent dynamic non-equilibrium under unsaturated conditions. Analysis demonstrates that this transition towards equilibrium conditions was a function of water content (Figure A.5b). With the limitation of a maximum of 20 s of $0g$ the criteria for establishment of quasi-steady-state and equilibrium conditions is at best an approximation, where the closest hydraulic potential to equilibrium occurs at the end of the $0g$ period. Criteria for determining reliable hydraulic potential data at equilibrium during $0g$ were obligatory because of noise inflicted by the strenuous environment of an aircraft flying parabolic profiles (i.e., periods of $1.8g$, and horizontal accelerations). Criteria included a minimum period of 7 s where the absolute value of g was no greater than $0.1g$. To ensure picking low noise data, the threshold of difference in two neighboring values was set to the resolution of the tensiometers (0.5 cm). Furthermore, values of hydraulic potential occurring at the end of $0g$ (averaged over 2 s) were only reported if no pumping activity occurred during $0g$. Hydraulic potentials determined to be at equilibrium using the described criteria are illustrated in Figure (A.5) (circles). Migration towards hydraulic potential equilibrium during $0g$ was faster in larger particle sizes (i.e. 2.5–3.5 mm glass beads) (not shown). This is attributed to

reduced tortuosity and higher hydraulic conductivity for larger pores.

Porous-Medium-Water Retention

Preliminary water retention data for 0.25–1 and 1–2 mm porous ceramic aggregates (Turface and Profile, respectively) for the initial drainage cycle are illustrated in Figure (A.6). The drainage porous-media water retention curves were generated by plotting tensiometer readings against volume pumped (converted to water content). We compared modeled ground-based retention data using the van Genuchten parameters to the microgravity data. Hydraulic potentials measured during parabolic flight are reduced in comparison to $1g$. The observed variation from the $1g$ reference is thought to be based on the following condition. In $1.8g$ water is drawn to the bottom of the cell by the increased gravitational force. In the $0g$ period water moves upward due to the gradient in hydraulic potential. As a result, measured matric potentials on parabolic flights are influenced by wetting conditions regardless of the direction of pumping. In addition, dynamic non-equilibrium at lower water contents partially explains the reduced hydraulic potentials compared to the modeled ground retention curves.

A.5.2 Saturated Hydraulic Conductivity

Gravitational acceleration had little effect on the measured pressure difference along the flow domain of densely-packed tubes. Loose packing resulted in a reduced pressure difference in $1.8g$ and an increase during periods of $0g$. This is indicative of a significantly different particle distribution scheme in $0g$ than in $1.8g$ where packing density allowed movement and rearrangement of porous-media particles and subsequent changes in cross sectional area for the flow process (Figure A.8). Table (A.2) lists the calculated saturated hydraulic conductivities. Porous ceramic aggregate saturated hydraulic conductivities measured are comparable to values reported by Steinberg et al. (2005) for Profile and Turface.

A.5.3 Imbibition

At the onset of $0g$, the water reservoir membrane volume was reduced to move water in contact with the bottom of the sample. Figure (A.9) illustrates the imbibition process during $0g$ when

water imbibes an initially dry Turface sample. In this capillary force-dominated flow condition, preferential flows appear that leave dry pockets or clusters behind which seem to increase with distance from the water inlet. Some of the air-pocket clustering is diminished by the redistribution of water draining under 1.8g. Video imagery will be analyzed to determine wetting front propagation with time for estimation of porous medium hydraulic properties and imbibition rates. Analysis will also consider influence of particle size on the imbibition process.

A.6   Summary and Conclusions

Automated measurement systems developed and tested on NASA's KC-135 aircraft provided valuable measurements of porous medium-water retention and hydraulic transport properties during parabolic-flight induced microgravity.

The measurement of water retention in microgravity is challenging because of the dynamic accelerational forces exerted on the crew and the hardware. Based on tensiometer and syringe pump control the water retention measurement system appeared to perform soundly in controlling water content in the substrate. Measured water retention data derived from tensiometer and pump data were within reasonable agreement to ground based measurements near saturation.

The short 20 s time window of 0g, followed by a period of 1.8g, limited equilibrium and steady state conditions under partially saturated conditions desired for these measurements. The porous medium water content determined the time to equilibrium based on reduced hydraulic conductivity at reduced water contents. Measured hydraulic potentials in microgravity fell below the 1g draining water retention curve likely due to the cyclic change in hydraulic potential and the associated vertical redistribution of water in the cells. The rate of redistribution dictated quasi-steady-state conditions as a function of water content.

Gravitational acceleration did not appear to affect the pressure gradient measured in the hydraulic conductivity cells of densely packed porous media. Saturated hydraulic conductivity, K_s, increased in loosely packed porous media during periods of 0g, likely due to a significantly different particle distribution scheme at 0g as opposed to 1.8g where packing density allowed movement of particulate porous media.

The observation of the imbibition process provides an opportunity to visually record the propagation of a wetting fluid and the extent of the dispersion in the wetting front, in addition to modeling this response afterwards.

These preliminary results demonstrate the limited capability for measurements of porous medium hydraulic properties in the microgravity environment of parabolic flight. Additional analysis of data will provide further insights into an extended water retention characteristic including hysteretic effects. Imbibition data analysis should also provide information regarding microgravity effects on the rate of wetting. Further testing in microgravity under sustained equilibrium conditions (i.e., space craft or ISS) is needed to definitively characterize microgravity effects on water retention over the entire range of water contents, and to advance model development for describing porous media hydrodynamic behavior.

Acknowledgments

A.7 References

Darcy, H., 1856. Dètermination des lois d'ècoulement de l'eau à travers le sable. p. 590594. In: Les Fontaines Publiques de la Ville de Dijon. Victor Dalmont, Paris.

Jones, S. B. and Or, D., 1998. A capillary driven root module for plant growth in microgravity. Adv. Space Res. 10:1407–1412.

Jones, S. B. and Or, D., 1999. Microgravity effects on water flow and distribution in unsaturated porous media: Analyses of flight experiments. Water Resour. Res. 4:929–942.

Levine, H. G., 2002. Water offset nutrient delivery system (WONDER). Tech. rep. Kennedy Space Center, Fl.

Levine, H. G., Georgiana, K. T. and Norikane, J. H. 2003. Fluid behavior under microgravity conditions within plant nutrient delivery systems: Parabolic flight investigations. SAE Tech. Paper No. 2003-01-2483. SAE Int., Warrendale, PA.

Norikane, J. H., Jones, S. B., Steinberg, S. L., Levine, H. G. and Or, D. 2004. Porous media matric potential and water content measurements during parabolic flight. Habitation 10:1–10.

Or, D., Jones, S.B., Tuller, M., Steinberg, S., Alexander, J.I.D., Diadzic, N., Redi, L.N., Kluitenberg, G., Ogden, F. L. and Heinse R., 2004. Unsaturated flow in zero gravity–lessons and challenges. In: ASA-CSSA-SSSA-CSSS Abstracts 2004 [CD-ROM], ASA, CSSA, and SSSA, Madison, WI.

Steinberg, S. L. and Henninger, D. L., 1997. Responses of water status of soybeans to changes in soil water potentials controlled by the water pressure in microporous tubes. Plant, Cell and Environ. 120(12):1506-16.

Steinberg, S. L., Alexander, I., Daidzic, N. E., Jones, S. B., Kluitenberg, G., Or, D., Reddi, L. N., and Tuller, M., 2002. Flow and distribution of fluid phases through porous plant growth media in microgravity: Progress to date. In: Proceedings of the 32nd International Conference on Environmental Systems (ICES). SAE Int., Warrendale, PA.

Steinberg, S. L., Kluitenberg, G., Jones, S. B., Diadzic, N., Reddi, L., Xiao, M., Tuller, M., Newman, R., Or, D., and Alexander, J. I. D., 2005. Physical and hydraulic properties of baked ceramic aggregates used for plant growth medium. J. Amer. Soc. Hort. Sci. 130(5):767-74.

van Genuchten, M. T., 1980. A closed-form equation for predicting the hydraulic conductivity of unsaturated soils. Soil Sci. Soc. Am. J. 44:892–898.

Table A.1: Bulk (packing) density and porosity for different porous media used in the water retention experiment.

Porous medium Size (medium)	Bulk density $[\text{g cm}^{-3}]$	Porosity $[\text{cm}^3 \text{ cm}^{-3}]$
0.25–1 mm (Profile)	0.658	0.737
1–2 mm (Turface)	0.616	0.754
1–2 mm (Turface)	0.602	0.773
1–2 mm (glass beads)	1.723	0.311
1–2 mm (glass beads)	1.688	0.325
2.5–3.5 mm (glass beads)	1.523	0.391

Table A.2: Average and standard deviation of saturated hydraulic conductivity K_s in $0g$, measured at different bulk densities.

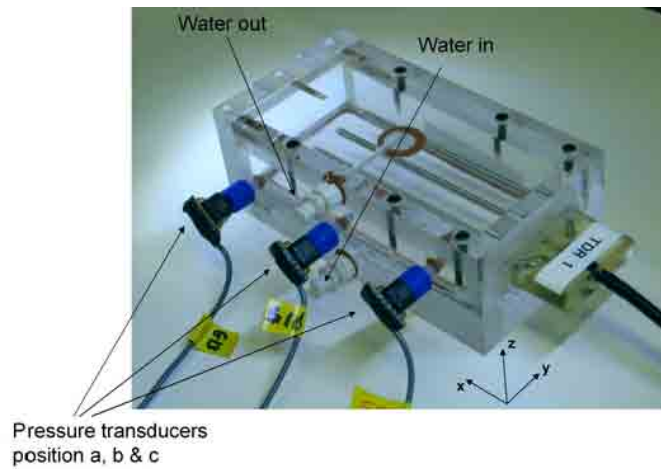| Porous medium Size (medium)	Bulk density $[\text{cm s}^{-1}]$	K_s $[\text{cm s}^{-1}]$	stdev $[\text{cm s}^{-1}]$
0.35-0.5 mm (glass beads)	1.56	0.090	0.007
0.6-1 mm (glass beads)	1.59	0.380	0.029
1–2 mm (glass beads)	1.55	1.394	0.094
1–2 mm (glass beads)	1.56	1.054	0.079
2.5–3.5 mm (glass beads)	1.46	6.343	1.012
0.25–1 mm (Profile)	0.62	0.295	0.039
0.25–1 mm (Profile)	0.67	0.140	0.009
1–2 mm (Turface)	0.61	1.250	0.109

Fig. A.1: Water retention measurement cell with tensiometers at positions a, b and c (height in cell: 0.5, 1 and 1.5 cm), and horizontally aligned TDR sensor. The water inlet and outlet used to control water in the cell is shown. The inlet is connected to the sintered porous plate at the bottom of the cell.
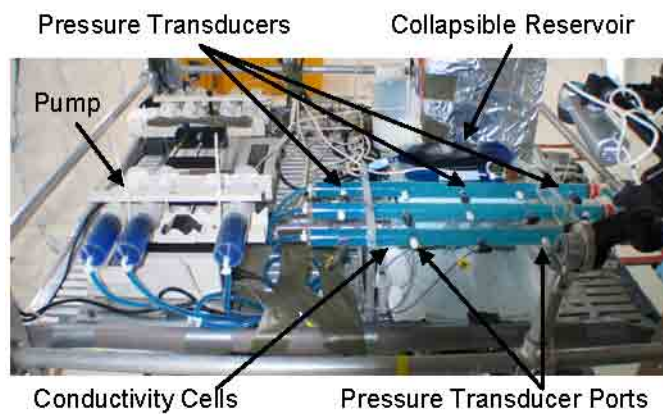

Fig. A.2: Setup for the measurement of saturated hydraulic conductivity of different porous media packed into cylindrical cells. The conductivity cells are equipped with 5 ports for pressure transducer hookup, of which 2–3 were used in the experiment. A precision syringe pump and collapsible reservoir are in the background.
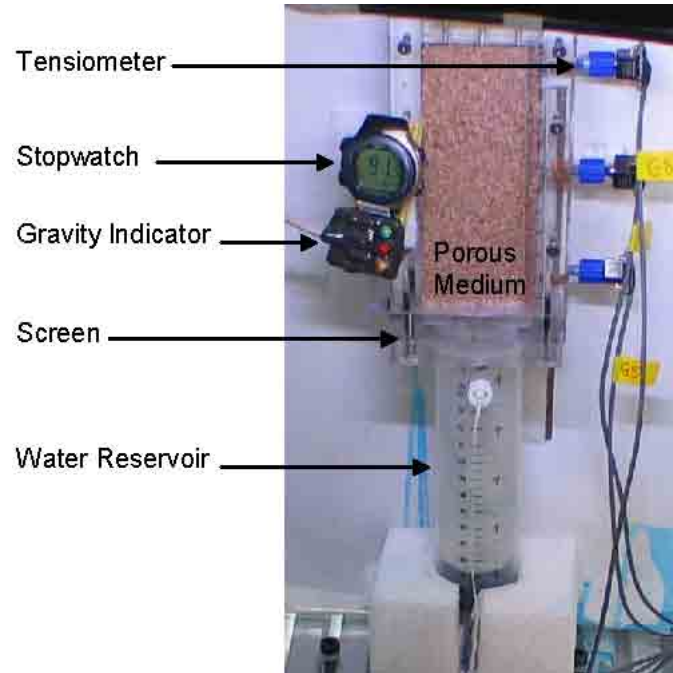
Fig. A.3: Water imbibition cell illustrating the porous-medium container, separation screen and water reservoir. Video imagery captured 15 frames per seconds at 600x800 resolution. Manual advance of the water level was adjusted during 1.8g to lie just below the substrate. Tensiometers provided hydraulic potential readings once the wetting front reached them.
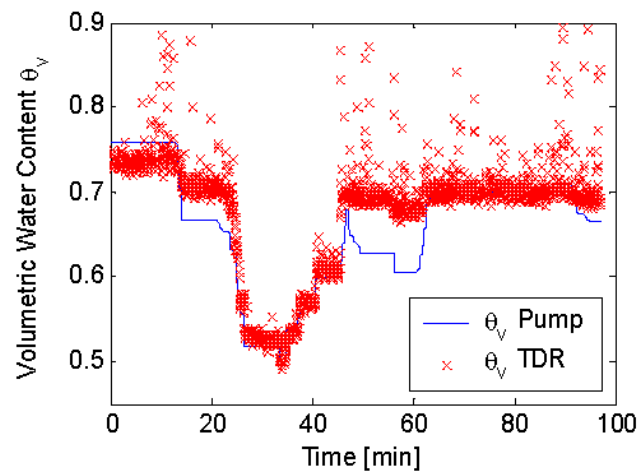

Fig. A.4: Volumetric water content in 1–2 mm baked ceramic aggregate (Turface) over the course of the multi-step drainage and wetting experiment. The solid line is the water content calculated from the pump with adjustments using the information from the bubble sensor. The symbols are the water contents derived from TDR measurements.
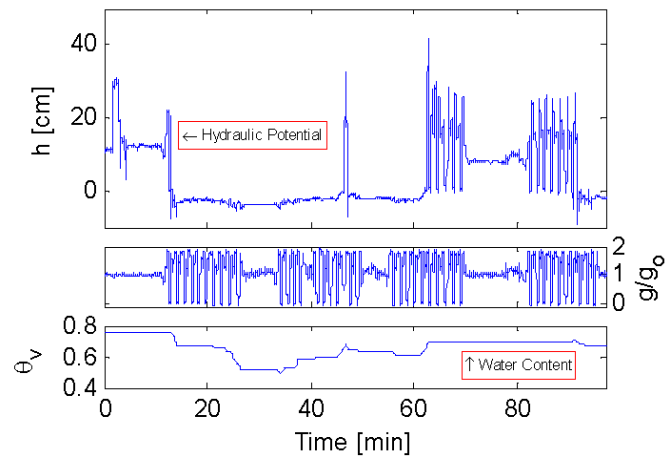
Fig. A.5: Time series of tensiometer response (hydraulic potential *h*) to varying *g*-forces, and water contents over the course of the flight in porous ceramic aggregate (Turface). Large positive hydraulic potentials represent periods when water was exiting out of the top of the cell. Since the outlet tube went upward into the storage reservoir, water standing in the tube exerted a hydrostatic pressure potential, proportional to the *g*-force, in 1*g* and 1.8*g* periods.
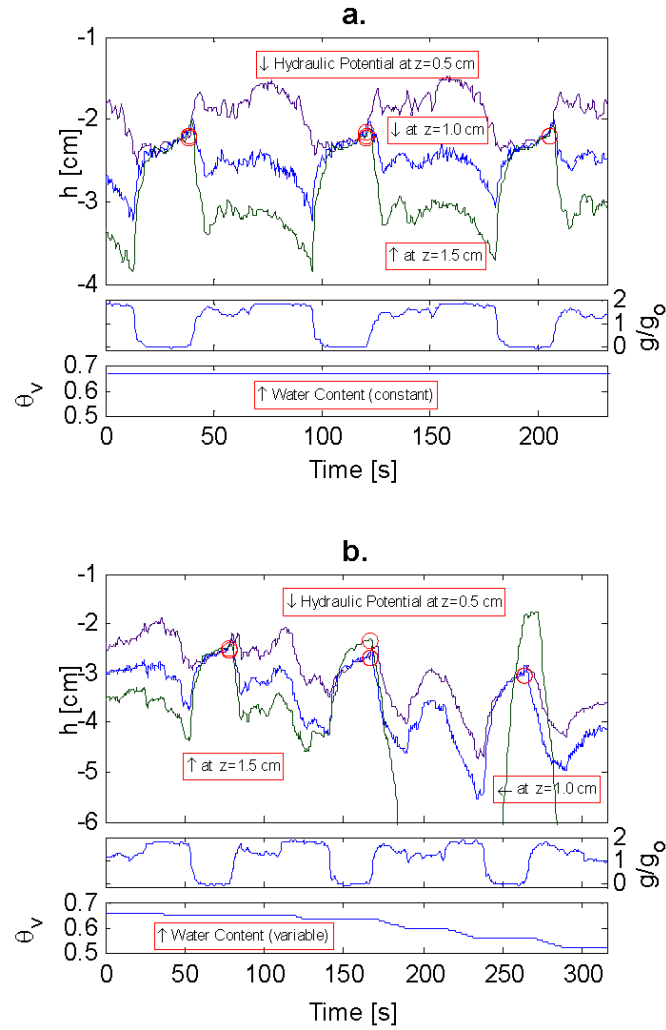
Fig. A.6: Time series of hydraulic potential, *g*-force and water content in porous ceramic aggregate (Turface) for three tensiometers at different heights (0.5, 1 and 1.5 cm, respectively). (a.) for 3 consecutive periods of 0*g* at a constant water content near saturation (θ_v=0.67), and (b.) for 3 consecutive periods of 0*g* at variable water content (θ_v=0.65, θ_v= 0.63 and θ_v= 0.56). The symbols (circles) indicate hydraulic potential values determined to be at quasi-equilibrium. Note that the upper tensiometer appears to hydraulically disconnect as water content decreases. Thereafter it tracked changes in cabin pressure.
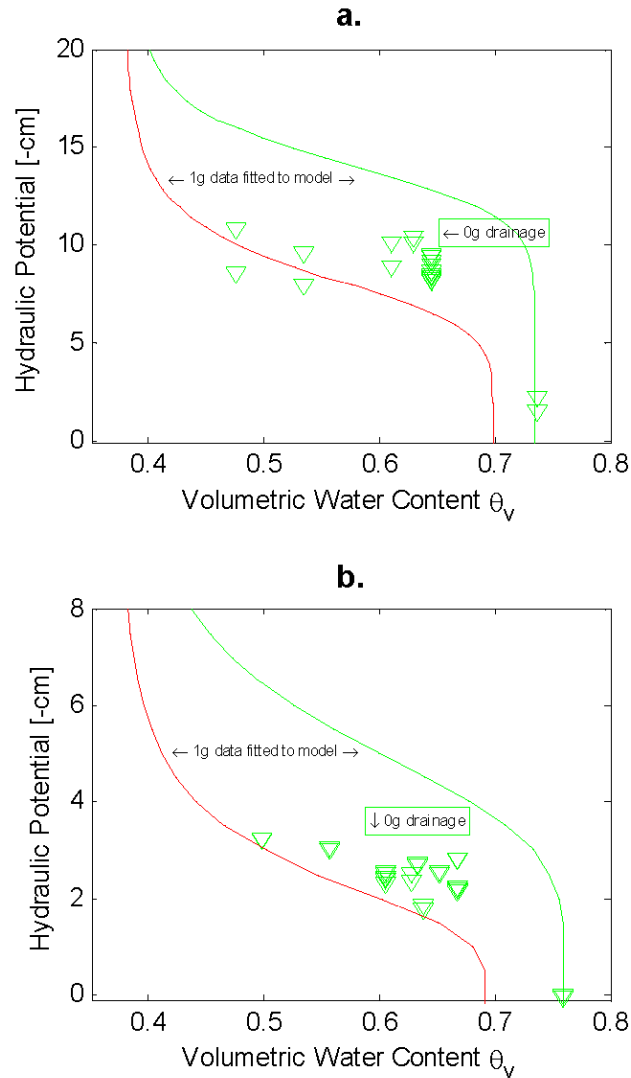
Fig. A.7: Comparison of 0*g* and 1*g* drainage porous-media water retention. Solid lines are predicted 1*g* reference curves. The symbols (∇) respond to 0*g* measured drainage data. (a.) for 0.25–1 mm porous ceramic aggregate (Profile) (Equation (25) parameters drainage: $\theta_s = 0.735$, θ_r=0.386, α=0.071 cm^{-1}, *n*=10.02; wetting: θ_s=0.698, θ_r=0.377, α=0.121 cm^{-1}, *n*=5.876) (b.) for 1–2 mm ceramic aggregate (Turface) (Equation (25) parameters drainage: θ_s=0.760, θ_r=0.366, α=0.198 cm^{-1}, *n*=4.523; wetting: θ_s=0.692, θ_r=0.369, α=0.428 cm^{-1}, *n*=3.605).
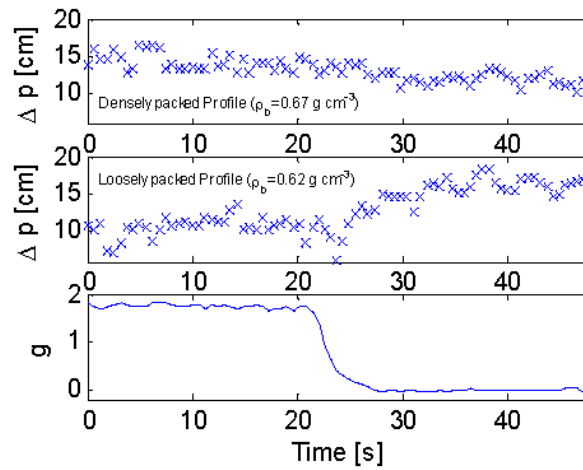
Fig. A.8: Time series of pressure potential difference along the flow domain of the conductivity cells for varying gravitational acceleration for densely (top) and loosely (middle) packed porous ceramic aggregate (Profile). Notice the greater differences in pressure potentials in the loosely packed cell between gravity levels.
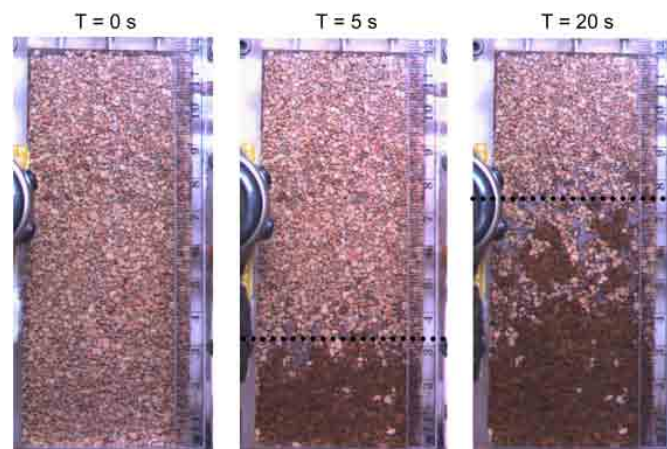
Fig. A.9: Water imbibition into dry Turface (1–2 mm) showing wetting front propagation at 0, 5 and 20 seconds into a 0g period. Clustering of dry particles at the Turface-Lexan interface indicates time-dependent preferential wetting or fingering.

APPENDIX B

PERMISSIONS AND RELEASE LETTERS

I. Letters for Chapter 2

Subject: FW: vzj article permission
From: Lisa Al-Amoodi <lalamoodi@agronomy.org>
Date: Mon, 5 Jan 2009 07:42:28 -0700
To: Robert Heinse <robert.heinse@usu.edu>

Hello Dr. Heinse,

I understand you spoke with Ann Edahl about a permission issue. I assume the article below is the article in question. Permission granted.

Thanks and best of luck with your dissertation.

Lisa Al-Amoodi

Measurements and Modeling of Variable Gravity Effects on Water Distribution and Flow in Unsaturated Porous Media

Robert Heinse[a,*], Scott B. Jones[a], Susan L. Steinberg[b], Markus Tuller[c] and Dani Or[d]

[a] Dep. of Plants, Soils and Climate, Utah State Univ., Logan, UT 84322-4820
[b] Universities Space Research Assoc., Mail Code EC3, NASA/JSC, Houston, TX 77058
[c] Dep. of Soil, Water & Environmental Science, The Univ. of Arizona, Tucson, AZ 85721
[d] Lab. of Soil and Environmental Physics, Ecole Polytechnique Fédérale de Lausanne, Switzerland
[*] Corresponding author (heinse@cc.usu.edu).

Lisa Al-Amoodi
Managing Editor

Books & *Vadose Zone Journal* http://www.vadosezonejournal.org

American Society of Agronomy * Crop Science Society of America * Soil Science Society of America
677 South Segoe Road
Madison, WI 53711-1086
TEL: 608-268-4966 FAX: 608-273-2021
www.agronomy.org | www.crops.org | www.soils.org

"Footprints in the Landscape: Sustainability through Plant and Soil Sciences"
ASA-CSSA-SSSA 2009 International Annual Meetings
November 1-5 | Pittsburgh, PA
https://www.acsmeetings.org/

From: Ann Edahl
Sent: Friday, January 02, 2009 1:27 PM
To: Lisa Al-Amoodi
Subject: vzj article permission

Hey Lisa,

Robert Heinse called today (Friday) about getting permission to use a VZJ article in full as a chapter in his dissertation VZJ 6:713-724. (V06-0105) He filled out an online form about six weeks ago but hasn't heard back. (He already has permission from his coauthors.)

I told him that you should be able to expedite the situation.

Thanks,
!nn

Ann Edahl
Associate Editor

American Society of Agronomy * Crop Science Society of America * Soil Science Society of America
677 South Segoe Road
Madison, WI 53711-1086
TEL: 608-268-3972
FAX: 608-273-2021
www.agronomy.org * www.crops.org * www.soils.org

Robert Heinse
Utah State University
Dept. Plants, Soils and Climate
4820 Old Main Hill
Logan, UT 84322-4820

November 13, 2008

Susan Steinberg
Senior Research Scientist
Universities Space Research Association
Johnson Space Center/NASA 2101·
NASA Rd 1
Houston, TX 77058

Dear Dr. Steinberg,

I am in the process of preparing my dissertation in the Plants, Soils and Climate Department at Utah State University. I hope to complete in December 2008.

I am requesting your permission to include the paper we co-authored in 2007 shown below. I will include acknowledgements and appropriate citations in this work and copyright and reprint rights in a special appendix.

Please indicate your approval of this request by signing in the space provided.

Thank you for your cooperation.

Yours sincerely,

Robert Heinse

I hereby give permission to Robert Heinse to reprint the following material in his dissertation.

Heinse, R., S.B. Jones, S.L. Steinberg, M. Tuller and D. Or (2007). Measurements and Modeling of Variable Gravity Effects on Water Distribution and Flow in Unsaturated Porous Media. Vadose Zone J. 6:713-724.

Signed:

Susan Steinberg

Robert Heinse
Utah State University
Dept. Plants, Soils and Climate
4820 Old Main Hill
Logan, UT 84322-4820

November 13, 2008

Markus Tuller
Associate Professor of Soil & Environmental Physics
University of Arizona
526 Shantz Building
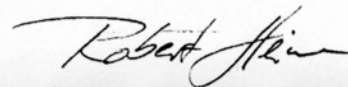Tucson, AZ 85721

Dear Dr. Tuller,

I am in the process of preparing my dissertation in the Plants, Soils and Climate Department at Utah State University. I hope to complete in December 2008.

I am requesting your permission to include the paper we co-authored in 2007 shown below. I will include acknowledgements and appropriate citations in this work and copyright and reprint rights in a special appendix.

Please indicate your approval of this request by signing in the space provided.
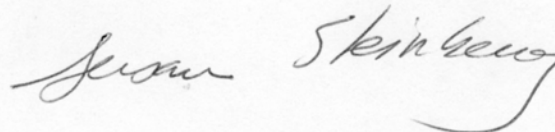
Thank you for your cooperation.

Yours sincerely,

Robert Hein

I hereby give permission to Robert Heinse to reprint the following material in his dissertation.

Heinse, R., S.B. Jones, S.L. Steinberg, M. Tuller and D. Or (2007). Measurements and Modeling of Variable Gravity Effects on Water Distribution and Flow in Unsaturated Porous Media. Vadose Zone J. 6:713-724.

Signed:

Markus Tuller

Robert Heinse
Utah State University
Dept. Plants, Soils and Climate
4820 Old Main Hill
Logan, UT 84322-4820

November 13, 2008

Dani Or
Professor
Chair in Environmental Physics of Terrestrial Systems
ETH Zürich
Universitätstrasse 16
8092 Zürich
Switzerland

Dear Dr. Or,

I am in the process of preparing my dissertation in the Plants, Soils and Climate Department at Utah State University. I hope to complete in December 2008.

I am requesting your permission to include the paper we co-authored in 2007 shown below. I will include acknowledgements and appropriate citations in this work and copyright and reprint rights in a special appendix.

Please indicate your approval of this request by signing in the space provided.

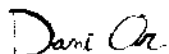Thank you for your cooperation.

Yours sincerely,

I hereby give permission to Robert Heinse to reprint the following material in his dissertation.

Heinse, R., S.B. Jones, S.L. Steinberg, M. Tuller and D. Or (2007). Measurements and Modeling of Variable Gravity Effects on Water Distribution and Flow in Unsaturated Porous Media. Vadose Zone J. 6:713-724.

Signed:

II. Letters for Chapter 5

Subject: RE: Copyright Permission Letter
From: Dawn Frenchak <dawn@sae.org>
Date: Fri, 9 Jan 2009 10:32:46 -0700
To: Robert Heinse <robert.heinse@usu.edu>

Dear Mr. Heinse,

I'm not sure if you received a response on this. If not, I'm sorry for the delay. I understand tha
you would like to use SAE Papers # 2006-01-2211 and 2005-01-2950 in your dissertation at Utah State
University.

Permission is hereby granted, and we request that the following credit line be used:

"Reprinted with permission from SAE Paper # XXXX-XX-XXXX* © XXXX** SAE International."

(*please insert the paper number and **year of publication)

Permission is for this one-time use only. New requests are required for subsequent editions, for
reprints or excerpts, or for other uses of the material.

Thank you for contacting SAE and for your cooperation.

Sincerely,
Dawn Frenchak
Intellectual Property Rights Administrator
SAE International
Phone: 001.724.772.8518; Fax: 001.724.776.3036
E-mail: dawn@sae.org

CONFIDENTIALITY NOTICE: This e-mail, and any attachments and/or documents linked to this email, are
intended for the addressee and may contain information that is privileged, confidential, proprietary
or otherwise protected by law. Any dissemination, distribution, or copying is prohibited. This
notice serves as a confidentiality marking for the purpose of any confidentiality or nondisclosure
agreement. If you have received this communication in error, please contact the original sender.

Please find the request-for-permission-to-reprint-forms for the two technical papers.
They will be part of my dissertation entitled: Characterization, Modeling and Design of Optimal
Plant-Growth Media for Reduced Gravity at Utah State University.

Thank you very much,
Robert Heinse
.

Robert Heinse
Utah State University
Dept. Plants, Soils and Climate
4820 Old Main Hill
Logan, UT 84322-4820

November 13, 2008

Gerard Kluitenberg
Professor
Soil and Environmental Physics
Kansas State University
Manhattan, KS 66506

Dear Dr. Kluitenberg,

I am in the process of preparing my dissertation in the Plants, Soils and Climate Department at Utah State University. I hope to complete in December 2008.

I am requesting your permission to include the paper we co-authored in 2006 shown below. I will include acknowledgements and appropriate citations in this work and copyright and reprint rights in a special appendix.

Please indicate your approval of this request by signing in the space provided.

Thank you for your cooperation.

Yours sincerely,

I hereby give permission to Robert Heinse to reprint the following material in his dissertation.

R. Heinse, G. Kluitenberg, K.S. Lewis, R.S. Austin, P.J. Shouse, G.B. Bingham, and S.B. Jones: "Integration of Heat Capacity and Electrical Conductivity Sensors for Root Module Water and Nutrient Assessment." SAE Technical Paper 2006-01-2211. The 36th International Conference on Environmental Systems (ICES), Norfolk, VI, July 17–20, 2006.

Signed:

Robert Heinse
Utah State University
Dept. Plants, Soils and Climate
4820 Old Main Hill
Logan, UT 84322-4820

November 13, 2008

Kelly Lewis
Acclima Inc.
2260 E Commercial St
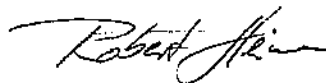Meridian, ID 83632

Dear Mr. Lewis,

I am in the process of preparing my dissertation in the Plants, Soils and Climate Department at Utah State University. I hope to complete in December 2008.

I am requesting your permission to include the paper we co-authored in 2006 shown below. I will include acknowledgements and appropriate citations in this work and copyright and reprint rights in a special appendix.

Please indicate your approval of this request by signing in the space provided.
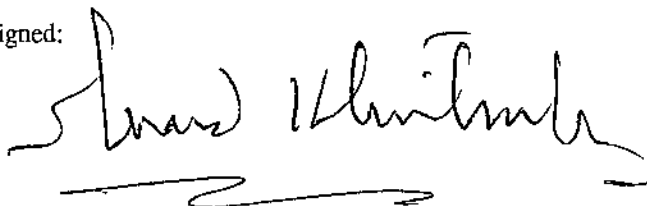
Thank you for your cooperation.

Yours sincerely,

Robert Heinse

I hereby give permission to Robert Heinse to reprint the following material in his dissertation.

R. Heinse, G. Kluitenberg, K.S. Lewis, R.S. Austin, P.J. Shouse, G.B. Bingham, and S.B. Jones: "Integration of Heat Capacity and Electrical Conductivity Sensors for Root Module Water and Nutrient Assessment." SAE Technical Paper 2006-01-2211. The 36th International Conference on Environmental Systems (ICES), Norfolk, VI, July 17–20, 2006.

Signed: _Kelly Lewis_ 11/14/08

III. Letters for Appendix B

Subject: RE: Copyright Permission Letter
From: Dawn Frenchak <dawn@sae.org>
Date: Fri, 9 Jan 2009 10:32:46 -0700
To: Robert Heinse <robert.heinse@usu.edu>

Dear Mr. Heinse,

I'm not sure if you received a response on this. If not, I'm sorry for the delay. I understand tha you would like to use SAE Papers # 2006-01-2211 and 2005-01-2950 in your dissertation at Utah State University.

Permission is hereby granted, and we request that the following credit line be used:

"Reprinted with permission from SAE Paper # XXXX-XX-XXXX* © XXXX** SAE International."

(*please insert the paper number and **year of publication)

Permission is for this one-time use only. New requests are required for subsequent editions, for reprints or excerpts, or for other uses of the material.

Thank you for contacting SAE and for your cooperation.

Sincerely,
Dawn Frenchak
Intellectual Property Rights Administrator
SAE International
Phone: 001.724.772.8518; Fax: 001.724.776.3036
E-mail: dawn@sae.org

CONFIDENTIALITY NOTICE: This e-mail, and any attachments and/or documents linked to this email, are intended for the addressee and may contain information that is privileged, confidential, proprietary or otherwise protected by law. Any dissemination, distribution, or copying is prohibited. This notice serves as a confidentiality marking for the purpose of any confidentiality or nondisclosure agreement. If you have received this communication in error, please contact the original sender.

Please find the request-for-permission-to-reprint-forms for the two technical papers. They will be part of my dissertation entitled: Characterization, Modeling and Design of Optimal Plant-Growth Media for Reduced Gravity at Utah State University.

Thank you very much,
Robert Heinse
.

Robert Heinse
Utah State University
Dept. Plants, Soils and Climate
4820 Old Main Hill
Logan, UT 84322-4820

November 13, 2008

Seth Humphries
Montana State University
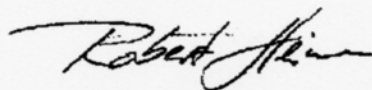Bozeman, MT 59717

Dear Dr. Humphries,

I am in the process of preparing my dissertation in the Plants, Soils and Climate Department at Utah State University. I hope to complete in December 2008.

I am requesting your permission to include the paper we co-authored in 2006 shown below. I will include acknowledgements and appropriate citations in this work and copyright and reprint rights in a special appendix.

Please indicate your approval of this request by signing in the space provided.

Thank you for your cooperation.

Yours sincerely,

I hereby give permission to Robert Heinse to reprint the following material in his dissertation.

R. Heinse, S.D. Humphries, R.W. Mace, S.B. Jones, S.L. Steinberg, M. Tuller, R. Newman and D. Or.: "Measurement of Porous Media Water Retention during Parabolic Flight Induced Microgravity." SAE Technical Paper 2005-01-2950. The 35th International Conference on Environmental Systems (ICES) and the 8th European Symposium on Space Environmental Control Systems (ESSECS), Rome, Italy, July 11–14, 2005.

Signed: _____   13–NOV–2008

Robert Heinse
Utah State University
Dept. Plants, Soils and Climate
4820 Old Main Hill
Logan, UT 84322-4820

November 13, 2008

R. William Mace
Research Associate
Utah State University
Logan, UT 84322

Dear Mr. Mace,

I am in the process of preparing my dissertation in the Plants, Soils and Climate Department at Utah State University. I hope to complete in December 2008.

I am requesting your permission to include the paper we co-authored in 2006 shown below. I will include acknowledgements and appropriate citations in this work and copyright and reprint rights in a special appendix.

Please indicate your approval of this request by signing in the space provided.

Thank you for your cooperation.

Yours sincerely,

Robert Hein

I hereby give permission to Robert Heinse to reprint the following material in his dissertation.

R. Heinse, S.D. Humphries, R.W. Mace, S.B. Jones, S.L. Steinberg, M. Tuller, R. Newman and D. Or.: "Measurement of Porous Media Water Retention during Parabolic Flight Induced Microgravity." SAE Technical Paper 2005-01-2950. The 35th International Conference on Environmental Systems (ICES) and the 8th European Symposium on Space Environmental Control Systems (ESSECS), Rome, Italy, July 11–14, 2005.

Signed: William Mace

Robert Heinse
Utah State University
Dept. Plants, Soils and Climate
4820 Old Main Hill
Logan, UT 84322-4820

November 13, 2008

Susan Steinberg
Senior Research Scientist
Universities Space Research Association
Johnson Space Center/NASA 2101
NASA Rd 1
Houston, TX 77058

Dear Dr. Steinberg,

I am in the process of preparing my dissertation in the Plants, Soils and Climate Department at Utah State University. I hope to complete in December 2008.

I am requesting your permission to include the paper we co-authored in 2006 shown below. I will include acknowledgements and appropriate citations in this work and copyright and reprint rights in a special appendix.

Please indicate your approval of this request by signing in the space provided.
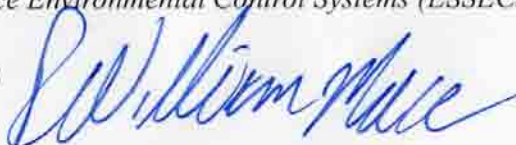
Thank you for your cooperation.

Yours sincerely,

Robert Hein

I hereby give permission to Robert Heinse to reprint the following material in his dissertation.

R. Heinse, S.D. Humphries, R.W. Mace, S.B. Jones, S.L. Steinberg, M. Tuller, R. Newman and D. Or.: "Measurement of Porous Media Water Retention during Parabolic Flight Induced Microgravity." SAE Technical Paper 2005-01-2950. The 35th International Conference on Environmental Systems (ICES) and the 8th European Symposium on Space Environmental Control Systems (ESSECS), Rome, Italy, July 11–14, 2005.

Signed:

Susan Steinberg

Robert Heinse
Utah State University
Dept. Plants, Soils and Climate
4820 Old Main Hill
Logan, UT 84322-4820

November 13, 2008

Markus Tuller
Associate Professor of Soil & Environmental Physics
University of Arizona
526 Shantz Building
Tucson, AZ 85721

Dear Dr. Tuller,

I am in the process of preparing my dissertation in the Plants, Soils and Climate Department at Utah State University. I hope to complete in December 2008.

I am requesting your permission to include the paper we co-authored in 2006 shown below. I will include acknowledgements and appropriate citations in this work and copyright and reprint rights in a special appendix.

Please indicate your approval of this request by signing in the space provided.
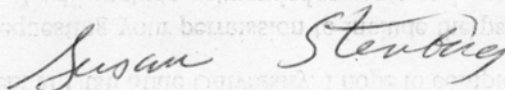
Thank you for your cooperation.

Yours sincerely,

Robert Hein

I hereby give permission to Robert Heinse to reprint the following material in his dissertation.

R. Heinse, S.D. Humphries, R.W. Mace, S.B. Jones, S.L. Steinberg, M. Tuller, R. Newman and D. Or.: "Measurement of Porous Media Water Retention during Parabolic Flight Induced Microgravity." SAE Technical Paper 2005-01-2950. The 35th International Conference on Environmental Systems (ICES) and the 8th European Symposium on Space Environmental Control Systems (ESSECS), Rome, Italy, July 11–14, 2005.

Signed:

Markus Tuller

Robert Heinse
Utah State University
Dept. Plants, Soils and Climate
4820 Old Main Hill
Logan, UT 84322-4820

November 13, 2008

Dani Or
Professor
Chair in Environmental Physics of Terrestrial Systems
ETH Zürich
Universitätstrasse 16
8092 Zürich
Switzerland

Dear Dr. Or,

I am in the process of preparing my dissertation in the Plants, Soils and Climate Department at Utah State University. I hope to complete in December 2008.

I am requesting your permission to include the paper we co-authored in 2006 shown below. I will include acknowledgements and appropriate citations in this work and copyright and reprint rights in a special appendix.

Please indicate your approval of this request by signing in the space provided.

Thank you for your cooperation.

Yours sincerely,

Robert Hein

I hereby give permission to Robert Heinse to reprint the following material in his dissertation.

R. Heinse, S.D. Humphries, R.W. Mace, S.B. Jones, S.L. Steinberg, M. Tuller, R. Newman and D. Or.: "Measurement of Porous Media Water Retention during Parabolic Flight Induced Microgravity." SAE Technical Paper 2005-01-2950. The 35th International Conference on Environmental Systems (ICES) and the 8th European Symposium on Space Environmental Control Systems (ESSECS), Rome, Italy, July 11–14, 2005.

Signed: Dani Or

VITA

CONTACT INFORMATION

    Ag. Sci. Bldg. Room 162   *Voice:* (435) 797-0406

    Department of Plants, Soils and Climate   *Fax:* (435) 797-2117

    Utah State University   *E-mail:* heinse@cc.usu.edu

    Logan, UT 84322-4820   http://www.usu.edu/soilphysics/

EDUCATION

Utah State University, Logan, Utah, USA

Department of Plants, Soils and Climate

Ph.D. Student, Soil and Environmental Physics

- Research Topic: "Characterization, Modeling and Design of Optimal Plant Growth Media for Reduced Gravity"
- Advisor: Scott B. Jones

Universität Leipzig, Leipzig, Germany

Department of Physics and Geosciences

Diplom (M.Sc.), Geophysics, March 2003

- Minors: Geology and Meteorology
- Thesis Topic: "Geophysical Investigation of Structure and Hydraulic Properties of Alluvial Clays on Example of the Elbe Flood Plains near Torgau, Germany"
- Advisor: Peter Schikowsky
- Major Professor: Franz Jacobs

PROFESSIONAL EXPERIENCE

Utah State University, Logan, Utah, USA

Graduate Research Assistant **2004–present**

Includes current Ph.D. research

Universität Leipzig, Leipzig, Germany

Research Fellow **April–December, 2003**

Geophysical estimation of retardation potentials of agricultural lands using integrated measurements

Universität Leipzig, Leipzig, Germany

Research Assistant **1999–2002**

Assisted with research and teaching

RESEARCH INTERESTS

My research area is environmental physics. In particular, I am interested in the integrative and complex array of processes governing the physical and hydrologic state of Earth systems at multiple spatial and temporal scales. In conducting my research, I aim to put feet in many waters, to bridge both disciplines and scales, to integratively study the environment in a holistic sense. My research focuses for example on the interface between sample and field scale through fostering the understanding of physical processes associated with fluid and gas transport at the pore/sample scale, and implementation for a variety of scales, ranging from field hydrology to plant-growth in space.

• Joint measurement and integrated interpretation of near-surface geophysical data to estimate water content, hydraulic conductivity and retarding properties of groundwater covering layers as part of a flood case risk assessment in flood catchment areas

• Geophysical characterization of transport and fate of snow melt to evaluate interactions between soil, vegetation and microclimate

• Reduced gravity impact on fluid configuration and flow as well as impact on oxygen transport in porous media intended to be used for plant growth in space

REFEREED PUBLICATIONS

Heinse, R., S.B. Jones, S.L. Steinberg, M. Tuller and D. Or (2007). Measurements and Modeling of Variable Gravity Effects on Water Distribution and Flow in Unsaturated Porous Media. Vadose Zone J 6:713-724.

Heinse, R., G. Kluitenberg, K.S. Lewis, R.S. Austin, P.J. Shouse, G.B. Bingham, and S.B. Jones (2006). Integration of Heat Capacity and Electrical Conductivity Sensors for Root Module Water and Nutrient Assessment. SAE Technical Paper 2006-01-2211.

Heinse, R., S.D. Humphries, R.W. Mace, S.B. Jones, S.L. Steinberg, M. Tuller, R. Newman and D. Or. (2005). Measurement of Porous Media Water Retention during Parabolic Flight Induced Microgravity. SAE Technical Paper 2005-01-2950.

Jones, S.B., R. Heinse, G.B. Bingham and D. Or (2005). Modeling and Design of Optimal Growth Media from Plant-Based Gas and Liquid Fluxes, SAE Technical Paper 2005-01-2949,

MANUSCRIPTS IN PREPARATION

Robinson, D.A., S.B. Jones, J.M. Blonquist, R. Heinse, I. Lebron and T. Doyle: Bright Martian Soil Dielectric Response Explained by Palagonite Type Structure. *Submitted to Proceedings of the National Academy of Sciences*

Heinse, R., S.B. Jones, D. Or, T.S. Topham, I.G. Podolskiy, D.H. Poritz and G.E. Bingham: Microgravity Configuration of Fluids in Unsaturated Porous Media: Measurements of Water Retention and Oxygen Diffusion on the ISS. *In preparation*

Heinse, R., S.B. Jones, G.E. Bingham and B. Bugbee: Optimizing Straticulate Plant-Growth Media for Improved Root Zone Performance and Management. *In preparation*

Heinse, R. and S.B. Jones: Towards Using Time-Lapse Electrical Resistivity Imaging for Improved Subsurface Snowmelt Characterization. *In preparation*

CONFERENCE PROCEEDINGS

Heinse, R. and P. Schikowsky (2003). Geophysical Assessment of Groundwater Protective Layers. 9th EEGS-ES Meeting, Prague 2003, Czech Republic.

LETTERS AND NEWS ARTICLES

Heinse, R., S.B. Jones, S.L. Steinberg, M. Tuller, and D. Or. (2007). Uncovering the Challenges of Watering Plants in Space. Crops, Soils, Agronomy CSA News V52 N12, pp. 2–3, Madison, WI, December 2007.

Jacobs, F. (2002). Hochwasserschutz durch Geoelektrische Deichdiagnose. Wirtschaft und Wissenschaft Transferbrief Leipzig, Agentur für Innovationsförderung und Technologietransfer GmbH, Leipzig, Germany, March

ABSTRACTS

Berger, P. A., R. Heinse, H. Abdu, M. Tuller, S.B. Jones, M.G. Schaap and J.F. Artiola (2008). Geophysical Characterization of Inactive Mine Tailings A First Step for Economical Design of Vegetative Covers. AGU Fall Meeting Abstracts, San Francisco, CA, December 8-12, 2008.

Berger, P. A., R. Heinse, M. Tuller, S.B. Jones and M.G. Schaap (2008). Physical and Hydrological Characterization of Mine Tailings—A First Step for Revegetation with Native Plant Communities. Agronomy Abstracts, ASA, Madison, WI.

Heinse, R., J. Carlisle and S.B. Jones (2008). Subsurface Snowmelt Patterns Identified using Time-Lapse Electrical Resistivity Imaging. Agronomy Abstracts, ASA, Madison, WI.

Heinse, R., S.B. Jones, D. Or, T.S. Topham, I.G. Podolskiy and G.E. Bingham (2008). Microgravity Implications of Water Distribution on Oxygen Diffusion Pathways in Unsaturated Porous Media. Agronomy Abstracts, ASA, Madison, WI.

Jones, S.B., D. A. Robinson, H. Abdu and R. Heinse (2008). Geophysical Techniques Uncover Soil Property Influence on Ecohydrological Processes. 93rd Ecological Society of America Annual Meeting, Midwest Airlines Center, Milwaukee, Wisconsin, Aug. 3 - 8, 2008.

Heinse, R., S.B. Jones, D. Or, M. Tuller, T.S. Topham, I.G. Podolskiy and G.E. Bingham (2008). Challenges of Watering Plants in Space: Water Retention and Distribution—What Have we Learned? 37th COSPAR Scientific Assembly, Montreal, Canada, 13-20 July 2008.

Jones, S.B., R. Heinse, D. Or, D. Poritz, T.S. Topham, I.G. Podolskiy and G.E. Bingham (2008). Oxygen diffusion measurements in porous media on the ISS: One piece of the puzzle for optimal root zone performance. 37th COSPAR Scientific Assembly, Montreal, Canada, 13-20 July 2008.

Heinse, R., S.B. Jones, D. Or, T.S. Topham, I.G. Podolskiy and G.E. Bingham (2007). Oxygen Diffusion Measurements in Unsaturated Porous Media on the International Space Station. AGU Fall Meeting Abstracts, San Francisco, CA, December 10-14, 2007.

Jones, S.B., R. Heinse, J. Šimunek, M. Tuller and D. Or (2007). Numerical Modeling of Unsaturated Flows in Variable Gravity During Parabolic Flight. AGU Fall Meeting Abstracts, San Francisco, CA, December 10-14, 2007.

Heinse, R., S.B. Jones, D. Or, T.S. Topham, I.G. Podolskiy and G.E. Bingham (2007). An Automated Oxygen Diffusion and Water Retention Measurement System for Microgravity. Agronomy Abstracts, ASA, Madison, WI.

Heinse, R., S.B. Jones, G.E. Bingham and B. Bugbee (2007). Optimizing Straticulate Plant-Growth Media for Improved Root Zone Performance and Management. Agronomy Abstracts, ASA, Madison, WI.

Jones, S.B., R. Heinse, D. Or, T.S. Topham, D.H. Poritz, I.G. Podolskiy and G.E. Bingham (2007). Oxygen diffusion measurements in partially saturated porous media onboard the International Space Station. Agronomy Abstracts, ASA, Madison, WI.

Heinse, R., S.B. Jones, B. Bugbee and G.E. Bingham (2007). Improving Root Zone Performance: Physical and Numerical Modeling of a Layered Plant-Growth Medium. USU Water Initiative, Spring Runoff Conference, Logan, UT 2007.

Heinse, R., S.B. Jones, B. Bugbee and G.E. Bingham (2006). Graduated Plant-Growth Media for Optimizing Gaseous, Liquid and Nutrient Requirements: Modeling, Design and Monitoring. AGU Fall Meeting Abstracts, San Francisco, CA, December 11-15, 2006.

Heinse, R. and S.B. Jones (2006). Porous-Media Water Retention and Distribution observed in Variable Gravity during Parabolic Flight. Agronomy Abstracts, ASA, Madison, WI.

Schikowsky, P., R. Heinse and D. Laass (2006). Complex Geophysical Measurements for Predicting Hydrogeological Properties of Alluvial Clays. SEG Hydrogeophysics Workshop, Vancouver, British Columbia, 31 July–2, August 2006.

Heinse, R., K.S. Lewis and S.B. Jones (2006). A Small-Scale Multifunctional Heat-Pulse Sensor for Soil Water Content and Electrical Conductivity. West Regional National Cooperative Soil Survey (WRCSS) and Western Society of Soil Science (WSSS) conference, Park City, Utah, June 19-23, 2006.

Lewis, K.S., R. Heinse, R. Austin, P. Shouse and S.B. Jones (2006). Measuring Electrical Conductivity Using A Low-Power Datalogging System. West Regional National Cooperative Soil Survey (WRCSS) and Western Society of Soil Science (WSSS) conference, Park City, Utah, June 19-23, 2006.

Heinse, R., K. Lewis and S.B. Jones (2006). Water Content and Electrical Conductivity Assessment using Small-Scale Multifunctional Heat-Pulse Sensors. USU Water Initiative, Spring Runoff Conference, Logan, UT 2006.

Heinse, R., Lewis, K., Kluitenberg, G. E., Bingham, G. and S. B. Jones (2006). Coupled Heat Capacity and Electrical Conductivity Measurements for Root Zone Water and Nutrient Assessment. Habitation 2006, Conference on Habitation Research and Technology Development. Rosen Plaza Hotel, Orlando, FL, February 5–8, 2006.

Jones, S. B. , Heinse, R., Or, D., Poritz, D. and G. E. Bingham (2006). Characterization and Analysis of Water Retention and Oxygen Diffusion in Plant Growth Media on Earth: Criteria for Comparison in Microgravity. Habitation 2006, Conference on Habitation Research and Technology Development. Rosen Plaza Hotel, Orlando, FL, February 5–8, 2006.

Heinse, R., Jones S. B. and D. Or. (2005). Inverse Modeling of Porous Media Unsaturated Hydraulic Properties in Microgravity. Agronomy Abstracts, ASA, Madison, WI.

Blonquist, J. M., Heinse, R., Ditthakit, P., Mace, B.,Lewis K. and S. B. Jones (2005). An Instrumented Soil Column For Teaching Unsaturated Flow And Transport Processes. Agronomy Abstracts, ASA, Madison, WI.

Jones, S. B., Heinse R., Bingham G. B. and D. Or (2005). Particulate Plant Growth Media for Reduced Gravity: Experiences and Challenges. Workshop on Granular Materials in Lunar and Martian Exploration, John F. Kennedy Space Center, Orlando, FL, Feb. 2–3, 2005.

Heinse, R., Jones S. B., Humprhies S. D., Mace R. W., Steinberg S. L., Tuller M., Newman R. and D. Or (2004). Porous Media Water Retention and Saturated Hydraulic Conductivity During Parabolic Flight Induced Microgravity. Agronomy Abstracts, ASA, Madison, WI.

Or, D., Jones S. B., Tuller M. , Steinberg S. L., Alexander I., Diadzic N., Reddi L. N., Kluitenberg G., Ogden F. L. and R. Heinse (2004). Unsaturated Flow in Zero Gravity—Lessons and Challenges. Agronomy Abstracts, ASA, Madison, WI.

Laass, D., Schwabe, J., Schikowsky, P. and Heinse, R. (2004). Einsatz der Geophysik bei hydrogeologischen Aufgabenstellungen. GeoLeipzig 2004—Geowissenschaften sichern Zukunft, Leipzig, Germany 2004.

Heinse, R., Laass, D. and Schikowsky, P. (2004). Common and Multi-Offset Ground Penetrating Radar in Assessing Soil Water Content Dynamics in the Vadose Zone. 85th Annual Meeting Pacific Division American Assoc. for the Advancement of Science, Logan, UT 2004.

Heinse, R. and Schikowsky, P. (2004). Geophysical Assessment of Groundwater Protective Layers. USU Water Initiative, Spring Runoff Conference, Logan, UT 2004.

Schwabe, J., Grützner, C., Heinse, R. and Schikowsky, P. (2004). Georadarmessungen für Hydrogeologische Aufgabenstellungen. Rundtischgespräch GEORADAR, Nossen, Germany 2003.

Heinse, R. and Schikowsky, P. (2004). Hochfrequente Elektromagnetische und Gleichstromgeoelektrische Untersuchungen zur Bewertung von Auelehmdeckschichten. Rundtischgespräch GEORADAR, Nossen, Germany 2003.

Heinse, R., Schikowsky, P. and Storz, W. (2003). Geophysikalische Untersuchungen zur Deckschichtbewertung—Ein Beitrag zum Grundwasserschutz. 63. Jahrestagung der Deutschen Geophysikalischen Gesellschaft, Jena, Germany 2003.

Heinse, R. Grützner, C., Schwabe, J. and Schikowsky, P. (2003). Georadarmessungen zur Bewertung von Auelehmdeckschichten - Ein Beitrag zum Grundwasserschutz. 63. Jahrestagung der Deutschen Geophysikalischen Gesellschaft, Jena, Germany 2003.

Heinse, R., Schikowsky, P. and Storz, W. (2003). Geophysikalische Untersuchungen zu Struktur und hydraulischen Eigenschaften von Auelehm am Beispiel der Elbaue bei Torgau. X. Arbeitsseminar Hochauflösende Geoelektrik, Kloster Nimbschen bei Leipzig, Germany 2002.

Heinse, R. Just, A. and Kürschner, D. (2002). Modelluntersuchungen zur elektrischen Vertikaltomographie in Gewässern. 62. Jahrestagung der Deutschen Geophysikalischen Gesellschaft, Hannover, Germany 2002.

Just, A., Helbig, K., Heinse, R., Flechsig, Ch., Jacobs, F. and Endler, R. (2001). Messungen mit einer neuen Elektrischen In Situ Apparatur (ELISA) in der Ostsee. 61. Jahrestagung der Deutschen Geophysikalischen Gesellschaft, Frankfurt, Germany 2001.

Just, A., Helbig, K., Heinse, R., Flechsig, Ch., Jacobs, F. and Endler, R. (2000). Messungen mit der Elektrischen In Situ Apparatur (ELISA) in der Ostsee. IX. Arbeitsseminar Hochauflösende Geoelektrik, Bucha/Sachsen, Germany 2000.

TEACHING EXPERIENCE

Teaching Assistant, Utah State University

- *Unsaturated Flow and Transport SOIL 6140*   (Spring 2007-present)
- *Environmental Soil Physics SOIL 6650*   (Fall 2005-present)

*Assisted students with homework assignments and laboratory data processing, graded homework assignments, and filled in as lecturer for the course.

Teaching Assistant, Universität Leipzig

- *Applied Geophysics/Engineering Geophysics I and II*   (Spring 2001–2003)

*Assisted students with homework assignments, graded homework assignments, demonstrated geophysical equipment for the laboratory section, and filled in as lecturer for the course.

Guest Lecturer, Utah State University

Single lectures on:

- *Water content measurements* for *Landscape Irrigation Mgmt. PLSC 5100*   (Spring 2006)
- *Time Domain Reflectometry (TDR)* for *Surface Hydrology SOIL 6600*   (Spring 2004)

HONORS & AWARDS

Named USU Water Fellow. Provided by the USU Water Inititative, 2008

Received GSS Travel Award. Provided by the Graduate Student Senate, Utah State University, 2005 and 2006.

Received Graduate Student Fellowship. Provided by the Dept. of Plants, Soils and Biometeorology, Utah State University, 2005/2006.

Invited Student Presenter. Don and Betty Kirkham Conference on Soil Physics, October 28–29, Logan, UT 2004.

AFFILIATIONS

AGU American Geophysical Union

ASA/CSSA/SSSA Soil Science Society of America

SEG Society of Exploration Geophysicists

SERVICE

Peer reviewer for *Near Surface Geophysics*, *Vadose Zone Journal*, *Geophysics*, *SAE Technical Papers* and *International Journal of Geomechanics*

Organizer of the *Utah State Water Speaker Series*   **2007–2008**

SPECIAL EXPERIENCES

NASA Parabolic Flight Opportunities

Reduced Gravity Office, Houston, Texas   **May, 2006**

Microgravity porous-media experiments

Underground Mine Experiments

Asse potassium salt mine, Lower Saxony, Germany   **June, 2003**

Geophysical measurements in a salt repository

Marine Research Vessel Cruises

Institut für Ostseeforschung Warnemünde, Germany   **April, 2000**

ELISA Electrical In-Situ Apparatus experiments   **February, 2001**